Investigating the Effect of Ultrasonic Consolidation on Shape Memory Alloy Fibres

By

Ross James Friel

Doctoral thesis submitted in partial fulfilment of the requirements of the award of Doctor of Philosophy of Loughborough University

June 2011

Abstract

This research was driven by the capability of the Ultrasonic Consolidation (UC) manufacturing process to create smart metal matrix composites for use within high value engineering sectors, such as aerospace. The UC process is a hybrid additive/subtractive manufacturing process that embeds fibres into metal matrices via the exploitation of a high plastic flow, low temperature phenomenon encountered at ultrasonic frequency mechanical vibrations. The research concerned an investigation of the use of the UC process for embedding Nickel-Titanium alloy (NiTi) shape memory alloy (SMA) fibres into Aluminium (Al) matrices which could potentially be used as vibration damping structures, stress state variable structures, as well as other future smart material applications.

It was hypothesised that the fibre volume fraction within a UC matrix was limited due to a reduction in foil/foil bonding, caused by increased fibre numbers, as opposed to the total level of plastic flow of the matrix material being insufficient to accommodate the increased fibre numbers.

This hypothesis was tested by increasing the NiTi SMA fibre volume fraction, within an Al 3003 (T0) metal matrix, beyond that of previous UC work. The metal matrix and the fibre matrix interface of these samples was then microscopically analysed and the overall UC sample integrity was tested via mechanical peel testing. It was found that a fibre volume fraction of ~9.8% volume (30 X Ø100 μm SMA fibres) was the maximum achievable using an Al 3003 (T0) 100 μm thick foil material and conventional UC fibre embedding.

A revised hypothesis was postulated that the interlaminar structure created during UC was affected by the process parameters used. This interlaminar structure contained areas of un-bonded foil and the increase of UC process parameters would reduce this area of un-bonded foil. Areas of this interlaminar structure were also thought to have undergone grain refinement which would have created harder material areas within the structure. It was suggested that maximum plastic flow of the matrix had not been

reached and thus the use of larger diameter NiTi SMA fibres were embedded to increase the effective SMA fibre volume fraction within Al 3003 (T0) UC samples. It was suggested that the embedding of SMA fibres via UC had an abrasive effect on the SMA fibres and the SMA fibres had an effect on the Al 3003 (T0) microstructure. It was further suggested that the activation of UC embedded SMA fibres would reduce the strength of the fibre/matrix interface and the matrix would impede the ability of the SMA fibres to contract causing a forceful interaction at the fibre to matrix interface, weakening the UC structure.

The investigation to test the revised hypothesis was broken down into three sections of study.

Study 1 was a methodology to determine the characteristics of the interlaminar surface created via UC and how this surface affected the nature of the consolidated sample. UC samples of Al 3003 (T0) were manufactured using a range of process parameters. The analysis involved optical microscopy to determine the UC weld density and the interlaminar surface; mechanical peel testing to quantify the interlaminar bond strength; white light interferometry to measure the interlaminar surface profile and microhardness measurements to determine the hardness of the interlaminar material.

Study 2 was a methodology to allow the analysis of the microstructural and mechanical interactions at the fibre/matrix interface, post-UC. Al 3003 (T0) samples were manufactured via UC using a range of process parameters with various NiTi SMA fibre diameters embedded. The analysis involved using mechanical peel testing to determine the interlaminar bond strength; optical microscopy to determine the level of fibre encapsulation; scanning electron microscopy and focussed ion beam analysis to analyse the fibre and matrix grain structures and microscopic interactions.

Study 3 was a methodology to investigate the fibre usage as would be expected from envisaged applications of an SMA containing metal matrix composite. Samples were manufactured using a range of UC process parameters with various SMA fibre diameters embedded and the embedded SMA fibres were subjected to different extension/contraction cycle numbers. The analysis involved using mechanical peel

testing to determine the interlaminar bond strength; optical microscopy to determine the level of fibre encapsulation and the interlaminar effect of fibre activation; fibre pullout testing to measurement the strength of the fibre/matrix interaction and load rate testing of the activated SMA fibres to monitor performance.

The interlaminar surface was found to affect the strength and density of interlaminar bonding during the UC process and the use of higher UC process parameters affected this interlaminar structure. Levels of un-bonded material were found within the interlaminar structure and these levels were found to decrease with increasing sonotrode amplitude and pressure with reducing speed. It was suggested that a specifically texture sonotrode could be developed to modify the interlaminar structure to the requirements of the intended sample application. The measurement of the interlaminar material hardness was unsuccessful and future work would likely require a different methodology to measuring this.

The work identified a grain refining effect of the embedded SMA fibres on the Al 3003 (T0) matrix material, (grain sizes were reduced from ~15 μm to <1 μm within 20 μm of the SMA fibres), as well as localised damage caused by the UC process to the SMA fibres. The performance of the activated SMA fibres established that this damage did not prohibit the ability of the SMAs to function however the compressive nature of the Al 3003 (T0) matrix was identified as reducing the ability of the SMA fibres to contract. Additionally it was found that the activation of SMA fibres within an Al 3003 (T0) matrix resulted in a reduction of the fibre/matrix interface strength which allowed fibres to be pulled from the composite with greater ease (a loss of ~80% was encountered after a single activation and extension cycle). The use of larger SMA fibre diameters allowed for the fibre volume fraction to be increased however the activation of these SMA fibres had a delaminating effect on the Al 3003 (T0) structure due to the size of the radial expansion of the SMA fibre.

The work furthered the understanding of the effect of UC on SMA fibres and highlighted the importance of the interlaminar surface in UC and that to increase the SMA fibre volume fraction to a useable level (25-50%) then an alternative fibre embedding method within UC is required. The fibre/matrix interface interactions during SMA activation have

implications in the ability of UC SMA embedded smart metal matrix composites to function successfully due to weakening effects on fibre matrix interface strength and the ability to achieve SMA fibre activation within the metal matrix.

Contents

Acknowledgement

I would like to thank my supervisor Dr. Russell Harris. His guidance, input and patience during my PhD have been excellent and have without doubt helped me to become someone capable of contributing to the wider academic community.

I would like to thank Mr. Andy Sandaver and Dr. Geoff West; their knowledge, experience and tutorage of all things metallurgical were key to this work and the discoveries within.

I would like to thank colleagues and technical staff at Loughborough University who have aided me during my PhD in some form or another.

My future wife Lisa deserves a medal for her patience and understanding during the completion of this PhD; you are my rock and compassionate ear. You have my deepest thanks and admiration.

Finally I would like to thank my parents; your hard work, love and support have allowed me a life that I am able to influence and shape. Without you I would be and have nothing; you have allowed me the opportunities and given me the wherewithal to take them – I am eternally grateful.

Publications

Journal Papers

- *Nanometre-scale fibre to matrix interface characterisation of an ultrasonically consolidated metal matrix composite*. **Friel, R.J. and Harris, R.A.** SAGE Publications, 2010, Proceedings of the Institution of Mechanical Engineers, Part L: Journal of Materials: Design and Applications, Vol. 224, No.1, pp. 31-40, ISSN: 1464-4207.

  (This paper was awarded as one of the journals top 5 most downloaded papers in 2010).

- *The effect of interface topography for Ultrasonic Consolidation of aluminium*. **Friel, R.J., Johnson, K.E., Dickens, P.M., Harris, R.A.** Elsevier, B.V., 2010, Materials Science & Engineering: A, Vol. 527, No.16-17, pp.4474-4483, ISSN: 0921-5093.

- *Activation response of ultrasonic consolidation embedded shape memory alloy fibres*. **Friel, R.J. and Harris, R.A.** Elsevier Ltd., 2011, Composites Part A: Applied Science and Manufacturing, ISSN: 1359-835X. (final preparation)

- *Fibre pullout performance of activated shape memory alloy fibres in metal matrix composites*, **Friel, R.J. and Harris, R.A.** Elsevier Ltd., 2011, Composites Science and Technology, ISSN: 0266-3538. (in preparation)

- *Increasing fibre volume fraction in shape memory alloy containing metal matrix composites produced via ultrasonic consolidation*, **Friel, R.J. and Harris, R.A.** Elsevier, B.V., 2011, Materials Science and Engineering: A, ISSN: 0921-5093. (in preparation)

Conference Publications

- *Smart Material Structures*. **Friel, R.J. and Harris, R.A.** Inaugural Ultrasonic Consolidation Technology Symposium, Ann Arbor, Michigan, USA, September 10th, 2008.

- *Field Repair and Replacement Part Fabrication of Military Components Using Ultrasonic Consolidation Cold Metal Deposition (Paper 22)*. **Schwope, L-A., Friel, R.J., Johnson, K., Harris, R.A.** NATO RTO-MP-AVT-163 Additive Technology for the Repair of Military Hardware, Bonn, Germany, October 19th-22nd, 2009. (*Invited presentation*).

- *Enabling Dissimilar Fibre Embedding and Explicit Fibre Layout in Ultrasonic Consolidation*. **Friel, R.J., Masurtschak, S., Harris, R.A.** 21st International Conference on Adaptive Structures and Technologies, State College, USA, October 4th-6th, 2010.

Acronyms

3D	Three Dimensional
Al	Aluminium
AM	Additive Manufacturing
CAD	Computer Aided Design
CAM	Computer Aided Manufacture
CFRP	Carbon Fibre Reinforced Polymer
CNC	Computer Numerical Control
DBFIB	Dual Beam Focussed Ion Beam
EBF3	Electron Beam Free Form Fabrication
EDM	Electro Discharge Machining
FBG	in-Fibre Bragg Grating
Fe	Iron
FEG	Field Emission Gun
FIB	Focussed Ion Beam
FRP	Fibre Reinforced Polymer
Ga^+	Gallium Ions
HIP	Hot Isostatically Pressed
HV	Vickers Hardness
LENS	Laser Engineered Net Shaping
LWD	Linear Weld Density
MEMS	Micro Electromechanical Systems
MMC	Metal Matrix Composite
MMF	Multi Mode Fibre
Mn	Manganese

MR	Magnetorheological
NEMS	Nano Electromechanical Systems
NiTi	Nickel-Titanium Alloy
Pt	Platinum
PU	Polyurethane
PVC	Polyvinyl Chloride
R_a	Average Surface Roughness
R_q	Root Mean Square Roughness
SEM	Scanning Electron Microscopy
SiC	Silicon Carbide
SiO_2	Silicon Dioxide
SLM	Selective Laser Melting
SLS	Selective Laser Sintering
SMA	Shape Memory Alloy
SME	Shape Memory Effect
SMF	Single Mode Fibre
SMP	Shape Memory Polymer
Sn-Ag	Tin-Silver Solder Alloy
Ti	Titanium
TiB_2	Titanium Diboride
UC	Ultrasonic consolidation
UHR	Ultra High Resolution
USA	United States of America
USW	Ultrasonic Welding
VGC	Variable Geometry Chevron
µCT	X-ray Microtomography

List of Figures

List of Tables

List of Equations

1 Introduction

1.1 Research Drivers

For this thesis there were three key drivers to motivate further research of the subject matter:

1. The possibilities that smart structures present to the engineering community.
2. The lack of apposite manufacturing techniques with regards to obtaining metal matrix based smart structures for mainstream engineering use.
3. The precursor work using Ultrasonic Consolidation (UC) that defined its key advantages and potential with regards to creating metal matrix based smart structures (Kong, 2005).

1.1.1 Smart Structure Possibilities

Smart structures, (also referred to as adaptive composite structures (Agnes, et al., 1999)):

"*typically feature a combination of sensors, actuators, and processors, which will permit them to respond intelligently and autonomously to dynamically-changing environmental conditions by capitalizing on embedded innovative functions*" (Thompson, et al., 1992).

The structures are engineered to respond to stimuli such as temperature, mechanical stress, a magnetic or electric field, moisture, pH, light, etc. The response to these stimuli is a controlled and variable response in the form of one or more material/structure property changes which is accorded through the use a smart material (also referred to as intelligent materials (Takahashi, 1988), and adaptive materials (Pinkerton, et al., 1996)).

This is a different approach to engineering than the common use of structures which are designed to have a performance that will always exceed, by several factors, the envisioned maximum performance of the healthiest component.

By following an adaptive route to structure operation a real time adaptable performance to the environment can be obtained through feedback and the integration of adaptable materials.

Many sectors are pursuing “smart” material and geometry exploitation with research in the aerospace (Barbarino, 2009) (Staszewski, 2004), automotive (Manz, 2001) (Peelamedu, et al., 1999), civil (Ansari, 1997) (Li, et al., 2007) and electronics (Chiodo, 2002) (Kang, 2006) industries. The results from smart structure research, that these industries are striving for, are as varied as the potential applications of smart structures. Some of the common goals are:

- Maintenance and safety improvement through the use of integral health and performance monitoring (Zagrai, 2010).
- Weight and complexity reduction through the reduction of part numbers (Kudva, 2004).
- Variability in response to match changing conditions (Bonello, 2005).
- Built in additional structural/material functionality (Salamone, 2010).

Examples

Magnetorheological (MR) dampers (see Figure 1) are now commonly found within the automotive and aerospace industries. These damper structures have a variable damping characteristic using a variable magnetic field to increase the apparent viscosity of the MR fluid (Figure 2). This variability is controlled via a closed loop system that uses feedback from onboard sensors to continually monitor and adjust fluid viscosity to match the dynamic situation. The magnetic field is typically applied via an electromagnet with field intensity varied in accordance with data received from onboard sensors.

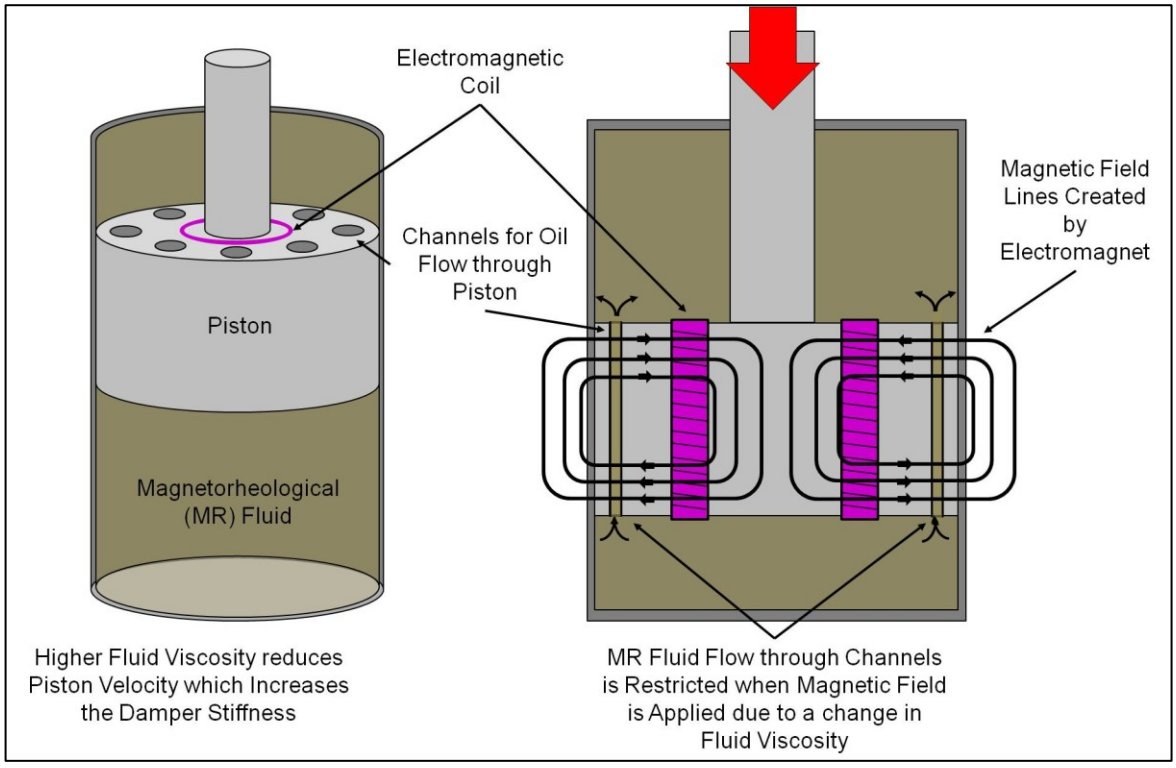

Figure 1 – Magnetorheological damper example schematic (Dyke, et al., 1996)

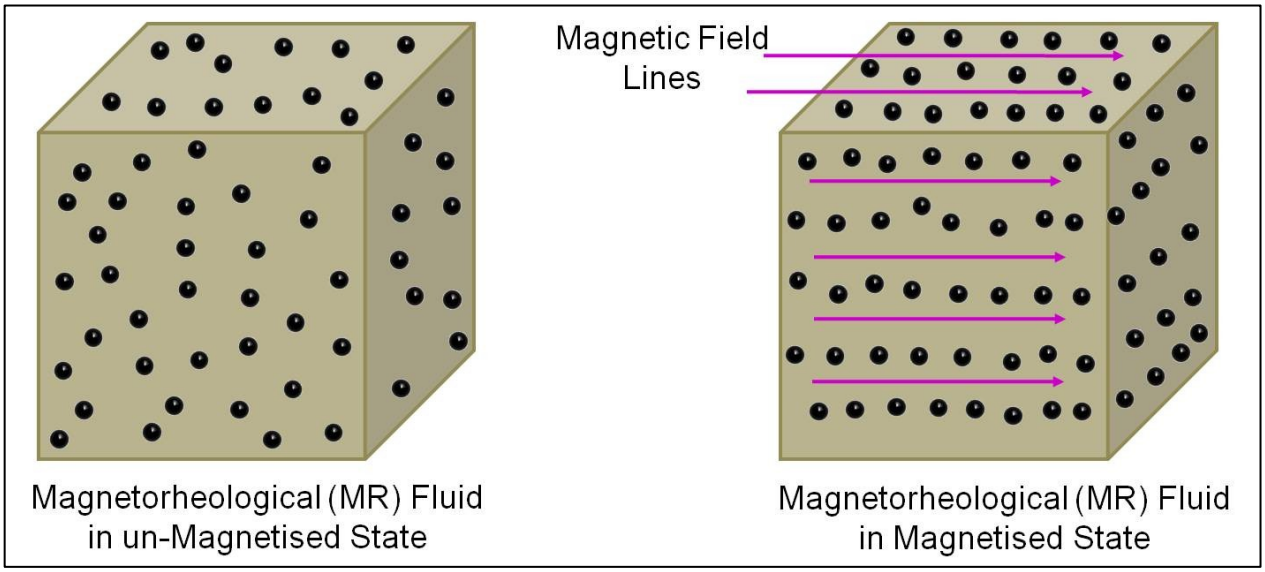

Figure 2- Schematic of magnetorheological fluid operation principal

Structural health monitoring beams and slabs have been used on six bridges in Canada to monitor structural health using in-Fibre Bragg Gratings (FBG) to measure static and dynamic strain (Tennyson, 2001). FBG's are formed into concrete beams and slabs that are pre-stressed using Carbon Fibre Reinforced Polymer (CFRP) (Figure 3). These

beams and slabs are then integrated into the bridge structure and provide information on strain and temperature over time. Engineers are then able to continuously monitor the bridges performance to ensure adequate performance, identify potential issues that may become apparent over time and gather data to determine maintenance procedures and schedules.

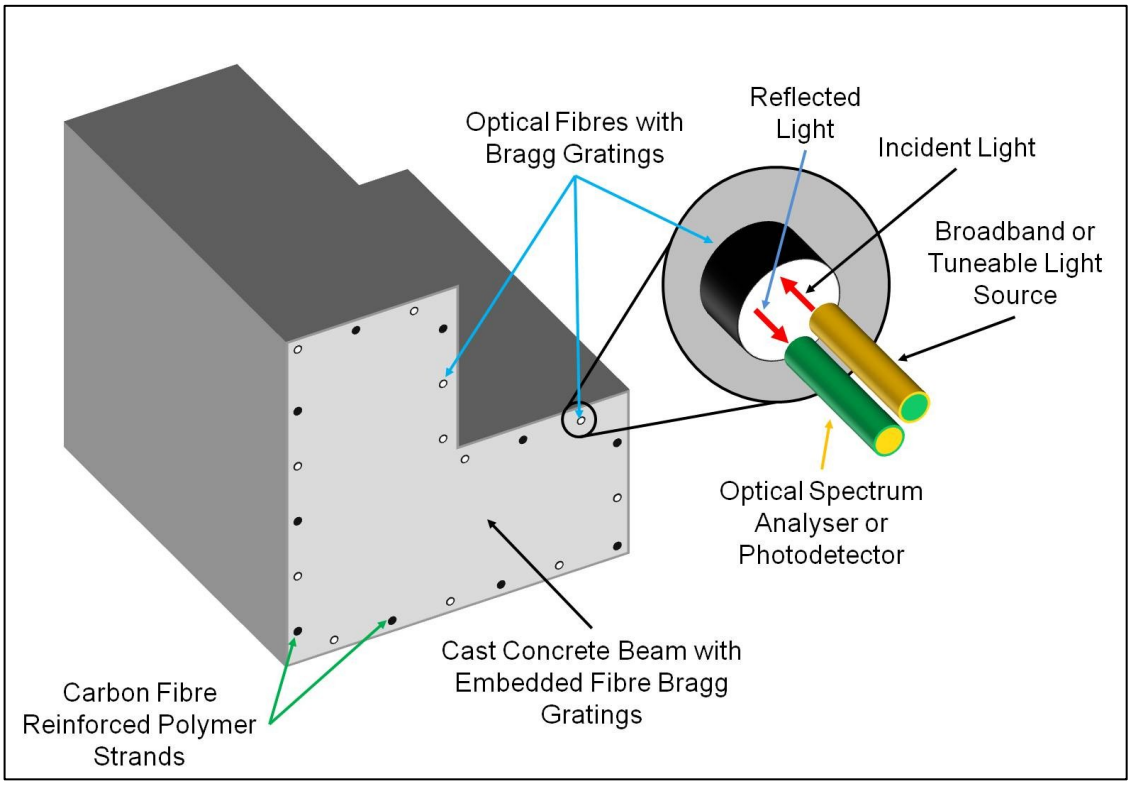

Figure 3 – Schematic of a smart concrete beam using embedded fibre Bragg gratings for structural health monitoring

1.1.2 Limitations of Traditional Technologies

The creation of fully integrated smart structures requires the combination of multiple, chemically distinct, materials into a single structure. This creates a composite of materials that have differing thermal and physical properties to each other. The common elements of many envisioned smart structure components, such as optical fibres, Micro Electromechanical Systems (MEMS), and shape memory materials are relatively fragile when compared to typical matrix materials and their associated traditional manufacturing techniques.

To overcome thermally and physically delicate component issues the use of liquid mediums, (e.g. oil (Peelamedu, et al., 1999), etc), or low temperature liquid to solid matrices, (e.g. thermosetting polymers (Pang, 2005), hydrating minerals such as cement (Li, et al., 2007), low temperature alloys such as Sn-Ag alloy (Coughlin, 2009), etc), are used to house the varying smart elements into a distinct structure. These matrices are suitable for smart structures however there is a distinct gap in functionality, mechanical and environmental performance as they do not allow the use of common engineering metal alloys, such as aluminium (Al) based, titanium (Ti) based and iron (Fe) based, as a matrix material. These alloys have significantly higher mechanical and temperature performance ranges over polymer or liquid or low temperature alloys. The use of a metal matrix to encapsulate sensor and actuator components within a single metal matrix structure is of significant interest to the engineering sector.

The use of a metal matrix to create a Metal Matrix Composite (MMC) is possible through a current range of manufacturing techniques; however the integration of continuous and/or delicate elements into these matrices, to create a smart structure, present certain pressure and/or temperature and/or stress issues that these techniques cannot yet resolve.

1.1.3 Opportunities Provided by Ultrasonic Consolidation

UC is a hybrid solid state metal additive/subtractive manufacturing process that combines ultrasonic metal seam welding and Computer Numerical Control (CNC) milling to fabricate solid metal components, layer by layer, from metal foil (White, 2000). Through the use of relatively low temperatures and pressures the UC process has been shown to be capable of embedding optical fibres for sensor use (Kong, et al., 2005) (Mou, et al., 2009), Shape Memory Alloy (SMA) fibres for actuation (Kong, et al., 2004) (Hahnlen, et al., 2010) and reinforcement fibres for strengthening (Li, 2009) (Yang, 2007), into metal matrices.

In addition to the embedding of fibres and components the UC process has also been proven to bond dissimilar materials together to form dissimilar metal matrices (Obielodan, 2010) which have the potential to be combined with embedded active and passive elements. The combination of these components coupled with the relative

geometric freedom that Additive Manufacturing (AM) permits places UC as a most attractive method with which to create metal matrix based smart structures.

However, UC is still a comparatively undeveloped manufacturing process with fundamental aspects of bond formation, plastic flow and embedded object performance uncertain. This research aimed to further the understanding of the matrix effects on embedded elements during UC, and vice versa, so as to help continue the development of smart metal matrix composites for a wide range of engineering applications.

1.2 Intentions of the Research

The most challenging type of smart structure to manufacture, and that which UC is most suited to, is metal matrix based smart structures. These structures are viewed as being a key technology of future aeronautic and astronautic structures (Committee on Aeronautical Technologies, 1992) and a viable commercial manufacturing technique has yet to be fully developed. Therefore for the purpose of this research, a focus has been put on metal based matrix composites suitable to future applications, such as airframe construction.

1.2.1 Aims and Objectives

The aim of this research was to understand the metal matrix effects on SMA fibres embedded via UC, and vice versa, at the micro and macro level. The objectives of the research investigation were:

- To evaluate fibre volume effect on interlaminar bond strength.
- To investigate higher fibre numbers embedded between two metal foils during UC than had previously been researched so as to identify possible limitations.
- To investigate interlaminar topography effects on the UC bonding process to ascertain any effect of topography on the effectiveness of UC.
- To understand how SMA fibres behave during UC.
- To investigate microstructure changes of the matrix due to fibre embedding.
- To evaluate the actuation performance of embedded SMA fibres.
- To evaluate fibre matrix integrity after SMA fibre activation.

1.2.2 Plan of Investigation

The overall method to the research work was formed into four distinct stages (

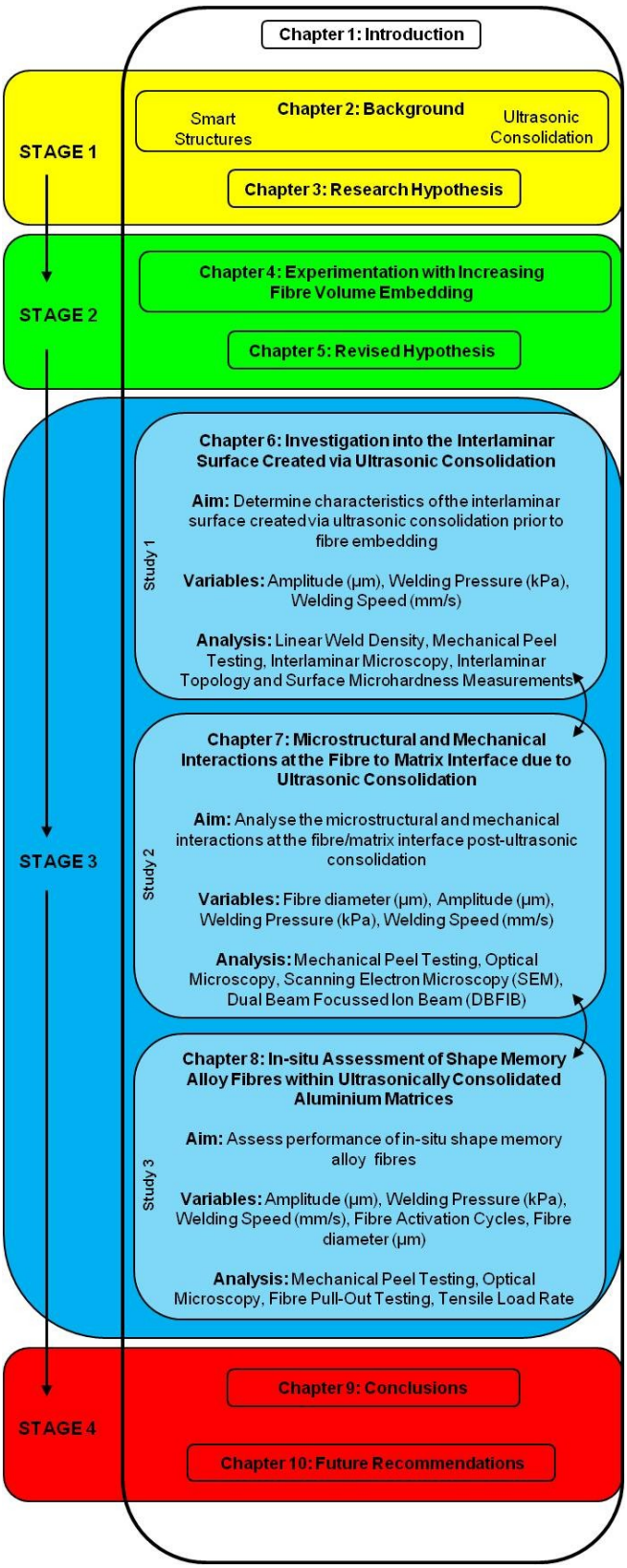

Figure 4).

STAGE 1:

After a background review (Chapter 2) of the area a research hypothesis was developed as a provisional conjecture to help guide the research (Chapter 3).

STAGE 2:

A method for experimentation into fibre volume increase during UC was devised and then carried out (Chapter 4). The results and discussion surround this work then resulted in a revised hypothesis (Chapter 5) to further the study.

STAGE 3:

To test the revised hypothesis three studies were carried out. Each of the studies developed the understanding of fibre embedding in UC. The first study (Chapter 6) was used to determine the characteristics of the interlaminar surface created via ultrasonic consolidation. The second study (Chapter 0) involved analysing the microstructural and mechanical interactions at the fibre/matrix interface. The third study (Chapter 8) was used to assess the performance of in-situ shape memory alloy fibres. The results garnered from the experimental studies were presented in a suitable fashion and discussed in depth with insight from both previous published work and new insight from the present work.

STAGE 4:

Conclusions (Chapter 9) and Future Recommendations (Chapter 10) were drawn from the research results and discussion and future recommendations that would further the present work and wider UC area as a whole were suggested.

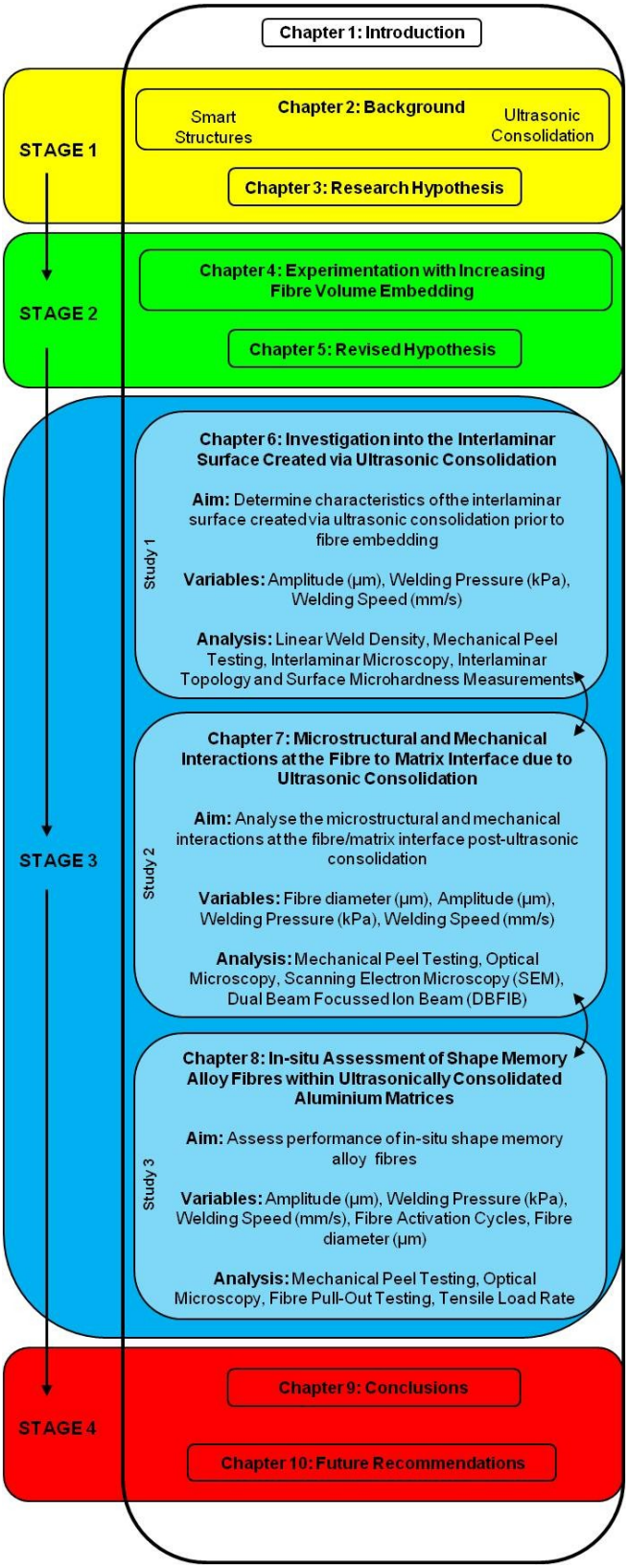

Figure 4 – Plan of investigation and thesis structure

2 Background

2.1 Smart Structures

2.1.1 Introduction

Smart structures are a relatively new development in engineering. A smart structure requires a matrix in or on which to house or support sensing and activating components. This matrix can be liquid based (Phulé, 2001), polymer based (White, et al., 2001), ceramic based (Dong, et al., 2005) or metal based (Bräutigam, et al., 2007).

The manufacture of liquid, polymer and ceramic matrix based smart structures, although still immature in development, are more easily achieved due to the use of solid to liquid phase transformations at relatively low temperatures; or none at all in the case of liquid based matrices. Metal matrix based smart structures are desirable for many applications due to the specific mechanical and thermal properties of the matrix material (Vogelesang, et al., 2000), however they present a manufacturing challenge due to their high temperature liquid phase which can destroy or damage the sensitive components required to create the smart structure (Recarte, et al., 2004) (Li, et al., 2003). The focus of this research is in the development towards metal matrix based smart structures and therefore the background review will be focussed on metal matrix based smart structures.

In order for a smart structure to be able to function there must be a form of monitoring that is sensitive to a particular or multiple sources of stimuli; and a form of activator to facilitate a response to stimuli; with both of these elements combined in a feedback system (see Figure 5). For the purpose of this research monitoring elements will be referred to as sensors and activation elements will be referred to as activators.

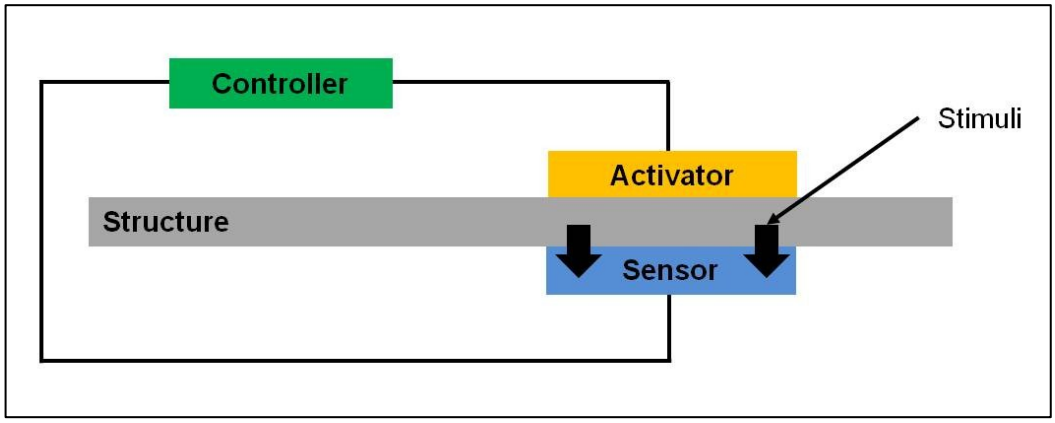

Figure 5 - Schematic of a Smart Structure Input/Output Setup

Research into smart structures has predominantly focussed on the use of shape change materials as activators due to their lower complexity, lower mass and greater reliability, when compared to mechanism based activators (Manz, 2001). These materials undergo a dimensional change when subject to an external stimuli such as temperature or electrical current. Common examples of these materials are piezoelectrics, shape memory polymers and shape memory alloys; (these materials are discussed in more detail in Section 2.1.3).

To provide information on which the activator can respond a sensor of some form is required. These sensors are chosen for the particular environmental stimuli to which they respond with common types being optical fibre based sensors, strain sensors, temperature sensors and piezoelectric based sensors; (these sensor types are discussed in more detail in Section 2.1.2).

In addition to the sensor and activator it is usual for a data processor or controller to be used to create the final smart structure. These controllers are required to monitor the data from the sensor and use this to control the activator in the required way to meet the changing conditions. These controllers, due to their size and complexity, are generally external to the structure and thus will not be researched in the present work.

2.1.2 Typical Sensor Types

There are many forms of potential activators that are viable for the creation of smart structures; however the focus of this background review will be on the sensor types that have been used most frequently for research in the field and which could potentially be

incorporated into a metal matrix. These include optical fibres, MEMS/Nano Electro Mechanical Systems (NEMS) and piezoelectric elements.

Optical Fibre based Sensors

Optical fibres are light waveguides that can be used for a variety of data transfer and sensor applications. A typical optical fibre will consist of a Silicon Dioxide (SiO_2) core as a pure consistent medium for transmitting the light wave, a cladding around the core which reflects the light back into the core and a buffer coating (typically polyvinylchloride (PVC) or polyurethane (PU)) which protects the core and cladding from damage and moisture contact (Allan, 1973) (Figure 6).

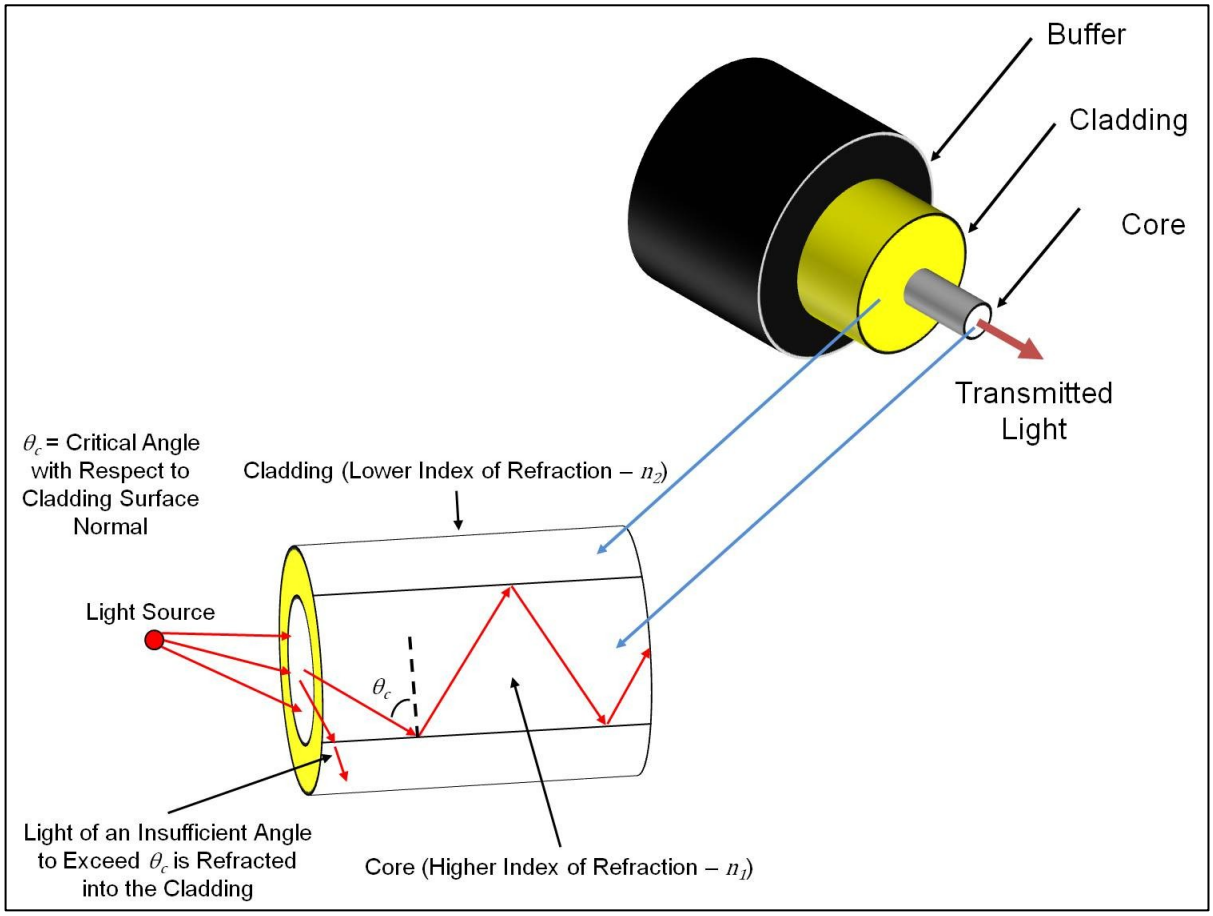

Figure 6 - Schematic of a single mode optical fibre showing principal of total internal reflection

The mechanism of optical fibre operation is through the exploitation of the total internal reflection phenomena. If a wave strikes a medium boundary at an angle larger than the critical angle (θ_c), with respect to the normal to the surface, then total internal reflection can occur (Equation 1). In optical fibres the refractive index of the core (n_1) is greater

than that of the cladding (n_2) allowing the critical angle to be exceeded and total internal reflection to take place (Figure 6). Any light that enters the core of the optical fibre at an angle less than the critical angle is refracted into the cladding where it is lost and therefore the light does not continue to traverse along the core.

$$\theta_c = sin^{-1}\left(\frac{n_2}{n_1}\right)$$

Equation 1 - Critical angle equation (Goff, 2002)

For communication use there are two different types of optical fibre: Single Mode Fibres (SMF) and Multimode Fibres (MMF). SMFs are capable of supporting only single propagation paths for light making them suited for longer distance communications as well as more accurate sensors. MMFs can support many propagation paths for light and are used for shorter distance communication and higher data transfer rate (Goff, 2002). SMFs generally have a core diameter ≤ 10 μm and require more specialised and expensive measurement equipment to use, compared to MMFs; but due to the fact that only one mode of propagation is present the light from a SMF is easier to focus and for measurements to be made with (Hill, et al., 1993). In practical application SMFs are more prone to damage than MMFs due to functioning only on a single propagation path and the smaller diameter core.

There are several proposed methods of using optical fibres as sensors for smart structures (Udd, 1995). These typically include, but are not limited to, Fabry–Pérot interferometric sensors (Bhatia, et al., 1996) (Liu, et al., 1997), two-mode fibre-optic sensors (Michie, 2000) (Zhou, et al., 2002), polarimetric fibre-optic sensors (Zhou, et al., 2002) (Bock, et al., 1996), and FBGs (Rao, 1997) (Takeda, et al., 2005) (Guemes, et al., 2002). In recent years much of the focus for fibre optic based sensors for conceptualised smart materials has been based on FBGs due to their ability to give an absolute measurement that is insensitive to fluctuations in the illuminating source, the fact that they can be directly created within an optical fibre without the need for diameter changes and complex fibre coupling, and due to their high range to resolution (Rao, 1997). Owing to this predominance of FBGs the operation of this sensor type will be discussed.

An FBG can detect the variation in strain and temperature experienced by the optical fibre (Hill, et al., 1997). This detection is performed by measuring the change in the

Bragg wavelength (λ_B) which is varied due to the change of spacing in a series of gratings that have been laser etched into the optical fibre core (Bennion, et al., 1996). These gratings change the effective refractive index (n_{eff}) of the fibre core in a periodic fashion (Figure 7). By exposing the grating containing core to a controlled broadband light source (λ_{broad}) and measuring the reflected wavelength, λ_B a profile for variation in strain or temperature can be produced (Kersey, 1996).

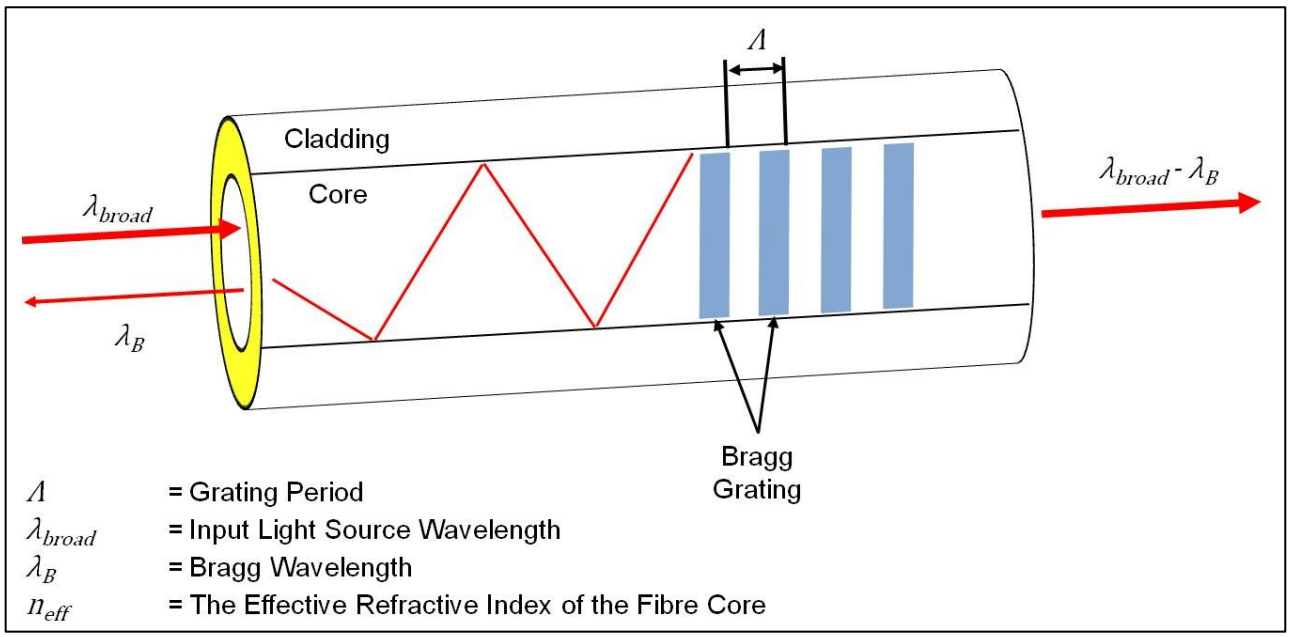

Figure 7 - Schematic of an in-fibre Bragg grating

The Bragg wavelength, λ_B is determined via the following relationship:

$$\boldsymbol{\lambda_B = 2\, n_{eff}\, \Lambda}$$

Equation 2 – Bragg wavelength relationship (Hill, et al., 1997)

MEMS/NEMS Sensors

MEMS/NEMS are terms used to describe micro or nano scale mechanical mechanisms that are powered by electricity (Gad-el-Hak, 2006). The emergence of NEMS has been possible due to improvement in the imaging and manufacturing techniques at the nano scale; however for the purpose of the theoretical applications of metal alloy based smart structures in this work the use of NEMS has little benefit over MEMS and thus the focus will be on MEMS.

There is a vast array of MEMS that are used in many industries however the majority are based on the transduction of many energy types for useful sensing or activation

applications (Judy, 2001). For the purpose of this background the focus of MEMS will be on MEM sensors. MEM actuator applications are wide ranging; however, for the purpose of the present work the intended smart structures are too large to allow MEM actuators to be effective in terms of usable force.

MEMS Thermal Sensors

The integration of a micro/nano-scale temperature sensing element into a small device with a thermally isolated supporting structure can be used to detect and then quantify temperature changes in the surrounding environment on the micro scale (Shi, et al., 2005). The thermal isolation of MEMS can be tailored by controlling thermal effusivity (Judy, 2001).

The size (typically 1-1000 μm (Spearing, 2001)) of the temperature sensing elements and the thermal isolation of this element within a MEMS allows for very accurate and fast thermal measurements due to the low thermal inertia provided by the small scale (Wood, et al., 1992).

MEMS Strain Gauge, Pressure Sensors and Inertial Sensors

The transduction of a mechanical signal into an electrical signal by the use of the change of resistance of a semiconductor material can make a highly sensitive (Kanda, 1991) small foot print strain gauge, pressure sensor or inertial sensor (Bennion, et al., 1996). The use of silicon piezoresistors is the most common form of strain signal transducer for MEMS sensor types because of the relative low cost of the material and manufacturing as well as the large sensitivity of resistive change to mechanical strain (Kanda, 1991).

MEMS based strain gauges are often now used in place of traditional strain gauges due to the added sensitivity that they provide over traditional resistive metal based gauges. MEMS pressure sensor are being used for accurate measurements in specific instances were small size is a necessity, such as for micro fluidic devices and micro biomedical devices (Chau, et al., 1988). MEMS based inertial sensors such as gyroscopes and accelerometers have become very common in consumer electronic devices such as mobile phones and video gaming technology. Due to the ‘single chip’ manufacture, low energy requirement and small payload size these inertial sensors are widely used.

The key characteristics of MEMS for their possible use in smart material structures are their relatively low weight, small size and low power consumption (Tang, 1997). However at the time of writing the cost of MEMS is still considerably higher than for many other sensor types however the relative cost will likely reduce as manufacturing techniques improve and industry uptake increases (Judy, 2001).

Piezoelectric based Sensors

Piezoelectric materials are ceramic based materials that produce an electrical response when subject to mechanical strain and produce a mechanical response when subject to an electrical current (Steinem, et al., 2007); this is known as the direct piezoelectric and converse piezoelectric effect respectively (Jaffe, 1958) (Figure 8). Due to this ability to both output and input mechanical strain piezoelectric materials can be used as sensors (Hea, et al., 2001) as well as actuators (Park, et al., 1997).

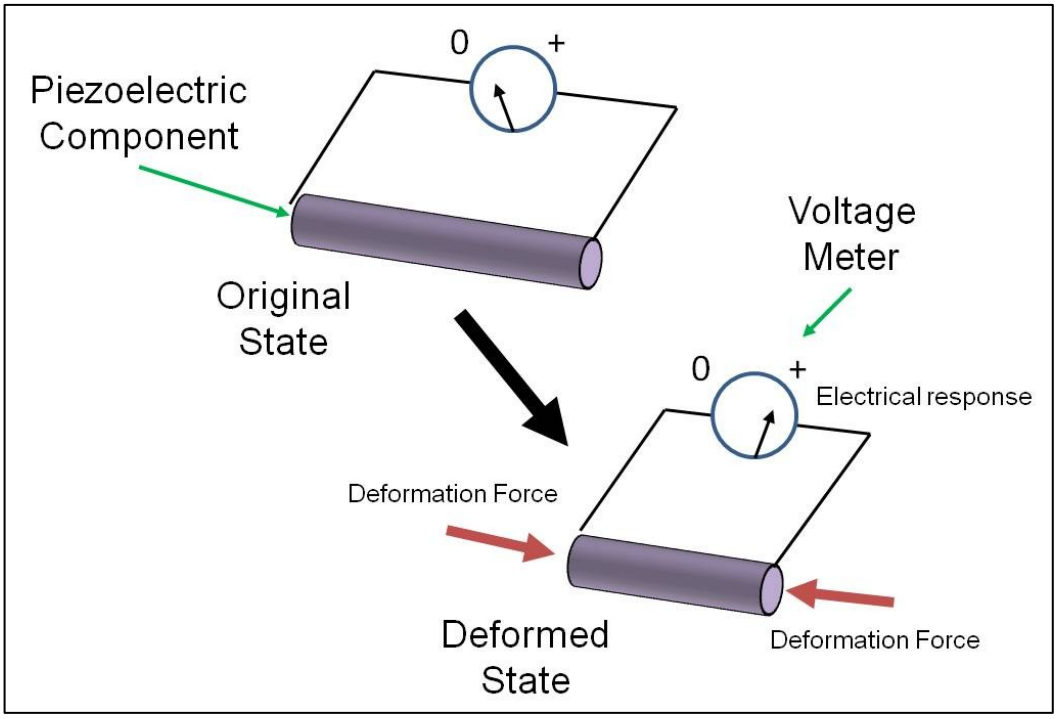

Figure 8 – Schematic demonstrating the piezoelectric effect

Piezoelectric Sensors

Piezoelectric sensors are regarded as a mature technology and their use for strain, pressure and acceleration measurement are common in many industries (Gautschi, 2002). For the acceleration sensing applications the piezoelectric is setup with a mass and the motion of this mass is monitored through the varying electrical response of the

piezoelectric element (Steinem, et al., 2007). Pressure monitoring is usually performed through the use of a membrane to exert the pressure to the piezoelectric element.

Piezoelectric materials have advantageous characteristics for sensing such as high modulus and thus minimal unwanted deflection, high signal linearity over a relatively large measurement amplitude and relative insensitivity to strong electromagnetic fields.

Piezoelectric materials are susceptible to damage from high and low temperatures and are unsuitable for measuring static loads due to a constant piezoelectric element length resulting in no measurable electrical output (Jaffe, 1958). This would mean many structural applications for piezoelectrics would be unsuitable due to stable static loads and the use of piezoelectric elements for strain measurement is therefore less popular than for pressure and acceleration measurements. As piezoelectrics are ceramic based materials their tensile strength is limited and the materials are brittle in nature. For accuracy of measurement additional stimuli to a structure, such as unaccounted for vibrations, may result in inaccurate measurements, therefore careful design must be used when using piezoelectric sensors.

Piezoelectric materials are relatively low cost but their performance will degrade over time, requiring replacement of the element (Tai, et al., 1996).

2.1.3 Typical Actuator Types

There are many forms of potential activators that are viable for the creation of smart structures; however the focus of this background review will be on the activator types that have been used most frequently for research in the field and which could potentially be incorporated into a metal matrix. These include piezoelectric elements, Shape Memory Polymers (SMP) and SMAs.

Piezoelectric Actuators

As previously stated, an applied electric current to a piezoelectric material will induce a mechanical response making them suitable as actuators (Figure 8). The actuation response of the piezoelectric is relatively small in its magnitude and very accurate in its motion thus piezoelectrics are well suited to high precision actuator situations (Okazaki,

1990). However due to the limited motion of the piezoelectric significant actuation distances, of millimetres and greater, are not possible.

Piezoelectric elements are already utilised in smart structures for the active vibration damping of machine structures. This application has been implemented commercially for high accuracy equipment (Dosch, 1992).

Shape Memory Materials

Shape memory materials are materials that have the ability to be mechanically deformed in various ways and can then be returned to their 'memory' state via the application of specific stimuli (Lendlein, 2010) (Otsuka, et al., 1998). This is referred to as the Shape Memory Effect (SME) and these materials can be metal based or polymer based; however the principal by which the SME operates for metal and polymers are different to each other.

Shape Memory Polymers

SMPs exhibit the SME (Figure 9) that allows them to be manufactured to a set shape and then subsequently, temporarily, deformed. The manufacturing process imparts a molecular network that is permanently set through the creation of cross links. The deformation process takes advantage of switching segments that maintain the shape until, typically, they are raised above the recovery temperature; at which point they revert back to their original 'as manufactured' shape (Lendlein, 2010). The returning stimulus for the polymers does not necessarily have to be temperature; however this is the most common activator stimuli type.

The applications of SMPs has so far been used for situations where expanding or forming of the polymer is utilised. However new applications are being continually researched. Much of the interest in SMPs is because of their high level of recoverable strain, low cost and low density making them particularly attractive for aerospace and automotive applications (Liu, et al., 2007). However, SMPs have a relatively slow response rate of activation (≥1 second) and are limited in ultimate thermal performance.

Shape Memory Alloys

SMA materials are metal based alloys that exhibit a natural phase change between Martensitic and Austenitic phases (Otsuka, et al., 1998) – refer to Figure 9.

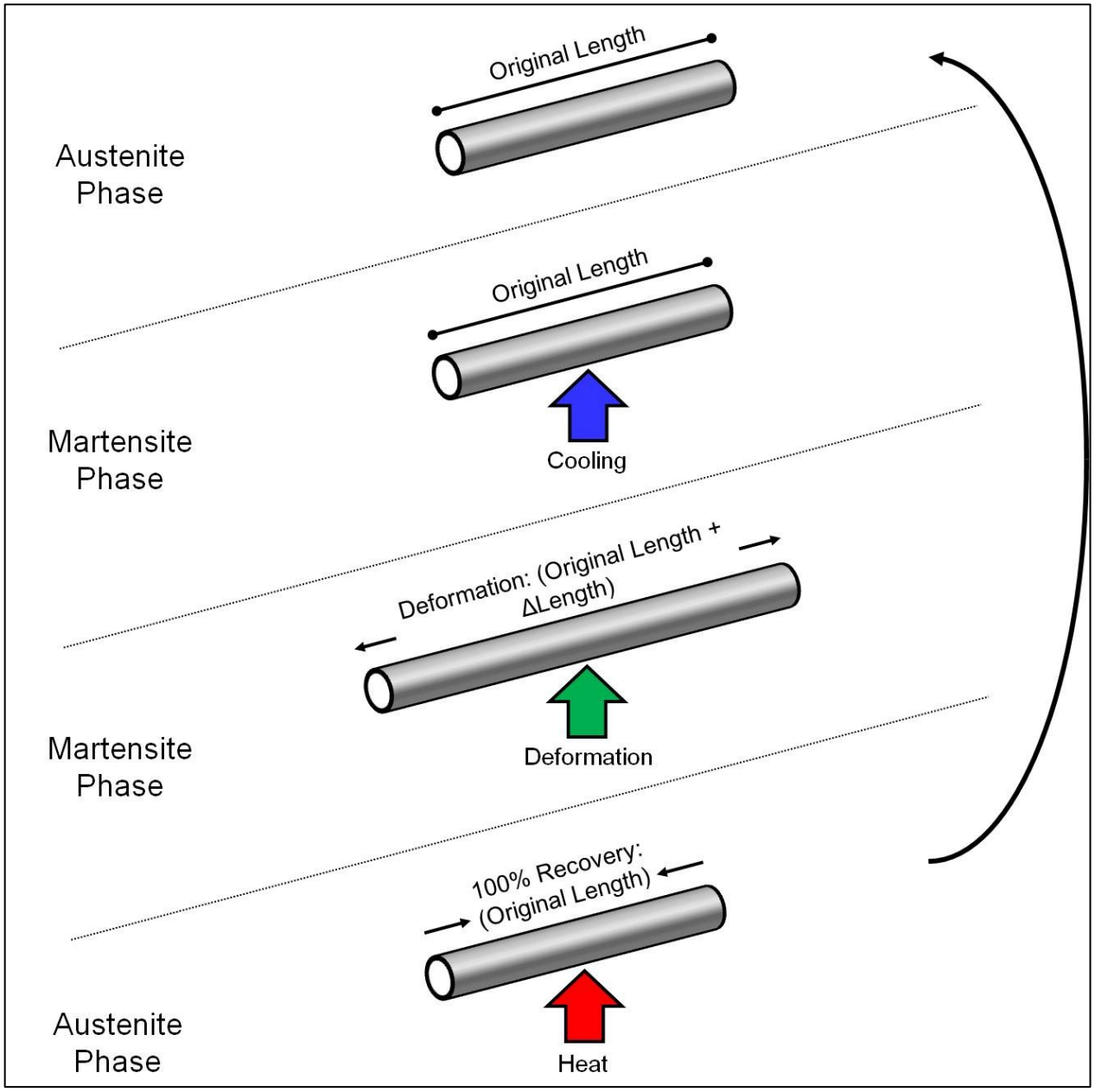

Figure 9 - Schematic of the Shape Memory Effect for a Single Phase Shape Memory Alloy

The three main alloy groups that exhibit this property are copper-aluminium-nickel, copper-zinc-aluminium-nickel and Ni-Ti. Ni-Ti alloys are the most widely used of the materials and have a range of properties that make them more robust, both mechanically and thermally, than optical fibres, piezoelectrics, and shape memory polymers.

As previously stated the mechanism by which the SME operates for SMA materials is different to that for SMP materials. The typical Martensitic to Austenitic phase for an

SMA is shown in Figure 10. M_s is the Martensitic start transformation temperature; M_f is the Martensitic finish transformation temperature; A_s Austenite start transformation temperature (typically 50-100°C); and A_f the Austenite finish temperature. The figure displays that strain deformation of the SMA material from M_s to M_f will be removed when the temperature reaches A_s at this point the strain returns to the original value at A_f. As the SMA cools it retains the strain rate from A_f as it returns to M_s. Due to the unavoidable energy dissipation within the strain/temperature system there is a level of hysteresis which is evident in Figure 10 (Ortin, et al., 2002).

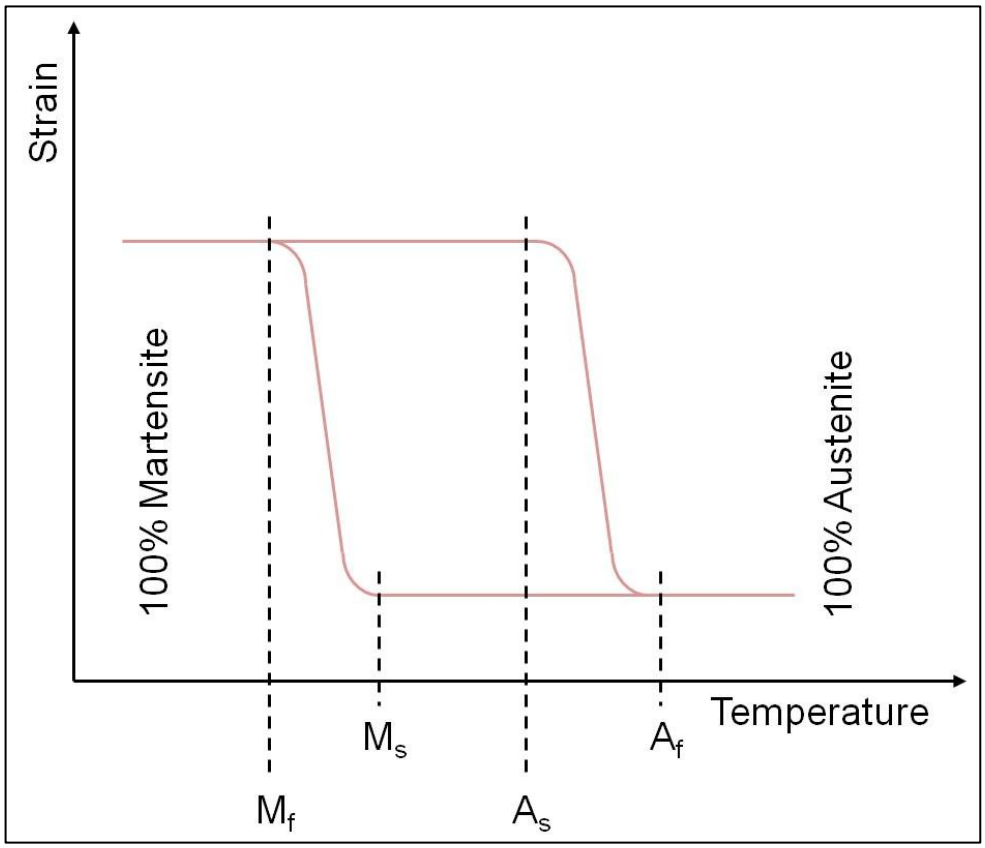

Figure 10 - Hysteresis curve for a typical shape memory alloy showing the key transformation temperatures

The use of SMAs within composite structures has been of significant research interest. By putting SMA fibres into polymer composites and then activating them the stiffness of the composite can be changed (Daghia, et al., 2008), the shape of the composite can be elastically deformed (Jung, et al., 2010) and the structure can be strengthened (Furuya, et al., 1993).

In addition to functioning as actuators NiTi SMA fibres are also capable of functioning as sensors by monitoring the electrical resistance of the SMA as it undergoes mechanical deformation (Wu, et al., 2000). This change in resistance can be related to the strain and thus a robust strain sensor can be created, free from the brittle nature of FBGs and piezoelectrics, the delicate nature of MEMS with superior actuation abilities and mechanical properties to SMPs. The SMA materials may be relatively expensive but have been concluded as the outstanding candidates for potentially embedding within a metal matrix to create a smart metal matrix composite due to them being both thermally and mechanically robust whilst being able to perform as both sensors and actuators.

2.1.4 Metal Matrix Based Smart Structures

Metal matrix based smart structures are regarded as a high value future development in the aerospace industry (Committee on Aeronautical Technologies, 1992), (Yousefi-Koma, et al., 2003) and have significant benefits over organic matrix based smart structures due to the superior performance of the metal matrix. MMCs possess several advantages to Fibre Reinforced Polymers (FRP)s such as: higher temperature capabilities, higher thermal conductivities, lower coefficients of thermal expansion, higher stiffness's and higher strengths (Rawal, 2001).

Work into creating adaptive composites using metal matrices has been focussed on creating structures which use shape change materials to change the stiffness/vibration characteristics of a structure (Schaller, 2003), (Straub, et al., 2004) shape change materials to change the stress state of a composite to improve strength (Taya, et al., 1993) and the use of shape change materials to perform structural movement (Loewy, 1997) (Hartl, et al., 2007).

Example

Boeing have designed and implemented a Variable Geometry Chevron (VGC) that is used on the exhaust of a turbofan jet engine attached to their commercial aircraft (Figure 11).

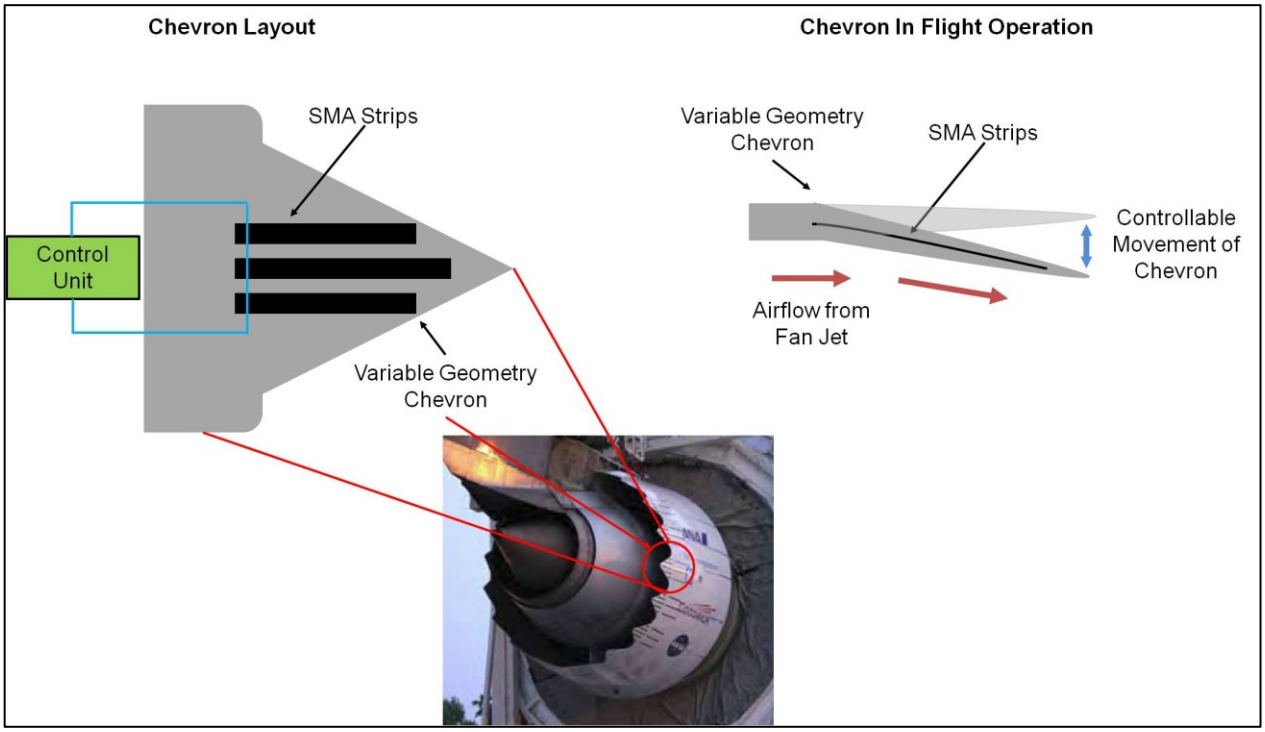

Figure 11 - Schematic of Boeings variable geometry chevron

This VGC is comprised of SMA strips within a metal matrix which acts as an actuation mechanism to change the geometry of the chevron without adding the weight, part number increase and complexity that a standard hydraulic or electric motor actuation mechanism would. The VGC is used by activating the SMA strips when the onboard sensors indicate that the aircraft is at low speed and altitude. The effect of the activation is that the chevron moves into the air flow from the jet fan engine which reduces the noise emitted by the aircraft. Using closed loop control the chevron can be maintained at the required air flow immersion throughout the entire flight of the aircraft. In addition to the noise reduction Boeing also found that the VGCs could be used to optimise the aircraft performance during the multiple flight conditions encountered during a typical flight (Calkins, et al., 2006).

The number of applications for metal matrix based smart structures is likely to grow as the technology is further understood however at present the manufacture of metal matrices that contain relatively high numbers of SMA fibres is still a challenge. To obtain significant actuation and stress levels from an SMA containing metal matrix it has been suggested that a SMA volume percentage of 25-50% is required (Armstrong, et al.,

1998). Therefore for a manufacturing method to be suitable a fibre volume fraction of this level is a likely requisite.

2.1.5 Suitable Current Manufacturing Techniques for Metal Matrix Based Smart Structures

The fabrication of polymer, low temperature metal alloy and ceramic based smart material structures is of less difficulty, due to the previously stated ability to create a fibre setup that is then infiltrated by a liquid which transforms to a solid at relatively low temperature; but is of less applicability to aerospace and automotive situations than the production of metal matrix based smart material structures. The focus of the present work is on the production of metal matrix based smart material structures and therefore the processes and research results of non-metal or low melting temperature metal based smart material structures will not be covered.

Traditional Manufacturing Techniques

Several manufacturing techniques are used to manufacture MMCs and in this section the main techniques will be discussed. The main techniques fall under three main sub-categories: deposition processes, solid-state processes and liquid processes (Evans, et al., 2003). The relative advantages and disadvantages of the traditional processes are shown in Table 1.

	Processes (Gärtner, et al., 2006) (Stoltenhoff, et al., 2002) (Papyrin, et al.,	**Solid-State Processes** (Thümmler, et al., 1993) (German, 1996) (Holzer, et al., 1999) (Atkinson, et al., 1991) (Kaczmar, et al., 2000) (Kalpakjian, et al., 2008) (Zhang, et al., 1999)				**Liquid-State Processes** (Hashim, et al., 1999) (Jiang, et al., 2003) (Srivatsan, et al., 1992) (Lira-Olivares, et al., 1997) (Torres, et al., 2009) (Clyne, et al., 1993) (Mortensen, et al., 1991)		
Process	Cold Spraying	Sintering	Hot Isostatic Pressing (HIP)	Extrusion	Diffusion Bonding	Stir Casting	Thermal Spraying	Infiltration
Advantages for MMCs	Low temperature; High density parts	Net shape; Good mechanical properties	Controllable grain structure; Dissimilar materials possible; High fibre volumes; Good mechanical properties	Fast; Well established process and equipment; Relatively low cost; Good mechanical properties	Low temperature; Suitable for various fibre types	Fast; Well established process and equipment; Relatively low cost; Good mechanical properties	Relatively low cost; Fine grain structure of matrix	Fast; Net shape; Relatively low cost; Good mechanical properties
Disadvantages for MMCs	Expensive; Powder material; High velocity powder can damage sensitive components	High temperature; Expensive; Powder material	Expensive; High pressure; High temperature; Slow	Limited geometries (constant cross-sectional profile only); Extrusion force/High pressure	Slow; Expensive; Limited geometries; Issues with oxides	Limited to particulates within metal matrix; High temperature; Post-process machining to obtain final geometry	Difficult to control spray velocity; High temperature; High porosity; High residual stresses	High temperature; Limited geometries (limited to mould shape)

Table 1 - Advantages and disadvantages of traditional metal matrix composite manufacturing techniques

There are several metal based traditional manufacturing techniques that have been covered however all these processes suffer from lack of geometric freedom and many require the expensive setup of specific tooling. As smart material structures are envisioned for future complex engineering applications the ability to manufacture superior geometry complexities directly from electronic data would have both cost and performance advantage.

Metal Additive Manufacturing Techniques

AM has been described as “An Industrial Revolution for the digital age” (Hopkinson, et al., 2006). To truly create future ready metal matrix based smart structures that can utilise the geometric complexity capable from computer based design then additive manufacturing systems are the most likely candidates for creating metal matrix based smart structures. In addition to the greater geometric freedom offered by AM there is the speed benefits of manufacturing directly from Computer Aided Design (CAD) in addition to the ability to insert elements between the layers of a manufactured sample. This may allow the creation of fully integrated metal matrix smart material structures.

The relative advantages and disadvantages of the main metal additive manufacturing techniques are given in Table 2.

	Selective Laser Sintering (SLS) (Gibson, et al., 2009) (Kruth, et al., 2005)	**Selective Laser Melting (SLM)** (Gibson, et al., 2009) (Kruth, et al., 2005) (Agarwala, et al., 1995)	**Laser Engineered Net Shaping (LENS)** (Hofmeister, et al., 2001) (Griffith, et al., 1999) (Lewis, et al., 2000)	**Electron Beam Free-Form Fabrication (EBF3)** (Taminger, et al., 2006) (Taminger, et al., 2006)
Advantages for MMCs	Low energy required to sinter binder; Net shape	Minimal post-processing; Range of materials (including super alloys)	Relatively fast; Range of materials; Mechanical properties	Relatively fast; Mechanical properties
Disadvantages for MMCs	Powder based; Post-processing to fully sinter components; Poor surface finish	Powder based; Residual stresses; High temperature; Poor surface finish	Powder based; Residual stresses; Reduced geometric complexity due to access requirements of large deposition head; Poor surface finish	Residual stresses; Reduced geometric complexity due to access requirements of large deposition head; Poor surface finish

Table 2 - Advantages and disadvantages of metal additive manufacturing techniques for metal matrix composites

A potential alternative to these traditional and additive manufacturing techniques is the UC process. This process is a hybrid process of additive manufacturing and traditional subtractive manufacturing. UC has been shown to be capable of producing MMCs which could potentially be used as smart structures (Kong, et al., 2004) (Mou, et al., 2009) and due to the early stage of the development of this process the subject of this thesis was to further the understanding of its use for the manufacture of future smart MMCs.

2.2 Ultrasonic Consolidation

2.2.1 Introduction

The UC process (Figure 12) was invented and patented by Dr. Dawn White (White, 2000) and is commercially owned and provided by Solidica Inc., USA. UC is a hybrid additive/subtractive manufacturing technology that combines Ultrasonic Welding (USW) with CNC machining by using an ultrasonic welder to join metal foils, layer by layer, and then periodic contour CNC milling to create a solid metal Three Dimensional (3D)

component (White, 2003) that replicates the original 3D CAD model. This permits the production of a diverse array of net shape components.

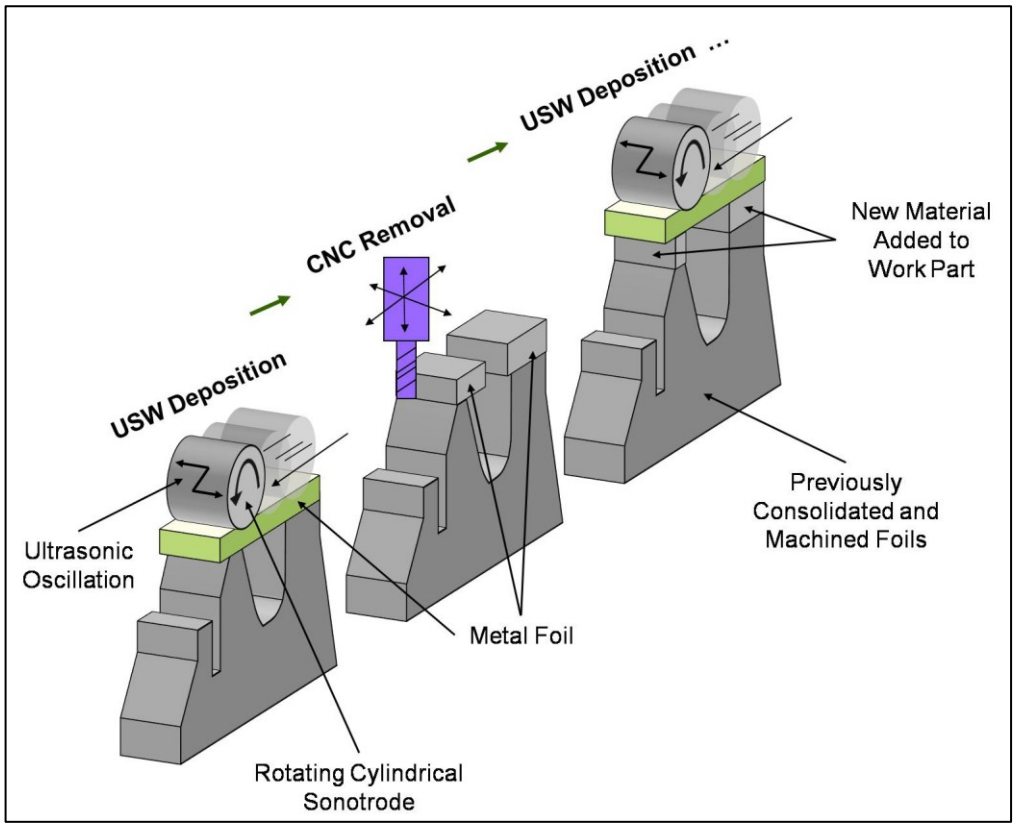

Figure 12 – Schematic diagram of the Ultrasonic Consolidation process (Schwope, et al., 2009, October 19-22)

During UC, energy generated from an ultrasonic transducer is transferred to a work piece through a roughened sonotrode in the form of ultrasonic oscillation. These oscillations, combined with a compressive normal force from the sonotrode, allow interlaminar metal flow with associated localised heating which is much lower than the melting temperature (typically <50% of the melting temperature (Jones, et al., 1956) (Joshi, 1971) (de Vries, 2004) (Daniels, 1965) (Okada, et al., 1963)), resulting in bonding at the consolidation interface.

2.2.2 Process Equipment

USW, the 'additive' component of the UC process, joins metal parts by transferring the energy of high frequency oscillations to the bond interface area between the parts to be welded. Electrical energy is transformed into high frequency mechanical vibration and

this mechanical vibration is transferred to the component material surfaces through the acoustically tuned sonotrode. The parts are oscillated together under pressure at ~20,000 cycles per second resulting in metal bonding.

***Benefits of Ultrasonic Welding*:**

- Electrical, mechanical and thermal coupling between similar and dissimilar metals
- Ability to weld dissimilar material thicknesses
- Plastic flow of metal during processing overcomes surface variability
- Solid state processing resulting in minimal heat build up issues causing material changes
- Relatively low energy costs per weld area

The main USW system components are as follows (Figure 13):

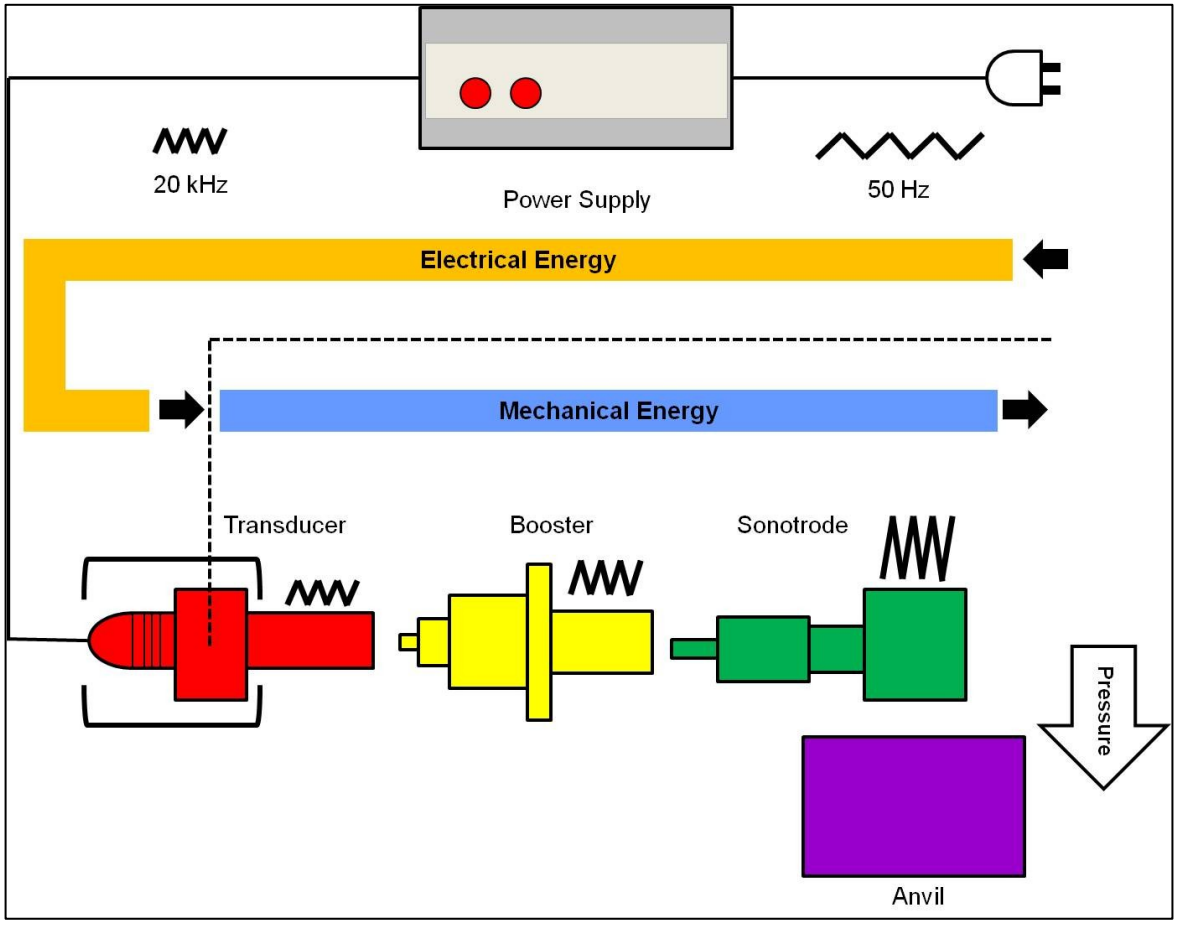

Figure 13 – Schematic of the components of an ultrasonic welding system

Power Supply

The power supply is used to convert the conventional mains electricity supply from 50/60 Hz to the high frequency supply needed to operate the ultrasonic stack at an ultrasonic frequency (typically 20 – 40 kHz). The power supply allows the amplitude of the ultrasonic oscillations of the sonotrode to be altered, which increases the energy supplied to the weld interface. The power supply also has inbuilt safety features to prevent the transducer from being damaged during the welding cycle by monitoring the feedback from the transducer so as to stop the cycle if the resistance to welding/oscillation is too high.

Transducer

The transducer, also known as the converter, is part of the ultrasonic stack and is the component of the system that converts the high frequency electrical signal into high frequency mechanical oscillations. Through a commutator the rotating cylindrical transducer is constantly connected to the electrical signal from the power supply. Within the transducer there are many ceramic piezoelectric elements that, when subjected to an alternating voltage, will cyclically expand and contract at the frequency of the voltage alternation. The energy conversion by the transducer from electrical to mechanical energy is highly efficient (typically ≥ 90%).

Booster

The booster acts as a couple between the transducer and the sonotrode and helps determine the amplitude of vibration produced at the tip of the sonotrode face. The booster is a resonant half-wave metal device that is typically made from titanium or aluminium (to help minimise mass and thus hysteresis of the system). A booster is specifically designed to resonate at the same frequency as the transducer that it is mechanically attached to. The booster is used as a rigid mounting point for the whole ultrasonic stack and acts as an amplifier to the transducer amplitude. The level of amplitude gain is specific to the booster.

Sonotrode

The sonotrode (also known as the horn) is the “tool” of the ultrasonic welder. It is the component that comes into direct contact and supplies the energy to the metal materials to be welded. A sonotrode is specifically designed for its intended application and will

typically be tuned to act as a half-wave length resonant device that will uniformly supply pressure and vibration to the metal parts to be welded. The sonotrode is mechanically fixed to the booster of the ultrasonic stack. The shape of the sonotrode determines the final amplitude that is experienced at the sonotrode face and hence the amplitude that will be used to weld two metal materials. To ensure adequate mechanical coupling and energy transmission between the sonotrode and the upper most metal material to be welded the sonotrode face is textured. Typical sonotrode materials are titanium, aluminium and steel. Titanium materials are favoured due to low loss of vibration and high strength; aluminium is often coated with chrome or nickel to reduce wear and steel is generally used for low amplitude applications were hardness is required.

Anvil

The anvil is not attached to the ultrasonic stack but is essential to the operation of the ultrasonic welding equipment. The anvil acts as the base for the metal materials to be bonded and provides the rigid platform to which the normal force, from the sonotrode, is applied. The anvil must be sufficiently strong and rigid to minimise deflection during the welding process and will typically be textured to prevent the slippage of the lower metal material. Slippage of the lower material would reduce the efficiency of the welding process and could lead to inadequate bonding being achieved.

2.2.3 The Commercial Ultrasonic Consolidation Equipment

Solidica, Inc. is currently the only manufacturer of the UC commercial equipment. The commercial UC machine is called Formation (Figure 14) and combines an ultrasonic seam welder with a titanium cylindrical sonotrode and 3-axis CNC machining centre. The process is operated through the use of proprietary software know as RPCam.

Figure 14 - The Formation ultrasonic consolidation equipment (Schwope, et al., 2009, October 19-22)

The schematic layout of the Formation process, the key machine components and the key process variables are shown in Figure 15 and Figure 16.

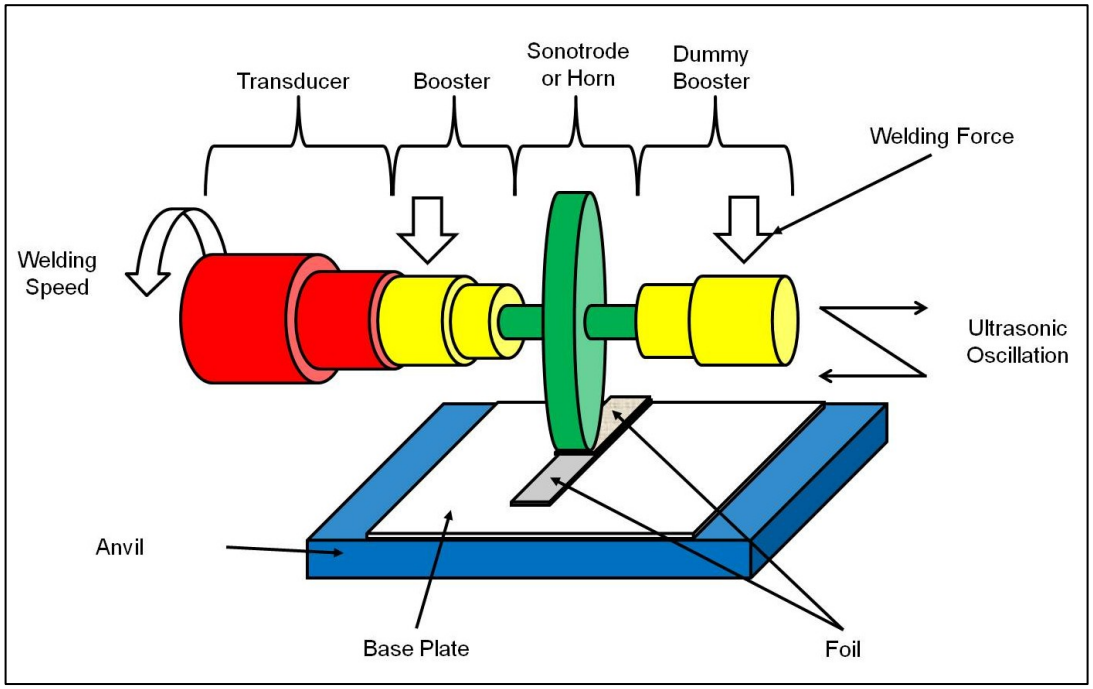

Figure 15 – Schematic of the Formation machines deposition assembly and process parameters

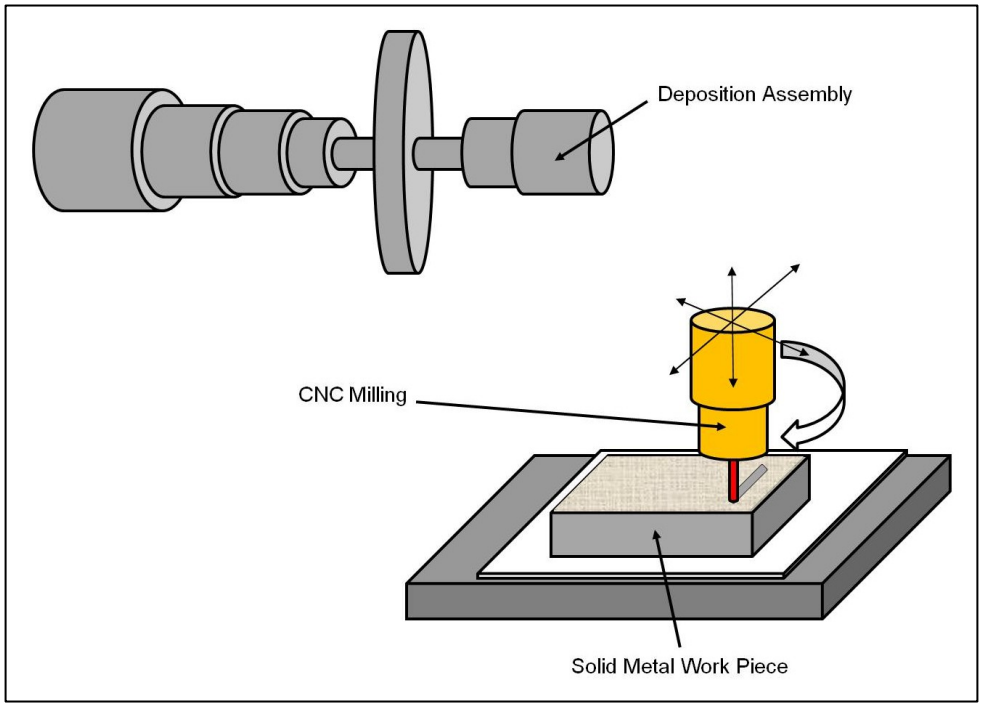

Figure 16 - Schematic of the Formation machines integrated machining centre

2.2.4 The Alpha Ultrasonic Consolidation Machine

For this research all samples were produced using the Alpha UC machine at Loughborough University that was supplied by Solidica Inc. (USA). This UC machine was a modified 3 kW ultrasonic seam welder operating at a constant 20 kHz frequency. The equipment consisted of a power supply, ultrasonic transducer, booster, and sonotrode (Figure 17 and Figure 18). The rotating sonotrode and machine carousel were electric motor driven. A pneumatic pressure system was used to supply the clamping force between the sonotrode and the work sample.

The Alpha UC machine did not have the integrated CNC equipment of the Formation machine. The benefit to the research work of using the Alpha UC machine was that smaller samples of only several foil layers could be quickly manufactured allowing for a large range of experimental factors to be quickly and accurately altered.

Power Supply

The power supply for the Alpha UC machine was a Branson BCA 900 20 kHz unit which converted the mains 50 Hz supply to the 20 KHz supply that was input to the transducer.

Transducer

The transducer for the Alpha UC system was a Branson 902JA. This is a lead-zirconate-titanate electrostrictive element containing converter and was used to convert the 20 kHz electrical supply into ultrasonic mechanical motion.

Booster

The booster for the Alpha UC system was a titanium 2:1 booster that was mounted within the UC machine stack.

Sonotrode

The model number for the sonotrode was an AmTech W1A90A27 tool steel sonotrode with a length of 234 mm and a tool diameter of 50.4 mm. The surface of the sonotrode tool contact area was Electro Discharge Machined (EDM) with the standard texture (5.89 µm average roughness (R_a)).

Anvil

The anvil for the Alpha UC system was a bespoke design manufactured from mild steel. The anvil was a two part construction; an 8 mm thick by 28 mm wide area with an EDM texture to match that of the sonotrode which was used to place and hold the work piece and a larger block of Al onto which the steel was bonded.

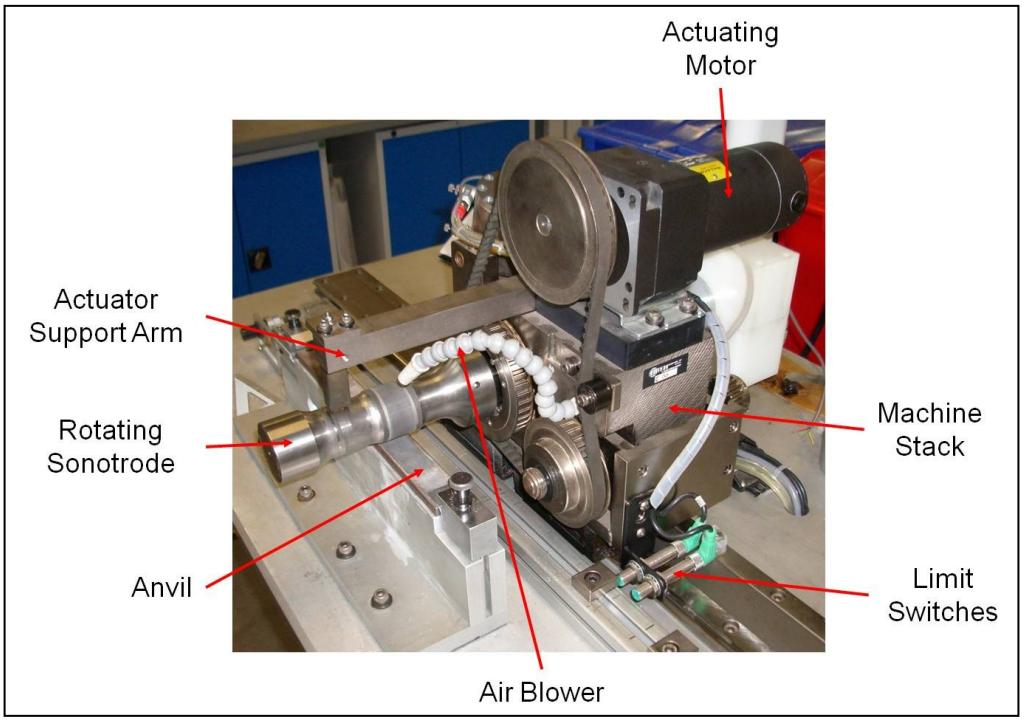

Figure 17 - The Alpha ultrasonic consolidation machine (front)

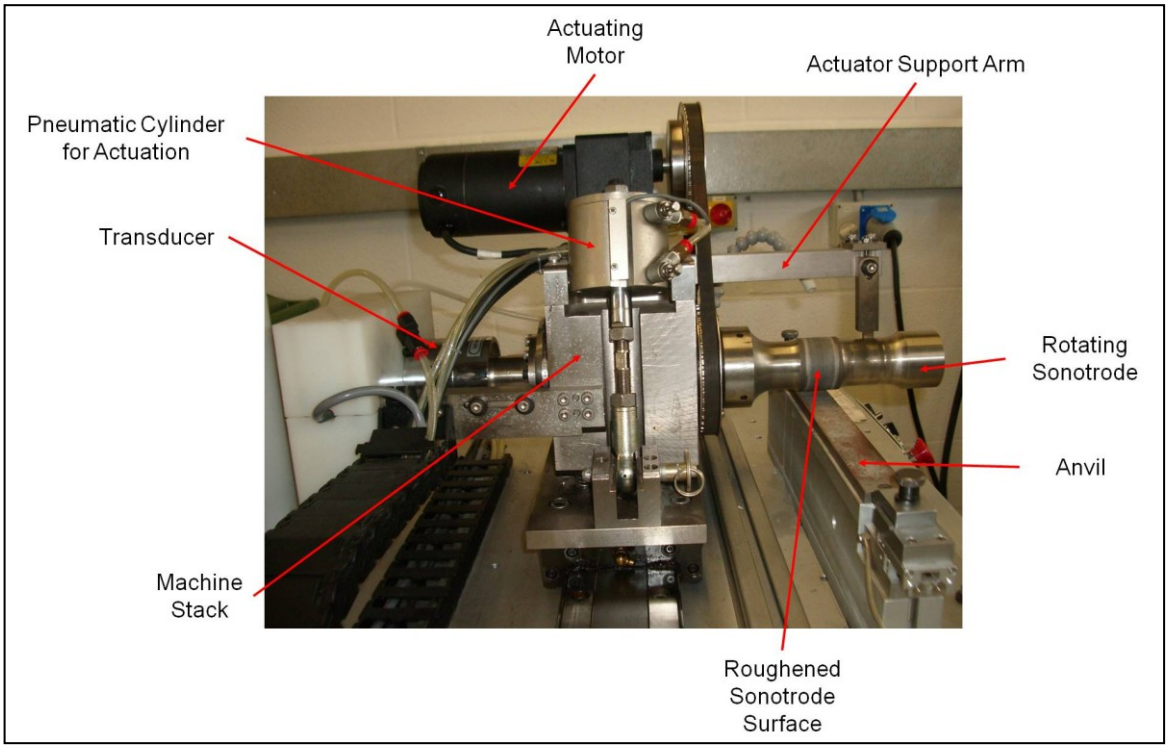

Figure 18 - The Alpha ultrasonic consolidation machine (rear)

There were three variable processing parameters on the Alpha UC machine. The parameters and their ranges were:

- The welding speed. The range of the welding speed was from static to 77 mm/s however during the work of Kong (Kong, 2005) it was found that a speed of range ≥27.8 mm/s and ≤43.5 mm/s was necessary to create robust bonding between aluminium alloy foils.
- The amplitude. This was the amplitude of the longitudinal sonotrode oscillation and is variable from 6.5 μm to 14.5 μm.
- The welding pressure. This is the pressure exerted on the weld sample that is sandwiched between the sonotrode and the anvil. The pressure is exerted by the pneumatic actuator (Figure 18) which holds the work sample against the anvil during welding. The contact pressure was variable from 0 kPa to 690 kPa (which equated to a clamping force on the work sample of between 0 and 70 MPa). Kong (Kong, 2005) found that a contact pressure of <103 kPa resulted in poor/no bond formation and >310 kPa resulted in excessive material deformation.

2.2.5 Bonding Process and Theory

UC induces plastic material flow and metal/metal bonding through the application of ultrasonic oscillation at a frequency of 20 kHz while exerting a normal force. Bonding takes place when the sonotrode comes into contact with the thin foil material and imparts its ultrasonic oscillations' to the foil material through the interaction of a roughened face on the sonotrode. The UC bonding process is the same as for USW metal welding and thus research into the bonding process of both metal USW and UC is applicable.

Previous research has shown that the key parameters in the UC process are (Langenecker, 1966):

- Welding Speed – this is the traverse speed of the sonotrode over the surface of the foils being bonded. It is known that usually the faster the welding speed the lower the density of the UC bonding, resulting in inferior mechanical properties.
- Amplitude – this is the peak to peak oscillation distance set for the sonotrode. It is known that usually a larger sonotrode oscillation results in superior UC bond quality I terms of density and mechanical properties.
- Welding Pressure – this is the pressure created at the foil/foil interface due to the normal force of the sonotrode onto the foil materials coupled with the reaction force from the machine anvil. It is known that a higher welding pressure usually results in a superior UC bond quality in terms of density and mechanical properties.

The USW process differs from other welding processes in that ultrasonic welding is a solid state mechanical process and the bonding between metal foils takes place at ≤50% of the metal foil melting temperature (Jones, et al., 1956) (Joshi, 1971) (de Vries, 2004) (Daniels, 1965) (Okada, et al., 1963). As a result of no material melt during the process there is no requirement for atmospheric control during the UC process and/or significant material preparation prior to welding. There are no fumes, powders, or excessive heat generated during the UC process thus the process is very safe. However, due to the nature of ultrasonic vibration interactions with the build material and machine

components audible high frequency sound is emitted during processing so ear protection must be worn when operating the equipment.

Bonding Theory

Research on ultrasonic metal welding processes has been ongoing since the 1960s and there is still no fully agreed upon single mechanism for the ultrasonic metal welding process due to a number of competing theories showing evidence as to their existence. There are at present four main mechanisms thought to take place during the ultrasonic metal welding process (Yang, et al., 2009): diffusion bonding, thermal fusion of the metal materials, mechanical interlocking and atomic forces across the metal/metal interface.

Diffusion bonding (Figure 19) across metal/metal interfaces is a phenomenon that takes place in manufacturing processes such as HIP (Mussman, 1999). The speed of the ultrasonic metal welding process is quicker than HIP however it is thought that the high cyclic stress rate during the ultrasonic process results in favourable conditions for element diffusion (Gunduz, et al., 2005). However, in studies of elemental mapping of post ultrasonic processed metal bond interfaces it has been shown that there is no elemental diffusion across the bond interface (Yang, et al., 2009).

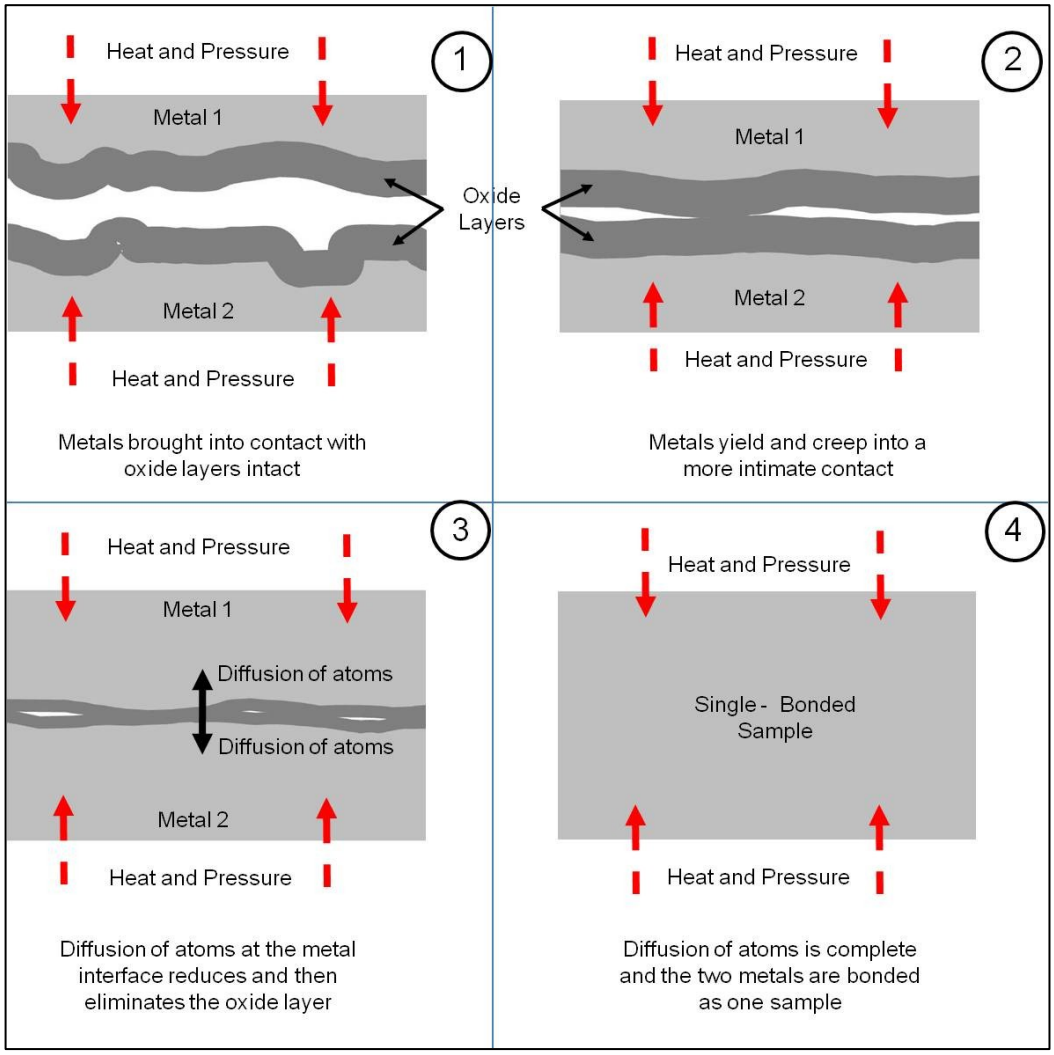

Figure 19- Schematic of the diffusion bonding process between two metals

Thermal fusion (Figure 20) of molten metal has not been observed in the majority of research results involving ultrasonic welding of metals and hence is normally described as a solid state, low temperature process (Jones, et al., 1956) (Joshi, 1971) (de Vries, 2004) (Daniels, 1965) (Okada, et al., 1963). There have been cases when researchers have concluded the presence of metal melting during specific material combinations and process parameters (Gunduz, et al., 2005). In this case the melting was thought to have significantly added to the strength of the welded samples. Measurements of the bond interface temperature during ultrasonic processing has determined a large range of interface temperature values, however there has so far been no agreement on the actual temperature level rise.

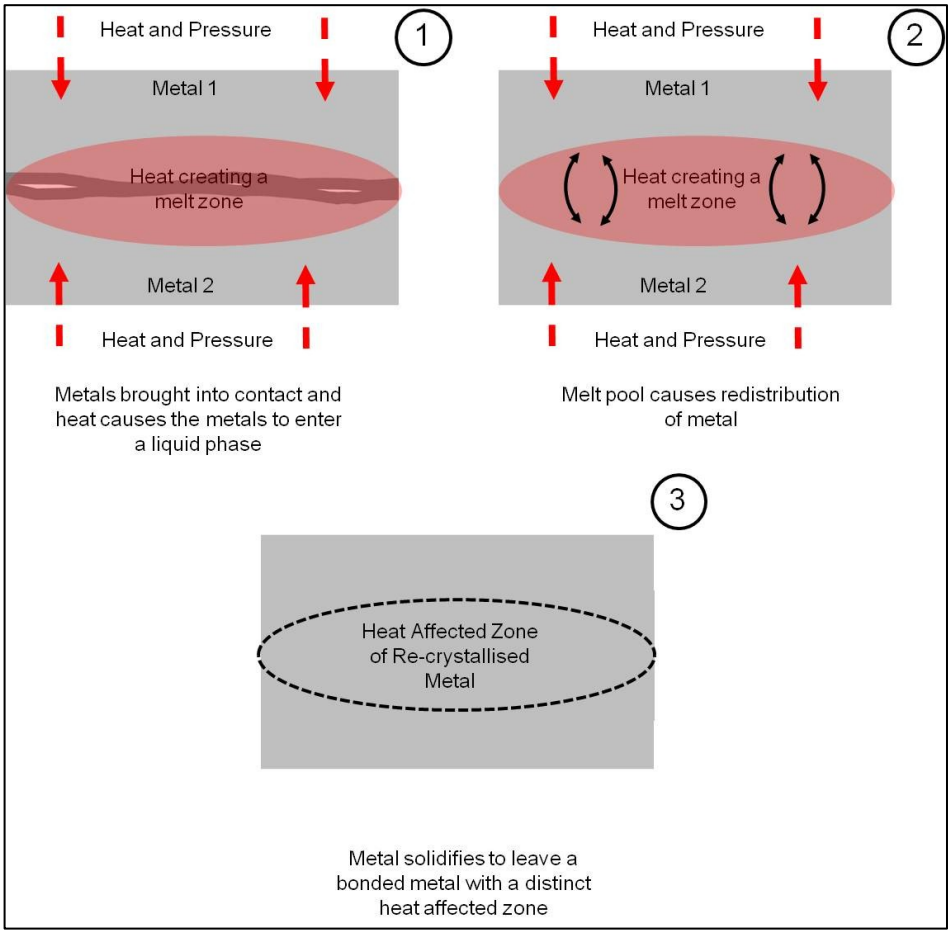

Figure 20 - Schematic of the thermal fusion bonding process between two metals

Mechanical Interlocking (Figure 21) may allow the combination of dissimilar metal materials, in terms of hardness and strength, to be ultrasonically welded together. It has been shown that when embedding significantly dissimilar materials into metal matrices via the use of ultrasonic processing that the material interaction is mechanical entrapment and not another process (Yang, et al., 2009). However, this process only appears to take place for materials with dissimilar structures and hardness's (Joshi, 1971).

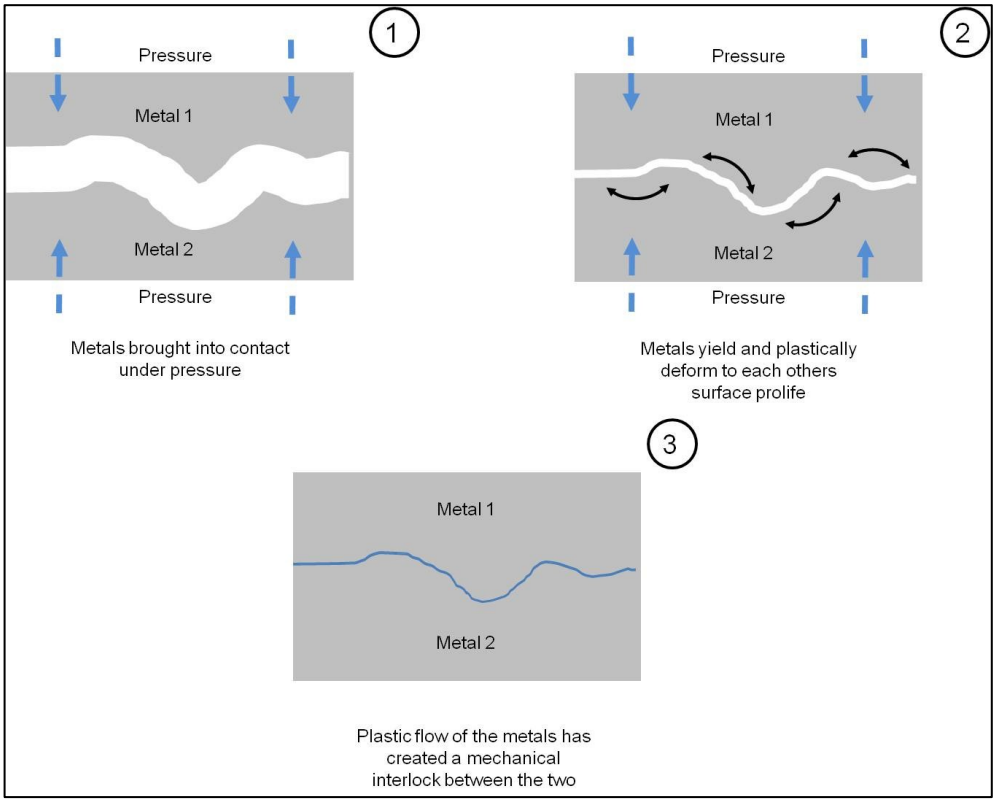

Figure 21 - Schematic of the mechanical interlocking bonding process between two metals

Atomic force (Figure 22) across the metal/metal interface is the preferred theory of many practitioners to explain the bonding process during UC (Kong, 2005) (White, 2003) (Yang, et al., 2009) (Langenecker, 1966) (O'Brien, 1991). The atomic force across the interface is thought to occur in the solid state and results in true metallurgical bonds between the metal layers. The prerequisites for atomic force across a metal interface are a clean layer with no oxide and intimate contact between the metal layers. During the ultrasonic welding process these two requisites are thought to be achieved for the majority of the bond interface due to the 'scrubbing' action of the sonotrode and the intimate contact created by the welding pressure from the sonotrode (Yang, et al., 2009).

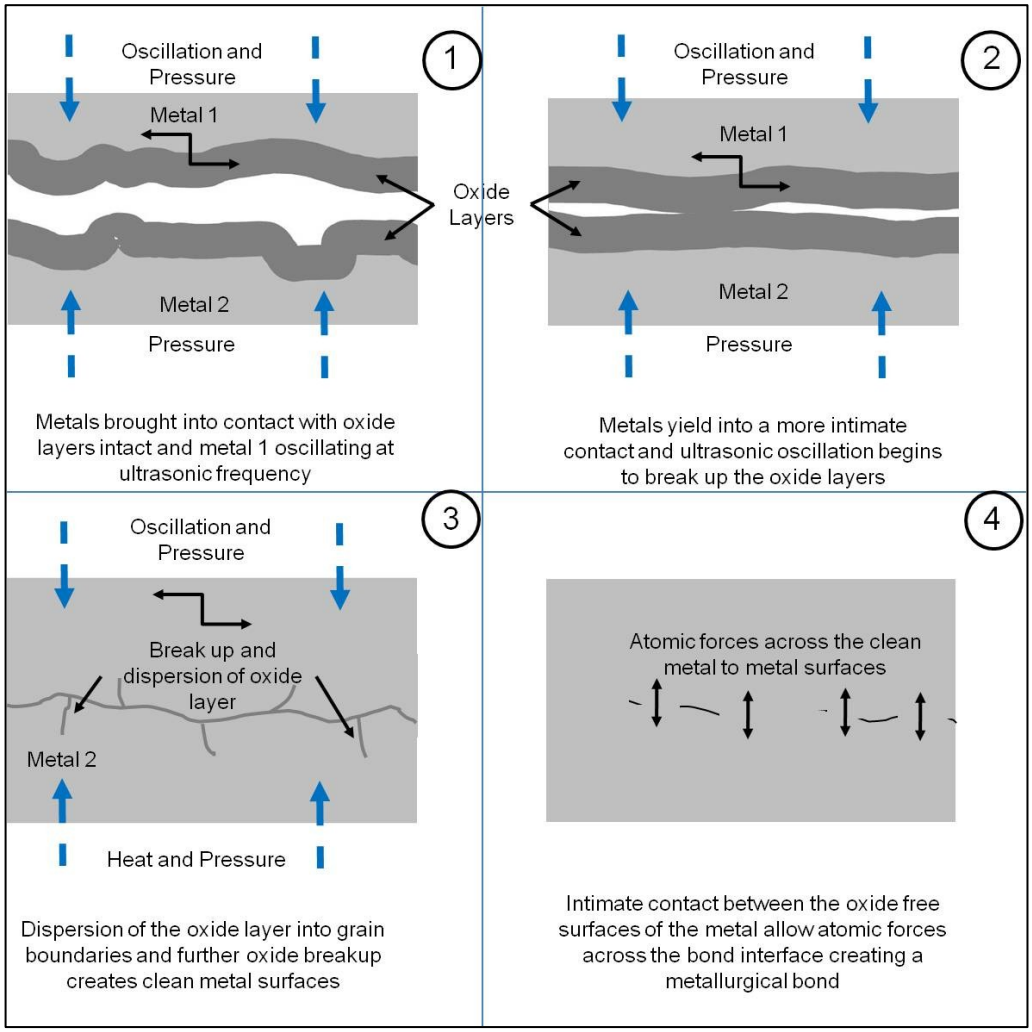

Figure 22 - Schematic of the atomic force bonding process between two metals

In addition to the four predominant theories of bonding there has been work suggesting that the Bauschinger effect or mechanical softening is taking place during UC/USW (Johnson, 2008) . The Bauschinger effect is a phenomenon within polycrystalline metals and depicts the mechanical mechanism by which the material is plastically deformed beyond the materials yield stress, in a particular direction, then fully unloaded; and then reloaded in the opposite direction. In theory the effect results in the yield stress, upon reloading, being less than the original yield stress of the material; this continual loading, unloading and then reloading continues to reduce the materials yield stress (Figure 23) (Bannantine, et al., 1990).

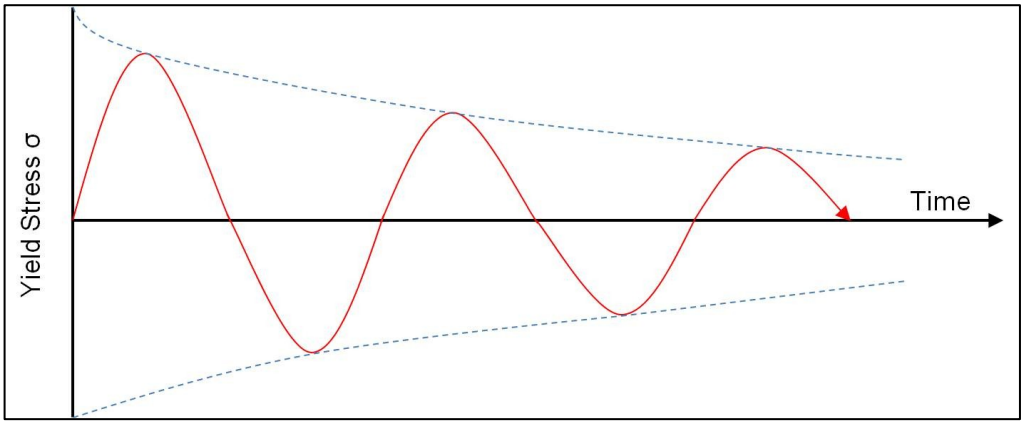

Figure 23 - The Bauschinger cyclic softening effect

The dislocations between the metals grain structure slip during the Bauschinger effect and will accumulate where the slip planes meet and 'tangle' (Orowan, 1959). When the load is removed and then reversed these dislocation slip lines effectively reduce the shear stress making the new movement less inhibited. These slip lines then become persistent slip bands along which shear stress is reduced.

Johnson (Johnson, 2008) hypothesised that the Bauschinger effect was taking place and suggested the three stages were involved in the UC/USW bonding process (Figure 24). During stage 1 he suggested that oxide layer removal began and instantaneous fretting of the asperity peaks occurred. At stage 2 the area of metal to metal contact quickly increases and continual fretting of the surfaces results in frictional heat generation which results in localised plastic deformation. The final stage is when the Bauschinger effect is suggested to occur and results in plastic deformation and a "deformation affected zone".

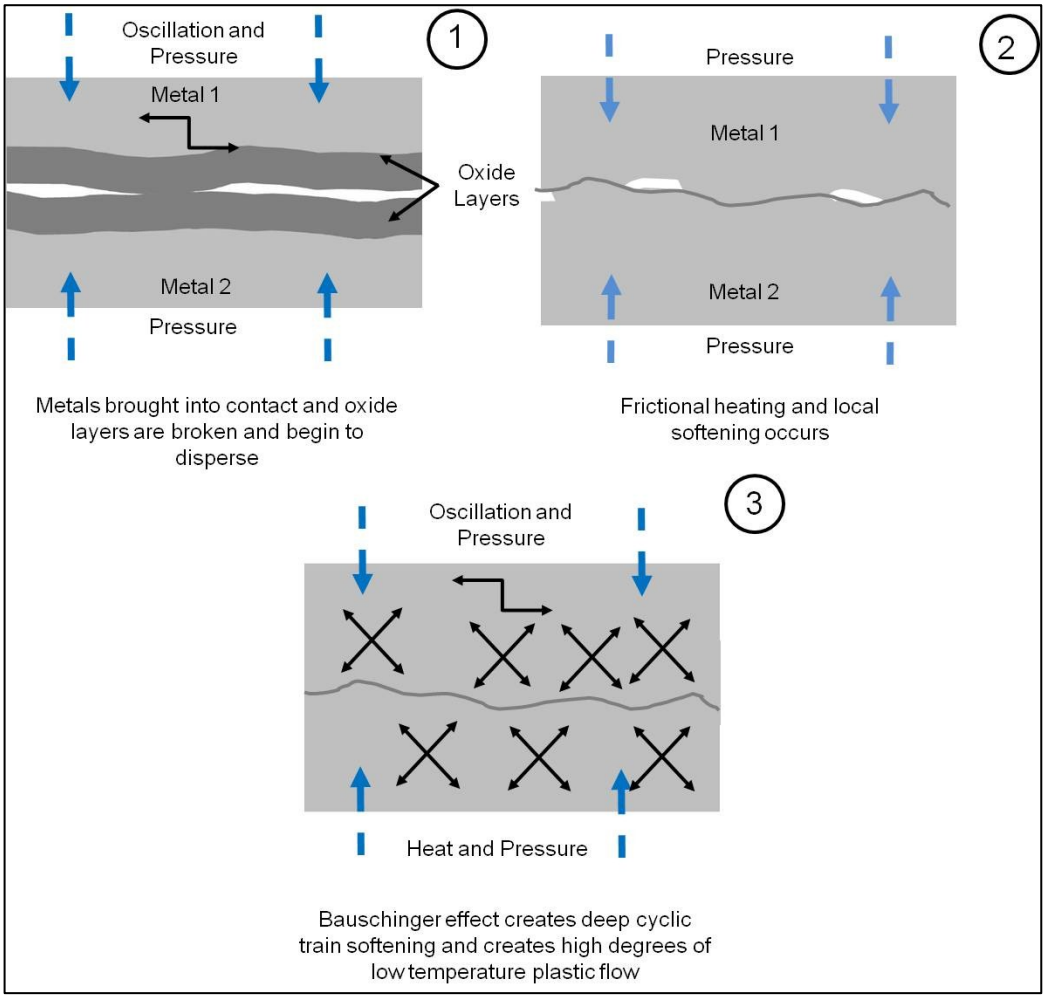

Figure 24 - Schematic of the Bauschinger effect/cyclic softening bonding process between two metals

The bonding process that occurs during UC/USW is still not clear and there is evidence for each of the different theories. However the theory that has accrued the greatest level of experimental evidence and that which is most accepted among USW practitioners is the theory of atomic force across the metal/metal interfaces that are as a result of the oxide dispersal caused by the high frequency oscillatory motion under pressure.

2.2.6 Weld Strength Model

To quantify the intensity of bonding, a measurement technique has been created by Kong, Soar and Dickens (Kong, et al., 2005) which was used to calculate the area of direct contact points after ultrasonic consolidation (Janaki Ram, et al., 2006) (Janaki Ram, et al., 2006). To enable comparisons of bond density the term 'Linear Weld

Density' (LWD) was used to represent the percentage of bonded length, $L_{b,}$ as a proportion of the total bond interface length, $L_{c,}$ for a given ultrasonically consolidated sample, and was expressed as:

$$LWD\ (\%)\ =\ \left[\frac{Lb}{Lc}\right] \times 100$$

Equation 3 – The linear weld density equation

This method involves the manual determination of voids within a bond interface studied at a microscopic scale. This makes user error a possible issue with the measurement of LWD however the technique has been proven to correlate the strength of a UC sample with the measured LWD; generally the greater the LWD the greater the samples strength.

2.2.7 Dissimilar Metal Bonding

There are many metal combinations possible with ultrasonic metal welding, however not all have been processed via UC. Figure 25 depicts the known metal combinations available through ultrasonic metal welding and UC.

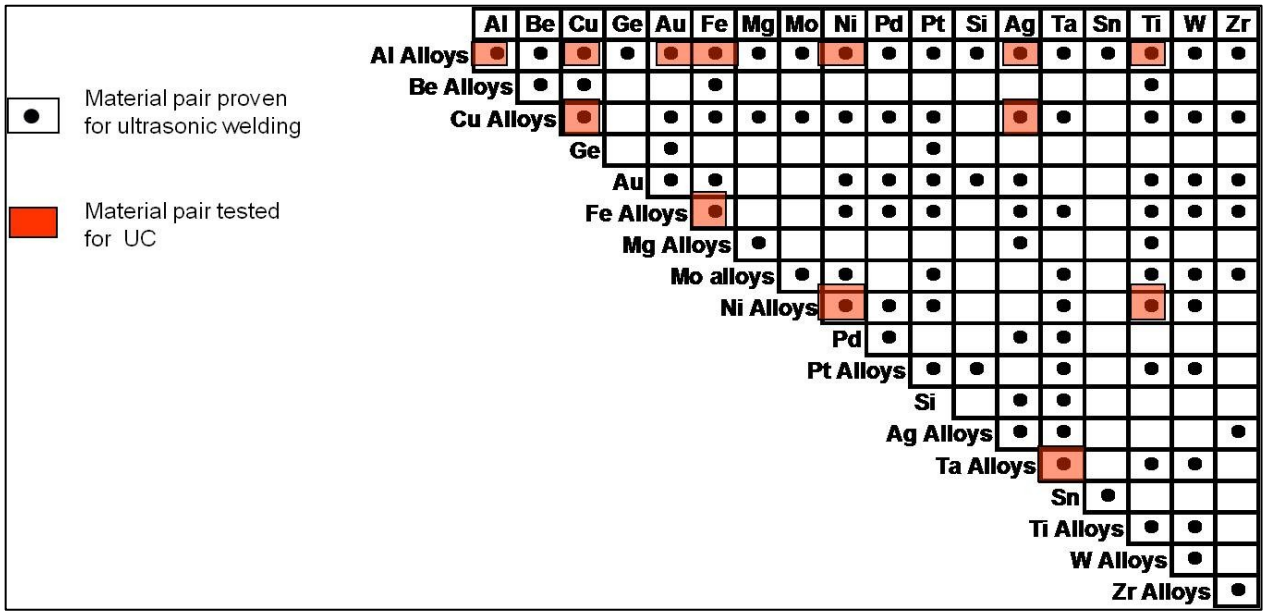

Figure 25 – A chart depicting which materials are ultrasonically weldable and which have directly been used with the ultrasonic consolidation process (Johnson, 2009) (O'Brien, 1991)

2.2.8 Component Embedding

There are several benefits of USW/UC, however a key attribute of the USW/UC process is that a significant level of low temperature and high plastic flow can occur within the material being processed; referred to as ‘acoustic softening’ or ‘volume effect’ in previous research (Kong, 2005) (Langenecker, 1966). This attribute can, and has, been exploited to allow the embedding of active (Kong, 2005) (Kong, et al., 2004), passive (Yang, 2007) and optical fibres (Kong, et al., 2005), as well as various other components (Kong, 2005) (Mou, et al., 2009), within an Al matrix (refer to Figure 27 steps a, b, and c for the embedding process and Figure 28 for an example of an embedded object).

The ‘volume effect’ takes place when the ultrasonic energy being inputted into the metal material increases the mobility of the dislocations between metal grains (Dawson, et al., 1970), (Langenecker, 1966), (Hansson, et al., 1978). In plastic deformation obstacles to dislocation movements, such as grain boundaries, result in the material obtaining a higher strength and stiffness from a higher yield stress – work hardening. To overcome this effect and reduce the yield stress energy input such as heat is required. During UC/USW this energy is provided in the form of ultrasonic energy and allows the reduction of yield stress with little temperature increase. Experiments by Langenecker (Langenecker, 1966) showed this phenomenon by obtaining stress-strain curves for static tensile tests in which samples were subject to ultrasonic excitation at 20 kHz (Figure 26). The graph on the right demonstrates the thermal requirements to obtain the same effect from the ultrasonic excitation. The result of this phenomenon is that plastic flow, due to reduced yield stress, during UC/USW is sufficient to encapsulate objects that would otherwise require temperatures of over 50% of the metal matrix melt temperature.

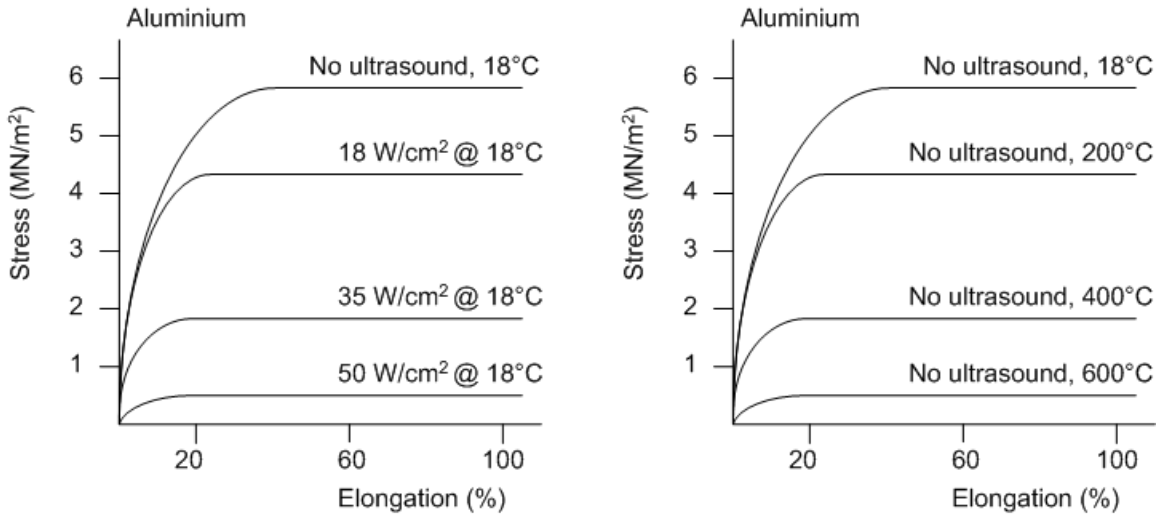

Figure 26 - Comparison of the equivalent energy requirements for ultrasonic vs. thermal energy (Langenecker, 1966)

Metal foil material is bonded to a base plate by the sonotrode. Onto this deposited foil fibres and/or other objects can be placed and secured. A second metal foil is then placed on top of the objects and the sonotrode then applies pressure and ultrasonic oscillations to the sample (step a). The yield strength of the metal foil is reduced due to acoustic softening (Langenecker, 1966) which, due to the pressure from the sonotrode, causes the foil to plastically deform around the objects between the foil layers (step b). The metal foil then creates an intimate contact with the previously deposited foil and a solid state bond is created (step c).

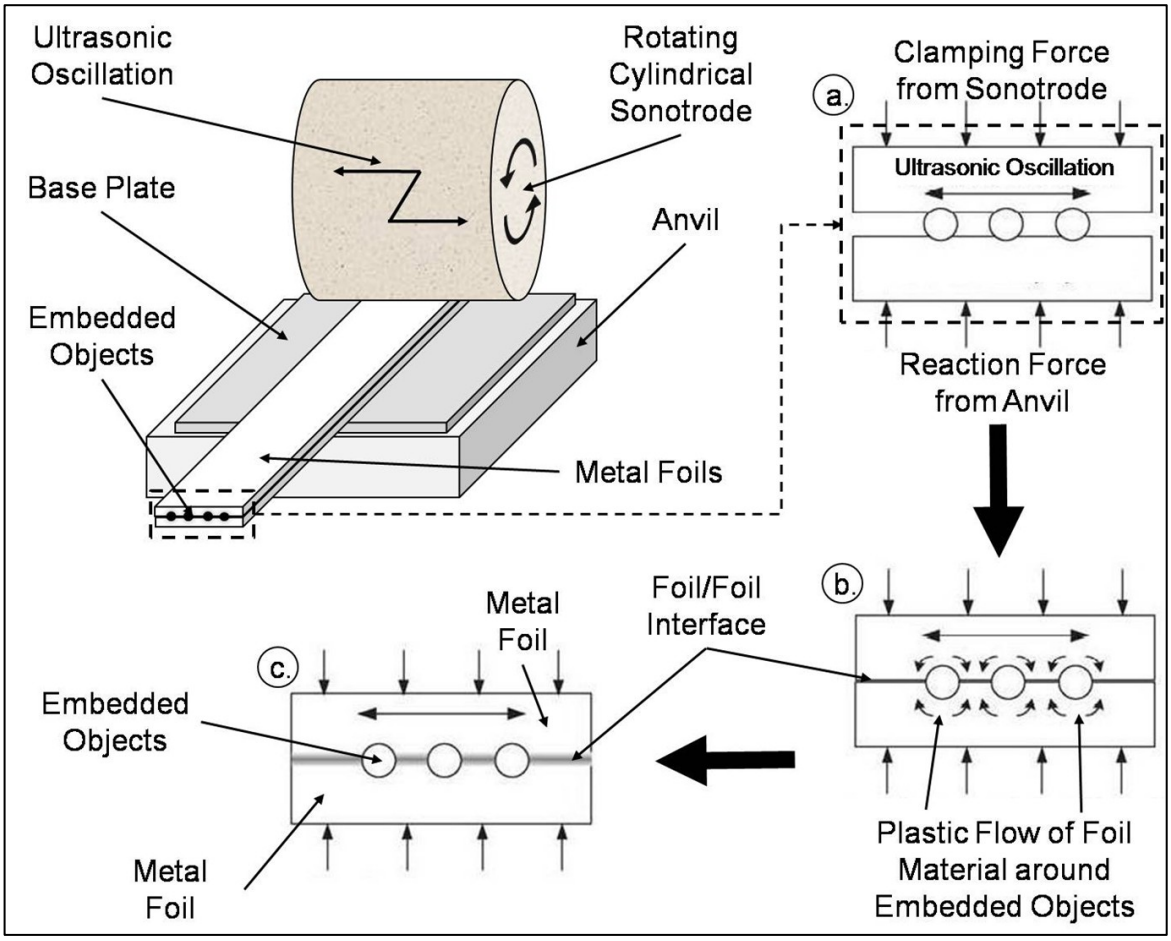

Figure 27 - Schematic diagram of the ultrasonic consolidation process for object embedment (Friel, et al., 2010)

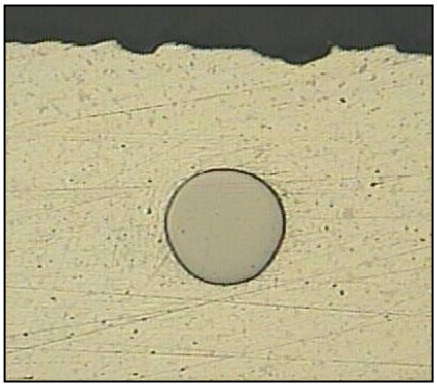

Figure 28 - Example of an embedded shape memory alloy fibre via ultrasonic consolidation

2.2.9 Suitability of Ultrasonic Consolidation for Smart Structures

The abilities of UC to be able to embed objects in solid metal matrices, bond dissimilar metals, take advantage of the geometric freedom provided by an AM process and as a solid state process with non-powder based materials makes UC very attractive and suitable for creating metal matrix based smart structures.

UC is solid state, uses relatively low cost foil materials, no atmospheric control, no/minimal pre-heat so relatively energy efficient and is able to exploit the volume effect.

Kong showed that it was possible to embed both SMA fibres (activators) and optical fibres (potential sensors) in metal matrices (Kong, 2005). Kong showed that the UC process is capable of embedding SMA fibres and still allowing them to retain their functionality. It was also shown that delicate single mode optical fibres could be embedded whilst still retaining their functionality. Mou, et al., 2009 was able to demonstrate that these single mode fibres could then be used as FBGs by laser etching. These FBG containing UC samples were then tested and the samples were able to function as structures with embedded strain sensors.

Hahnlen, et al., 2010 was able to further demonstrate that SMA fibres could be successfully embedded into metal matrices via UC and that these fibres retained their functionality. In addition this work demonstrated that via the continual measurement of the electrical resistance of the SMA fibres they could be used to detect increase in strain and temperature to the UC structure. This effectively was a UC structure that contained both activators and sensors in unison. This therefore was a clear demonstration of the potential of UC to create smart structures.

UC shows the potential to be very effective at creating complex geometry metal matrix composite based smart structures, however the technology is still young and the aim of this research is to help mature the process by understanding the interaction of the metal foil matrix with embedded fibres and vice versa.

2.3 Summary of Background

The background has shown that there are currently several different sensing and actuating components available for the creation of future smart structures. Of the discussed components SMA materials appear to have the best combination of mechanical properties, cost, and functionality to make them the most suitable candidate for creating smart metal matrix structures. As SMAs can function as both actuators and sensors there is a possibility of only requiring SMA fibres within a metal matrix to create a smart structure.

The current processes for manufacturing metal matrix composites generally operate at an elevated temperature which can have an adverse effect on sensitive components and thus prevent them from being included or remaining functional within a metal matrix based smart structure. The most widely used MMC manufacturing techniques are based on traditional methods and thus are limited in geometric freedom and often require significant levels of post processing. To pursue the maximum potential of smart MMCs one should consider manufacturing methods based on additive techniques which have significant advantages over traditional processes. Of the AM related metal technologies, UC is the only non-powder based process that does not require a large amount of post processing and operates at low temperature and in the solid state.

These factors make UC very attractive and suitable for creating metal matrix based smart structures and SMA fibres are an excellent candidate for sensor and actuators within a smart MMC.

To assess the suitability and issues surrounding the manufacture and use of SMA containing MMCs made via UC, a process experimental study was formulated.

Previous research has been carried out into the embedding of SMA fibres into Al matrices (Kong, 2005) (Kong, et al., 2004). However, there had only been a relatively low SMA fibre volume fraction embedded into an Al matrix using UC (15 fibres; approximately 5 % by volume (Kong, et al., 2004)). Increasing this fibre volume fraction would potentially allow SMA UC structures to achieve greater activation force densities due to the greater fibre volume fraction being activated. SMA fibre volume fractions of

approximately 50% have been achieved via conventional manufacturing methods (HIP) for creating Al/SMA composites (Armstrong, et al., 1998). A volume fraction of ≥25% has stated as being required to significantly affect the stress performance of a smart MMC.

UC has already been demonstrated to be capable of producing MMC based smart structures (Hahnlen, et al., 2010). This capability was achieved thought the use of SMA fibres.

3 Research Hypothesis

Several researchers have researched the use of UC to embed fibres into aluminium matrices (Kong, et al., 2004) (Li, et al., 2008) (Yang, 2007) (Hahnlen, et al., 2010). This previous research has shown the ability of UC to perform as a metal matrix composite manufacturing method with possible future capabilities for creating smart structures.

Kong (Kong, et al., 2005) demonstrated that a fibre volume fraction of (5%) SMAs was capable with a UC manufactured, aluminium matrix based, metal composites. This volume fraction is less than that achieved via other manufacturing methods (HIP - (Armstrong, et al., 1998)); and is insufficient for the intention of creating an adaptive composite for use within a smart structure system ((Furuya, et al., 1993) (Armstrong, et al., 1998) (Hamada, et al., 1998)).

This research aims to further the UC process towards creating higher SMA fibre volume fraction containing metal matrix composites that may be used within future smart structures.

It was hypothesised that the fibre volume fraction within a UC matrix was limited due to a reduction in foil/foil bonding, caused by increased fibre numbers, as opposed to the total level of plastic flow of the matrix material being insufficient to accommodate the increased fibre numbers. This was to be tested by increasing the fibre volume fraction beyond that of Kong's work (Kong, 2005) *and then determining by microstructural analysis of the matrix, the fibre/matrix interface and the UC sample integrity whether or not the maximum plastic flow of the matrix was reached.*

4 Experimentation into Embedding Increasing Fibre Volumes using Ultrasonic Consolidation

4.1 Introduction

This chapter details the experimentation that was carried out to identify the effect that SMA fibre number increase was having on the final UC sample. This work was to test the hypothesis and identify key factors that may have been influential in the embedding of SMA fibres into aluminium matrices.

4.2 Methodology

The UC machine used was the same as for previous research at Loughborough University (Kong, 2005) (Kong, et al., 2005) (Mou, et al., 2009) (Kong, et al., 2004) (Li, 2009) (Kong, et al., 2005) (Kong, et al., 2005) (Kong, et al., 2003) (Kong, et al., 2004) (Mariani, et al., 2010) - the Alpha UC machine. This machine was previously detailed in section 2.2.3.

To determine how the fibre volume fraction affected the UC bond interface and to identify the key issues in increasing the number of fibres, tests were conducted with varying numbers of 100 µm Flexinol SMA fibres embedded into Al 3003 (T0) ultrasonically consolidated matrices. The fibre numbers, and their relative volume fractions, that were embedded into the Al 3003 (T0) foils were: 0 (0% - reference control sample), 10 (~3.2%), 15 (~4.9%), 20 (~6.5%), 25 (~8.2%), 30 (~9.8%), 35 (~11.5%) and 40 (~13.1%).

To permit maximum matrix plastic flow to enable the high number of fibres relatively high UC process settings were used: 12.28 µm amplitude, 276 kPa welding pressure, and 34.5 mm/s welding speed. These Alpha UC machine process parameters had previously

been identified as suitable for embedding multiple SMA fibres into Al matrices by Kong (Kong, 2005) (Kong, et al., 2004) (Kong, et al., 2005).

4.2.1 Materials

For the sample production during this initial and subsequent research the foil material used was Al 3003 alloy in the annealed state (T0). This foil material was 25 mm wide, 100 μm thick and was supplied by United Aluminum Corporation, USA. Al 3003 is a widely available Manganese (Mn) based alloy that is used extensively in chemical processing, domestic appliances, and heat exchangers as well as for general sheet metal work.

The practical reasons for using this material were: it had been previously shown to be successful as both a bulk and fibre embedding UC matrix material suitable for peel testing and microstructural analysis (Kong, et al., 2004); Al 3003 (T0) requires minimal surface preparation prior to the UC processing; it would be able to be compared directly to previous work and the work of others using the same material (Kong, 2005) (Kong, et al., 2005) (Kong, et al., 2004) (White, 2003) (Kong, et al., 2005) (Johnson, 2008) (Kong, et al., 2005) (Kong, et al., 2003) (Kong, et al., 2004); and it was readily available in the prescribed thickness and width as a continuous foil material.

Al 3003 (T0) has the advantage of being in the annealed state therefore any microstructural changes that would have been present in the strain hardened versions (e.g. Al 3003 H18) were removed and thus any microstructural observations could be attributed to the UC or fibre embedding process.

The properties of Al 3003 (T0) are given in Table 3.

Material Property	Value
Density (g/cm³)	2.73
Hardness (Brinell)	28
UTS (MPa)	110
Tensile Yield Strength (MPa)	41.4
Elongation at Break (%)	30
Modulus of Elasticity (GPa)	68.9
Poisson's Ratio	0.33
Shear Modulus (GPa)	25
Shear Strength (MPa)	75.8
Electrical Resistivity (ohm-cm)	0.00000349
Melting Temperature (°C)	643-654
Elemental Composition (%)	Al (96.7 - 99), Mn (1 - 1.5), Cu (0.05 - 0.2), Fe (max 0.7), Si (max 0.6), Zn (max 0.1), Other (max 0.15)

Table 3 – Mechanical, thermal, electrical and compositional properties of aluminium 3003 (T0) alloy

The material used as the SMA fibre was Flexinol™ NiTi wire. Flexinol™ (Dynalloy, Inc. USA) is a 'single mode' NiTi alloy. This was the material used for previous work at Loughborough University (Kong, 2005) (Kong, et al., 2004). The Flexinol™ wire was readily available both in terms of quantity and cost (approx. £6 per metre) for the research work and was available in a variety of diameters; (50, 100, 150, 250 and 375 μm).

Kong (Kong, 2005) (Kong, et al., 2004) had previously shown that SMA fibres were still functional after UC embedding and that they were sufficiently strong and ductile to perform fibre pullout testing which was deemed an intrinsic testing methodology in characterising the fibre matrix interface during UC.

The mechanical, thermal and physical properties of Flexinol™ SMA fibre are listed in Table 4.

Material Property	Value	
	Austenitic	Martensitic
Density (g/cm³)	6.45	
UTS (MPa)	754 - 960	
Tensile Yield Strength (MPa)	100	560
Elongation at Break (%)	15.5	
Modulus of Elasticity (GPa)	28	75
Poisson's Ratio	0.3	
Shear Modulus (GPa)	10.8	28.8
Electrical Resistivity (Ω-cm)	0.000076	0.000082
Melting Temperature (°C)	1240 - 1310	
Elemental Composition (%)	Ni (55), Ti (45)	

Table 4 – Mechanical, thermal, electrical and compositional properties of Flexinol™ NiTi shape memory alloy

4.2.2 Sample Fabrication

The fabrication of the Al/SMA samples (as illustrated in Figure 27) comprised of: firstly ultrasonically consolidating three 100 µm thick layers of Al 3003 (T0), consecutively onto an Al 1050 supporting base plate (150 mm long × 1.2 mm thick × 28 mm wide) (Figure 29 - Step 1). The required number of SMA fibres were then cut to length (~200 mm in length each) and placed equidistant from each other on top of the deposited foil layer, straightened, pre-strained and secured into place (Figure 29 - Step 2). A fourth Al 3003 (T0) foil layer was then placed on top of the SMA fibres and the previously ultrasonically consolidated Al foils and then ultrasonically consolidated to form the Al/SMA fibre matrix composite (Figure 29 - Step 3).

All SMAs were pre-strained prior to being embedded as Kong (Kong, 2005) had identified that UC process parameters from the higher end of the identified processing window could possibly be inducing the shape memory effect (SME). To ensure this did

not occur in the present work the SMA fibres were extended from 200 mm to 210 mm, (5% extension, the recommended value by the manufacturer), using a Lloyd Instruments LRX material testing machine (Figure 31) prior to being embedded into the Al 3003 (T0) foil matrix.

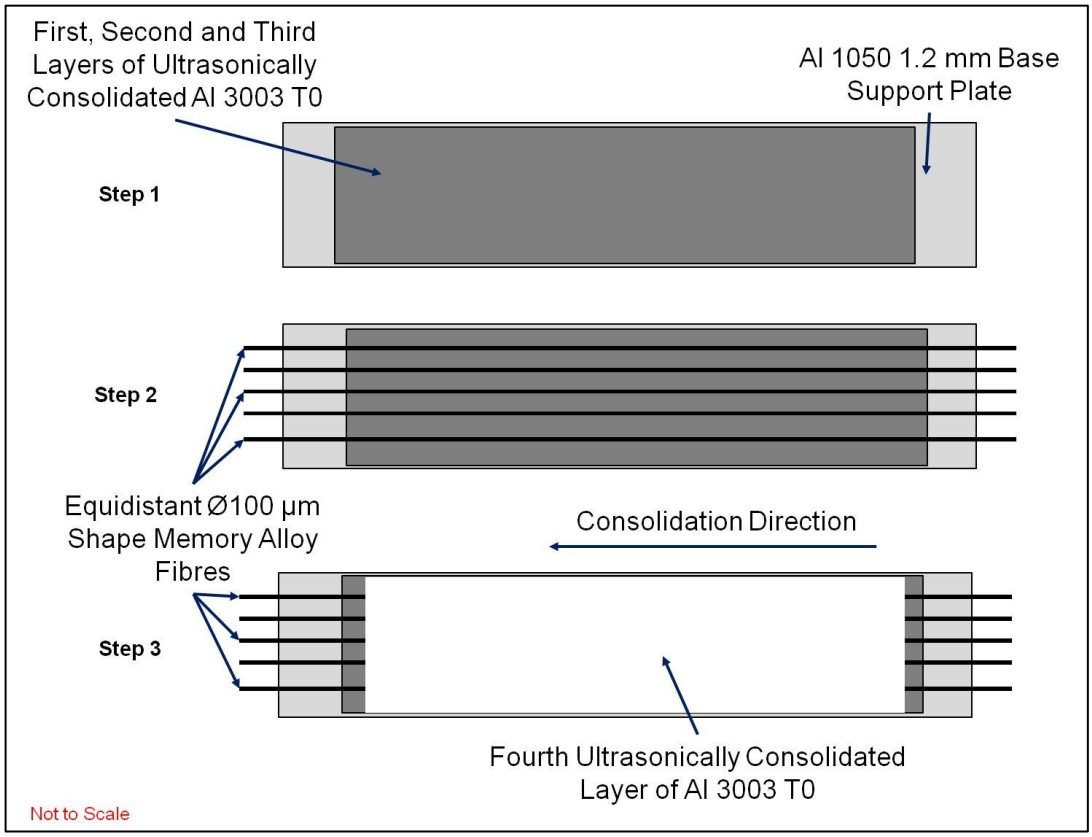

Figure 29 - Schematic of the shape memory alloy/aluminium matrix composite sample preparation procedure

4.2.3 Optical Microscopic Analysis

For qualitative analysis of the fibre embedment the manufactured samples were sectioned perpendicular to the longitudinal direction of the fibre using a cutting disc (Figure 30). The sectioned SMA–Al MMC was then mounted in Buehler Varidur thermosetting polymer and ground on 240, 400, 600 and 1200 grit SiC paper for 2 minutes each. The samples were then polished using 6 µm and 1 µm diamond paste for 4 minutes each. Final polishing of the samples was performed for 5 minutes using 0.1 µm colloidal silica. To prevent cross-contamination and surface degradation to the prepared Al surface the samples were thoroughly rinsed with soapy deionised water and

blow dried between each grind and polish stage. The finished samples were then stored in a sealed, clean, desiccated container to avoid contamination post polishing and drying.

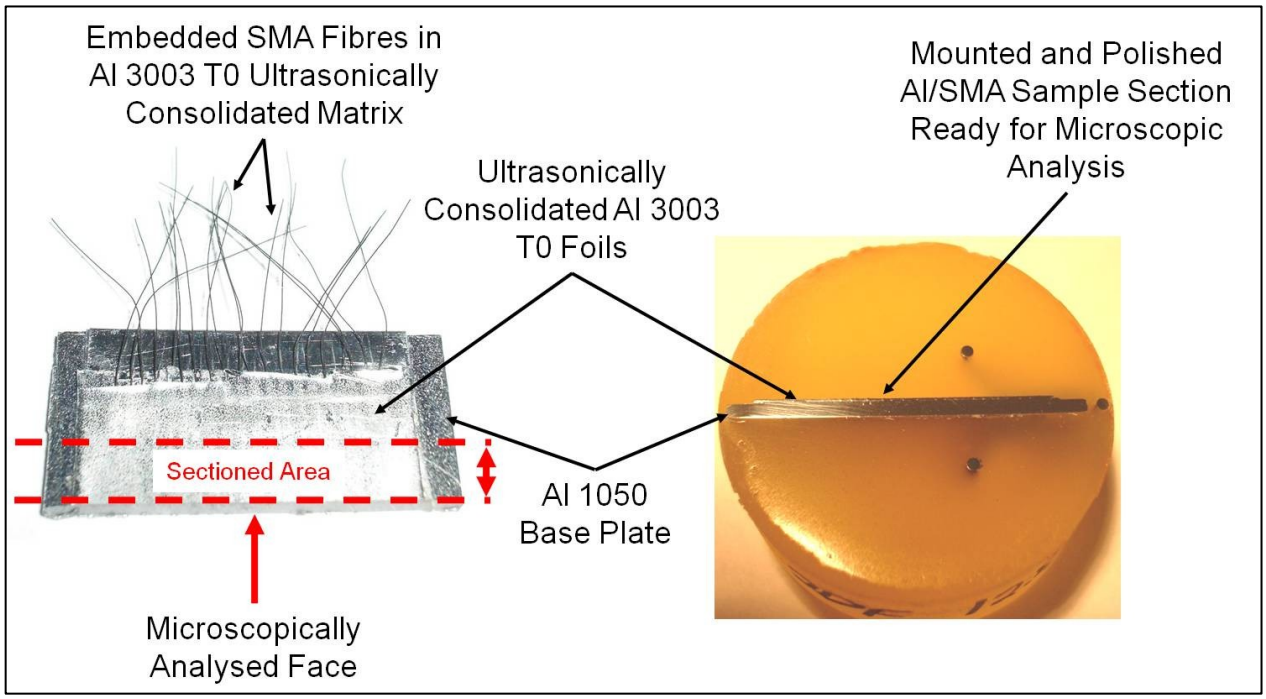

Figure 30 - Example of aluminium/shape memory alloy sample sectioning and mounting for microscopic analysis

Microscopic analysis of the mounted samples was performed using an Olympus microscope with digital image capture capabilities. Images were captured at magnifications of 5x, 20x, 50x and 100x.

4.2.4 Mechanical Peel Testing

To quantify the effect of the increased fibre volume fraction on the interlaminar bond strength the samples were peel tested and compared to a non-fibre containing Al 3003 (T0) UC sample that had been manufactured with the same 12.28 µm amplitude, 276 kPa pressure, and 34.5 mm/s weld speed process parameters. This peel testing was carried out in accordance with BS EN2243-2:1991 which had been previously used for quantifying the UC interlaminar bond strength (Kong, 2005) (Kong, et al., 2004). A bespoke peel testing apparatus was attached to a Lloyd Instruments LRX material testing machine (Figure 31) and used to peel samples that had been mounted (Figure

32). The excess unbonded foil length used to hold the UC sample was 100±5 mm in length.

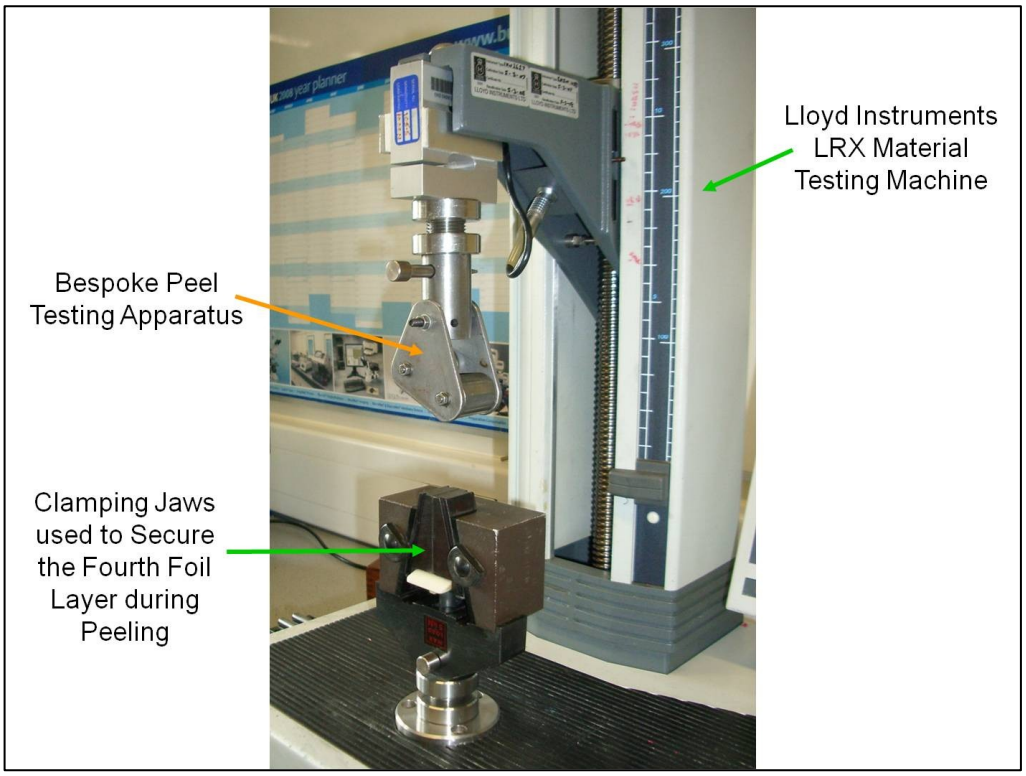

Figure 31 - The Lloyd Instruments LRX material testing machine with the attached bespoke peel testing apparatus

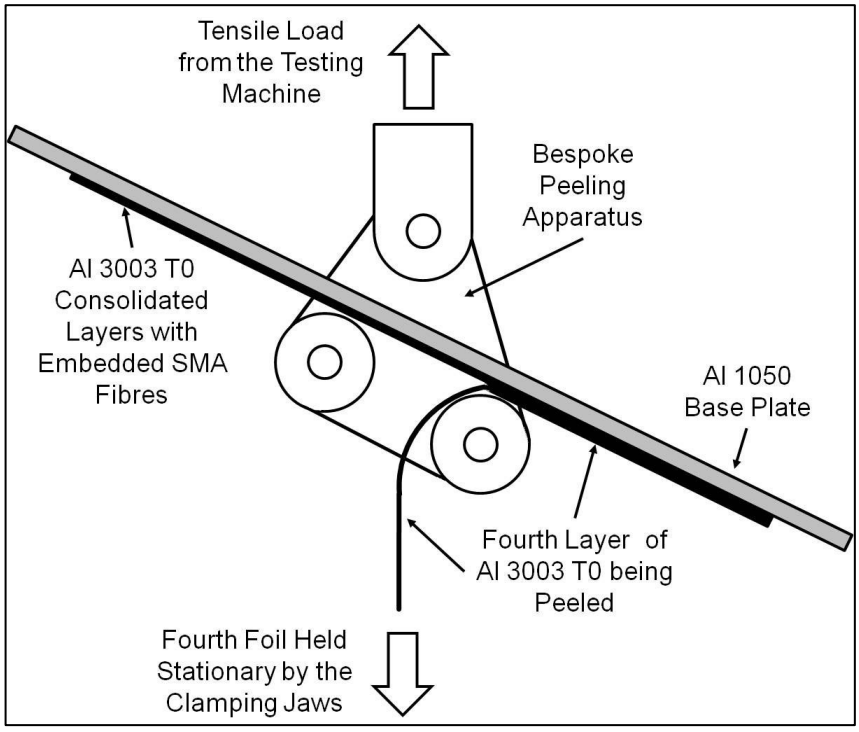

Figure 32 - Schematic of the sample mounting technique within the bespoke peel testing fixture

The peel testing parameters were a tensile loading speed of 50 mm/min and the testing was set to stop when the peel force dropped to 10% of the maximum load measured. All testing was performed at 21 ±5°C and all samples were thermally conditioned at the ambient testing lab temperature for at least 24 hours prior to testing. Three samples for each variety (number of fibres) were peel tested in addition to the samples produced for microscopy.

4.3 Results and Discussion

4.3.1 Sample Fabrication and Microscopic Analysis

The embedding of multiple 100 µm diameter SMA fibres into ultrasonically consolidated Al 3003 (T0) matrices was successful for 10 – 30 fibres however the embedding of 35 and 40 fibres was unsuccessful in all attempts. Using 35 or 40 fibres resulted in delamination of the fourth foil layer which consequently halted their manufacture.

Therefore, the greatest fibre numbers for a single foil Al 3003 (T0) layer that were successfully embedded was 30 fibres (~9.8% volume).

Mounted sample preparation of those that maintained their post-UC integrity was successfully performed. However, grinding and polishing of the samples to a 0.1 µm finish was difficult due to scratching of the relatively soft Al 3003 (T0) by particles of the relatively hard NiTi fibres. The samples were sufficiently polished to allow accurate and detailed imaging of the fibre/matrix area in the bond interface.

Figure 34 shows the typical fibre and bond interface visual that was encountered for samples comprising 10 and 15 fibres. The fibre/matrix interface displayed an intimate contact between the fibres and the Al 3003 (T0) matrix indicating that the plastic flow of the foil matrix during the UC process was sufficiently high to fully encapsulate the fibres and create a dense foil/foil bond interface.

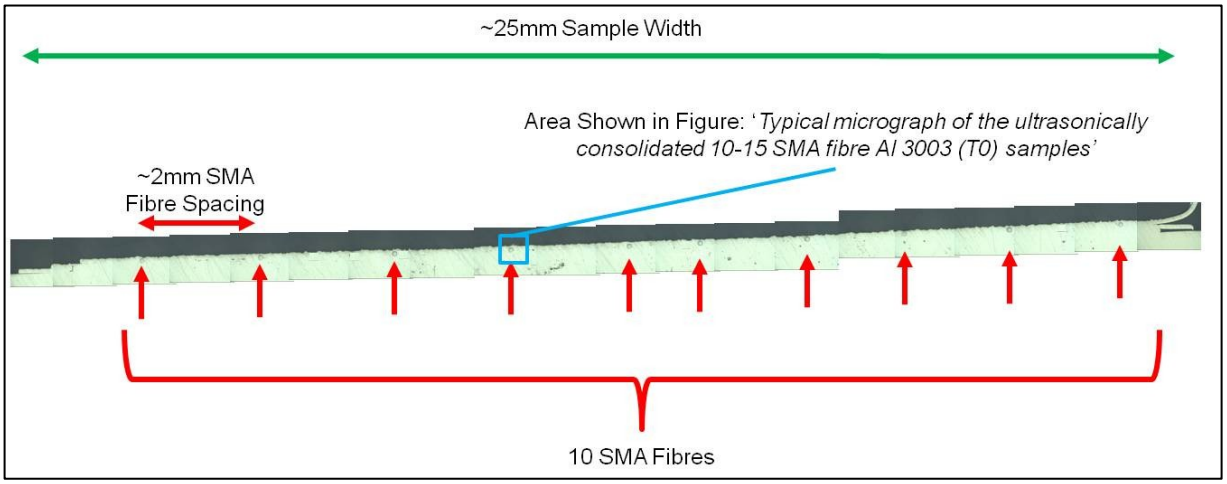

Figure 33 – Complete cross-section of a 10 shape memory alloy fibre/aluminium 3003 (T0) sample

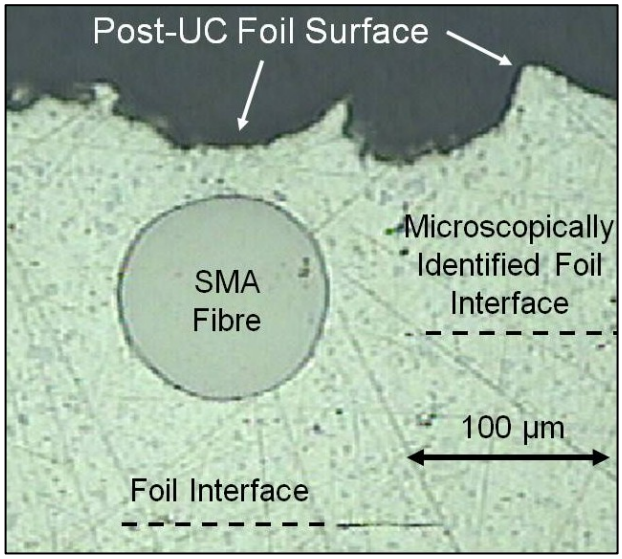

Figure 34 - Typical micrograph of the ultrasonically consolidated 10-15 shape memory alloy fibre/aluminium 3003 (T0) samples

Figure 35 shows a typical fibre and bond interface that was encountered when embedding 20 fibres. The fibre/matrix interface was still primarily intimate but porosity of the interface was perceptible across a number of samples as was porosity at the foil/foil interface. These signs of porosity were possibly due to the maximum level of plastic flow during the UC processing being exceeded and thus full fibre encapsulation as well as full foil/foil interface bonding was not achieved.

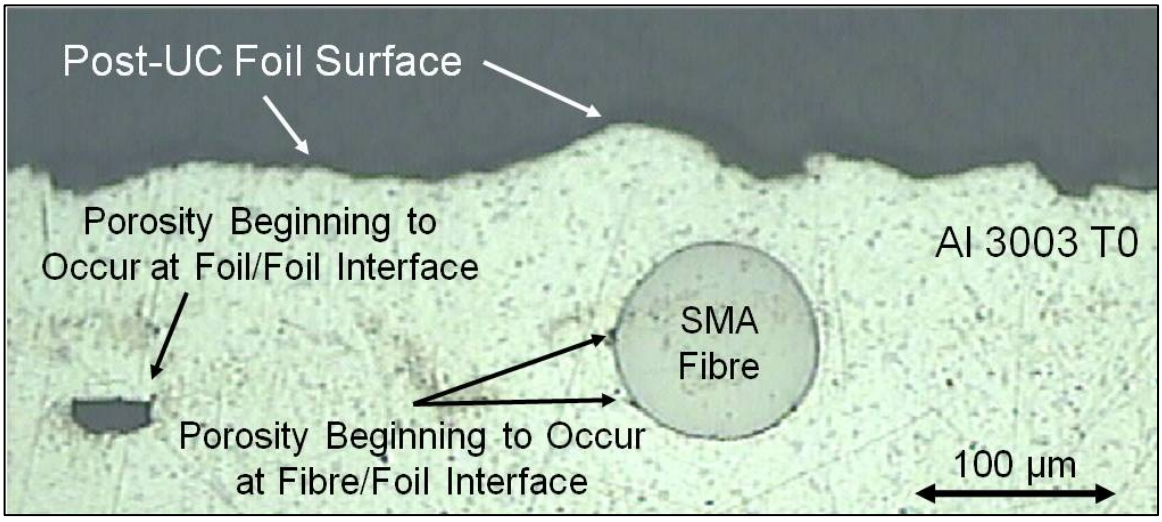

Figure 35 - Typical micrograph of the ultrasonically consolidated 20 shape memory alloy fibre/aluminium 3003 (T0) samples

Figure 36 shows the typical fibre and bond interface visual that was encountered for 25 and 30 fibre embedding. The fibre/matrix interface was significantly reduced than for 10 and 15 fibre embedding and porosity at the interfaces were larger and more numerous than for 20 fibre embedding. The visual difference between 25 and 30 fibre embedded samples' foil and fibre interface quality was not evident at this magnification. The porosity level around the fibres indicated that the level of plastic flow of the foil material during UC processing was insufficient to create a fully dense fibre to matrix interface. Likewise the level of porosity at the foil/foil interfaces signified that the fibre volume fraction was hindering the bonding process between the foil layers during the UC processing.

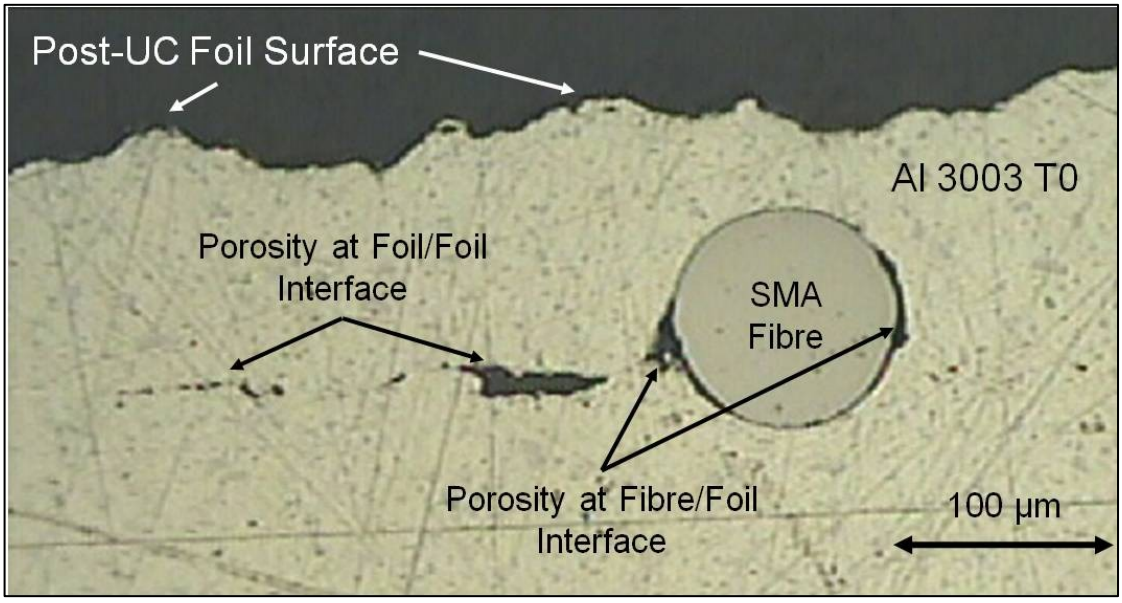

Figure 36 - Typical micrograph of the ultrasonically consolidated 25-30 shape memory alloy fibre/aluminium 3003 (T0) samples

Figure 37 shows the resultant delamination that was found to occur when manufacturing of the 35 and 40 fibre containing samples. The bonding between foil layers appeared to be inhibited by the greater volume of fibres and thus adequately robust samples for sectioning and peel testing were not possible. The foil surface that the fibres were to be forced onto were apparently still deformed in a similar fashion to the upper surface of the post-UC processed fourth foil for the other samples. This further suggested that the effect of the previously deposited foil on the fibre being embedded may be of significance.

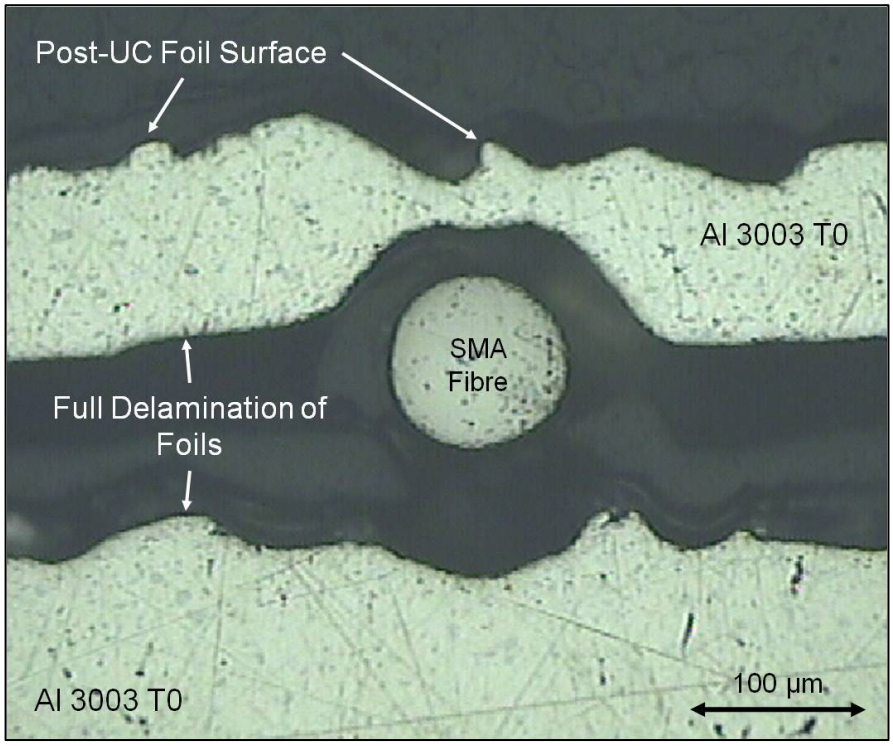

Figure 37 - Typical micrograph of the ultrasonically consolidated 35-40 shape memory alloy fibre/aluminium 3003 (T0) samples

In all samples manufactured it was evident that the fourth UC deposited layer was significantly deformed by the contact with the machine sonotrode; (see "Post-UC Foil Surface" in Figure 34, Figure 35, Figure 36 and Figure 37). This surface had previously been shown by Johnson (Johnson, 2008) to have undergone a significant level of plastic deformation and sub-grain refinement due to the direct contact with the sonotrode and ultrasonic excitation of the foil material. This implied that the surface contact between the previously deposited foil (sonotrode deformed) and the bottom of the SMA fibre would be different in characteristics to the surface contact between the fourth foil (virgin material) and the top of the SMA fibre.

4.3.2 Peel Testing

Peel testing of the Al 3003 (T0) samples containing 0, 10, 15, 20, 25 and 30 SMA fibres was successfully completed and the average maximum peel load (N) for the three samples of each fibre number tested are presented in Figure 38. The samples of 35 and 40 fibres were not successfully tested due to their interlaminar bond strength being insufficient to allow the testing to be performed.

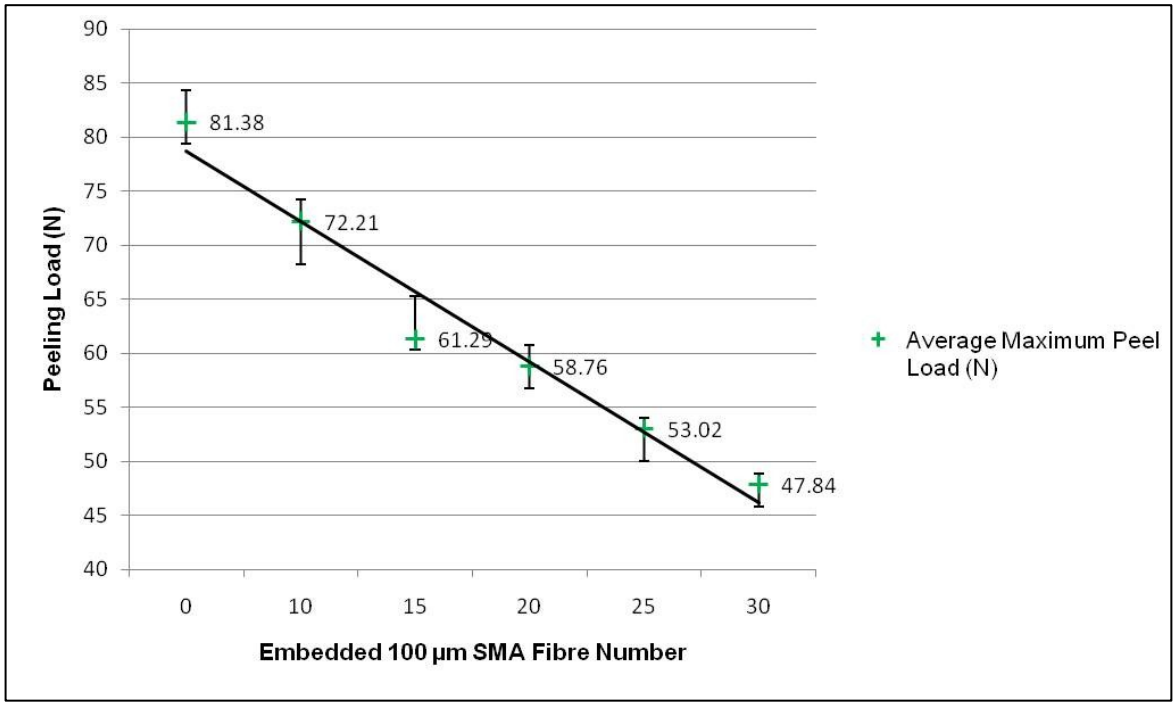

Figure 38 - A graph showing the average maximum peel load for ultrasonically consolidated aluminium 3003 (T0) samples with embedded shape memory alloy fibres

The trend of the peel testing showed that the increasing fibre volume fraction had a negative effect on the maximum peel load of the UC Al 3003 (T0) laminate structure. The average maximum peel load for the control samples (zero fibres) was 81.38 N. The reduction in average maximum peel load with respect to the samples with no fibres embedded was: 11.27% (72.21 N) for 10 fibres; 24.69% (61.29 N) for 15 fibres; 27.80% (58.76 N) for 20 fibres; 34.85% (53.02 N) for 25 fibres, and 41.21% (47.84 N) for 30 fibres.

A total reduction of 41.21% in average peel load, compared to zero fibres, resulted when 30 fibres were embedded in the matrix. This reduction was less than 50%; however an increase in fibre numbers to 35 and 40 resulted in no significant foil/foil bonding taking place and minimal peel load resistance. These results were interpreted to highlight that the foil/foil contact was not the only significant factor in the creation of interlaminar bonding during the UC process. The increase of fibre volume fraction is limited in the level of encapsulation by the volume of plastic matrix material flow. However, the reduction of peel resistance does not appear to be completely dependent on the plastic flow of the matrix material around the fibres. A reduction to the relative motion and

surface area of the foil material relative to the UC sample could be incurred as a result of the increasing number of fibres which would prevent metal to metal contact and bonding from occurring.

The post peeled Al 3003 (T0) samples were observed to have areas of material that appeared to have not been plastically deformed from their original foil as-rolled state. To assess this observation in greater detail a micrograph of the surface of a sample was taken and is presented in Figure 39. The initial interpretation was that some areas of the foil material were not involved in the foil/foil bonding process as they were not deformed. An interesting note was that the area of the apparently un-bonded foil material constituted a greater area of material than the interlaminar porosity (LWD measurements) noted in sectioned samples. This suggests that foil/foil contact may be occurring, giving an appearance of bonding during the LWD measurements, but metallurgical bonding is not occurring and the foils are only in contact with each other.

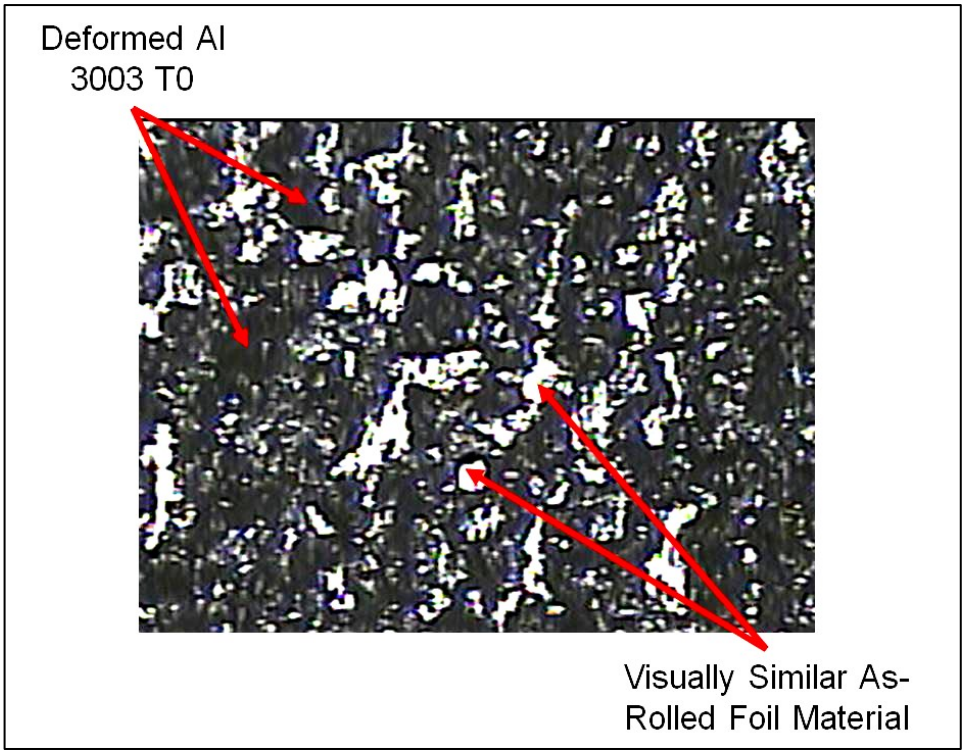

Figure 39 - Optical micrograph at 5× magnification of an aluminium 3003 (T0) interlaminar ultrasonically consolidated surface

4.4 Summary of Increasing Fibre Volume Embedding Experimentation

There were several insights gained from increasing the fibre volume fraction and using optical microscopy and mechanical peel testing to analyse the results. The increasing fibre numbers resulted in greater porosity at the fibre/foil interface and the foil/foil interface. These effects resulted in the UC Al 3003 (T0) SMA MMC samples having reduced peel resistance with increasing SMA fibre numbers. The maximum peel load reducing effect by the SMA fibres was found to significantly increase at greater than 30 fibres which highlighted that the plastic flow of the Al 3003 matrix and the inherent foil/foil contact was not the only significant factor in achieving interlaminar bonding during UC.

Upon microscopic investigation of these post peel tested samples there were apparent areas of un-bonded Al 3003 (T0). The amount of un-bonded area appeared greater than that which was visually identified through microscopic cross-sections of the pre-peeled UC samples. Therefore the interlaminar bonding process was highlighted by the post-UC peel testing to be more porous than was apparent from microstructural cross sectioning. This interlaminar surface was found to be a series of peaks and troughs resultant from sonotrode contact and the subsequent UC bonding process. Johnson (Johnson, 2008) previously had shown that the post UC upper foil layer had undergone plastic deformation and grain refinement. This grain refinement was thought to have resulted in a harder material and thus the post-UC surface was theorised to be made of harder and softer areas. The relationship between process parameters and the interlaminar structure created during UC and the possible effect of the sonotrode on the material hardness were unknown and likely significant on the fibre embedding process during UC. Determining the characteristics of the interlaminar surface created via UC prior to fibre embedding would aid in the understanding of fibre embedding via UC.

The plastic flow of the Al 3003 (T0) around the SMA fibres was observed in this instance and in previous work (Kong, 2005) (Kong, et al., 2004). This plastic flow was observed for fibre diameters of 100μm and was found to result in porosity at higher fibre numbers.

The size of objects that can be embedded within the Al 3003 (T0) matrix was not altered however the use of larger SMA fibres could increase the fibre volume fraction while maintaining a lower number of fibres. The interactions between the SMA fibres and the Al 3003 (T0) matrix were not documented in terms of the grain structure interactions that take place during the UC process. These interactions would likely involve two separate instances: The fibre interacting with the underside of the as-rolled foil that is placed onto the fibres and the interaction of the fibre with the sonotrode altered previous foil layer. Analysing the microstructural and mechanical interactions at the fibre/matrix interface, post-UC could help elucidate fibre embedding via UC.

The interaction between the fibre and matrix was noted as being intimate in contact when porosity was not present within the bond interface. As SMA fibres, and any adaptive metal matrix composite that would be manufactured containing them, are shape change materials the nature of the interaction between matrix and fibre was a dynamic one. Extension and activation of UC embedded fibres could create internal stresses within a UC structure and alter the fibre/matrix interface. Assessing the performance of UC embedded SMA fibres and their interaction with the metal matrix upon activation would aid in understanding the issues with regards to creating SMA containing UC adaptive composites.

As a result of the insight gained from the experimentation a revised hypothesis was presented and three studies were formulated to test this hypothesis.

5 Revised Hypothesis

It is postulated that the interlaminar structure created during UC is affected by the process parameters used. This interlaminar structure contains areas of un-bonded foil and the increase of amplitude, welding pressure and welding speed would reduce this area of un-bonded foil. This could be tested by manufacturing UC samples with a range of UC process parameters, peeling the samples and then detailing the interlaminar structure to identify un-bonded foil areas.

This interlaminar structure is the surface onto and into which the SMA fibres are embedded and this surface has come into contact with the UC machines sonotrode prior to fibre embedment. This sonotrode contact was shown by Johnson (Johnson, 2008) *to create a refined grain structure in areas of the contacted foil. It is hypothesised that this refined grain structure would likely be harder than the un-refined grain structure and thus a surface of uneven material hardness would have been created which has implications for fibre embedding during UC. To test this hypothesis hardness testing of the foil material that has come into contact with the sonotrode would establish if the matrix material has become harder or not.*

Higher fibre numbers within the UC foil/foil interface result in greater porosity and a less robust UC sample. It is hypothesised that the maximum plastic flow of the matrix material during UC has not been reached and it is instead the reduction of foil to foil oscillatory motion that causes the lack of UC bonding and not the level of plastic flow. To test this hypothesis larger fibre diameters will be embedded into the matrix material, which would require greater plastic flow but allow relative foil/foil motion to remain high, and these samples will be analysed microscopically and quantified via peel testing.

The embedded SMA fibres are embedded into two different surfaces of the matrix material: the as-rolled foil surface and the sonotrode contacted surface. The interaction between the fibre and matrix is hypothesised to have a work effect on the as-rolled matrix materials microstructure and the grain refined matrix material is hypothesised to have an abrasive effect on the fibre. This will be tested through the micro grain structure

analysis of the fibre/matrix interface, post UC, to determine any grain refinement and the nature of the fibre/matrix interaction.

Prior work into UC embedded SMA fibres was shown possible by Kong (Kong, et al., 2004) and the activation of the fibres in-situ was subject to preliminary investigation which demonstrated its feasibility. However, evidence as to the effect of the activation on the UC matrix material and the fibres themselves was not investigated in depth.

It is hypothesised that the activation of UC embedded SMA fibres will reduce the strength of the fibre/matrix interface and the matrix will impede the ability of the SMA fibres to contract causing a forceful interaction at the fibre to matrix interface weakening the structure. This hypothesis will be tested by activating UC embedded fibres in-situ and then measuring their speed and force of response. The fibres will then be pulled from the matrix to measure any potential loss of fibre/matrix interaction and the UC sample will be peel tested to identify any loss of strength caused through fibre/matrix interaction during SMA fibre activation.

The investigation based on the revised hypothesis was broken down into three sections of study (Figure 40).

Study 1 (Section 6) Describes a methodology to determine the characteristics of the interlaminar surface created via UC and how this surface affects the nature of the consolidated sample. This interlaminar characterisation was necessary with regards to understanding the type of surface that is present in the UC sample prior to fibre embedding. This information was then able to aid in understanding the microstructural profiles that were likely to be encountered in Study 2.

Study 2 (Section 0) Describes a methodology to allow the analysis of the microstructural and mechanical interactions at the fibre/matrix interface post-UC. These interactions would allow further insight into the role of the SMA fibres during the UC embedding process and what was occurring at the microstructural level for both the foil and fibre materials. This information was then able to aid in understanding the interaction between the matrix and fibre which was useful when moving to Study 3.

Study 3 (Section 8) Describes a methodology to investigate the fibre usage as would be expected from envisaged applications of the SMA/Al metal matrix composite. The specific effects of in-situ fibre activation and extension on the fibre matrix dynamic would provide invaluable data for optimising future applications of the UC technology.

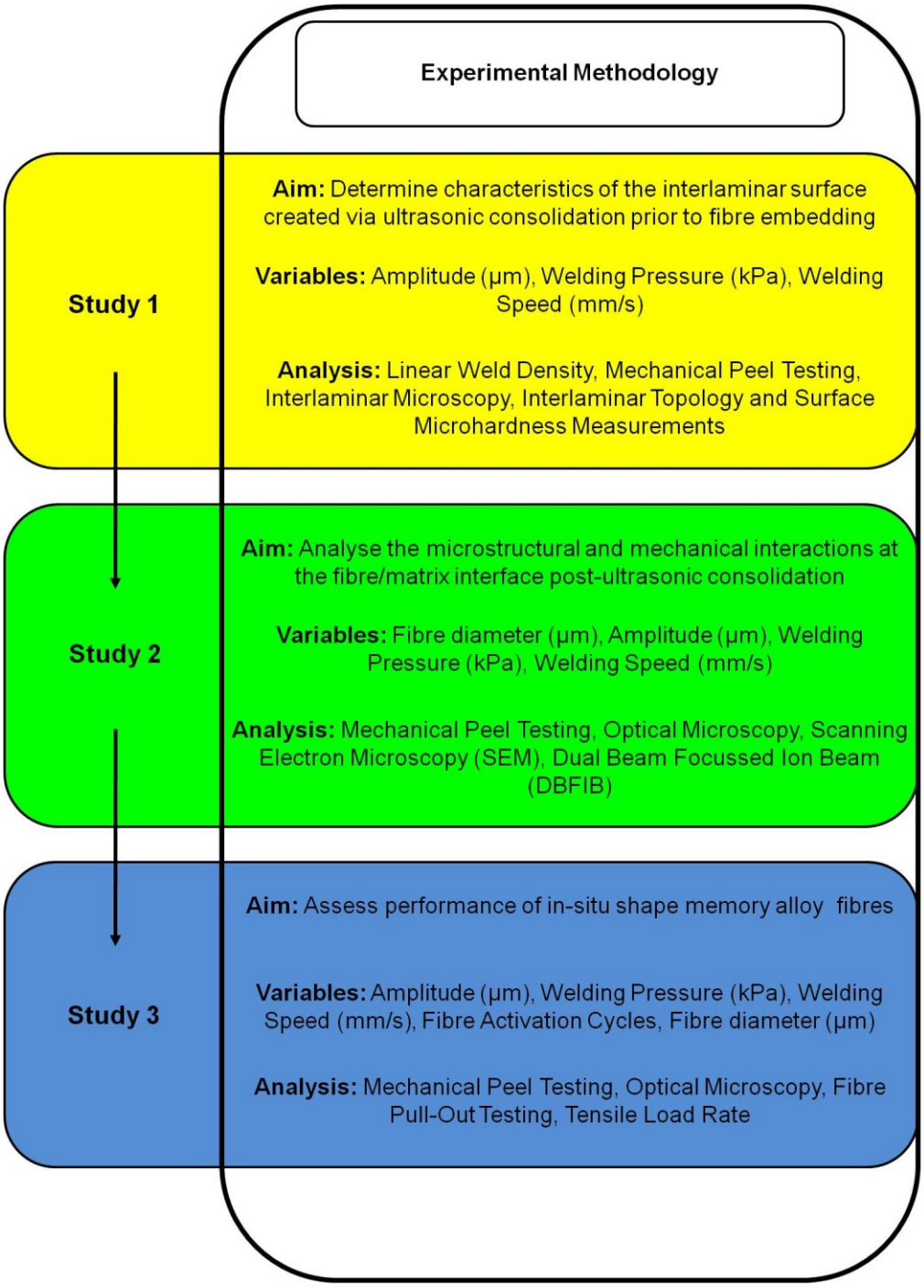

Figure 40 - Methodology Process and Studies

6 Investigation into the Interlaminar Surface Created via Ultrasonic Consolidation

6.1 Introduction

Research into the sonotrode surface roughness effects has highlighted phenomena during UC (Janaki Ram, et al., 2006) (Johnson, 2008). The findings were that the sonotrode surface roughness not only determines the foil to foil contact surfaces but also is a main factor in determining the level of plastic flow, work hardening and mechanical properties of the UC sample. This work did not identify the effect of process parameters on this interlaminar surface or that investigate material property changes that may have been caused by the sonotrode contact.

This research was aimed at furthering the understanding of the sonotrode effect on the monolithic UC structure to help understand how process parameters are represented in terms of changes in the interlaminar characteristics, such as area of bonded foil, topological profile and material property changes.

6.2 Methodology

6.2.1 Mechanical Peel Testing

As with previous work (Kong, et al., 2004) the mechanical performance of the bonding in UC produced samples was verified by ultrasonically consolidating Al 3003 (T0) monolithic samples with different processing parameters. The peel testing was carried out in the same method as in section 4.2.4 however the sample preparation did not involve the step of embedding fibres as the samples for this experiment were monolithic structures and they were produced with a range of process parameters so that the effects of these parameters could be determined.

Peel testing allowed for bond quality to be quantitatively analysed by assessing a set of samples average resistance to peeling for a given set of UC process parameters. It was shown in earlier work (Kong, et al., 2005) that the greater the LWD, the higher the peel strength of the sample.

Three samples for each set of processing parameters were tested; the combinations of processing parameters used for making the samples are shown in Table 5. The amplitudes used were 10.41, 12.28, and 14.26 μm (50, 70 and 90% of the machines capability respectively). The contact pressures used were 207, 241, 276 and 310 kPa (30, 35, 40, and 45 psi respectively). The weld speeds used were 34.5 and 43.5 mm/s.

Welding Speed (mm/s)	Sonotrode Amplitude (μm)	Welding Pressure (kPa)
34.5	10.41	207
		241
		276
		310
	12.28	207
		241
		276
		310
	14.26	207
		241
		276
		310
43.5	10.41	207
		241
		276
		310
	12.28	207
		241
		276
		310
	14.26	207
		241
		276
		310

Table 5 - The combinations of processing parameters used to produce the monolithic ultrasonically consolidated peel testing samples

The process parameters that were investigated were based on the process window work defined by Kong (Kong, 2005) (Kong, et al., 2004). The parameters that had previously

been shown to result in what was deemed as unacceptable LWD/ peel test performance were not investigated in this study.

6.2.2 Analysis of Linear Weld Density

To quantify the density of bonding LWD was used to represent the percentage of bonded length as shown in Equation 3.

One sample for each set of processing parameters was sectioned into start, middle and finish sections (Figure 41) which were then mounted in Buehler Varidur resin. Each sample was then ground and polished as described in section 4.2.3. After polishing no chemical etching was used, unlike previous research (Kong, 2005). The reason for this was that it was found that etching of the Al 3003 (T0) resulted in biased etching of the Mn intermetallics which then made it difficult to determine porosity at the bond interface as opposed to excessive etching. After etching an Olympus BX60M optical light microscope with a 100x magnification lens was used to analyse the samples and obtain images, using a QImaging Micropublisher 3.3MP camera, for LWD assessment. Seven images, along the bond interface, for each mounted sample section were obtained.

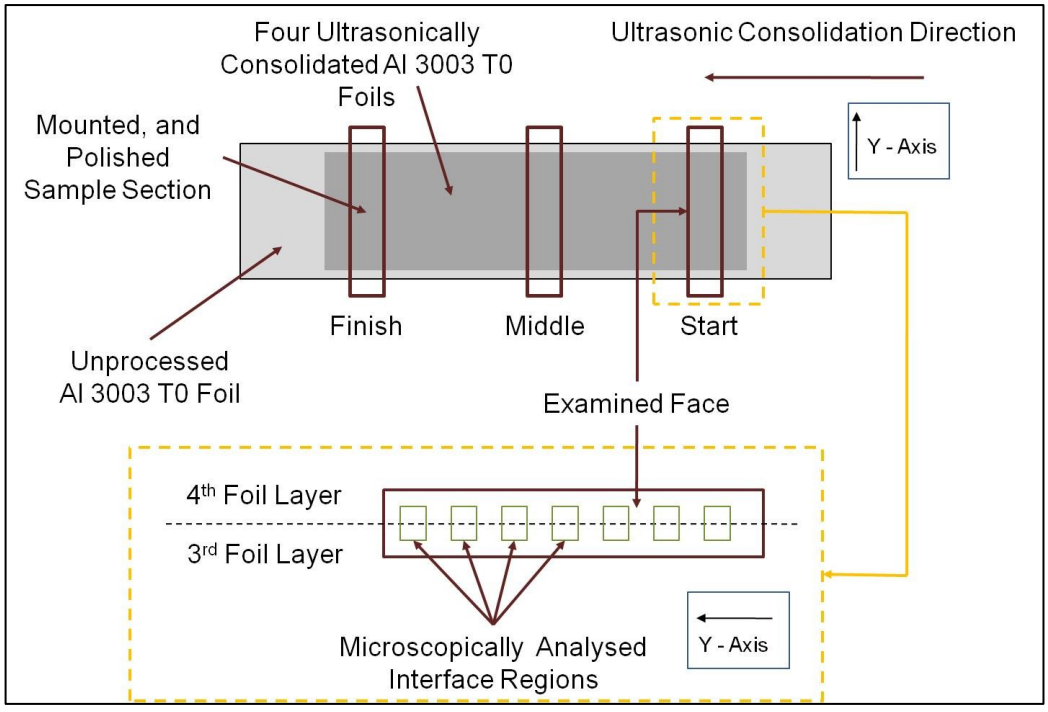

Figure 41 - Schematic showing specimen sample extraction regions for microscopic analysis to determine linear weld density

The images were each assessed to visually determine the bonded length (L_b) and interface length (L_c) before calculating the LWD (see Equation 3 and Figure 42). For all the images obtained for each sample set, an average of the LWD was calculated and then used as the actual LWD for the monolithic Al 3003 (T0) samples produced using those specific processing parameters.

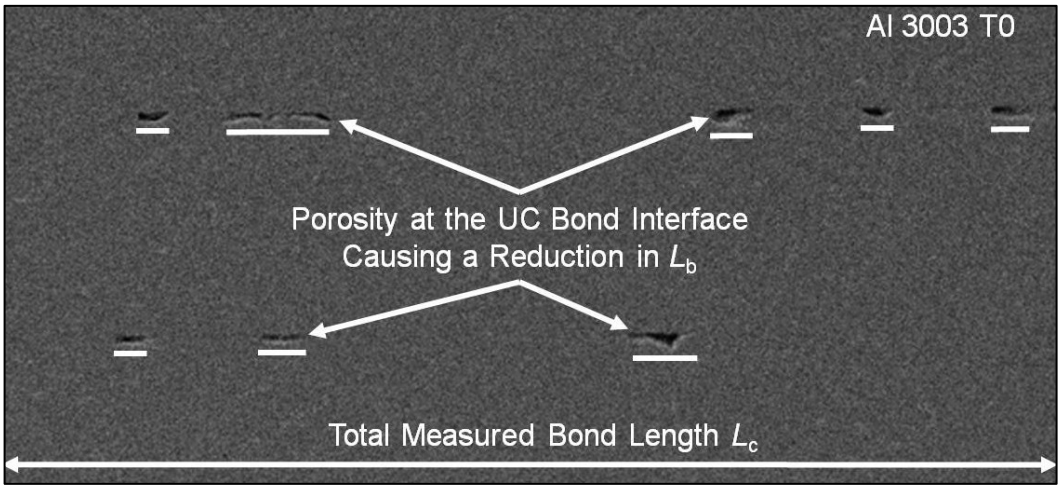

Figure 42 - Example of the determination of linear weld density (Friel, et al., 2010)

6.2.3 Microscopic Analysis of Post Peel Tested Interlaminar Surface

Johnson (Johnson, 2008) showed that during UC processing the sonotrode imprints its own unique surface roughness structure onto the processed foils' surface. This texture imprint, or 'transfer function' acts as one of the major factors in determining the number and geometry of point to point contacts between surfaces when the next foil layer is deposited onto this previously textured layer. The residual texture of the processed foil was also analysed after processing by forcibly removing it from its consolidated state with the previous foil layer.

This research investigated the interlaminar foil surface topography, after undergoing peel testing, of Al 3003 (T0) ultrasonically consolidated monolithic foil structures (refer to Figure 43). The topography was microscopically analysed using a Leica DM 6000

optical light microscope for a variety of Al 3003 (T0) samples produced using a variety of UC processing parameters (see Table 5).

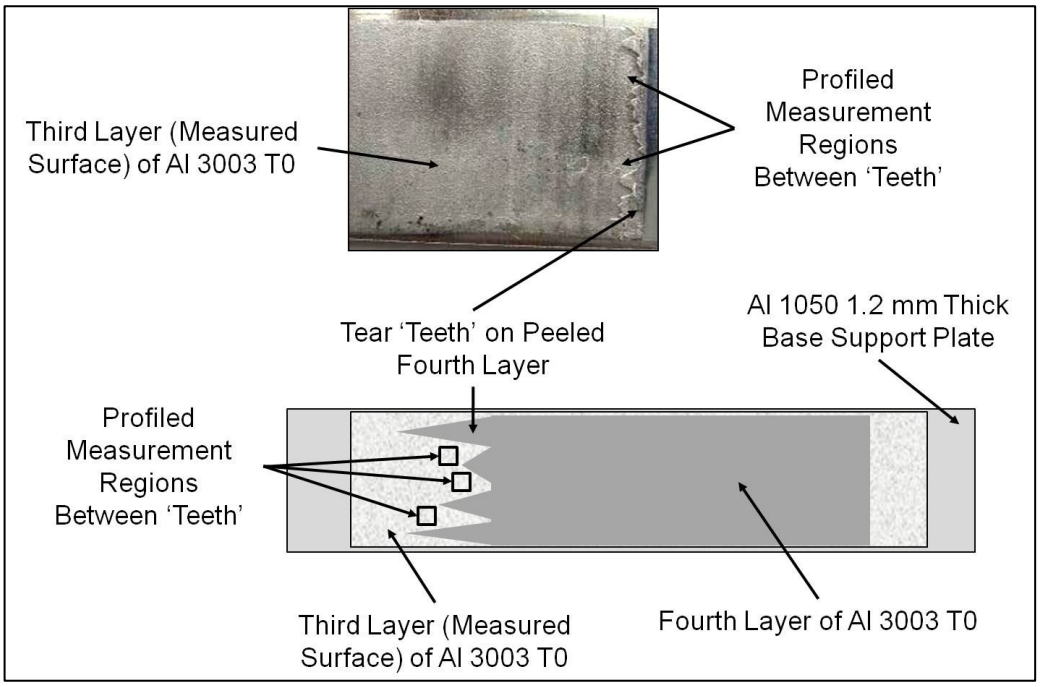

Figure 43 - Image and schematic showing the interlaminar surface assessment region on the consolidated aluminium 3003 (T0) monolithic sample post peel testing

The samples were prepared and peel tested as described in sections 4.2.1 and 4.2.4 before being microscopically analysed while deformation of the sample from peel testing was likely, the bonded area was to be indentified and compared over multiple processing parameters and samples to identify if there was variation of the produced profiles and thus was a representative measurement of interlaminar bonded area. The samples were not polished or etched as this destroyed the complex topographic structure that was present, which opposed the aims of the work.

6.2.4 Post Peel Tested Interlaminar Surface Roughness Mapping

To contribute to a further understanding of the interlaminar structure present in the Al 3003 (T0) monolithic structures the surface roughness profile of the samples was measured to allow for a quantitative analysis of the sample topography. This type of profiling allowed for accurate determination of the R_a and Root Mean Square Roughness

(R_q) values for the interlaminar structure for various processing parameters as well as creating a comprehensive 3D topographical map.

The profiling system used for taking the 3D measurements was a Zygo NewView 5000™ white light interferometer with a 10x magnification objective lens. The NewView 5000™ uses non-contact scanning white light interferometry to obtain high Z-resolution images. The processing variables used during the measurements are shown in Table 6, these parameters were set within the proprietary software (MetroPro version 8.1.5 – see Figure 44).

Measurement Variable	Variable Setting
Objective Lens	Mirau 10x
Measurement Array Size	640 x 480 at 30 Hz
Manual Image Zoom	2x magnification
Field of View	X: 0.35 mm Y: 0.26 mm
Height Resolution	≤0.1 nm
Frequency Domain Analysis (FDA) Resolution	High
Scan Length	100 µm bipolar
Mid Mod	1%
Stitch Image Number	9 = 3 columns x 3 rows
Stitch Image Overlap	25%
Stitched Image Size	X: 0.87 mm Y: 0.66 mm

Table 6 - Zygo NewView 5000 system parameter settings

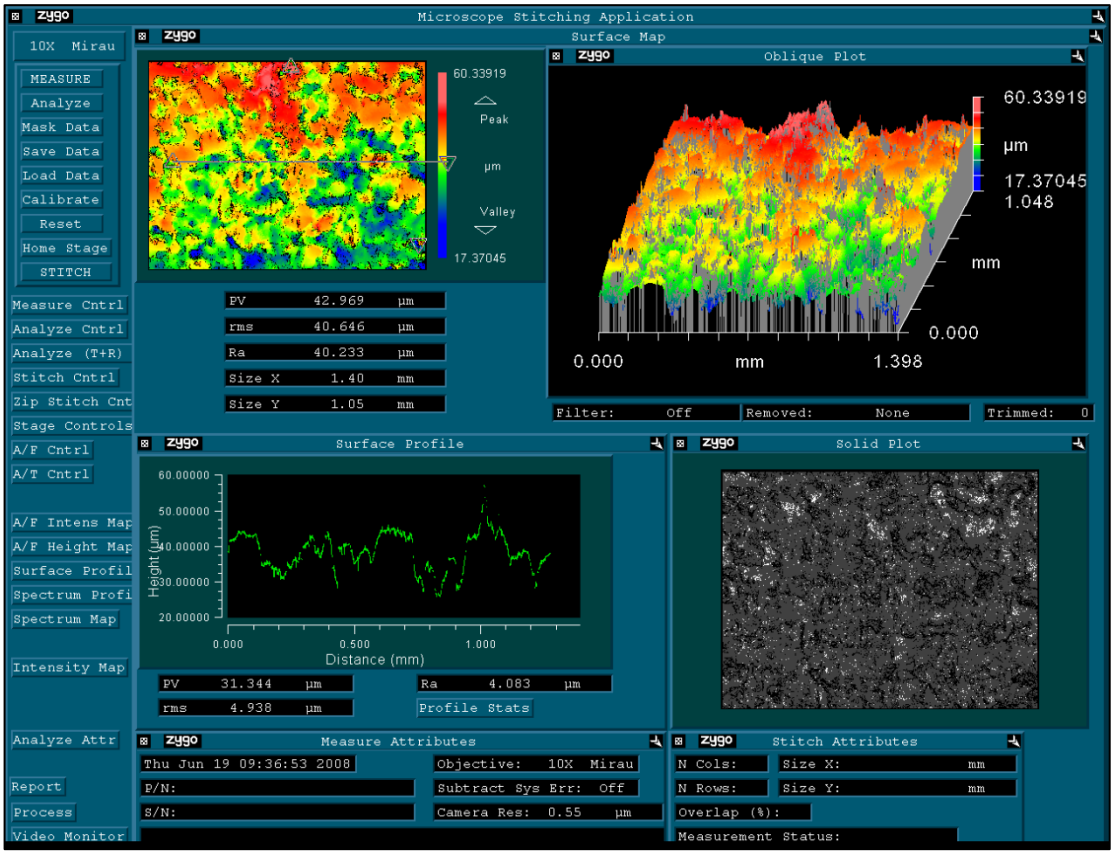

Figure 44 - A screenshot of the MetroPro version 8.1.5 operational software for the Zygo NewView 5000 surface profiler

The measurement area for each sample was variable due to the variable nature of the 'teeth' profile produced during peel testing however Figure 43 shows the approximate location of the measurements used for each sample. Three measurements were taken for each sample and the sample data was analysed using TalyMap Gold 4.1 software. Due to the highly uneven surface present and due to the angle of some faces of the material being too steep, a level of data loss was present. This data loss was rectified via the use of an in built approximation algorithm within the TalyMap software that filled in the data loss by observing the average profile and nearby faces to create a 'best fit'. The R_a and R_q values for the surface were measured using the software after this processing was complete.

All surface roughness measurements were taken at a temperature of 21±2 °C and each sample was thermally conditioned at this temperature for at least 24 hours prior to measurement.

6.2.5 Assessment of Post Peel Tested Interlaminar Material Hardness

It had, in previous work, been discussed that ultrasonic welding of metals had a strain work hardening effect on the material within the ultrasonically affected zone (Kong, 2005) (Janaki Ram, et al., 2006) (Janaki Ram, et al., 2007). However, there was minimal information on the actual level of increase of strain work hardening and how UC process parameters affected this level. The focus of the present work was to measure the increase in interlaminar material hardness post UC processing.

The measurements taken were via the use of a Buehler Micromet™ 2100 microhardness material tester. This tester was equipped with a Vickers diamond indenter and therefore all hardness measurements were Vickers Hardness (HV) measurements.

The measurement locations were the same as shown in Figure 43 with the indenter contact area being microscopically identified so that the material being tested had in fact been in contact with the sonotrode and/or upper foil surface and was not virgin foil material (refer to Figure 45). Six measurements were taken in a 2x3 formation at areas at least 20 μm away from each other (due to the highly irregular interlaminar surface it was not possible to maintain an entirely regular measurement pattern). Each measurement, performed to EN ISO 6507, was taken using a load of 200 g which was applied for 25 seconds to ensure minimal elastic recovery of the Al 3003 (T0) material when the load was removed.

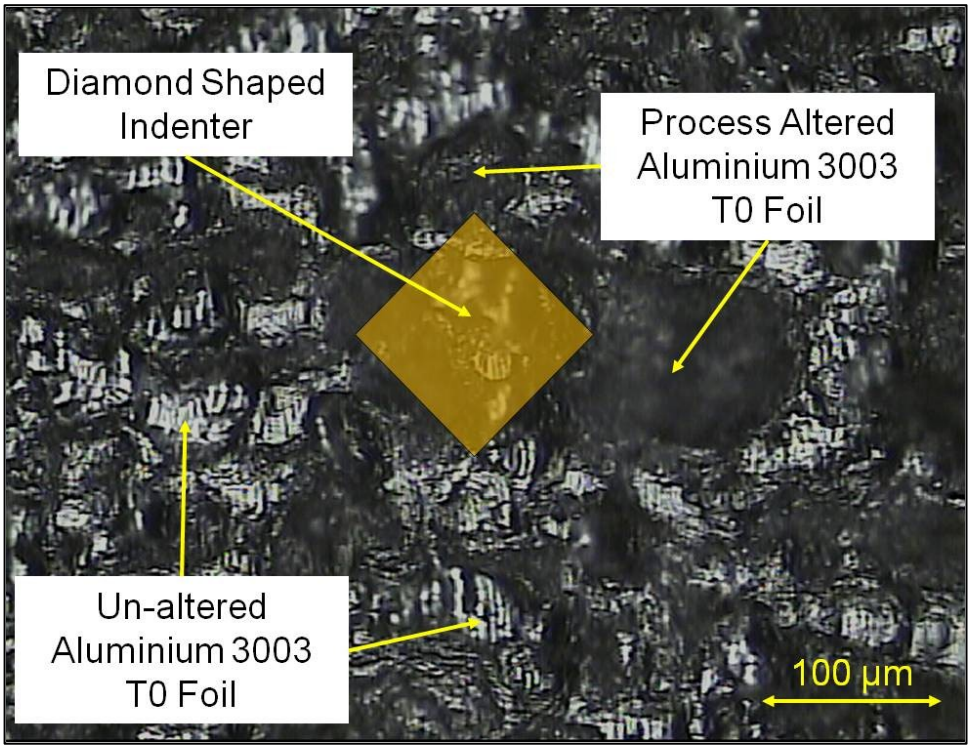

Figure 45 - Schematic representation of the microhardness test indentation image on a typical aluminium 3003 (T0) sample micrograph

Using the attached microscope the diagonals of the diamond shape were measured and computed by the microhardness testing equipment to obtain the HV value using the following equation:

$$HV = \frac{2\,F\,sin\left(\frac{\theta}{2}\right)}{L^2}$$

Equation 4 – The Vickers material hardness determination equation

F is the applied load (kg), *L* is the average length of the diagonals of the diamond shaped indentation (mm) and *θ* is the angle in degrees between opposite faces of the pyramid (136° for a Vickers pyramid hardness indenter as in this case).

The equipment and the test samples were all kept at 22±2 °C and this is the temperature at which all hardness tests were carried out after a period of 24 hours thermal conditioning. For each sample the six measured HV values were averaged and used as the overall value for that particular sample.

6.3 Results and Discussion

6.3.1 Peel Testing Results of Al 3003 (T0) Samples

Peel test sample production was successful for the full range of processing parameters in Table 5. The samples were tested in the peel testing apparatus. Figure 46 shows the two main failure modes of the peel test samples that were encountered. The more abrupt failure mode was found to occur with samples produced using the processing parameters of 12.28 – 14.26µm with a contact pressure ≥241 kPa. The more abrupt failure mode resulted in a more uniform tear pattern at the non-bonded/bonded foil interface while the elongated failure mode resulted in a pattern of 'tear teeth'.

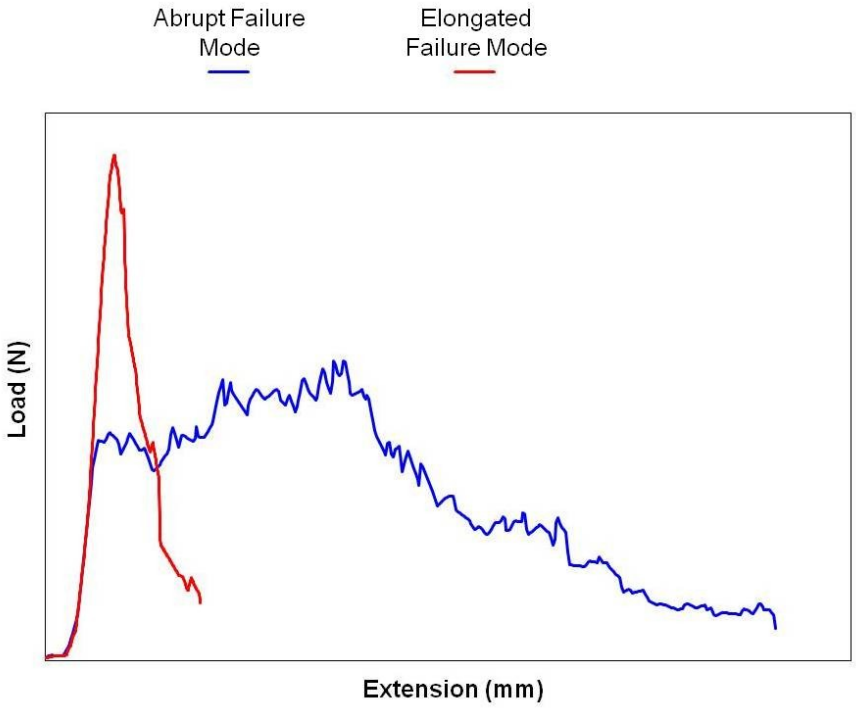

Figure 46 – The typical peeling load vs. extension graph showing the two different forms of failure mode

The more elongated peeling indicated that tear propagation through the bonded Al 3003 (T0) foil was not hindered in the same manner as for the abrupt tear pattern. This ease of tear suggested that the underlying bond contacts were fewer in number and/or were sufficiently weak to allow tear propagation to continue.

The peel test results for the Al 3003 (T0) ultrasonically consolidated samples are shown in Figure 47 and Figure 48. The samples produced using a welding speed of 34.5 mm/s resulted in samples with a greater peel force than samples produced using a welding speed of 43.5 mm/s. The peel force achieved was 93.10 N for 34.5 mm/s compared to 71.18 N for 43.5 mm/s. The higher speed processing would reduce contact time between the sonotrode and the specific foil material area and thus reduce the amount of ultrasonic excitation which resulted in a reduction of peel strength.

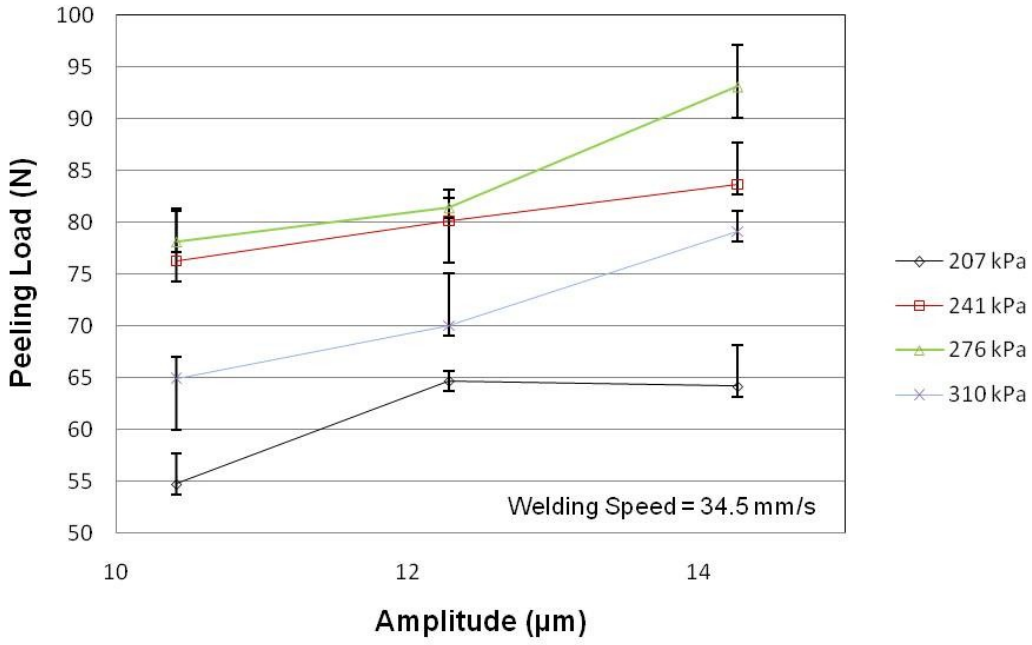

Figure 47 - The peel testing results for aluminium 3003 (T0) ultrasonically consolidated samples produced using a welding speed of 34.5 mm/s

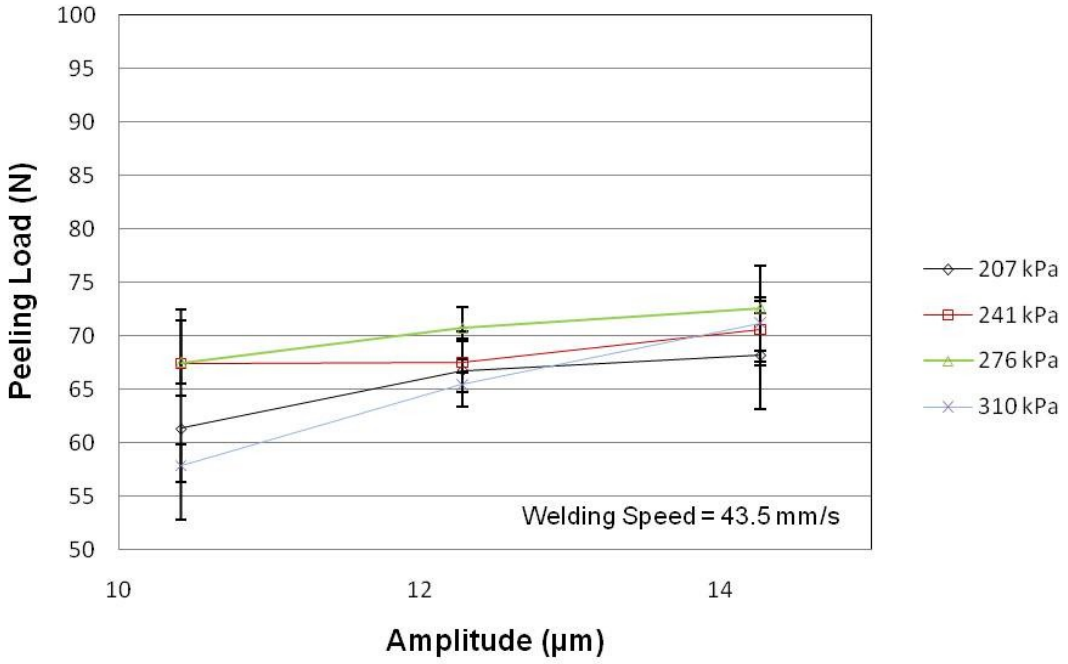

Figure 48 - The peel testing results for aluminium 3003 (T0) ultrasonically consolidated samples produced using a welding speed of 43.5 mm/s

Higher peel strength was achieved through the use of a greater sonotrode amplitude suggesting that the greater the relative motion of the bonding foil to the substrate the more effective and robust the interlaminar bonding. The use of higher welding pressures generally resulted in higher peel strength; however this was not the case while using the highest pressure of 310 kPa. The use of this higher pressure resulted in a decrease of peel strength which was counter to the trend. There is a possibility that the reduction in weld strength at the higher pressure was as a result of the transducer/booster/sonotrode UC machine element, (refer to Figure 13), being impeded by the higher welding pressure. The higher pressure exerted as a normal force to the oscillation of the sonotrode, may have reduced the amplitude and/or frequency of the oscillations and thus reduce the excitation level of the foil.

6.3.2 Linear Weld Density Results of Al 3003 (T0) Samples

Samples were manufactured, sectioned, mounted and polished for the LWD analysis of the ultrasonically consolidated Al 3003 (T0) monolithic samples produced using the

parameters in Table 5. The results of this analysis can be seen in Figure 49 and Figure 50.

For the Al 3003 (T0) samples produced using a welding speed of 34.5 mm/s and 43.5 mm/s the LWD was found to generally increase with an increase in amplitude and pressure. The maximum LWD for Al 3003 (T0) samples was 93%. As with the peel test data a welding pressure of 310 kPa was found to result in a lower LWD which added credence to the theory of amplitude/frequency loss of the sonotrode from excessive sonotrode normal force. The LWD was variable for each of the sample sections and seven analysis regions. However, the measured increase in average LWD correlated with the previous results of increased peel strength.

The average LWD was not found to vary for the start middle and finish regions of the UC samples.

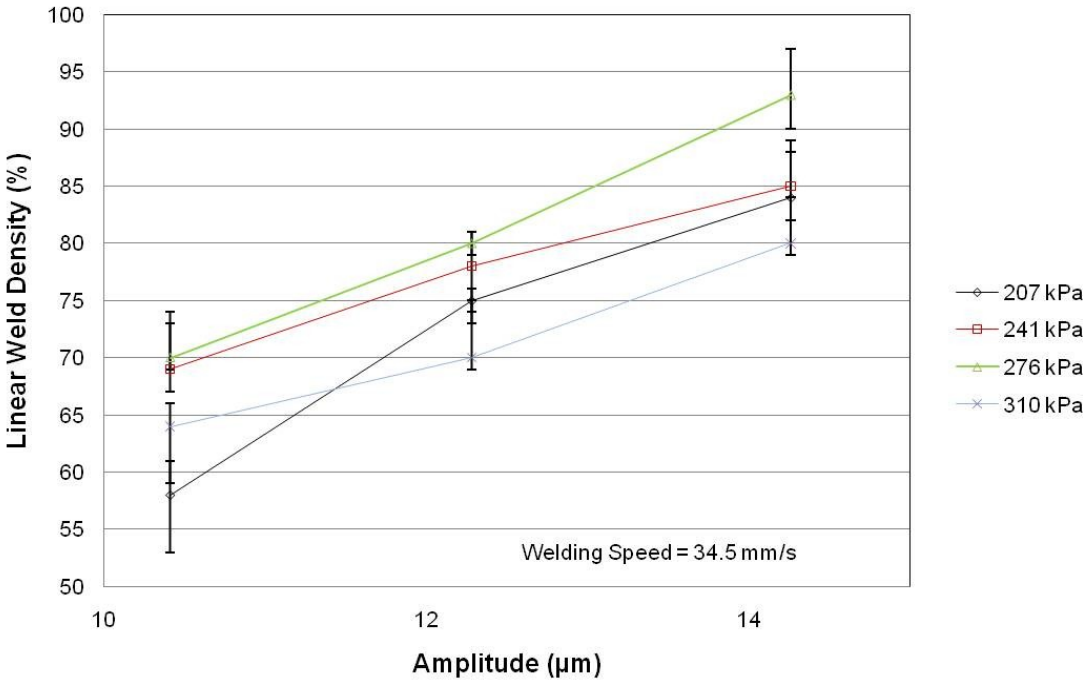

Figure 49 - Linear weld density of aluminium 3003 (T0) ultrasonically consolidated monolithic samples produced using a welding speed of 34.5 mm/s

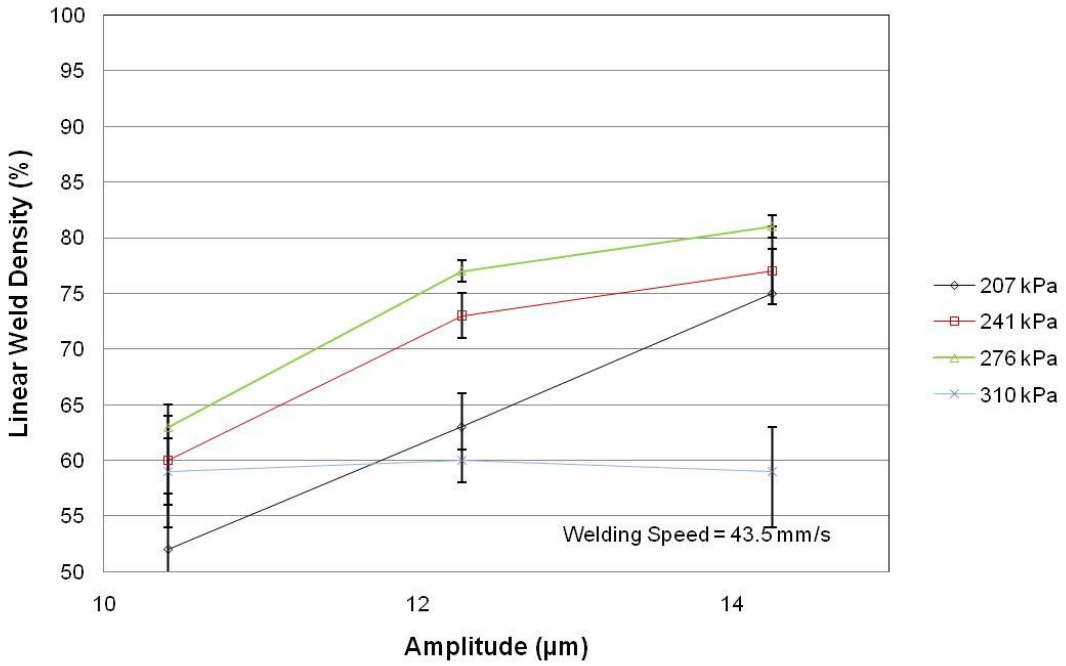

Figure 50 - Linear weld density of aluminium 3003 (T0) ultrasonically consolidated monolithic samples produced using a welding speed of 43.5 mm/s

Results from the peel strength analysis and LWD corresponded with greater LWD resulting in greater peel strength of the samples. This suggests that a higher amplitude and/or pressure and/or lower speed created a more dense interlaminar structure between the foil layers with greater strength being achieved.

6.3.3 Microscopy of Post Peel Tested Interlaminar Surface

The optical microscopy of the post peel tested sample surface was successfully carried out. Figure 51 depicts a typical example of the structure found in the interlaminar region of the post peel tested Al 3003 (T0) samples.

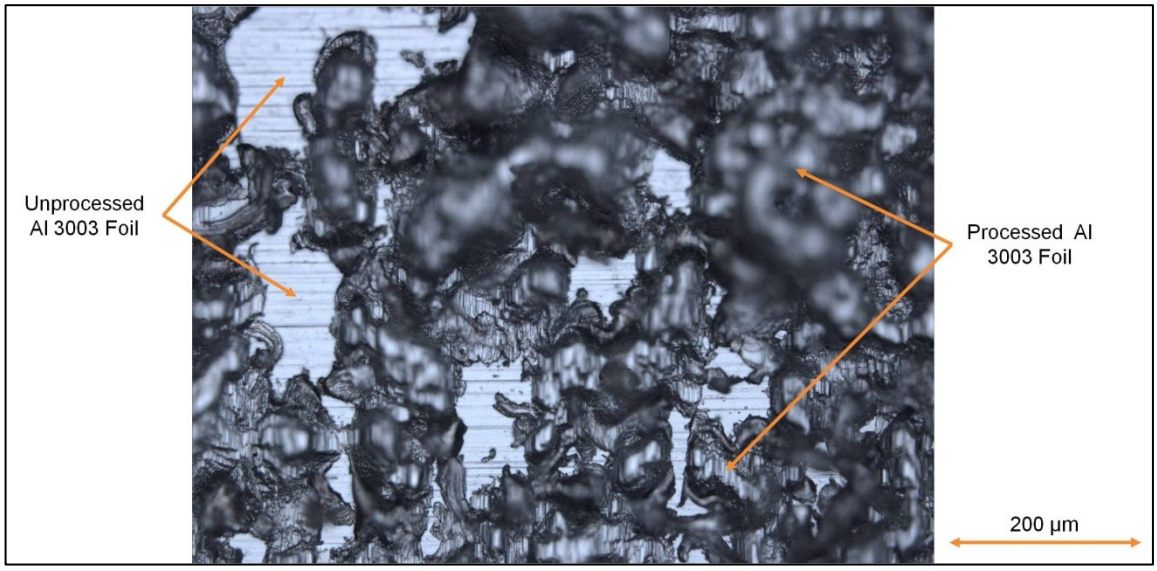

Figure 51 – An optical micrograph of a typical aluminium 3003 (T0) interlaminar ultrasonically consolidated surface showing altered and unaltered foil regions

Figure 51 highlights the finding that post-peel testing there was foil material that did not visually appear to have been in contact with the UC machine sonotrode or the opposing foil material. By using a conglomeration of micrographs a 3D representation of the typical interlaminar structure was generated (Figure 52). This highlighted the peak and trough nature of the interlaminar UC surface and identified a region of the samples that were apparently virgin foil like in their appearance suggesting these regions were not involved in the UC bonding process.

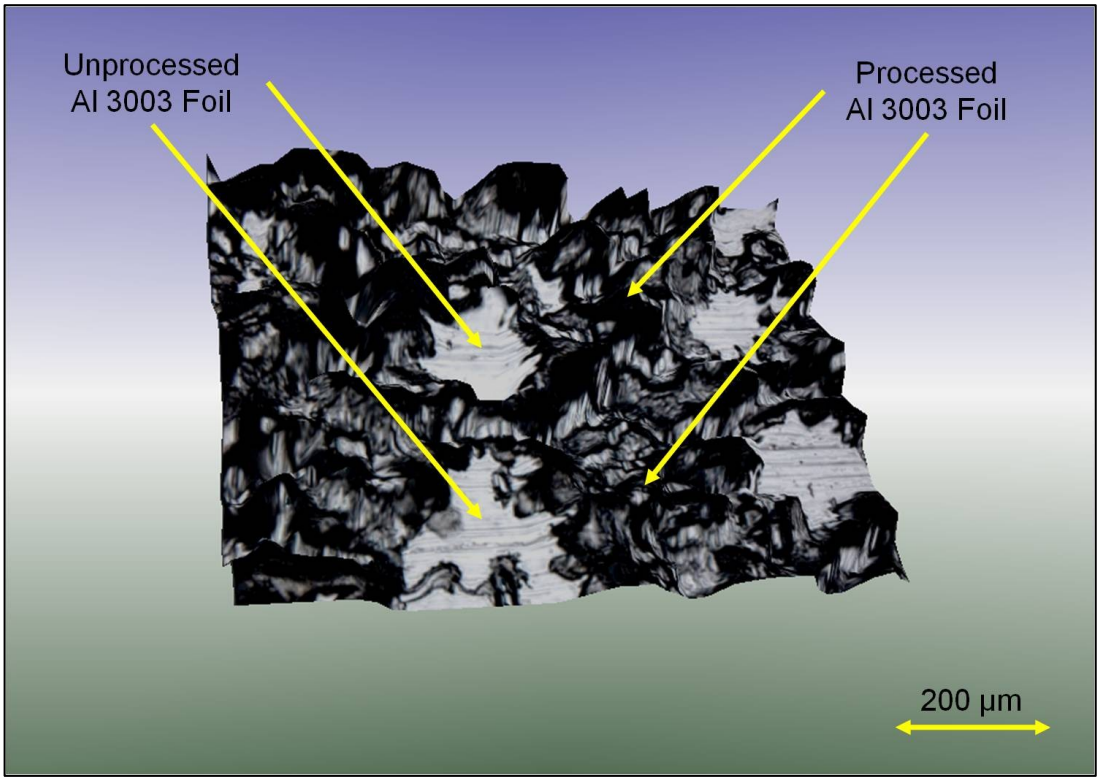

Figure 52 – A three dimensional optical micrograph of a typical Al 3003 (T0) interlaminar ultrasonically consolidated surface showing altered and unaltered foil regions

The comparison of processing parameters to this virgin like structure (Figure 53 and Figure 54) showed that higher pressure, higher amplitude and slower speeds resulted in a surface composed of smaller areas of unaltered virgin like material. This indicated that increasing the UC processing amplitude and pressure while reducing speed involved more of the foil surface in the UC bonding process which could be identified through a greater LWD; higher peel strength and smaller virgin like material areas, post peel testing.

The characterisation of this interlaminar structure in microscopic detail added new data to the UC area and contributed in a published paper by the author (Friel, et al., 2010).

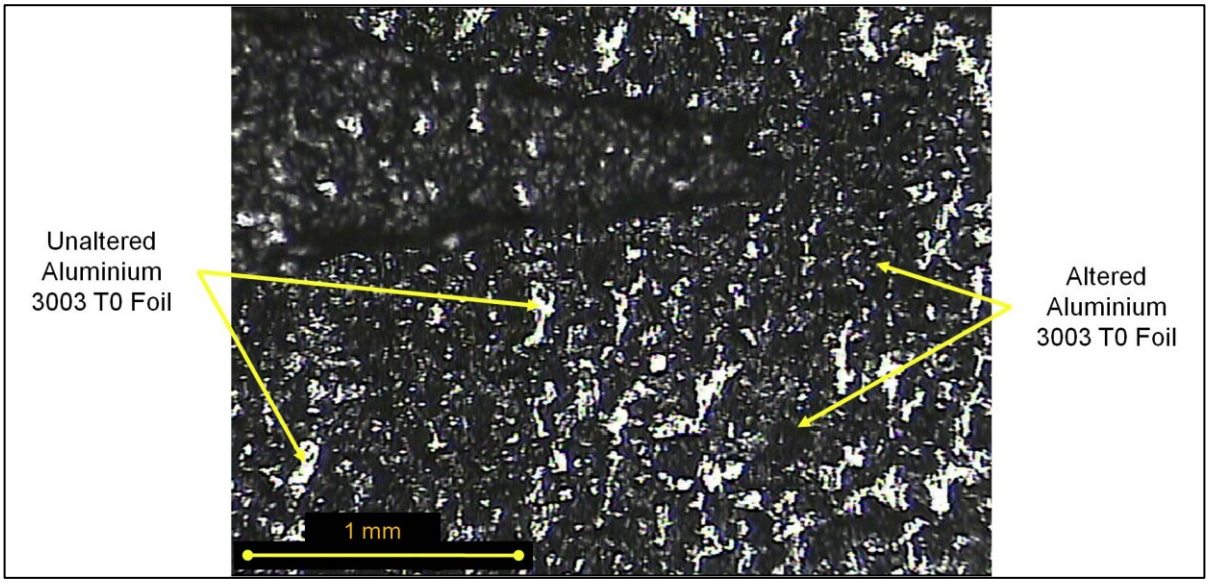

Figure 53 – An optical micrograph at 5x magnification of an aluminium 3003 (T0) interlaminar ultrasonically consolidated surface produced using 10.41 µm amplitude and 241 kPa welding pressure showing altered and unaltered foil regions

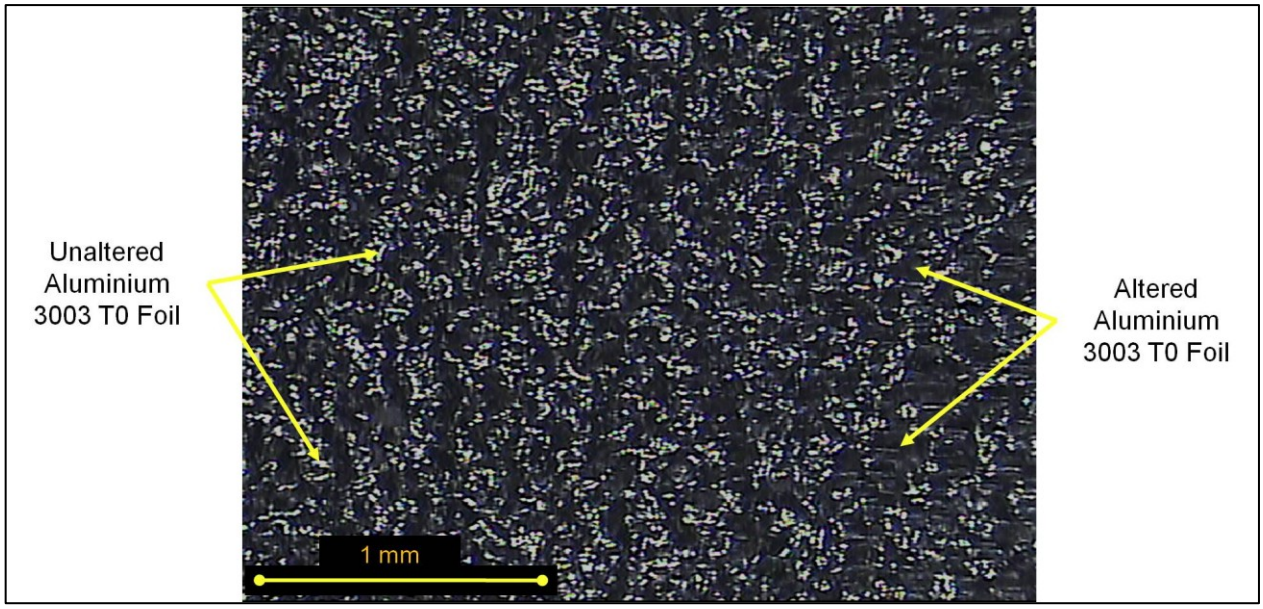

Figure 54 - An optical micrograph at 5x magnification of an aluminium 3003 (T0) interlaminar ultrasonically consolidated surface produced using 14.26 µm amplitude and 276 kPa welding pressure showing altered and unaltered foil regions

6.3.4 Post Peel Tested Interlaminar Surface Roughness Mapping

The optical surface profiling of the interlaminar surfaces of Al 3003 (T0) peeled samples was successfully carried out. The profiles showed that as the processing amplitude and welding pressure were increased and the speed decreased the surface became smoother and more uniform in its overall processed area. The full results for the measured surfaces are presented in: Table 7, Figure 55, Figure 56, Figure 57, Figure 58 and Table 8.

Sonotrode Amplitude (μm)	**Welding Pressure (kPa)**	**Average R_a (μm)**	**Average R_q (μm)**
10.41	207	5.03	6.77
	241	4.81	6.70
	276	4.76	5.88
	310	5.44	7.02
12.28	207	4.88	6.72
	241	4.22	6.66
	276	4.28	5.72
	310	5.25	6.82
14.26	207	4.85	6.29
	241	4.13	6.45
	276	4.14	5.70
	310	5.20	6.74
As-Rolled Foil	N/A	0.09	0.11

Table 7 – Average aluminium 3003 (T0) interlaminar R_a and R_q measurements for various ultrasonic consolidation process parameters at 34.5 mm/s welding speed

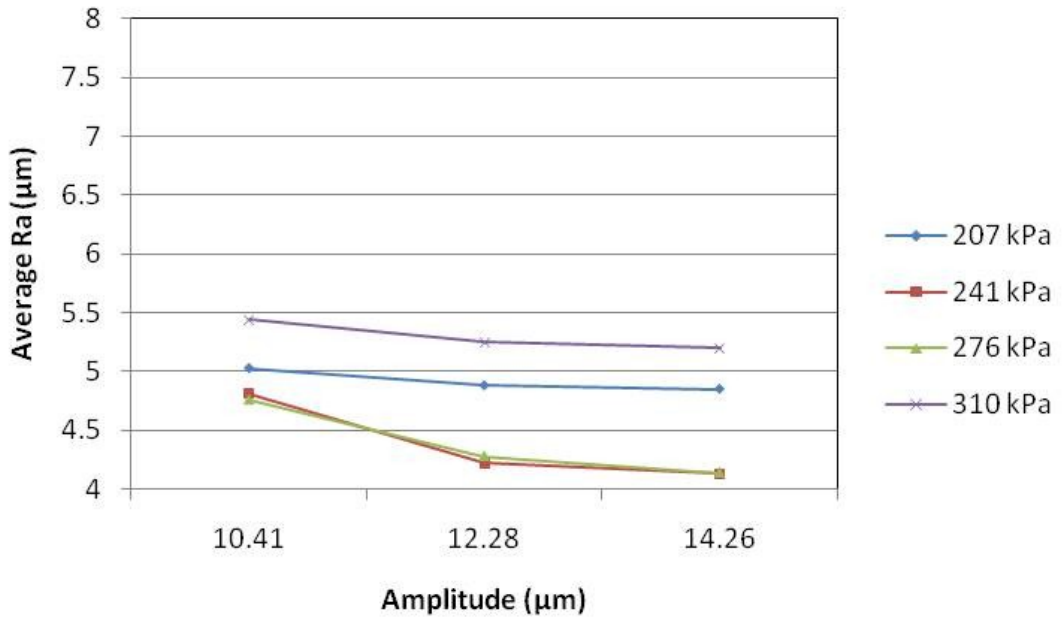

Figure 55 - Average aluminium 3003 (T0) interlaminar Ra measurements for various ultrasonic consolidation process parameters at 34.5 mm/s welding speed

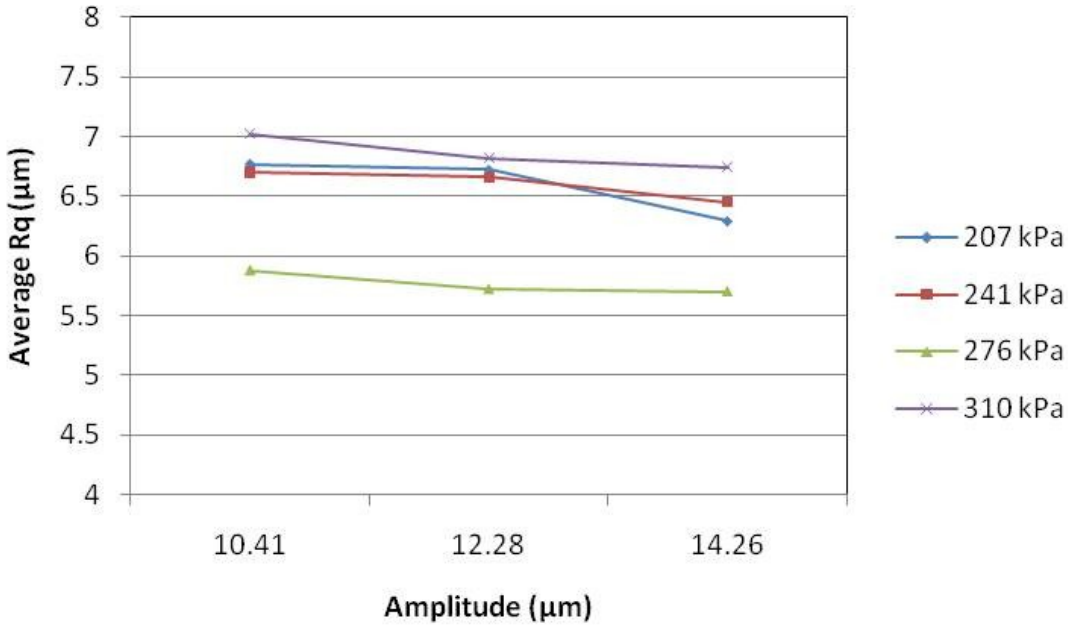

Figure 56 - Average aluminium 3003 (T0) interlaminar Rq measurements for various ultrasonic consolidation process parameters at 34.5 mm/s welding speed

Sonotrode Amplitude (μm)	Welding Pressure (kPa)	Average R_a (μm)	Average R_q (μm)
10.41	207	5.49	7.03
	241	5.37	6.99
	276	5.24	6.53
	310	5.84	7.36
12.28	207	5.29	6.92
	241	5.22	6.78
	276	4.87	6.32
	310	5.25	7.09
14.26	207	5.21	6.89
	241	5.03	6.52
	276	4.71	5.86
	310	5.20	7.90
As-Rolled Foil	N/A	0.09	0.11

Table 8 - Average aluminium 3003 (T0) interlaminar R_a and R_q measurements for various ultrasonic consolidation process parameters at 43.5 mm/s welding speed

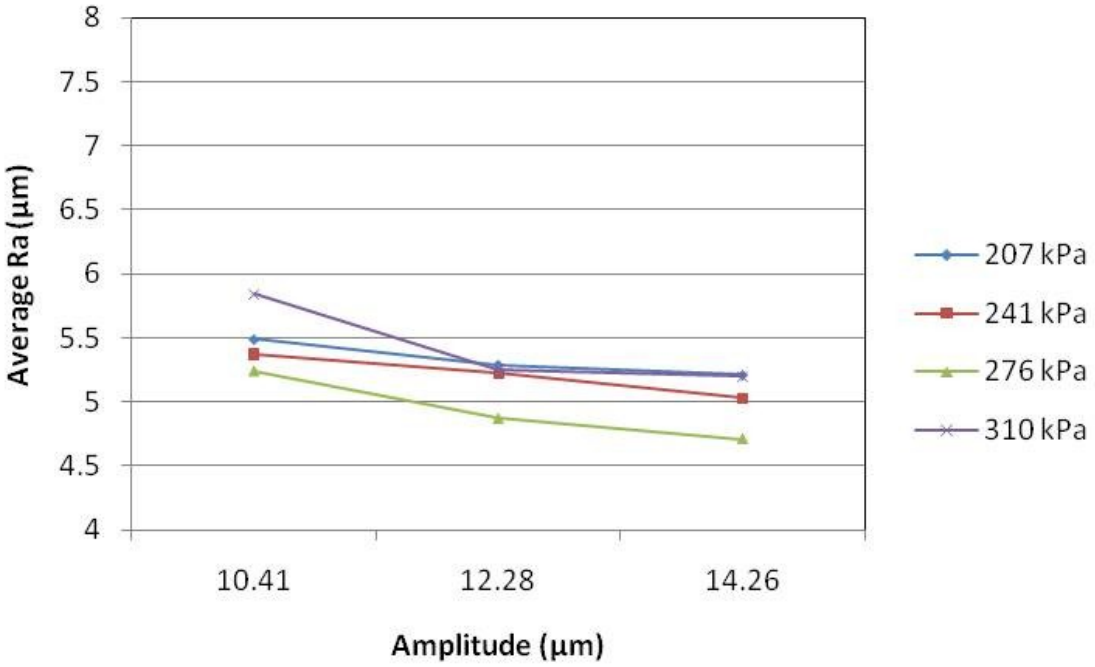

Figure 57 - Average aluminium 3003 (T0) interlaminar Ra measurements for various ultrasonic consolidation process parameters at 43.5 mm/s welding speed

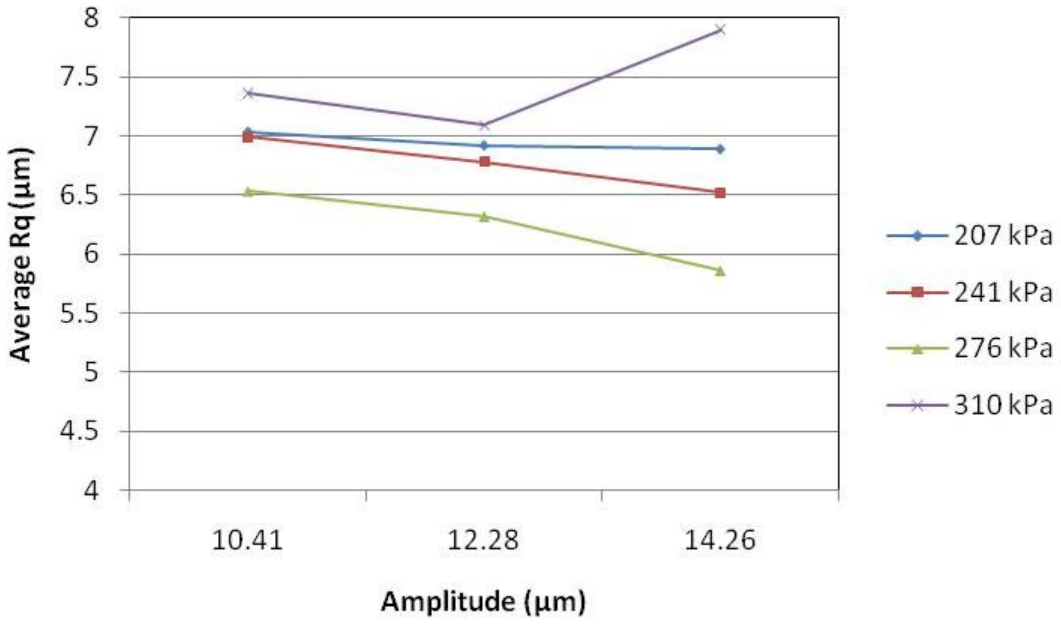

Figure 58 - Average aluminium 3003 (T0) interlaminar Rq measurements for various ultrasonic consolidation process parameters at 43.5 mm/s welding speed

Figure 59 shows a typical surface profile of a sample produced at a lower amplitude and contact pressure. The surface could be seen to have a region of dark blue where the surface was relatively deformed; this corresponded to troughs identified in section 6.3.3.

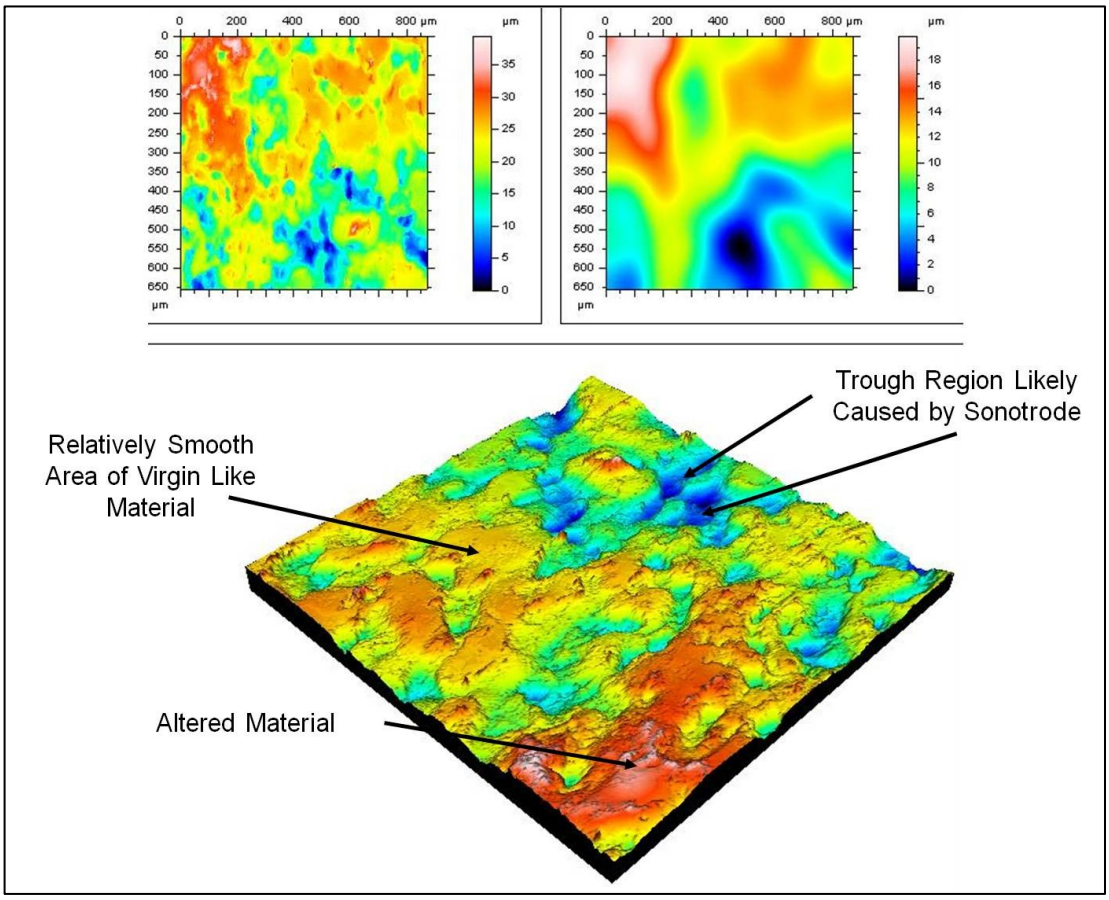

Figure 59 – Surface profile of the interlaminar region for an aluminium 3003 (T0) sample produced via the parameters: 10.41 µm, 241 kPa 34.5 mm/s

Figure 60 shows a typical surface profile of a sample produced at a higher processing amplitude and contact pressure. The profile showed that the overall surface roughness was lower and there were fewer regions of the relatively deep troughs representing the deformed material.

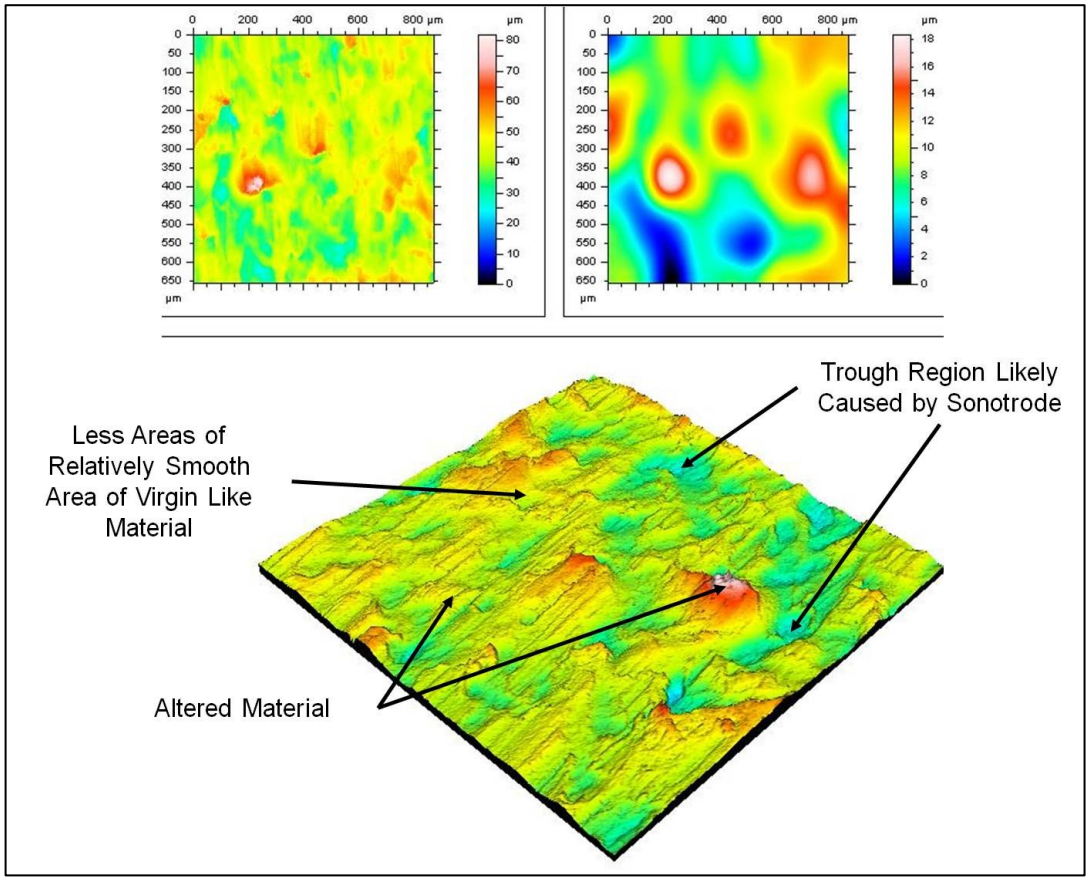

Figure 60 - Surface profile of the interlaminar region for an aluminium 3003 (T0) sample produced via the parameters: 14.26 µm, 276 kPa 34.5 mm/s

Figure 61 shows a typical surface profile of a sample produced at the same levels of high processing amplitude and contact pressure, and also with a higher speed. The surface showed that the overall surface roughness was higher and there were more regions, (compared to Figure 60), of the relatively deep troughs representing the sonotrode deformed material. This indicated that increasing the welding speed increased the area of unbonded foil and thus resulted in a lower LWD and hence lower peel strength.

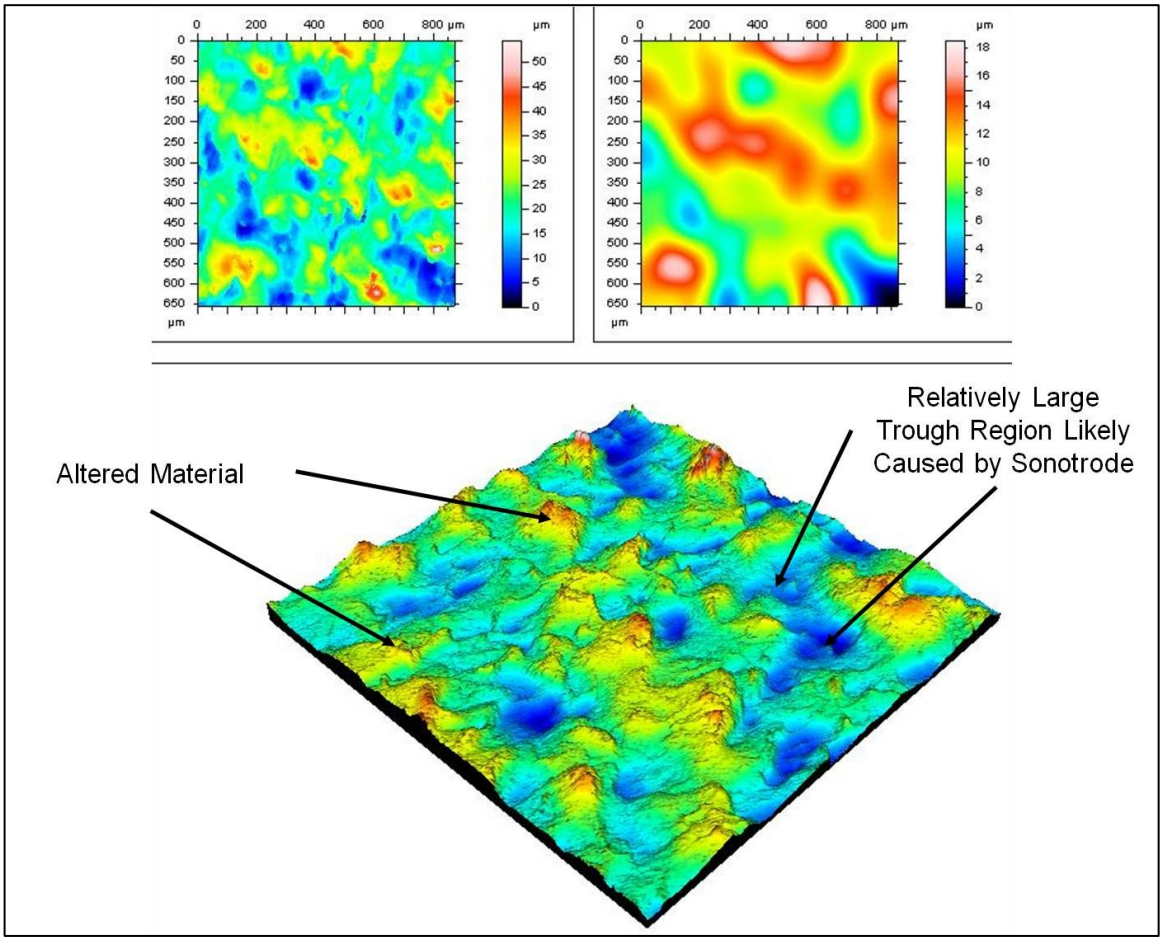

Figure 61 – Surface profile of the interlaminar region for an aluminium 3003 (T0) sample produced via the parameters: 14.26 µm, 276 kPa 43.5 mm/s

The interlaminar surface mapping of UC samples for variable processing variables was a unique piece of research in the UC area and significantly contributed data to the authors published paper (Friel, et al., 2010).

6.3.5 Post Peel Tested Interlaminar Material Hardness

The interlaminar material hardness testing using a Vickers microhardness machine was performed for the samples produced using the process parameters in Table 5. Performing the measurements highlighted issues in the limitations of the equipment being used. Due to the highly uneven surface caused by sonotrode contact and peel testing, (see sections 6.3.3 and 6.3.4), the accurate placement and uniform load application for the diamond indenter was not possible. The data collected showed the Vickers hardness could vary from ~20HV to ~140HV within a single sample. It was not

possible to state if these values were correct since it was observed during indentation that, due to the highly uneven surface roughness, lateral material displacement was occurring. This lateral displacement of the surface 'peak' resulted in a partial indentation of the sample and/or measurement of a flatter region adjacent to the material peak. As it was theorised that the peak was the material that would have undergone the greatest level of work hardening during UC processing this inability to accurately measure the HV values of these peaks has resulted in the rejection of this data.

Using the Hall-Petch relationship, (Equation 5), dictates that if the foil material involved in the formation of bonding at the foil/foil interface underwent grain structure refinement then this would result in a harder material.

$$\sigma_y = \sigma_0 + k_y d^{-1/2}$$

Equation 5 –Hall-Petch Equation (Furukawaa, et al., 1996)

Where σ_y is the yield stress of the material, d is the grain size, σ_0 is the friction stress and k_y is a constant of yielding.

The issue of the 'peak' material in the UC bond being harder than subsequent foil layer deposition has implications in terms of fibre embedding as a hard 'peak' will be more resilient to yielding thus presents an uneven and anisotropic material into which fibre embedding would take place.

6.3.6 Summary of Interlaminar Surface Results

Li, D. and Soar, R. (Li, et al., 2009) showed that a lower roughness, (3.44 μm R_a in their case), sonotrode topology can result in inadequate bonding during UC; this was thought to be due to the lack of ultrasonic energy transfer into the foil material due to a high level of sonotrode slippage and energy loss when compared to a rougher material. The present work combined with additional published work by the author (Friel, et al., 2010) suggests that the sonotrode material texturing effect is of fundamental importance to the quality of components produced via UC.

Generally, the higher the LWD, the higher the peel strength of UC samples was found to be. The optical microscopy and surface profiling signified that when a relatively constant

sonotrode topology was used, then the process parameters of amplitude, welding pressure and welding speed had a significant effect on the interlaminar topology and bond density created during UC. An increase in weld force and amplitude and a reduction in welding speed revealed that the un-bonded foil areas, shown to be present in the UC interlaminar region, were reduced in maximum size but increased in number. This suggested that these three processing parameters had the effect of creating a more intimate contact between the foil layers during UC processing which resulted in a residual interlaminar bond of lower void volume.

The LWD was not found to vary for the start middle and finish regions of the UC samples. This suggested that the weld density, although variable in analysed cross-sections, did not differ significantly along the total length of the bond.

Using the welding pressure of 310 kPa did not improve LWD and peel strength compared to 276 kPa. The postulated theory for this was the relatively high weld pressure resulted in a reduction in the relative oscillatory motion and/or frequency of the sonotrode due to elevated levels of contact friction between the sonotrode and anvil/sample. This reduction in oscillatory motion would lower the relative motion of the unprocessed foil with the previously processed foil, which could result in a reduction in bonding density achieved.

The LWD was shown to increase with processing amplitude and weld pressure for samples welded at 34.5 mm/s and 43.5 mm/s. This increase was shown via interlaminar microscopy and surface profiling. The greater the processing amplitude used, the smaller the unprocessed foil areas within the sample became. This reduction in unprocessed material led to a greater LWD and hence an improved peel test performance. A reason that the higher amplitude created this more refined peak and valley profile was possibly due to the greater lateral movement of the sonotrode creating a wider surface to surface contact area between the sonotrode and the upper foil layer. The foil to foil contact area was also maximised due to the greater lateral movement of the second foil layer over the first. This greater lateral movement combined with greater weld force resulted in a smoother interlaminar topology and therefore a greater foil surface to surface real area of contact.

During peel testing the samples with the smaller void areas and hence more contact points resulted in a greater resistance to tear propagation within the material. This was evident from the ‘tear teeth’ profile created when the sample failed during peeling. The samples with the smoother interlaminar topology resulted in a more brittle failure with only small teeth patterns, where as the samples with greater unprocessed foil areas resulted in tear teeth patterns that were more pronounced and indicated a more ductile failure mode.

From the surface profiles it was evident that the ‘peak and valley’ surface created by the sonotrode on the foil was complex and variable. This variability helped explain the high variance when calculating the LWD using perpendicular mounted sections.

In addition to the variation of LWD there was also a discrepancy between the area of the unaltered foil material present in the interlaminar microscopy and surface profiling when compared to the LWD. The microscopy and surface profiling of the post peel tested samples displayed an area of unaltered foil that exceeded all the LWD measurements for the sample processing parameters. There was a possibility that during the UC bonding process the peak material was bonding to the new foil layer however this layer also undergoes a relatively high level of plastic flow that allowed the foil to ‘fill’ the voids (troughs) and press against the unaltered foil areas of the previous foil layer. This plastic flow was not coupled with sufficient oscillatory motion and pressure to induce foil to foil bonding, however during cross-sectional optical microscopy the intimate contact of the foils was observed as being a fully dense bond. When the samples were subsequently peeled this unbonded material was removed leaving the relatively virgin like foil.

Although the hardness measurements were unsuccessful the theory that the peak material was work hardened during the UC process implied that the material that fibres were being embedded onto was not of the same mechanical and topological properties of the virgin foil material. This however remains only a theory as the data to back up the theory was not achieved in this instance.

The investigation into the interlaminar surface created via UC had shown that there was a more complex surface to fibre interaction taking place during fibre embedding due to

the sonotrode contact with the Al 3003 T0 prior to fibre embedding. To study in detail what these interactions were an experimental methodology was devised.

7 Microstructural and Mechanical Interactions at the Fibre to Matrix Interface due to Ultrasonic Consolidation

7.1 Introduction

Research into the microstructure encountered at the UC foil/foil bond interface (Johnson, 2008) has shown the unique insights that the Dual Beam Focussed Ion Beam (DBFIB) process could offer in terms of cross-sectioning and visualising material grain structures. The same insight was expected to be possible at the fibre/matrix interface of a UC MMC using DBFIB. A methodology to analyse the fibre/matrix interface in detail via the use of DBFIB was designed for this purpose.

The fibre volume experimentation (Section 4) had suggested that the maximum plastic flow of the Al 3003 matrix was not the cause of sample failure which was instead attributed to the number of fibres being embedded. The use of larger diameter fibres in fewer numbers may allow for greater volume fractions to be achieved. To test this theory fibres of diameters greater than 100 μm were embedded and the subsequent effect on the matrix was determined via the use of optical microscopy, Scanning Electron Microscopy (SEM), and DBFIB.

7.2 Methodology

7.2.1 Fibre Sample Manufacture

To ensure that the effect of the main UC process parameters, as well as the fibre volume size, were taken into account Al 3003 (T0) samples containing 10 SMA fibres

were manufactured using a variety of UC processing parameters. The UC processing parameters used are detailed in Table 9. For each set of parameters three SMA/Al samples were produced. Each of these samples had 10 embedded fibres of the same diameter, either: 50, 100, 150, 250 or 375 μm. The manufacturing procedure using the various process parameters was the same as in section 4.2.1.

All SMAs were pre-strained prior to being embedded as Kong (Kong, 2005) had identified that UC process parameters from the higher end of the identified processing window could possibly be inducing the SME. To ensure this did not occur in the present work the SMA fibres were extended from 200 mm to 210 mm, (5% extension, the recommended value by the manufacturer), using a Lloyd Instruments LRX material testing machine (Figure 31) prior to being embedded into the Al 3003 (T0) foil matrix.

Welding Speed (mm/s)	Sonotrode Amplitude (μm)	Welding Pressure (kPa)
34.5	10.41	241
		276
		310
	12.28	241
		276
		310
	14.26	241
		276
		310
43.5	10.41	241
		276
		310
	12.28	241
		276
		310
	14.26	241
		276
		310

Table 9 - The combinations of processing parameters used to produce the varying fibre diameter ultrasonically consolidated test samples

7.2.2 Mechanical Peel Testing of Various Fibre Diameter Containing Samples

The peel testing was carried out in the same method as in section 4.2.4. The peel testing allowed for bond quality to be quantitatively analysed by assessing a samples average resistance to peeling for the given weld interface. The effect of the diameter of the embedded fibres and the process parameters in combination on the maximum peel load was quantified.

To factor in the effects of the main UC process parameters and fibre volume Al 3003 (T0) samples containing 10 SMA fibres were manufactured using a variety of UC processing parameters. The UC processing parameters used are detailed in Table 9.

7.2.3 Optical Analysis of Fibre to Matrix Interface

As in section 4.2.3 a sample for each of the variations was sectioned perpendicular to the longitudinal direction of the fibre using a cutting disc. This was to allow for a qualitative analysis of the fibre/matrix interface. The sectioned SMA Al MMC was, after sectioning, mounted in Buehler Konductomet 1 thermosetting polymer and then ground, polished and stored as in section 4.2.3. The reason for using Konductomet 1 in place of Buehler Varidur was that this material was electrically conductive due to a significant inclusion of carbon black and thus it was suited to the electron and ion based analysis techniques in the future sections of this study.

The samples were analysed using an Olympus BX60M microscope with a QImaging Micropublisher 3.3MP digital camera for image capture. Images were captured at magnifications of 5x, 20x, 50x and 100x.

7.2.4 Electron and Ion Beam Analysis of Fibre to Matrix Interface

Using Johnson's research (Johnson, 2008) as a guide to the possibilities of DBFIB for UC investigation, new insight was thought to be possible at the fibre/matrix interface of a UC MMC. A methodology to analyse the fibre/matrix interface in detail via the use of DBFIB was designed for this purpose. The equipment used for the analysis via SEM and

DBFIB was a Nova 600 NanoLab, Ultra High Resolution (UHR) Field Emission Gun (FEG)- SEM/Focussed Ion Beam (FIB) machine (FEI Company™), Figure 62. The Nova 600 was able to be used to both ion mill and image selected areas at the fibre matrix interface of the SMA/Al 3003 (T0) samples as well as perform SEM analysis.

Figure 62 - Nova 600 NanoLab, ultra high resolution field emission gun-scanning electron microscope and focussed ion beam machine

Grain structure analysis of the fibre–matrix interface and the Al matrix adjacent to the fibre was performed by using a FIB to create a cross-section at an identified area. These areas were selected within and around the fibre trench, which was the deformed region that resulted from a SMA fibre being embedded into the Al matrix via UC and then removed after peel testing. For grain structure analysis of the fibre–matrix interface the SMA fibre was still embedded within the Al matrix so that a full structural analysis of both the Al and NiTi could be conducted simultaneously.

Previous research (Kong, et al., 2004) had not used DBFIB or UHR SEM analysis to observe the fibre–matrix interface. During the SEM and FIB analysis of the fibre–matrix interface, conducted in the present work, it was found that the fibre exhibited previously unidentified phenomena. As a cross-reference to the newly identified embedded SMA

fibre structure both SEM and FIB analyses were also performed on virgin (un-embedded) SMA fibre structures.

Fibre to Matrix Interface Analysis

The fibre containing samples used for identifying the grain structure at the fibre/matrix interface had been sectioned and mounted in Buehler Konductomet 1 thermosetting polymer and ground to the 1200 grit stage. FIB milling was conducted prior to SEM and FIB analysis. Due to high operational cost of FIB and the lengthy preparation time per sample, three samples for each of the parameters in Table 10 were produced and analysed.

SMA Fibre Diameter (μm)	Sonotrode Amplitude (μm)	Contact Pressure (kPa)	Welding Speed (mm/s)
100	12.28	276	34.5
	14.26	310	34.5
250	12.28	276	34.5
	14.26	310	34.5
375	12.28	276	34.5
	14.26	310	34.5

Table 10 - The combinations of processing parameters used to produce the varying fibre diameter ultrasonically consolidated test samples for focussed ion beam/scanning electron microscope analysis

The interface to the left and right of the embedded SMA fibres (Figure 63) was analysed by depositing a thin layer of Platinum (Pt), to protect the underlying structure during the ion milling process, and then using the Gallium (Ga^+) FIB to machine away the Al 3003 and SMA fibre (Figure 64). The milled pit was approximately 30 x 30 x 30 μm and allowed for SEM and FIB imaging of the high ion polished surface at the SMA/Al 3003 (T0) interface.

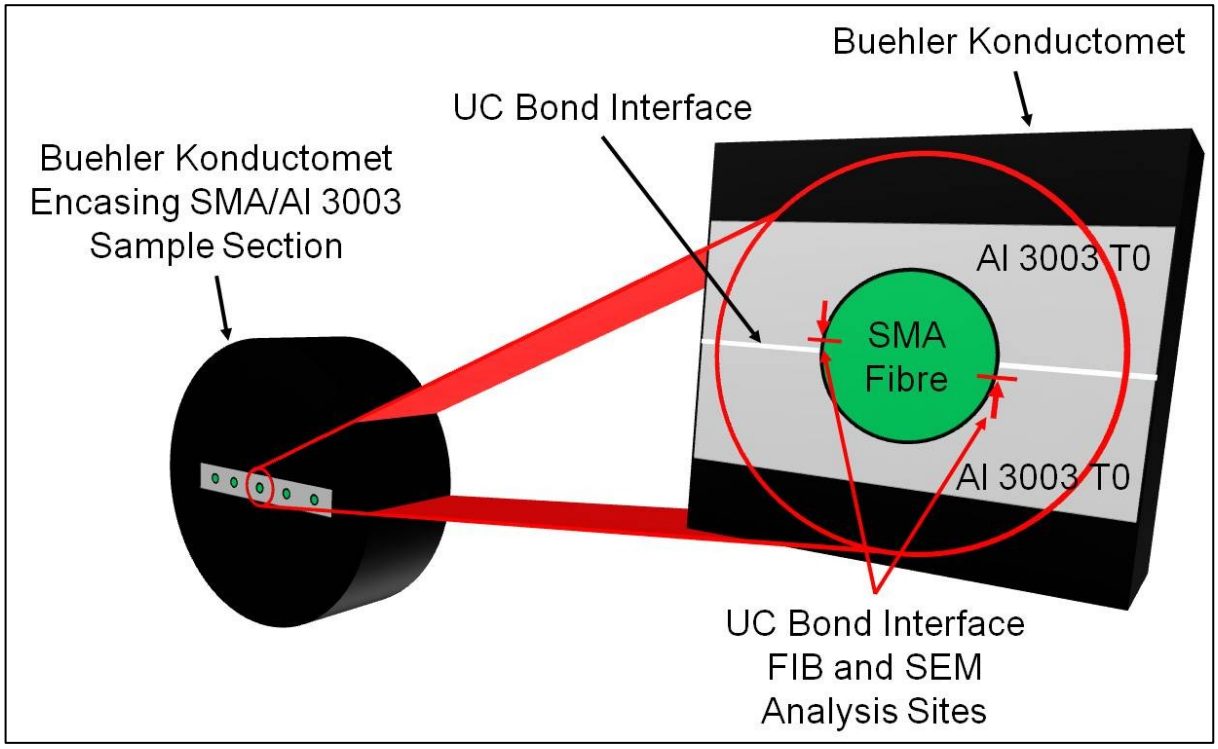

Figure 63 – Schematic of the fibre/matrix interface analysis area

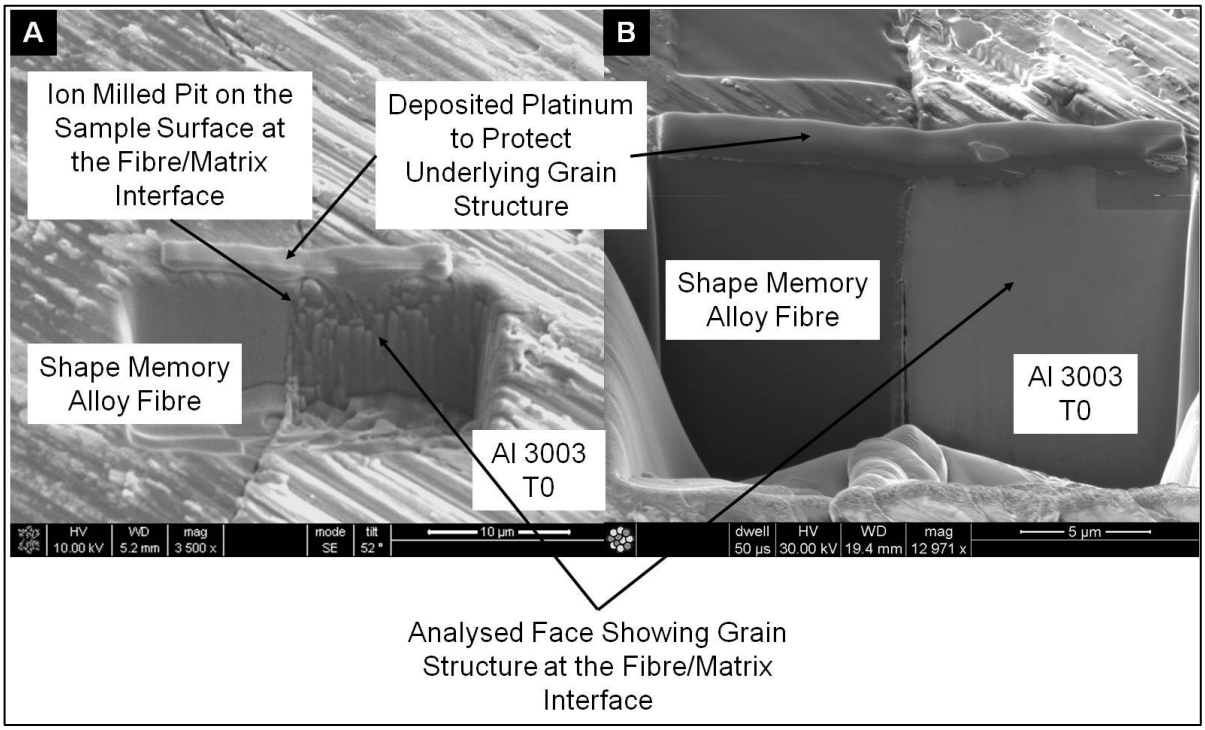

Figure 64 - Example scanning electron microscopy and focussed ion beam images of the fibre/matrix analysis A) Post platinum deposition during ion milling B) post ion milling

Adjacent Matrix Analysis

Due to the relatively small image width available using the FIB cross-sectioning process a more inclusive image of the grain structure at the fibre matrix interface would require cross-sectioning perpendicular to the longitudinal line of the fibre lay. Owing to the relatively large volume of material above and below the fibre/matrix interface (~100 µm and ~300 µm respectively) it was unfeasible to mill a cross-sectional pit via FIB to the SMA/Al interface. To overcome this issue the SMA/Al sample was sectioned (Figure 65 - Step 1) and separated, and the SMA fibre removed (Step 2) at which point the third and fourth foil layers were mounted on a standard SEM stub with the SMA trench facing upwards (Step 3).

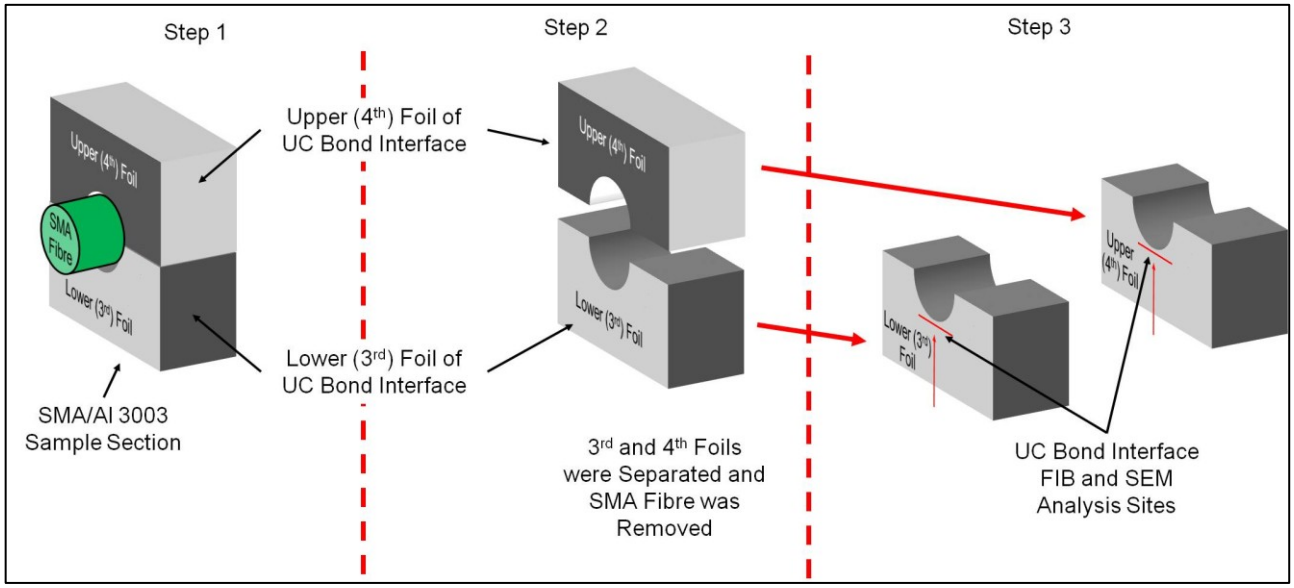

Figure 65 - Schematic of the adjacent matrix analysis focussed ion beam and scanning electron microscopy sample area

Both the upper, (Figure 66), and lower, (Figure 67), foil layers were analysed by depositing a thin layer of platinum, to protect the underlying structure during the ion milling process, and then using the Ga^+ ions to machine away the Al 3003. The milled pit was approximately 30 x 30 x 30 µm and allowed for SEM and FIB imaging of the high polished surface adjacent to the SMA/Al 3003 (T0) interface.

Due to high operational cost and preparation time per sample, one sample (one upper and one lower foil for each set of parameters) for each of the parameters in Table 10 was produced and analysed.

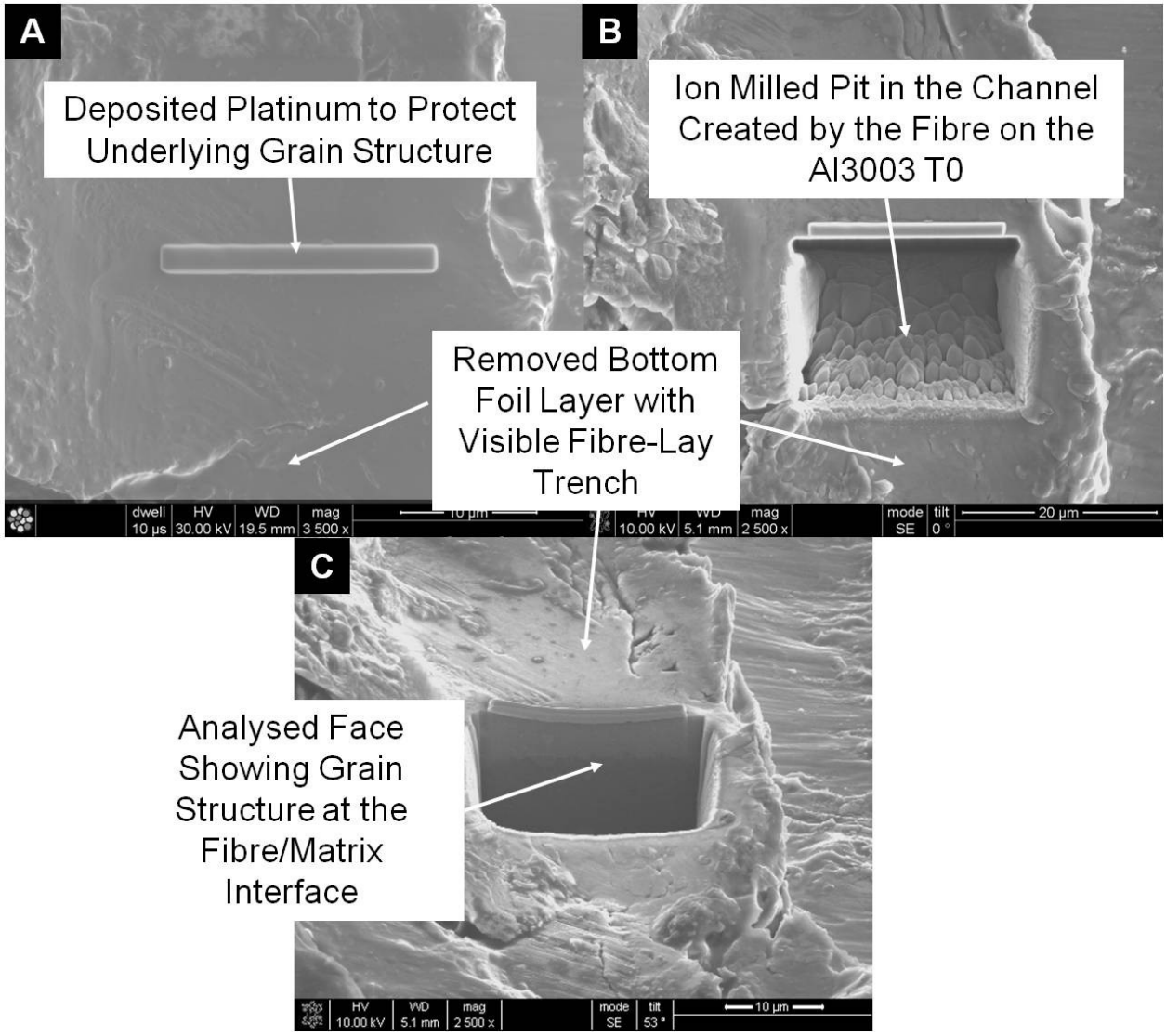

Figure 66 - Images highlighting the focussed ion beam cross sectioning procedure when analysing the fibre/matrix grain structure for the lower (3rd) foil layer: A) deposited platinum B) ion milling of observation pit C) the analysed face within the fibre created trench

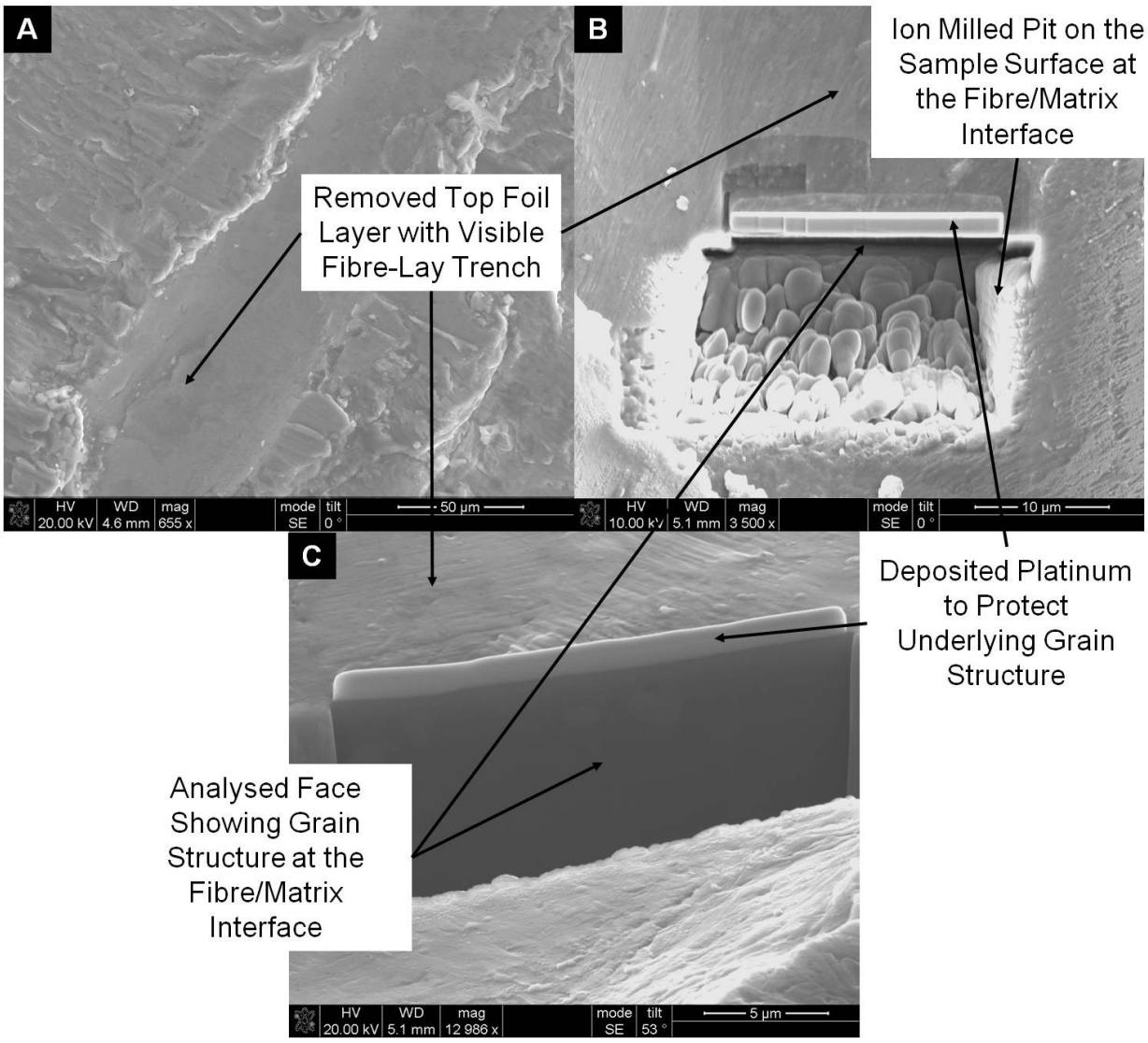

Figure 67 - Images highlighting the focussed ion beam cross sectioning procedure when analysing the fibre/matrix grain structure for the upper (4th) foil layer: A) deposited platinum B) ion milling of observation pit C) the analysed face within the fibre created trench

7.3 Results and Discussion

7.3.1 Peel Testing Results of Various Fibre Diameter Containing Samples

The manufacturing of the various fibre diameter samples was completed and the peel testing performed. The results of the analysis are detailed in Figure 68 to Figure 73.

Figure 68, Figure 69 and Figure 70 show the peel testing results for the various fibre diameter samples manufactured using a weld speed of 34.5 mm/s. The data highlighted that increasing the amplitude and weld pressure resulted in greater peel strength of the samples. For fibre diameters of 50, 100 and 150 μm the peel strength of the samples was reduced when compared to data from section **Error! Reference source not found.** and the increase in diameter from 50 to 150 μm had a progressively detrimental effect on the peel strength of the samples. This was not the case for 250 and 375 μm fibres. The addition of these fibres resulted in an increase to the peel strength of these samples. This result appears to run counter to the trend, however due to the greater level of plastic flow caused by the 250 and 375 μm fibres the foil/foil contact may have been increased which resulted in a higher strength UC sample.

This research into the effect of larger fibre diameters on the peel performance of UC matrices was a unique set of data which offered novel insight into the effects of larger fibre diameters on the UC matrix materials.

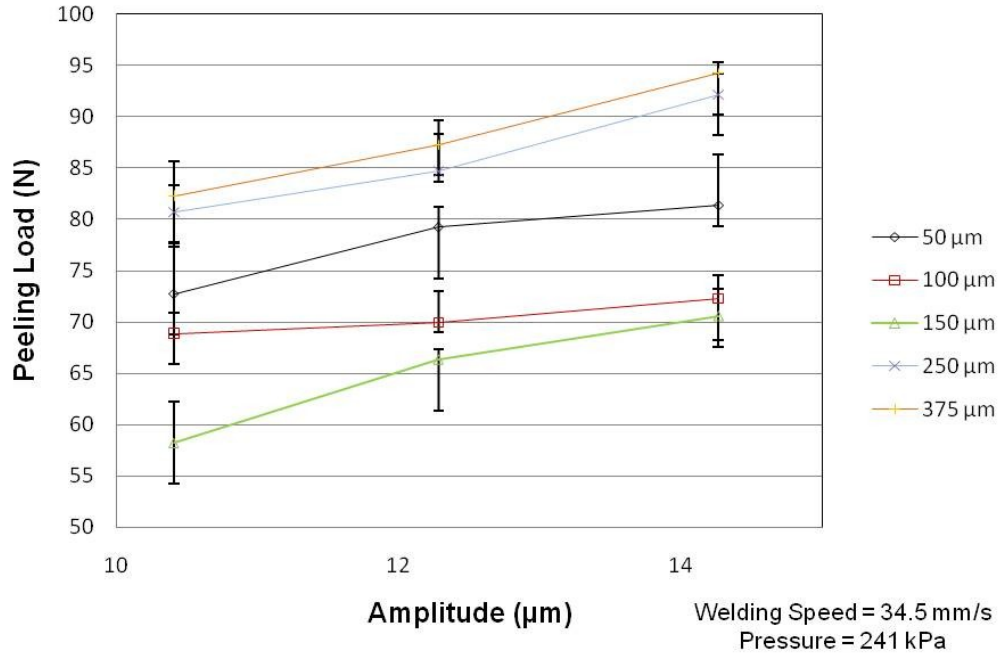

Figure 68 - The peel testing results for aluminium 3003 (T0) ultrasonically consolidated samples with ten embedded NiTi fibres of various diameter produced using welding speed of 34.5 mm/s and welding pressure of 241 kPa

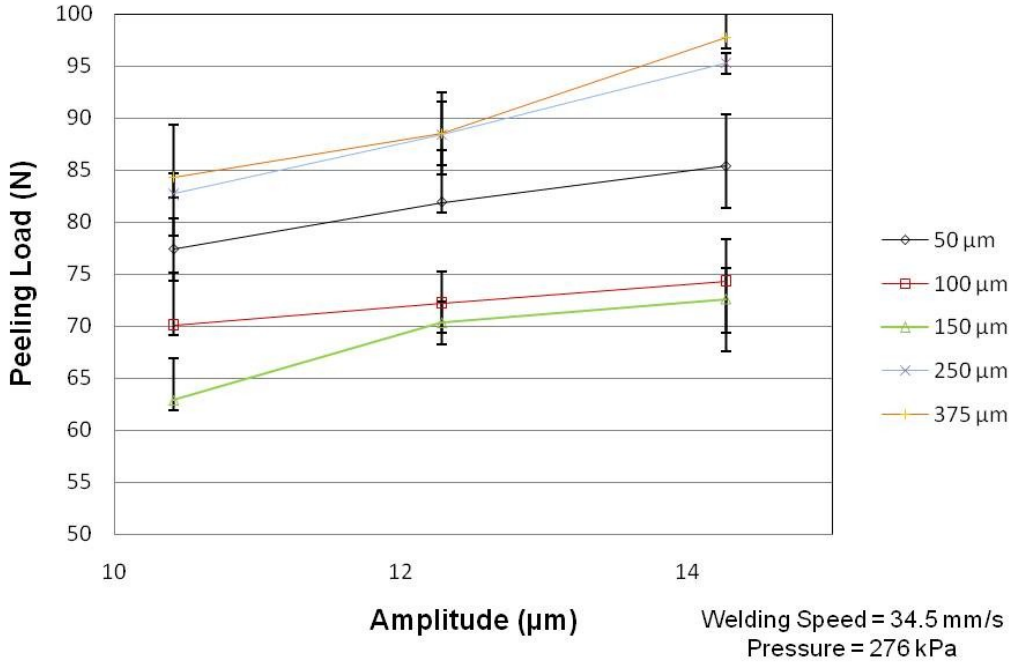

Figure 69 - The peel testing results for aluminium 3003 (T0) ultrasonically consolidated samples with ten embedded NiTi fibres of various diameter produced using welding speed of 34.5 mm/s and welding pressure of 276 kPa

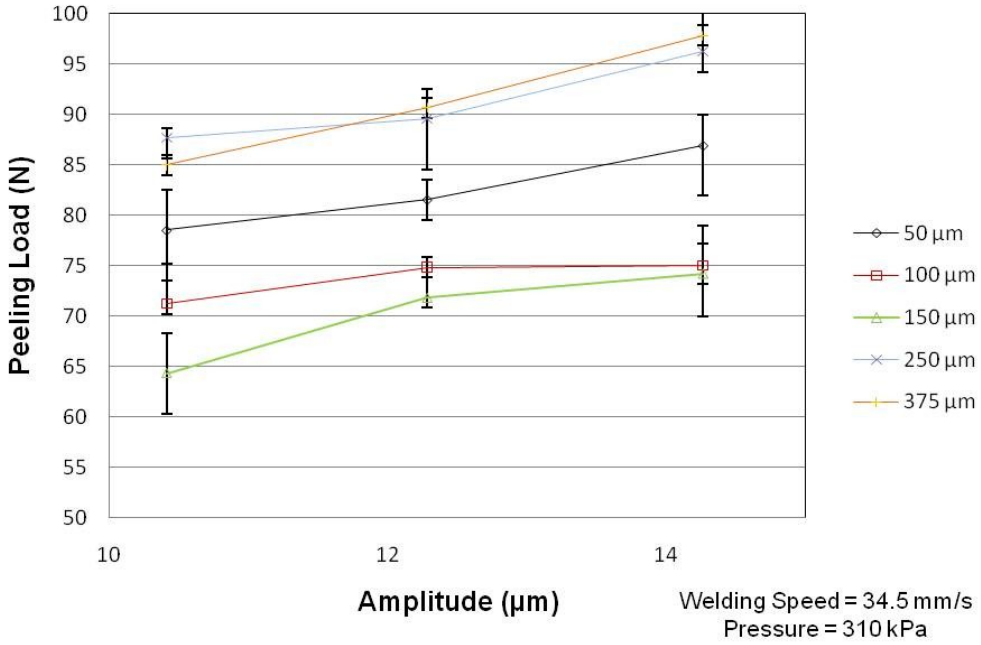

Figure 70 - The peel testing results for aluminium 3003 (T0) ultrasonically consolidated samples with ten embedded NiTi fibres of various diameter produced using welding speed of 34.5 mm/s and welding pressure of 310 kPa

Figure 71, Figure 72 and Figure 73 show the data obtained using the higher weld speed of 43.5 mm/s. This data demonstrated that increasing the welding speed had a negative effect on the peel strength of the fibre embedded samples. This was a similar effect as for the non-fibre containing samples suggesting that a reduction of ultrasonic processing time resulted in reduced flow around the embedded fibres and reduced bond strength.

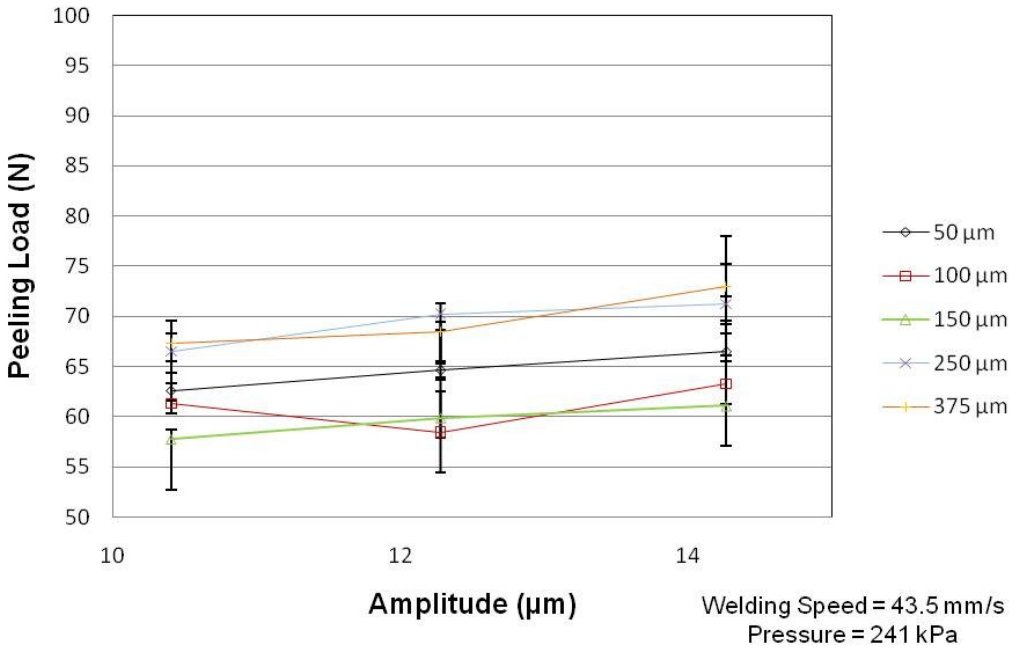

Figure 71 - The peel testing results for aluminium 3003 (T0) ultrasonically consolidated samples with ten embedded NiTi fibres of various diameter produced using welding speed of 43.5 mm/s and welding pressure of 241 kPa

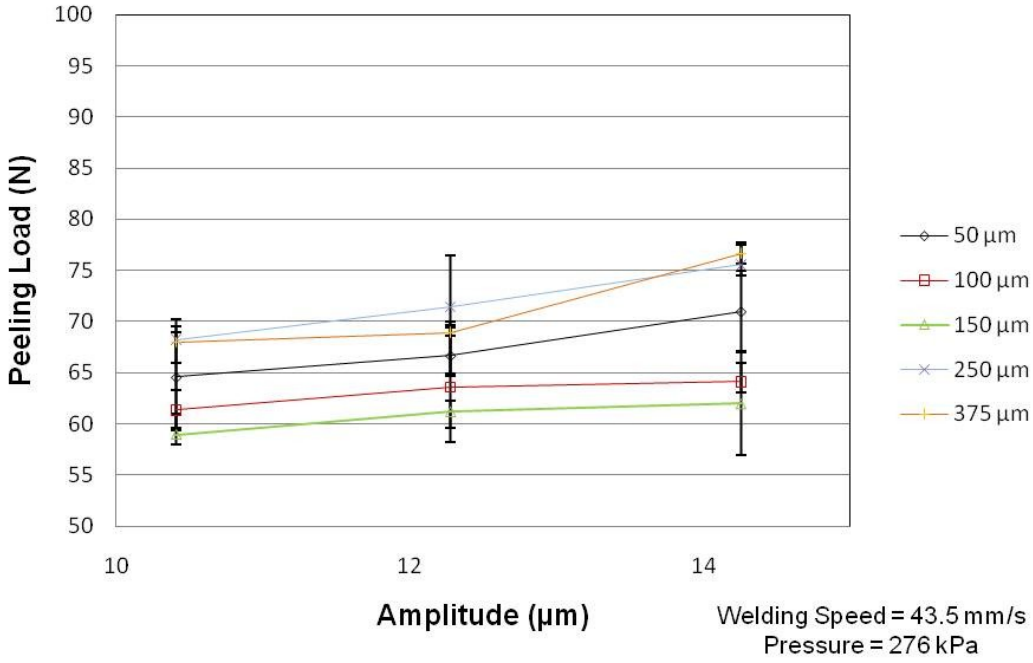

Figure 72 - The peel testing results for aluminium 3003 (T0) ultrasonically consolidated samples with ten embedded NiTi fibres of various diameter produced using welding speed of 43.5 mm/s and welding pressure of 276 kPa

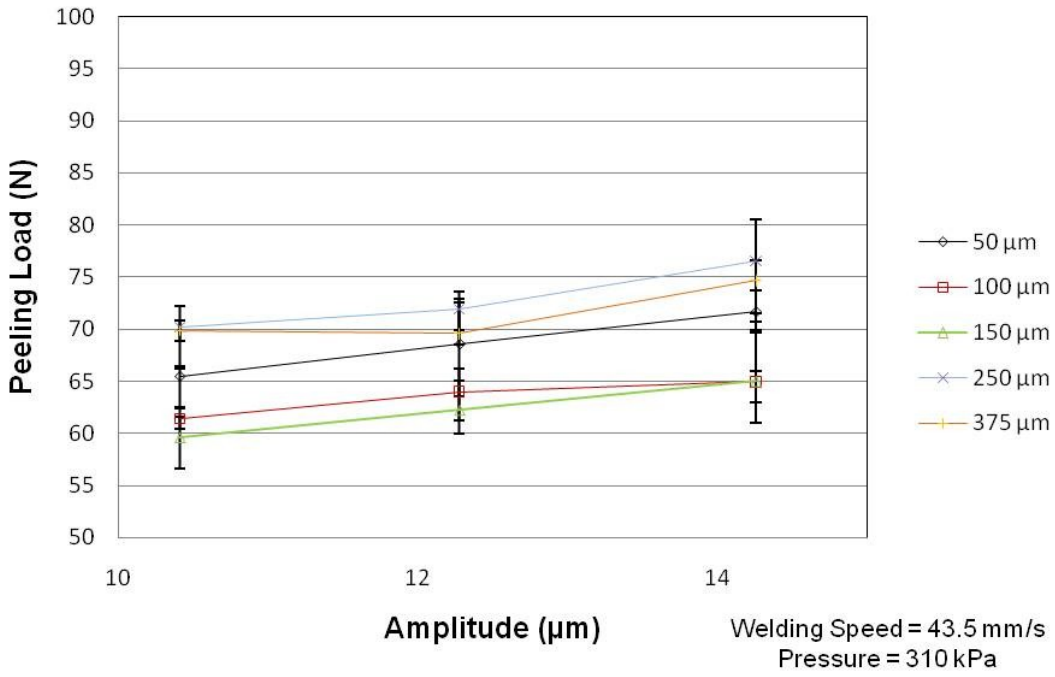

Figure 73 - The peel testing results for aluminium 3003 (T0) ultrasonically consolidated samples with ten embedded NiTi fibres of various diameter produced using welding speed of 43.5 mm/s and welding pressure of 310 kPa

The embedding of various fibre diameters and specifically the embedding of diameters greater than 100 µm raised the prospect of using fewer fibres of larger diameters to act as superior functional elements in a UC manufactured component. The greater fibre diameters have been shown to be possible and to also improve the peel strength of the Al 3003 (T0) samples. The ability to embed larger diameters of SMA fibres while still achieving a full integrity UC sample suggested that higher numbers of SMA fibres did not restrict the achievement of UC bonding due to the level of plastic flow they required from the matrix but due to impeding of the oscillatory motion of the matrix material between the fibres. With a greater number of fibres across the foil/foil interface the ability for the matrix material to have come into sufficiently high contact pressure and achieve sufficient oscillatory motion was reduced. By reducing the fibre numbers and increasing the fibre diameter the void between adjacent fibres could be at a sufficient size to allow foil/foil bonding to be possible. This represents useful, new, information in increasing actuation force (larger diameter fibres have larger maximum pull forces) from an SMA fibre embedded UC component.

7.3.2 Optical Analysis of Fibre to Matrix Interface

Optical analysis of the various fibre diameter samples was carried out. This showed that the plastic flow of the matrix around all the various fibre diameters was sufficient to create a largely void free interface between the matrix and fibres, (see Figure 74, Figure 75 and Figure 76).

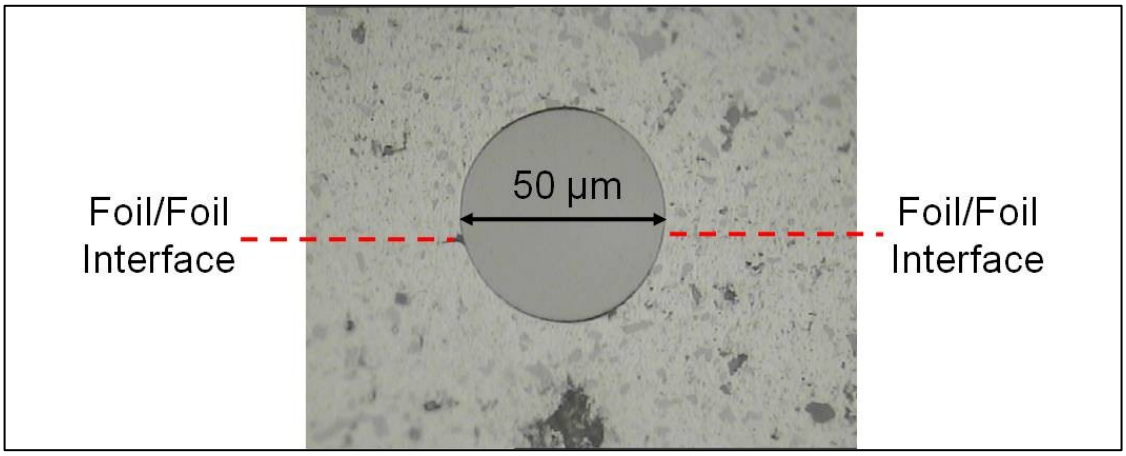

Figure 74 - A micrograph example of a 50 µm NiTi fibre embedded in an ultrasonically consolidated aluminium 3003 (T0) matrix

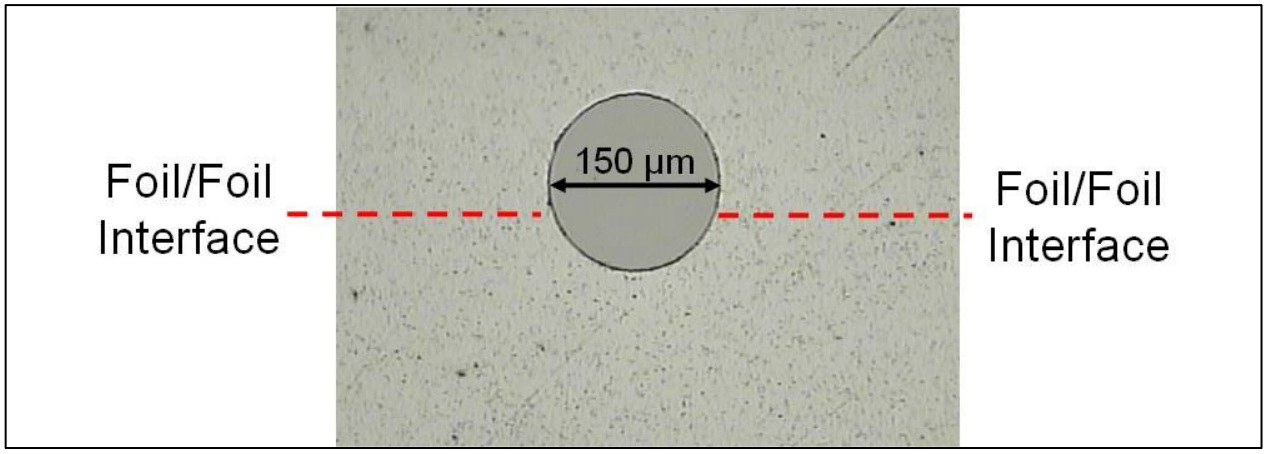

Figure 75 - A micrograph example of a 150 µm NiTi fibre embedded in an ultrasonically consolidated aluminium 3003 (T0) matrix

It was observed from the micrographs that the embedded fibres did not embed 50% into both the upper and lower foil layers. The fibres appeared to be embedded further into the foil being deposited onto the top of the fibre. This may have been due to the uneven surface and anisotropic mechanical properties of the previous foil layer being more

resistant to the plastic flow required for fibre embedding and due to the upper foil/fibre interface being closer to the ultrasonic energy source (sonotrode). Closer proximity to this source may have increased the level of energy within the material and increased grain boundary mobility.

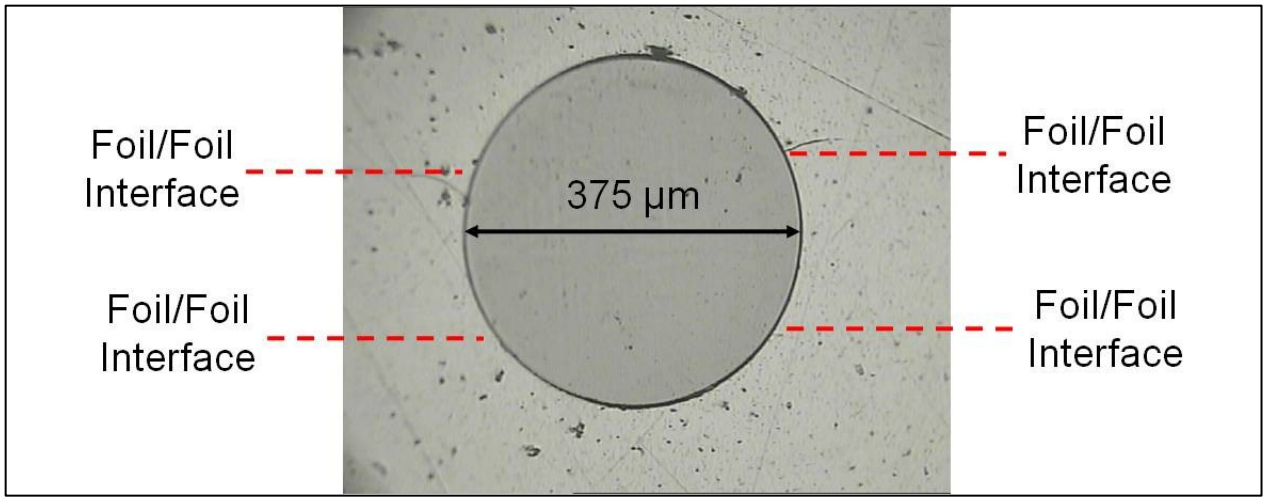

Figure 76 - A micrograph example of a 375 µm NiTi fibre embedded in an ultrasonically consolidated aluminium 3003 (T0) matrix

Full foil layer penetration was observed for the 250 and 375 µm diameter fibre samples which was the mechanism that allowed the fibres to embed into the sample. This layer penetration was necessary to embed the fibres fully into the Al 3003 (T0) matrix however this penetration may have only been possible due to the relatively low yield strength of Al 3003 (T0).

7.3.3 Electron and Ion Beam Analysis of the Fibre to Matrix Interface

Sample manufacture using the parameters in Table 10 was conducted. The samples were successfully prepared and analysed using the DBFIB equipment.

Figure 77 shows the average grain sizes for the upper foil, lower foil, and fibre/matrix interface on both sides of the fibre at four measurement regions. Region 1 was within 5 µm of the fibre/matrix interface; Region 2 was within 5-10 µm of the fibre/matrix interface; Region 3 was within 10-15 µm of the fibre/matrix interface and Region 4 was within 15-20 µm of the fibre/matrix interface. The measurement of average grain size

was performed using the mean linear intercept method with a circular traverse (Johnson, 2008). The legend format for the graphs in Figure 77 is: NiTi fibre diameter (µm), Sonotrode Amplitude (µm), Welding Pressure (kPa) (i.e. 100 µm, 12.28 µm, 276 kPa).

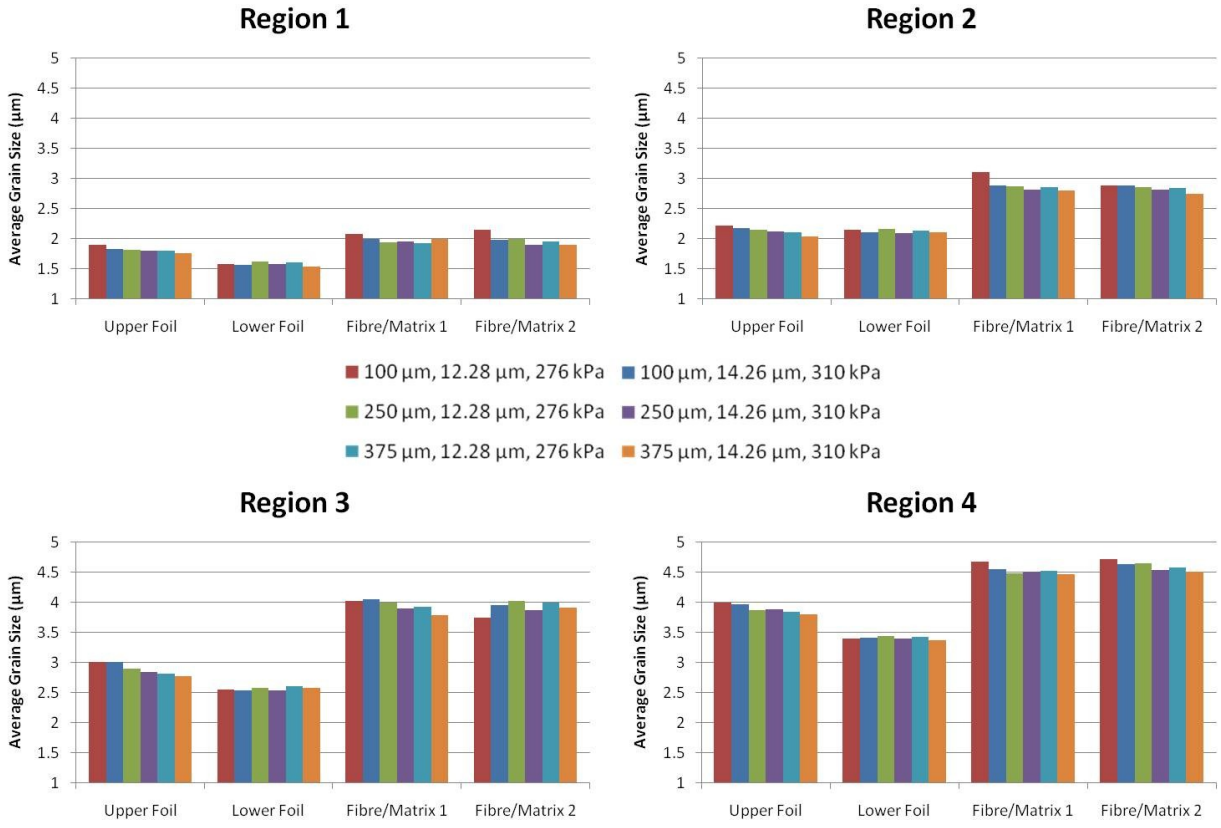

Figure 77 - Graphs showing the measured average aluminium 3003 (T0) grain size at the four regions for different NiTi fibre diameters and ultrasonic consolidation processing parameters

The grain size measurements showed that both the upper and lower foil regions at the fibre interface had a smaller average grain structure than the regions along the sides of the fibre. An increase in fibre diameter, welding pressure and amplitude resulted in a more refined grain structure characterised by a lower average grain size.

SEM analysis of the trench created by the SMA fibre showed that there was greater plastic deformation to the upper foil (consolidated after fibre placement) than the lower foil (consolidated prior to fibre placement). The lower foil-fibre interface had a greater level of void inclusion than the upper foil-fibre interface.

The inner trench surfaces had a visibly low surface roughness which corresponded to the low surface roughness of the embedded SMA fibres. Small, rougher, regions were visible which represented the void areas around the fibres.

The average grain size of the Al 3003 (T0) was lower than pre-UC processing within 20 μm of an embedded SMA fibre (typically <1 μm). The region ≥20 μm exhibited a grain structure comparable to the pre-UC Al 3003 (T0) foil material (1 μm – 15 μm grain size). The greatest levels of grain size reduction were observed at the upper and lower foil, relative to the normal force exerted by the sonotrode, of the fibre/matrix contact. Figure 78 and Figure 79 show the FIB and SEM images of the grain structures in close proximity to the SMA fibres.

There were regions of sub-grain refinement at and within close proximity (<1 μm) of the embedded fibres and the sizes of these sub-grains varied from 1 nm to 2 μm.

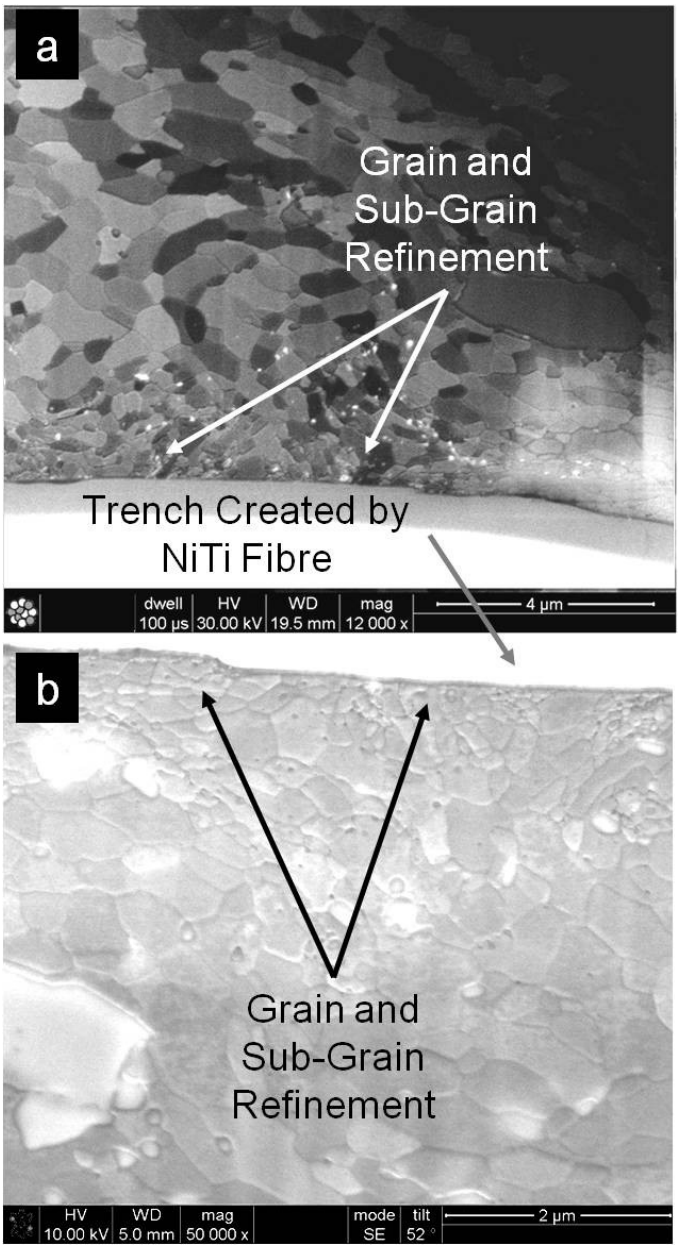

Figure 78 - Grain structure of the aluminium 3003 (T0) matrix around the shape memory alloy fibre: (a) focussed ion beam cross-section and image of the grain structure of the underside of the deposited foil post-fibre placement (upper foil layer) and (b) ultrahigh resolution scanning electron microscopy image (rotated 180◦) showing (a) at higher magnification

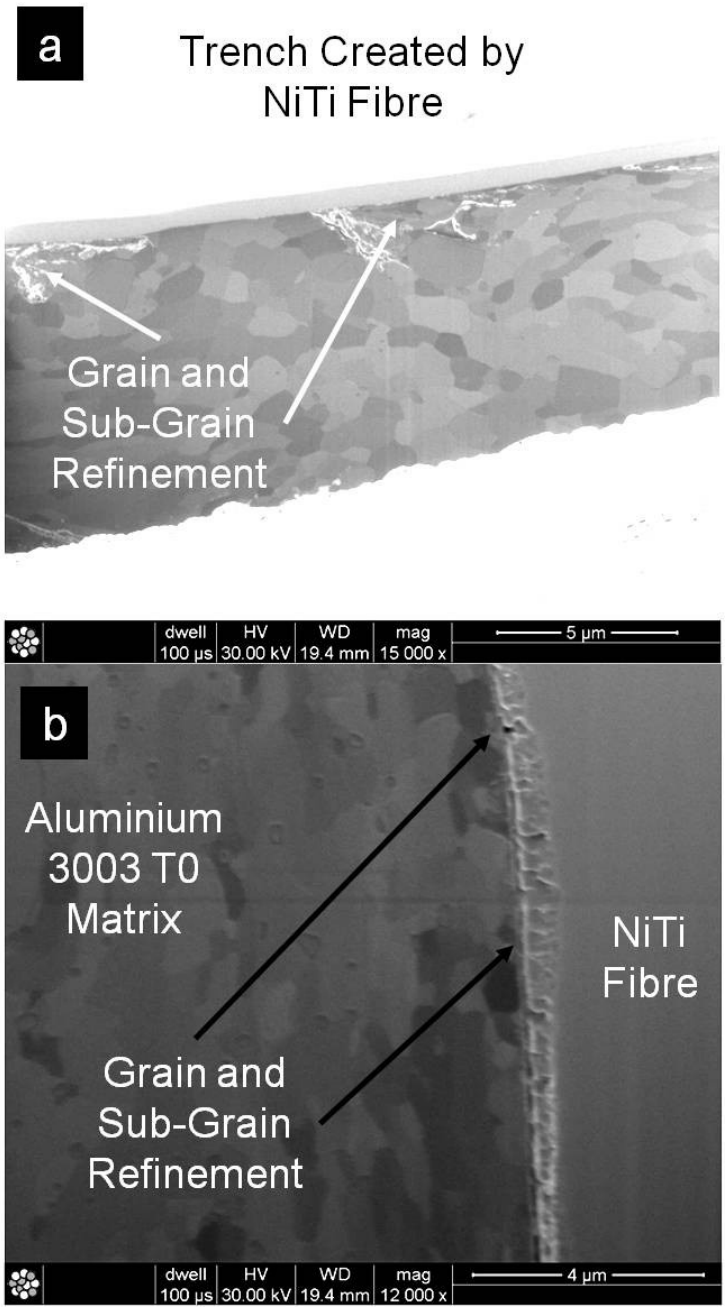

Figure 79 -Grain structure of the aluminium 3003 (T0) matrix around the shape memory alloy fibre: (a) focussed ion beam cross-section and image of the grain structure of the upside of the deposited foil pre-fibre placement (lower foil layer) and (b) focussed ion beam cross-section and image of the grain structure of the upper foil matrix adjacent (left side) to the shape memory alloy fibre

Figure 80 and Figure 81 show the virgin SMA fibre and fibre/matrix interfaces at high magnification. A common characteristic that was exhibited by the SMA fibre was a high level of surface cracking to approximately 1 µm depth into the SMA fibre surface. This

cracking was also seen to cause larger scale deformation of the fibre surface (Figure 81b), which was apparently exacerbated by the plastic flow of the Al matrix; an extreme case is illustrated, however, this process was documented to a lesser extent in several other FIB images/cross-sections. In all cross-sections there was no evidence of grain growth across the interface.

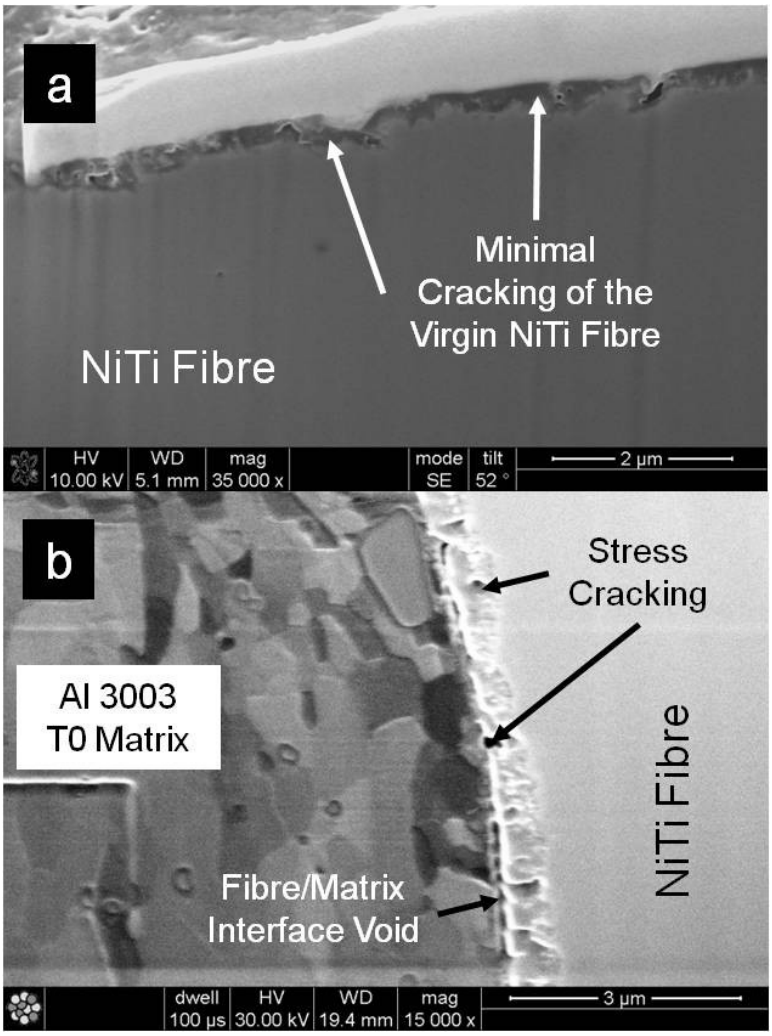

Figure 80 - Pre- and post-ultrasonic consolidation images of the shape memory alloy fibre: (a) focussed ion beam cross-section and ultrahigh resolution scanning electron microscopy image of the virgin (pre-ultrasonic consolidation) shape memory alloy fibre surface and (b) focussed ion beam cross-section and image of the cracking of the shape memory alloy fibre and void inclusions (post-ultrasonic consolidation)

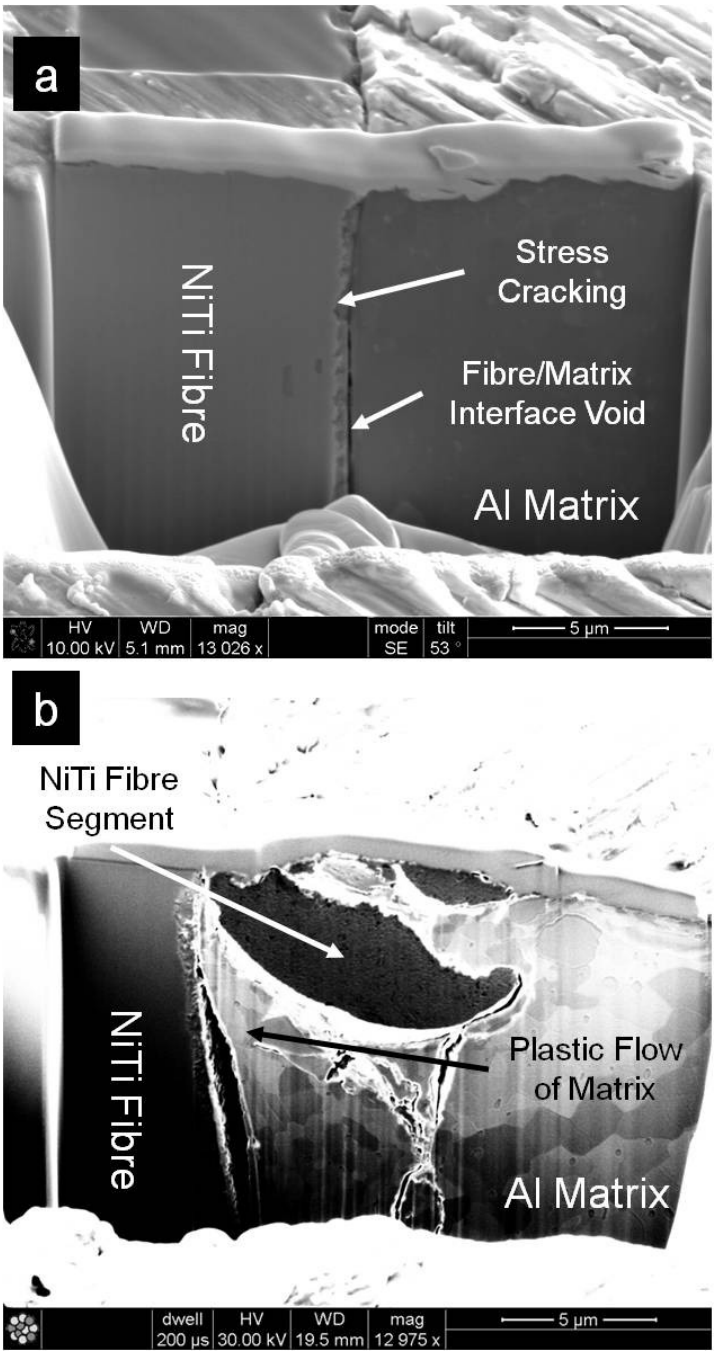

Figure 81 - Fibre matrix interface images between the aluminium 3003 (T0) matrix and shape memory alloy fibre: (a) scanning electron micrograph of the focussed ion beam cross-section showing the specific damage and void inclusion at the fibre/matrix interface and (b) focussed ion beam cross-section and image showing the specific damage and then subsequent forceful matrix material flow at the fibre/matrix interface

A high level of plastic flow resulted in an intimate contact between the fibre and the matrix with encapsulation being on average approximately ≥95 % complete for the

averaged visual analysis performed by the researcher during the DBFIB exploration. Although there was a high level of encapsulation, the majority of the plastic deformation occurred in the top foil layer that was being processed which was evidenced by the fibre being embedded to a deeper extent within the upper foil layer in comparison with the lower foil layer.

The direct sonotrode to foil contact resulted in the sonotrode imparting a roughened surface onto the foil. This uneven surface has been shown to include regions of highly refined sub-grain structure (Johnson, 2008) which would be expected to present a harder material (Li, et al., 2008) for the fibre to embed into and thus potentially make the process more resistant to plastic flow and prone to void inclusion. During the deformation of this uneven, post UC processed surface, a level of plastic flow occurred which appeared to result in a high inclusion of surface oxides into the underlying fibre/matrix material (Figure 79a). This oxide inclusion could alter the properties of the Al 3003 (T0) matrix and affect the mechanical performance of the MMC, as the oxide is brittle compared to the relatively ductile Al bulk matrix.

The grain structure in the vicinity (<20 μm) of the embedded SMA fibre resulted in a significant level of grain refinement. The level and geometry of the refined matrix areas varied around the fibre suggesting the mechanism was not exactly the same for each region (i.e. regions 1-4).

At the fibre/matrix contact area at the bottom of the SMA fibre (Figure 79a) to the previously deposited Al layer; the grain refinement was in deformed ‘pockets’ that appeared random in location with regards to the SMA fibres. These pockets were likely a result of the previous direct sonotrode to surface contact, which was shown to create regions of highly refined sub-grain ‘peaks’ on the surface of the deposited Al foil (Johnson, 2008). A possible scenario was that when the fibre was forced onto this previously deposited, harder, foil by the sonotrode and the resultant reaction force and ultrasonic energy caused the greater embedding, of the fibre, into the upper, softer, layer of foil. Therefore the embedding process was not a 50:50 split, in terms of embedding depth, between the upper and lower foil layers. These hard ‘peaks’ also appeared to be forced back into the surrounding matrix material by the SMA fibre and this, as previously mentioned, resulted in a relatively high level of oxide and void

inclusion, but with little grain refinement to the surrounding area. However this forceful insertion of the peaks did appear to result in a relatively large realignment of the surrounding grain structure and flow direction.

Fibre/Matrix regions 1 and 2 exhibited a degree of grain refinement with apparent sub-grain pockets (Figure 79b, Figure 80b, and Figure 81b). These sub-grain pockets, to the left and right of the fibre, were only identified in the previously deposited foil and not in the upper foil layer. These pockets could be the hard ‘peak’ structures, caused by direct sonotrode contact, that were mentioned previously. These sub-grain regions in the lower foil and the surrounding grain structure showed the same flow patterns as the area below the SMA fibre; this could be due to the same forcing of the sub-grain peak back into the matrix.

The matrix region above the SMA fibre exhibited a highly refined sub-grain structure that followed a conical shape directly above the fibre (Figure 78a and b). The level of grain refinement reduced as the matrix flowed around the fibre towards the foil to foil interface. This region of the foil was never in contact with the sonotrode and/or previously deposited foil; therefore this sub-grain refinement was likely to be caused by the fibre/matrix interaction in the presence of high levels of ultrasonic energy. This effect showed similar results to the identified sonotrode to foil interaction and suggested that ultrasonic energy transmission through the foil material was sufficiently high to create the high levels of sub-grain refinement at the foil to fibre interface.

In addition to the identified sub-grain regions above the fibres a relatively high level of oxide inclusion within the matrix was witnessed. This oxide inclusion within the matrix suggested that there may be a sufficiently high level of grain mobility that surface oxides were included and dispersed among the grain boundaries of the matrix material.

The fibre/matrix interface was approximately ≥95% matrix to fibre direct contact. Although this contact was metal to metal it appeared, from nano-scale investigation, that there was no grain growth across the interface (Figure 79b and Figure 80b). In addition to this the UC process had an apparent fatiguing effect on the surface of the SMA fibre. This was represented by small scale cracking of the fibre surface to a depth of approximately 1 μm. Although for the majority of the images taken this cracking was

apparently a small surface effect, in some instances this cracking had led to sections (maximum size observed: 10μm in length) of the fibre being sheared off from the bulk of the fibre. This shearing was coupled by infiltration of the matrix material behind the fragment and towards the fibre. This suggested that the fracturing occurs early enough in the UC process to allow for the fibre segment to move and for the matrix to have time to flow behind the segment (i.e. this fracturing had occurred during UC processing, not post processing). From analysis the matrix material that flowed behind the segment exhibited the same sub-grain structure and oxide inclusion that was found at the bottom foil to fibre interface. A reason for this may be that the hard area of the matrix, the sub-grain refined peak, was increasing the fatigue and maximum stress to the surface of the fibre and aided this fracturing of the fibre (i.e. these hard peaks were acting as an extra abrasive agent during the UC processing). Li (Li, et al., 2008) suggested that some high hardness results for the area around a Silicon Carbide (SiC) fibre in a UC Al matrix maybe due to dispersion of Titanium Diboride (TiB_2) particles at the fibre/matrix interface. Although the SMA fibres were not purposefully coated, they do have an unavoidable oxide layer on the surface, the same process that has dispersed fragments of the TiB_2 may also have caused the cracking and then separation of external SMA fibre fragments in this instance. The TiB_2 particles were a coating on the SiC fibres and may have been dispersed in a similar way to the exterior of the SMA fibres in the current work. This highly erosive mechanism of ultrasonic work hardening and hard matrix material pockets may also help explain the damage caused to fibres during UC in other research (Kong, et al., 2005).

7.3.4 Summary of Microstructural and Mechanical Interactions at the Fibre to Matrix Interface

The microstructural and mechanical evidence suggested that the fibre/matrix bonding mechanism was mechanical entrapment by the matrix around the fibre as opposed to a chemical or atomic diffusion type bond. Due to the fibres not bonding to the matrix the inclusion of fibres reduced the area of matrix to matrix contact and appeared to act in a similar way to voids within the bond area for fibres of 50, 100 and 150 μm. The use of

larger fibre diameters increased the plastic flow of the matrix resulting in greater matrix to matrix interaction which increased the matrix to matrix bond strength.

The presence of the SMA fibre itself may have induced a sonotrode-like effect due to the matrix grain structure adjacent to the fibre. This sonotrode-like effect was a description to compare to work which identified a reduction of foil material grain sizes caused by the direction contact of the sonotrode to the foil surface material during UC (Johnson, 2008).This may have resulted in a refined grain structure at the fibre matrix interface.

The plastic flow of the matrix coupled with the UC process appeared to damage the surface of SMA fibres to varying degrees. This damage had not been previously identified and was a unique finding of this research as was the sonotrode-like effect of the embedded fibre material.

To assess what effect these interactions, between the fibre and matrix, may have had on the embedded SMA fibres and to further characterise the fibre/matrix interface an experimental methodology was devised to assess, in-situ, the performance of the embedded SMA fibres.

8 In-situ Assessment of Shape Memory Alloy Fibres within Ultrasonically Consolidated Aluminium Matrices

8.1 Introduction

To assess the activation response of embedded SMA fibres in UC Al 3003 (T0) structures a thermo-mechanical analysis method was formulated to monitor the effect of the Al matrix and UC process on the SMA fibres of various diameters. When heated to an activation temperature, 70°C in this instance, a pre-strained SMA fibre will undergo a phase change and revert back to its original shape; provided the pre-activation deformation was not in excess of the maximum recoverable deformation. The activation temperature is normally achieved by the use of an electrical current being passed along the SMA fibre.

8.2 Methodology

8.2.1 Activation of Embedded Shape Memory Alloys

The method of sample production is shown in Figure 82, three layers of Al 3003 (T0) were UC processed and bonded to an Al 1050 support plate (150 mm long, 1.2 mm thick, and 28 mm wide). A single (length: 200±5 mm SMA) fibre of 50, 100, 150, 250 or 375 µm diameter was then placed on top of the sample and embedded between a fourth Al 3003 (T0) foil using the same processing parameters as were used for the previous three foils. As in section 7.2 the SMA fibres were pre-strained 5%, by length, prior to embedding to prevent the SME inhibiting fibre/matrix bond integrity in the first instance. The UC parameters that were used to embed the fibres are detailed in Table 9 and three samples for each set of parameters and fibre diameter were manufactured and tested (270 in total).

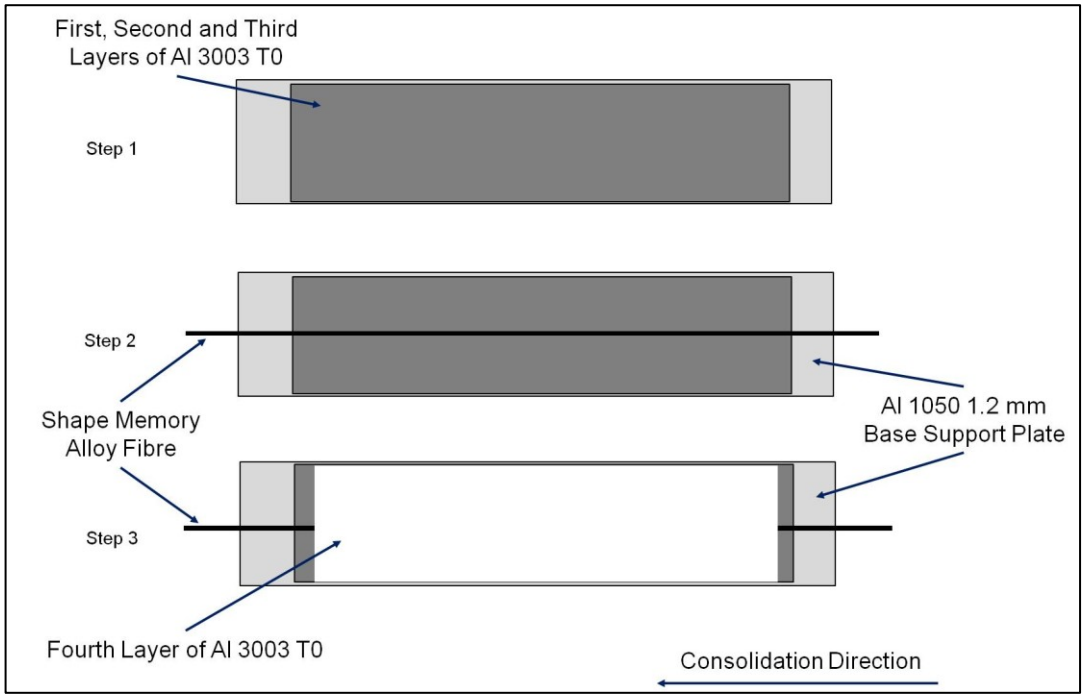

Figure 82 - Schematic of the shape memory alloy/aluminium matrix activated sample preparation

The activation procedure was to mount the two fibre ends, which had been insulated using silicone tubing, in a Lloyd Instruments LRX material testing machine and set the tensile load to 0.25 N (Figure 83). The temperature of both ends of the SMA fibre was monitored using K-type thermocouples attached using an adhesive in the same procedure as was demonstrated by Kong (Kong, 2005). An electrical current of 350 mA at 3V was applied across the fibre using a variable power supply. Using the timer for the material testing equipment in combination with the thermocouple data and tensile data the speed of activation temperature attainment, rate of load and maximum load achieved by the SMA were recorded. The SMA fibre was then activated and subsequently strained to 5%; the data from the SMA fibre was collected on the first, fifth and tenth cycle for comparison. For the first, fifth and tenth cycle the SMA temperature was allowed to stabilise at 21±2°C to maintain a standard baseline from which the temperature would need to increase to the activation temperature. This procedure was also carried out for five un-embedded SMA fibre lengths, of each of the fibre diameters, which acted as a reference to which the embedded fibre values were compared.

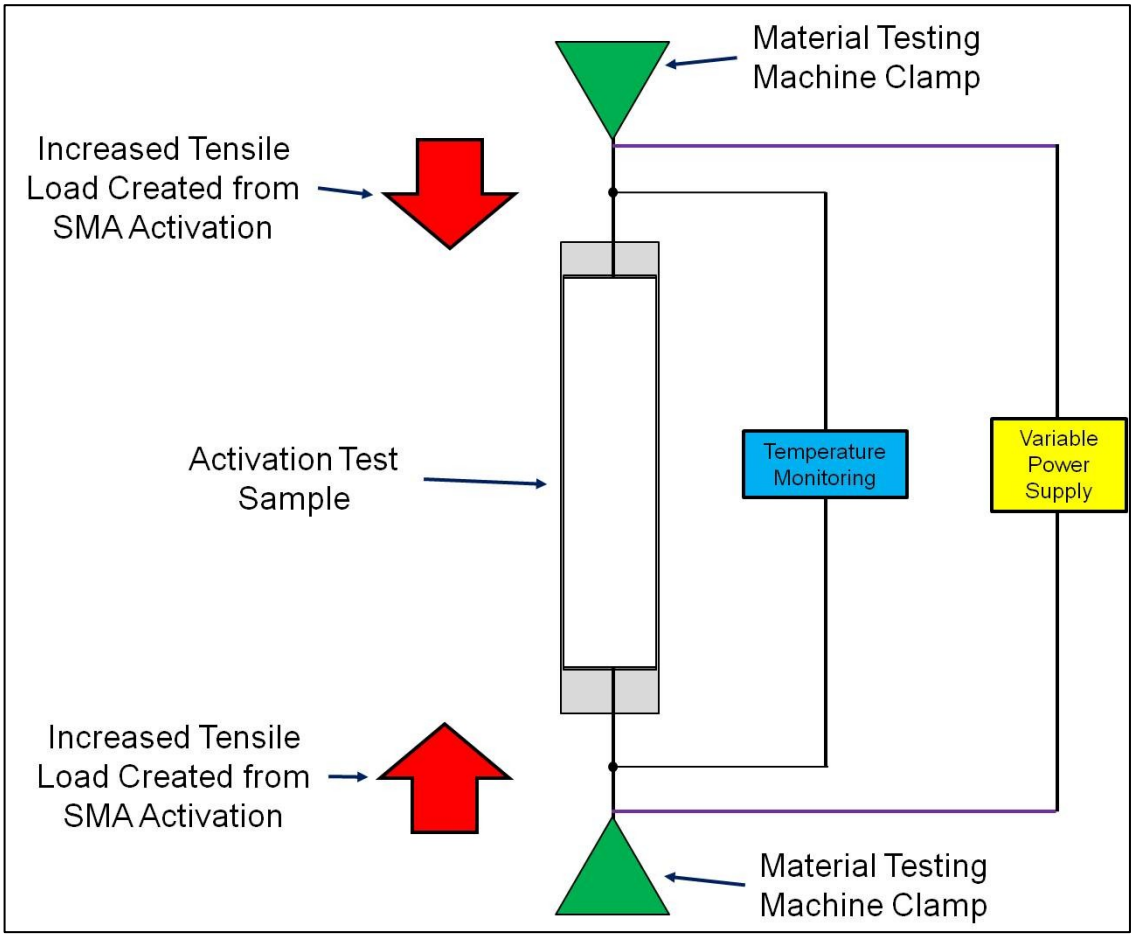

Figure 83 – Schematic of the activation sample mounting setup for fibre activation testing

8.2.2 Fibre Pull Out Testing of Shape Memory Alloy Fibres

To quantitatively assess the mechanical interaction between the SMA fibre and the Al 3003 (T0) matrix prior and post activation a testing methodology was devised. This methodology used a technique shown successful by Kong (Kong, 2005) to assess the maximum fibre pullout force and the characteristics of the fibre/matrix interaction.

The samples were produced to the specifications shown in Figure 84. As with previous samples three layers of Al 3003 (T0) were deposited onto an Al 1050 base plate. A single SMA fibre of 50, 100, 150, 250 or 375 µm was then placed onto the bonded foils before being embedded using a fourth Al 3003 (T0) foil layer. Four samples for each of the processing parameters in Table 9 and for each of the fibre diameters were processed (360 samples in total).

Each sample was placed in a bespoke bracket (Figure 85) which was attached to a Lloyd Instruments LRX material testing machine and the longer fibre end was clamped to the machine. The tensile loading was performed at 0.5 mm/min for a total distance of 3 mm during which the maximum load was recorded.

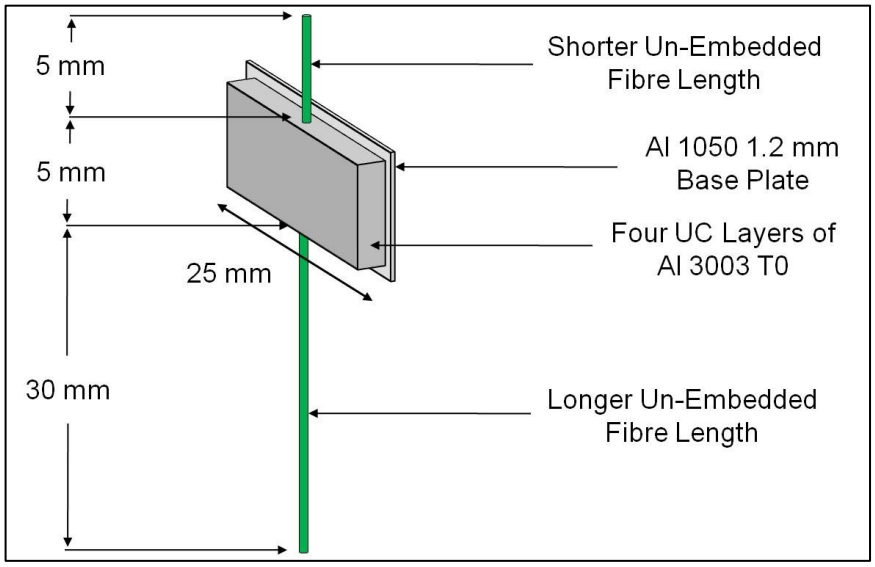

Figure 84 - Schematic of the fibre pull out test sample

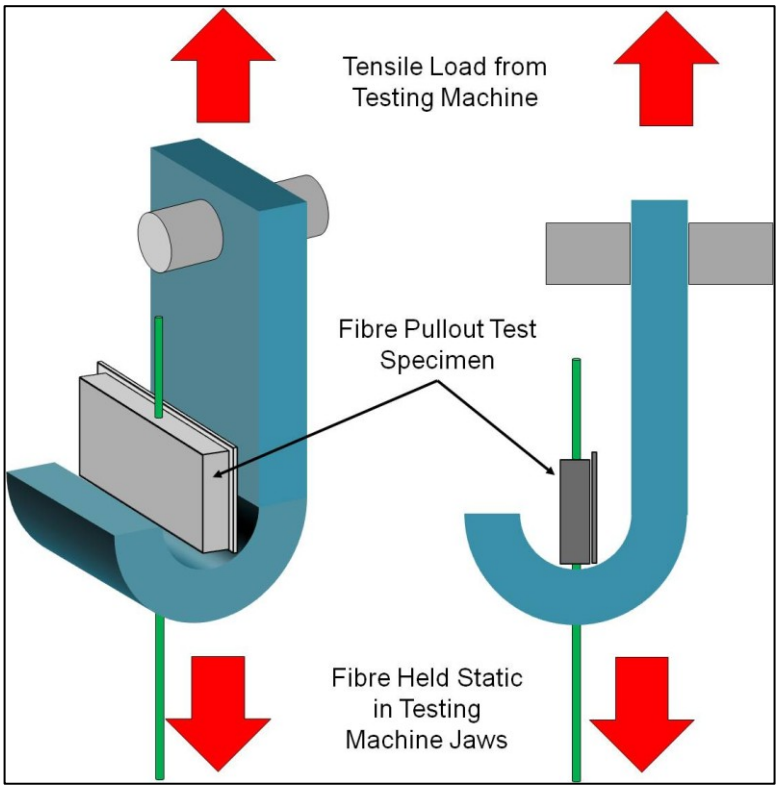

Figure 85 – Schematic of the fibre pull out test rig

To assess the effects of fibre activation/extension cycling of the embedded SMA fibres on the fibre/matrix interface strength five samples (Figure 84) for each of the fibre diameters were manufactured using the UC processing parameters of 12.28 μm amplitude, 276 kPa pressure and 34.5 mm/s weld speed. These samples were then mounted in the Lloyd Instruments LRX material testing machine with both fibre ends securely clamped. The fibres were then activated in the same manner as section 8.2.1 using one, five or ten cycles. These cycled samples were then setup as in Figure 85 and then loaded at 0.5 mm/s for 3 mm while maximum load was recorded.

8.2.3 Optical Microscopy of Activated Aluminium/Shape Memory Alloy Fibre Samples

To visually assess any possible variation in the fibre matrix interface, post fibre activation, each of the samples from section 8.2.1 were cross sectioned perpendicular to the longitudinal direction of the fibre using a cutting disc. The sectioned SMA Al MMC was mounted in Buehler Varidur thermosetting polymer and then ground, polished and stored as in section 4.2.3.

The samples were analysed using an Olympus BX60M microscope with a QImaging Micropublisher 3.3MP digital camera for image capture. Images were captured at magnifications of 5x, 20x, 50x and 100x.

8.2.4 Mechanical Peel Testing of Activated Aluminium/Shape Memory Alloy Fibre Samples

During the extension and the activation of the SMA fibres a degree of expansion due to Poisson's ratio was expected. To assess any effect on the interlaminar strength of an SMA/Al sample ten activation cycles were performed prior to mechanical peel testing.

The samples from section 7.2.2 were placed in a kiln set at 75°C for ten minutes to activate the embedded SMA fibres. This method was used rather than the more complex method of electrical activation of individual fibres since the Al matrix was unlikely to undertake any significant structural change at the temperature of 75°C

(Ferrasse, et al., 1997). The samples were mounted in a Lloyd Instruments LRX material testing machine (refer to Figure 83) and all ten fibres were then strained with a 5% extension. The samples were then removed from the testing machine and placed in the kiln to activate the SMA fibres within the Al matrix and return them to their original strain state. The samples were then remounted in the Lloyd Instruments LRX material testing machine. This procedure was repeated for 10 cycles.

The peel testing was carried out in the same method as in section 4.2.4. The peel testing allowed for bond quality to be quantitatively analysed by assessing a samples average resistance to peeling for the given weld interface. The effect of the diameter of the embedded fibres, the process parameters and the activation/extension cycle, in combination, on the maximum peel load was quantified.

8.3 Results and Discussion

8.3.1 Activation Results of Embedded Shape Memory Alloy Fibres

The samples for the fibre activation testing were successfully manufactured and tested. The process parameters used to manufacture the samples did not have a consistent measurable effect on the activation response of the embedded SMA fibres. The performance of the embedded SMA fibres was different to that of the un-embedded fibres and therefore the results for each embedded fibre diameter was averaged and compared to the un-embedded fibre (Figure 86).

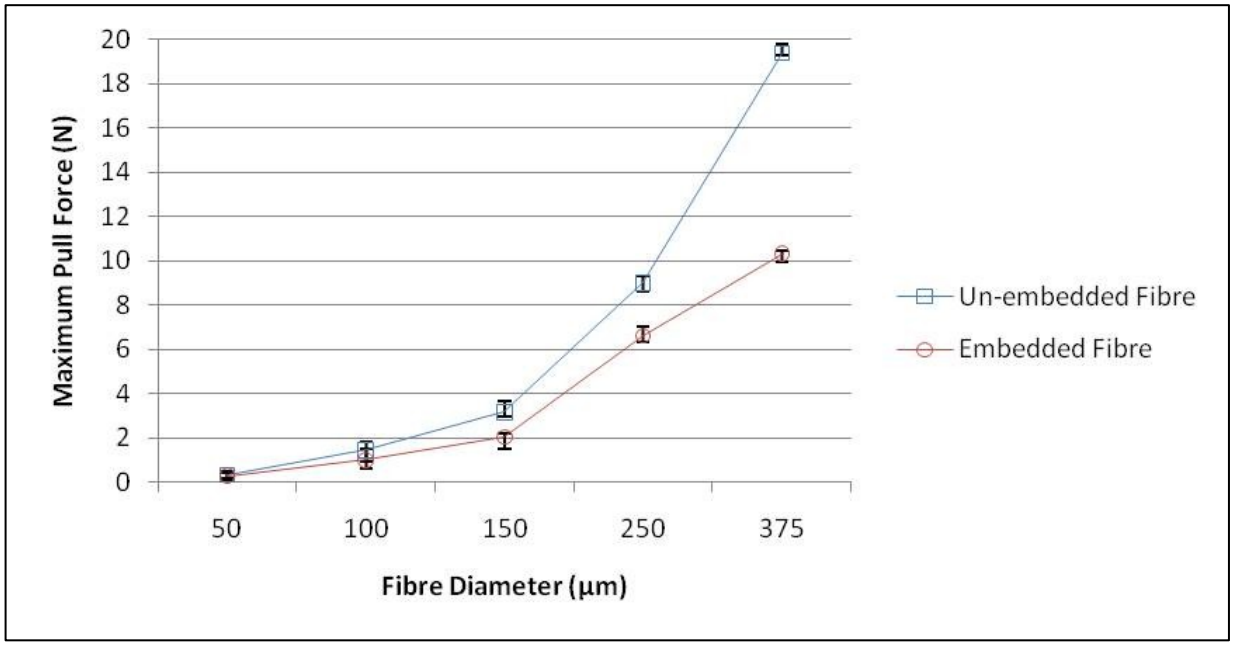

Figure 86 – Maximum pull force data for embedded and un-embedded shape memory alloy fibres in aluminium 3003 (T0) matrices

The maximum pull force exhibited by the embedded fibres was less than that of the un-embedded fibres. The fibres were embedded in the pre-strained state and it was suggested that due to this any axial contraction of the SMA fibres required a radial expansion. Therefore the SMA fibre would work against the compression of the matrix material and thus would be impeded in exerting the maximum pull force.

The activation response times of both the embedded fibres and un-embedded fibres were less than 1 second in all cases. The speed of activation was quicker than the measure equipment used was able to accurately measure and the response time was thought to be less than or equal to 100 milliseconds; which was identified in research activating SMA fibres that were not embedded in a metal matrix (Potapov, et al., 2000). The fibre damage identified in the previous section did not appear to affect the performance of the embedded fibres.

The electrical current required for activating the embedded fibres was higher than for the un-embedded fibres (which were activated using the manufacturer's recommendations). This was possibly due to the high conductivity of the Al 3003 (T0) matrix reducing the efficiency of the activation temperature attainment process. Although not measured it

was an observation by the researcher that the speed at which the embedded fibres returned to room temperature was faster than that of the un-embedded fibres suggesting that the Al 3003 (T0) matrix was functioning in a similar manner to a heat sink which had possible implications for the future use of UC embedded SMAs.

The SMA performance testing in terms of response time and maximum pull force were unique in their method and findings for the UC research community. The identification of a hindrance to fibre contraction and activation temperature by the metal matrix represented new insight.

8.3.2 Non-Activated Shape Memory Alloy Fibre Pull-Out Results

The manufacture of the fibre pullout samples was successfully completed. The data from the experiments is presented in Figure 87 to Figure 92.

The data showed that an increase in fibre diameter generally resulted in a higher fibre pull out load. In addition to this the use of a higher weld pressure, amplitude and lower welding speed resulted in higher fibre pullout loads. This was thought to be due to the fact that the higher processing parameters appeared to induce a greater level of matrix plastic flow which was shown in section 0 to lead to a more intimate and more compressive fibre/matrix interface.

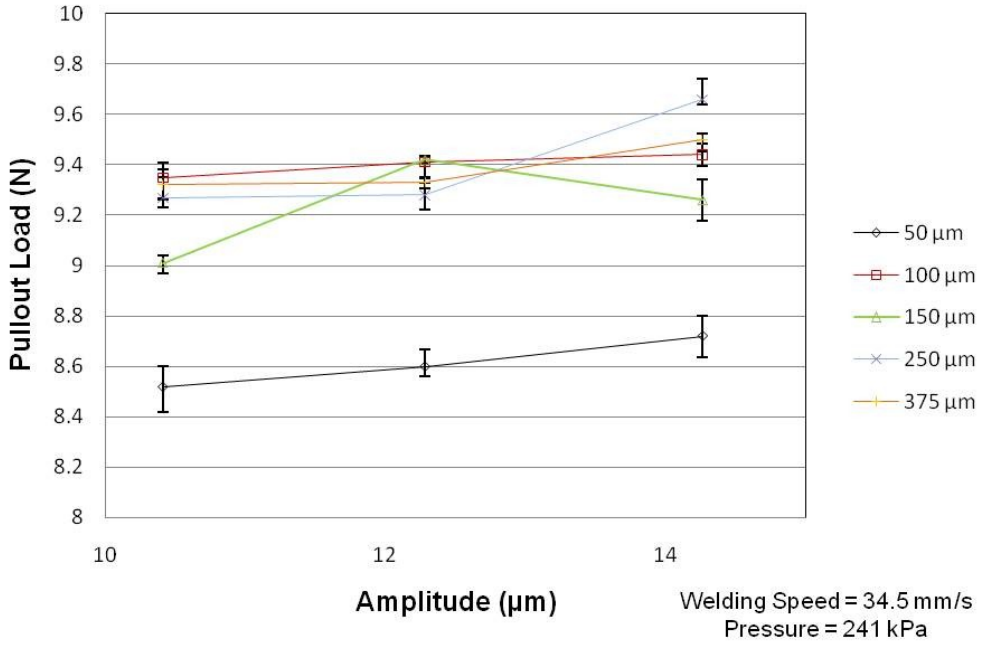

Figure 87 - Pullout test results of various NiTi fibre diameter specimens ultrasonically consolidated at 34.5 mm/s welding speed 241 kPa welding pressure

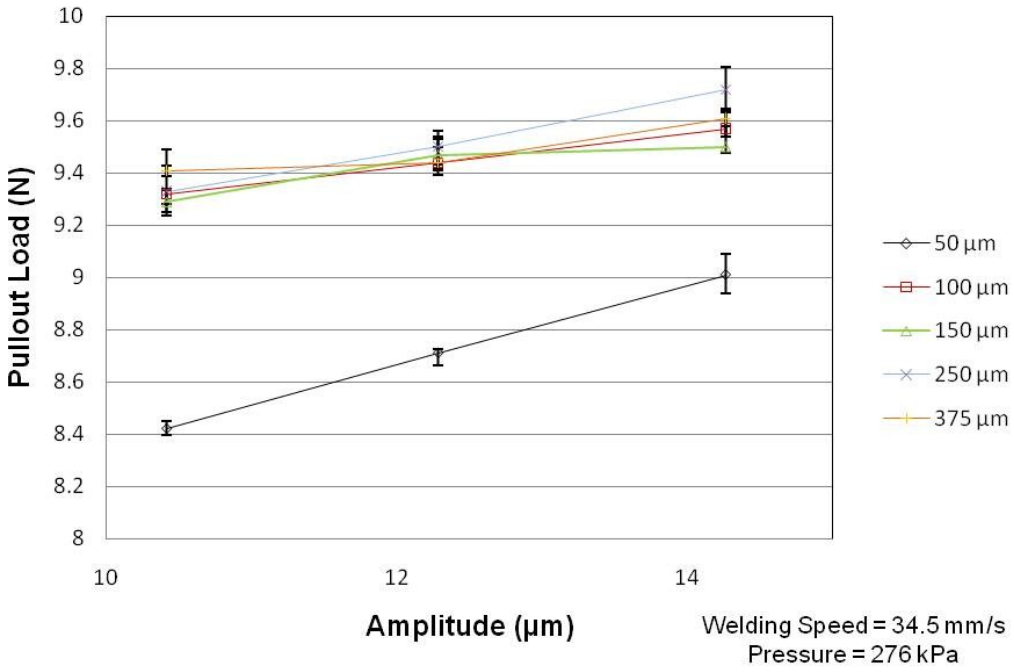

Figure 88 - Pullout test results of various NiTi fibre diameter specimens ultrasonically consolidated at 34.5 mm/s welding speed 276 kPa welding pressure

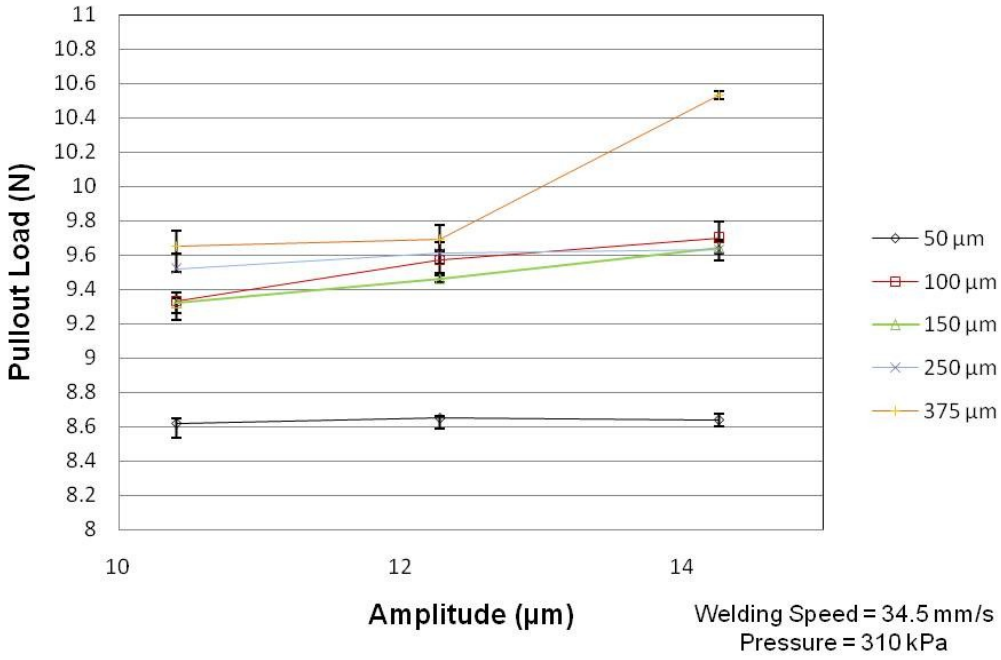

Figure 89 - Pullout test results of various NiTi fibre diameter specimens ultrasonically consolidated at 34.5 mm/s welding speed 310 kPa welding pressure

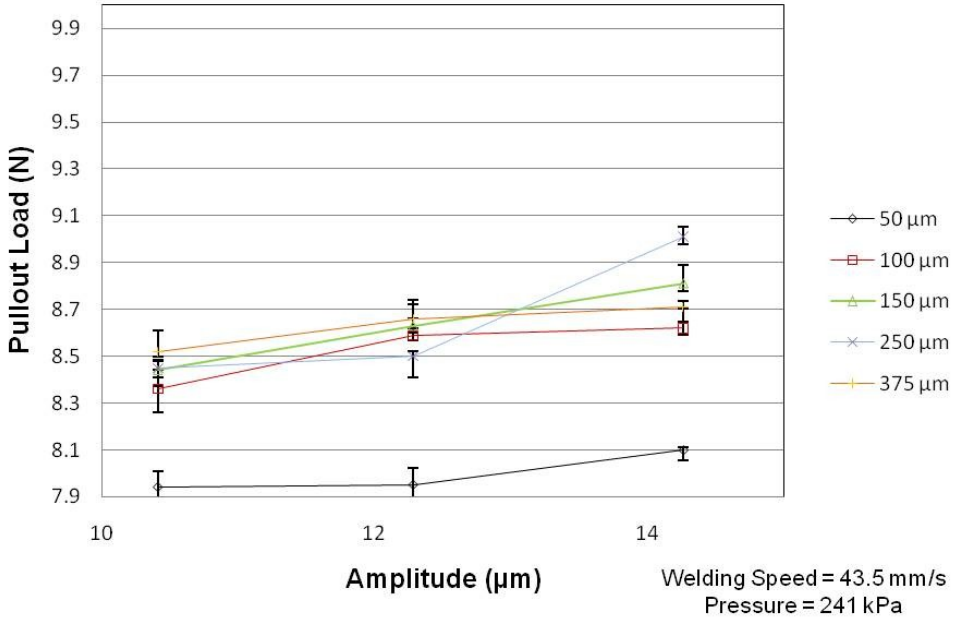

Figure 90 - Pullout test results of various NiTi fibre diameter specimens ultrasonically consolidated at 43.5 mm/s welding speed 241 kPa welding pressure

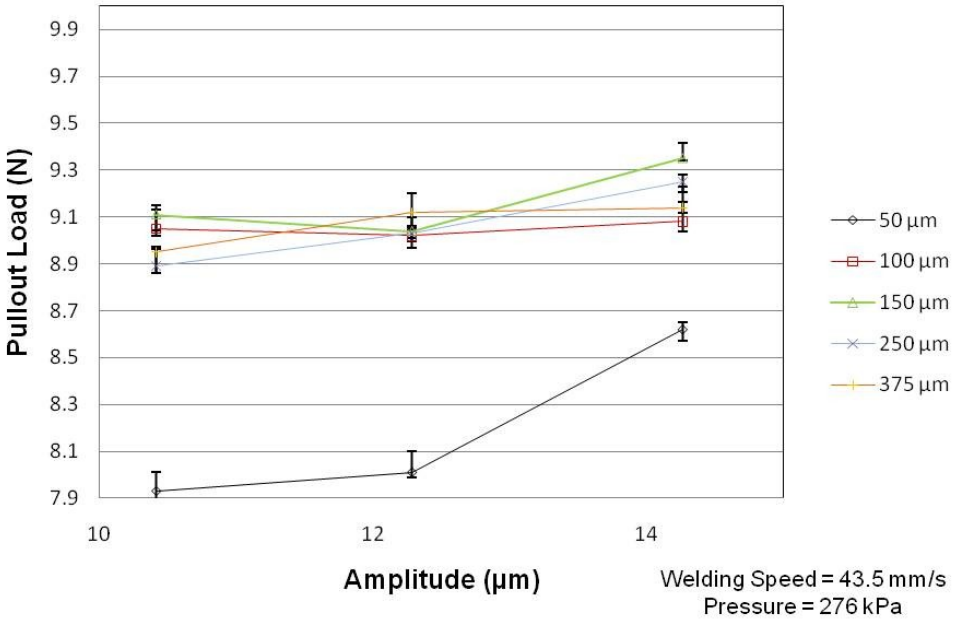

Figure 91 - Pullout test results of various fibre NiTi diameter specimens ultrasonically consolidated at 43.5 mm/s welding speed 276 kPa welding pressure

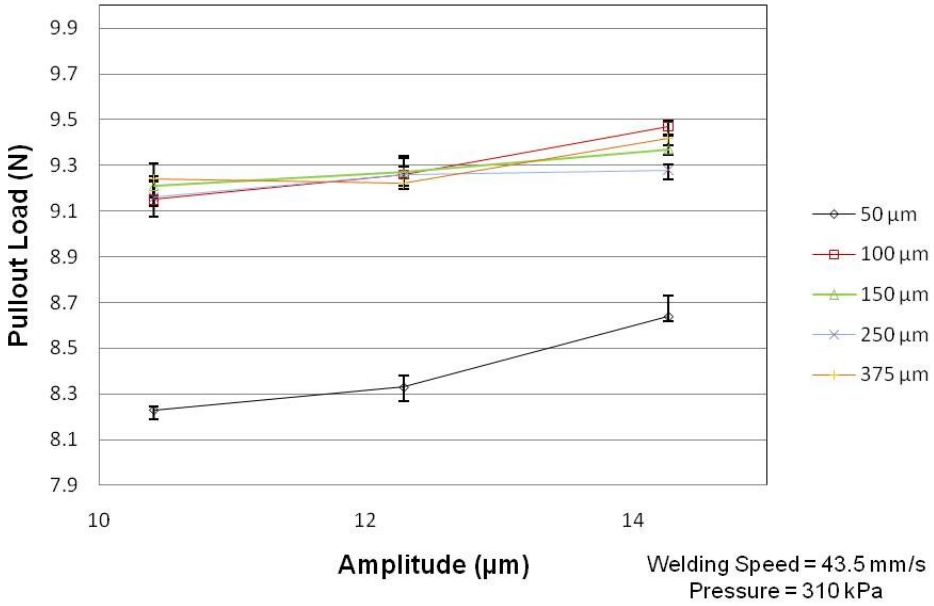

Figure 92 - Pullout test results of various fibre NiTi diameter specimens ultrasonically consolidated at 43.5 mm/s welding speed 310 kPa welding pressure

The use of pre-strained SMA fibres appeared to have prevented the SME taking place during the UC embedding process. This resulted in the fibre pullout testing being

relatively unaffected by the issues of low fibre pullout results encountered by Kong (Kong, 2005).

8.3.3 Activated Shape Memory Alloy Fibre Pull-Out Results

The activation and re-straining of the fibre pullout test samples was successfully completed. The data collected is represented in Figure 93.

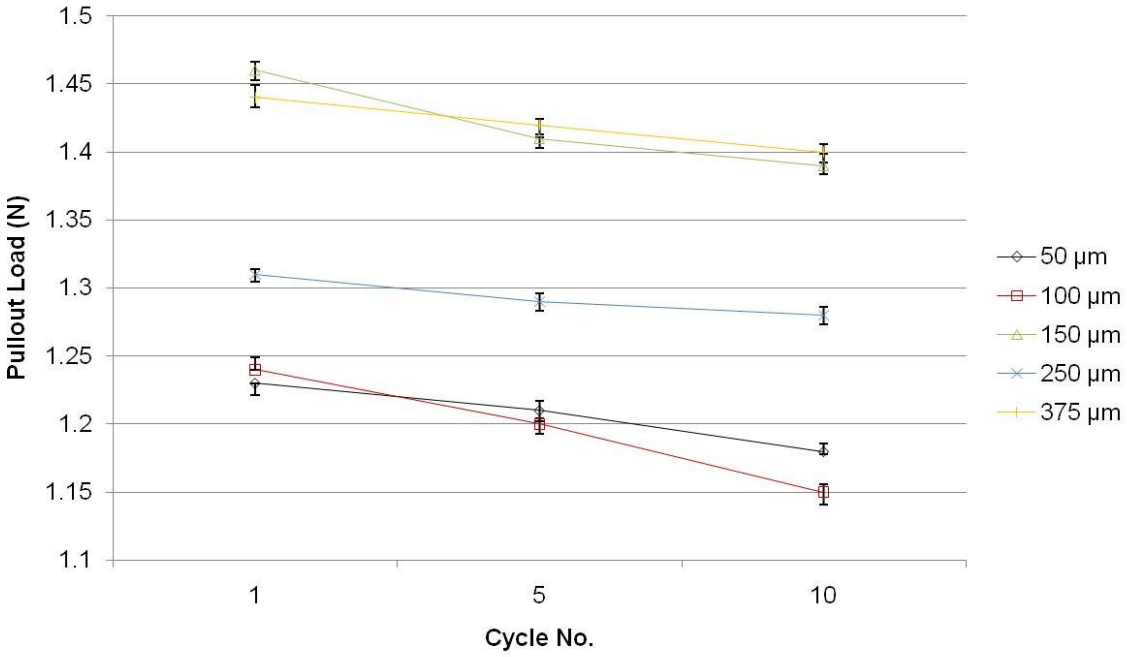

Figure 93 – Activated fibre pullout test results of various NiTi fibre diameter specimens ultrasonically consolidated at 34.5 mm/s welding speed 276 kPa welding pressure and 12.28 µm amplitude

The SMA fibre pullout testing data showed that after one cycle the fibre pullout load has significantly lower than for the un-activated samples. This loss of pullout load was exacerbated by the addition of five and ten cycles. This was possibly related to the inability of the embedded fibres to exert the maximum fibre pull force. When the fibre was activated it contracted axially and expanded radially which resulted in a plastic expansion of the matrix. This expansion appeared to result in a loss of the mechanical compression on the SMA fibre. Therefore when the post-activated fibre was pulled it required less force due to the loss of the mechanical interface between the fibre and matrix material.

8.3.4 Optical Microscopy of Activated Shape Memory Alloy Fibre Samples

When analysed, the activated fibres showed a higher level of fibre to matrix intimacy than for non-activated samples (Figure 94). This further suggested that the expansion of the SMA fibre during activation was having a deformation effect on the matrix at the fibre/matrix interface.

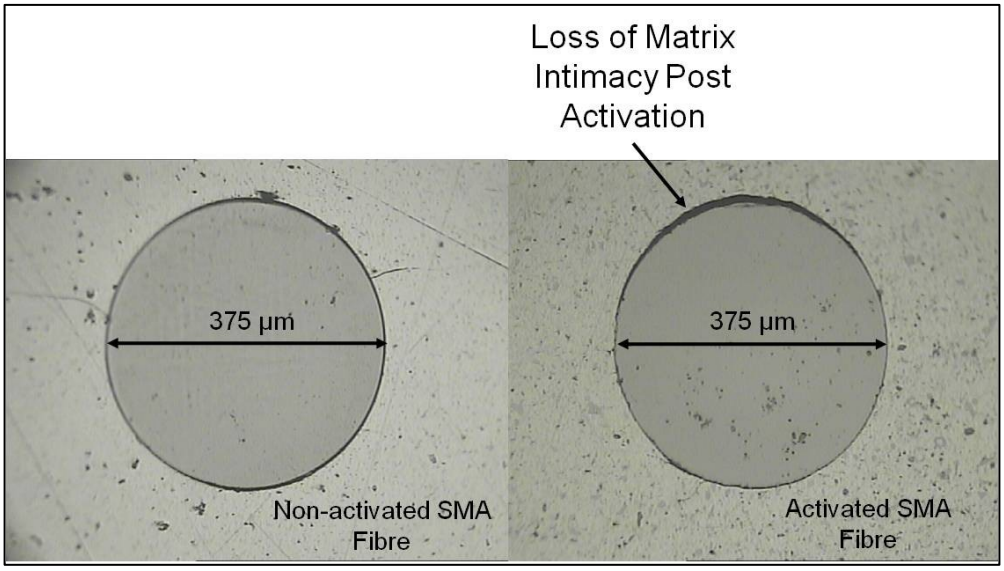

Figure 94 – Micrograph showing the Non-activated and activated shape memory alloy fibre within the aluminium 3003 (T0) matrix

In addition to the loss of matrix intimacy the larger fibre diameters exhibited damage to the interlaminar region of the matrix (see Figure 95). This damage for the larger SMA fibre samples was not universal but in some cases the separation of the foil/foil bonds by the expansion of the larger diameter fibres was significant.

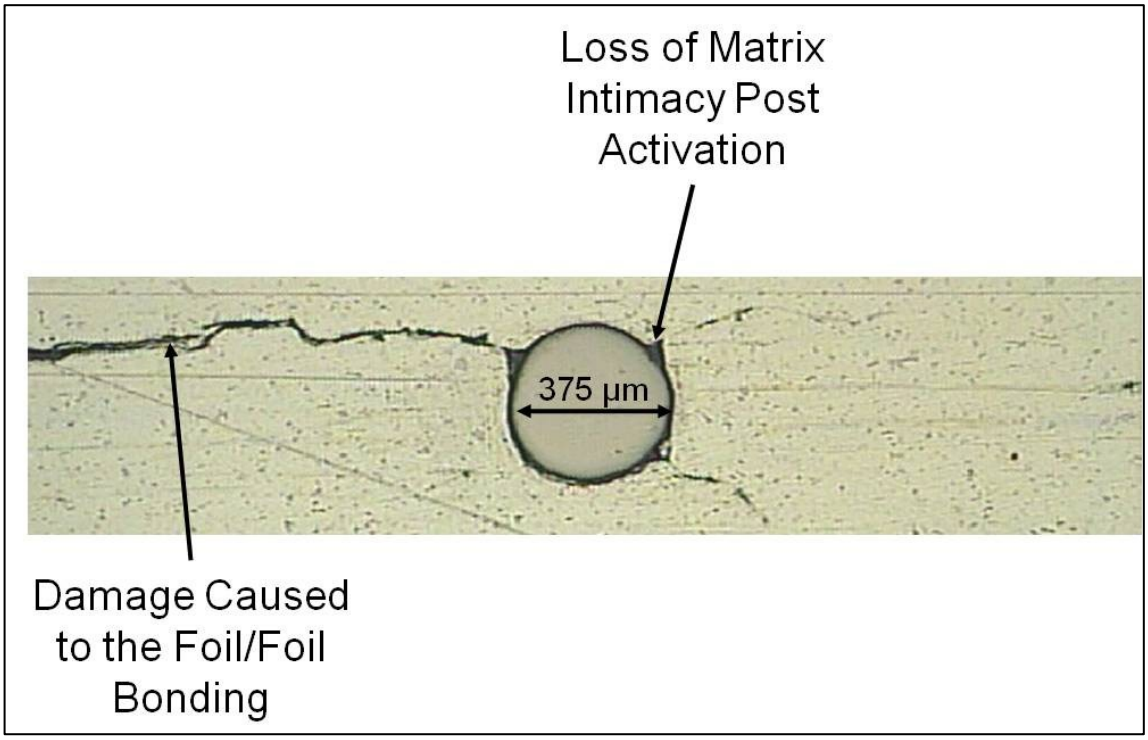

Figure 95 - Micrograph of activated 375 µm diameter NiTi fibre within an aluminium 3003 (T0) Matrix

8.3.5 Mechanical Peel Testing Results of Activated Shape Memory Alloy Fibres

The samples produced for the peel testing were successfully manufactured and the SMA fibres cycled. The cycled samples were successfully peel tested and the data is shown in Figure 96.

There was a reduction to the peel strength of the samples when compared to data in Figure 69. This reduction was possibly due to the weakening of the foil/foil bonding caused by the expansion of the SMA fibres during activation. Although the peel strength had been reduced the level of reduction was not sufficient to cause full foil/foil delamination and thus the samples still retained the majority of their integrity.

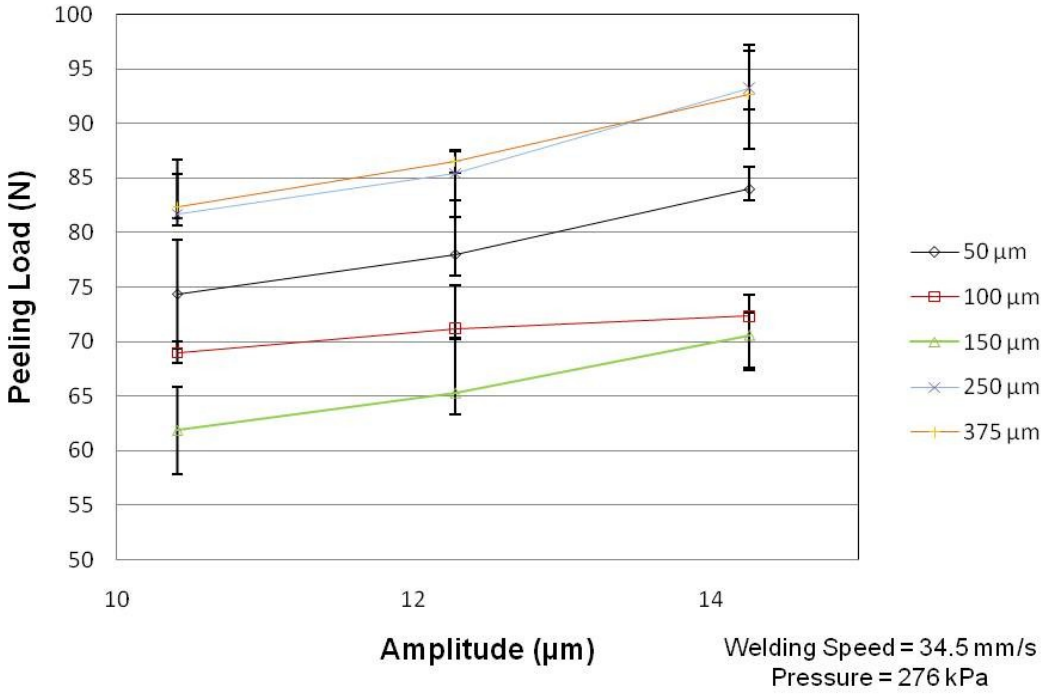

Figure 96 – Post activation peel testing results of various NiTi fibre diameter specimens ultrasonically consolidated at 34.5 mm/s weld speed 276 kPa weld pressure

8.3.6 Summary of In-Situ Assessment of Shape Memory Alloy Fibres within Ultrasonically Consolidated Aluminium Matrices

The non-activated SMA fibre pullout results were not affected by the SME as with previous research (Kong, 2005). The activation of SMA fibres in Al 3003 (T0) matrices required the radial expansion of the SMA fibres. This expansion appeared to be hindered by the Al 3003 (T0) matrix which resulted in a reduced pull force exerted by the SMA fibres. In addition to the reduced pull force the expanding fibre caused the matrix material to plastically deform and thus resulted in a significant reduction of the fibre pull-out strength after one cycle.

The expanding larger diameter SMAs appeared to cause foil/foil delamination after being activated. The peel strength of activated fibre containing samples was reduced. However, the sample integrity appeared to be maintained.

The reduction of peel strength and the delamination caused by activated SMA fibres was a unique finding of this research.

9 Conclusions

Fibre volume fraction was increased from previous work into fibre embedding via UC (Kong, 2005) (Li, 2009) (Yang, 2007). This fibre volume fraction was not as high as that obtained by other manufacturing methods and it was concluded that a UC is incapable of reaching of obtaining 50% or greater fibre volume fractions without an alternative method to fibre placement.

The interlaminar topography was investigated and it was concluded that by changing the processing settings used during UC it was possible to increase the apparent bonded area, resulting in better peel testing performance; however this increased bonded area appeared to still be dependent on the interlaminar topology profile. When compared to the LWD measurements there was apparently more unbonded foil material in the optical and roughness measurements. This greater density in LWD measurements could be due to the plastic flow of the upper foil material filling the gaps and achieving an intimate contact with the previous foil without sufficient energy to achieve bonding.

This work uniquely investigated the activation issues on fibre/matrix integrity of SMA MMCs produced via UC. The identified fibre damage did not appear to inhibit the activation response of the SMA fibre material. The maximum pull force of the SMA fibre was inhibited by the compressive nature of the Al 3003 (T0) matrix. This compressive force was lost when the fibres were activated and then strained which resulted in low fibre/matrix integrity. Higher process parameters did not alter the fibre matrix strength after fibre activation and did not alter the performance of the fibre in terms of response time. A single cycle of the SMA fibres resulted in a loss of fibre pullout strength which was possibly due to the expanding fibre plastically deforming the matrix material and, upon straining, the original fibre diameter was no longer in contact with the matrix material.

This work has uniquely identified that the embedded fibres appeared to have a sonotrode like effect on the surrounding metal matrix by reducing the grain size and inducing work hardening during UC processing. This effect was most abundant in the foil

that was placed on top of the fibre and then consolidated. This virgin material was found to be more susceptible to plastic ‘acoustic softening’ flow and therefore the fibre embedment was not 50:50 but was instead more deeply embedded into the top foil layer. The UC process coupled with areas of matrix of the previously deposited foil can damage embedded SMA fibres through a combination of surface cracking and plastic flow. The, peaked structure of the previously deposited foil layer was often observed to be inverted back into the matrix material after SMA fibre embedding.

The highest processing pressure (310 kPa) did not achieve the best bonding via UC. The reason for this may have been because of the higher pressure putting the sonotrode under greater load and thus artificially reducing the amplitude of oscillation; which in turn would reduce the success of UC bonding.

Fibres of larger diameters were able to be embedded into Al 3003 (T0) matrices using standard processing parameters and, due to the superior actuation force, it was possible to have a greater pull force with a lower number of fibres. The larger diameter fibres were more resistant to fibre pullout when compared to the smaller diameter fibres, some however, when activated the larger diameter fibres caused delamination to the UC matrix. This delamination resulted in a reduction of the peel strength of the sample.

The fibre/matrix bonding mechanism was concluded to be mechanical entrapment as no grain growth was identified across the fibre/matrix interface and no evidence of chemical/diffusion bonding was identified with deconstructed samples. The higher process parameters were found to increase the intimacy of the fibre/matrix interface by increasing the fibre pull out force required to remove the un-activated fibre from the matrix.

The metal matrix was found to decrease the efficiency with which the SMA fibre could reach the activation temperature; however, there was no response rate difference once the activation temperature was attained. The greater conductivity of the matrix material, compared to air, appeared to allow the SMA fibre to cool more quickly which may help future smart material applications by allowing faster SMA cycle times.

There were several novel discoveries within this work which contribute to optimising UC for creating SMA containing MMCs for smart structure applications.

10 Future Recommendations

The hypothesis that the sonotrode was encountering a loss in amplitude at the higher processing pressures should be investigated. This could be investigated through the use of a laser vibrometer to monitor the sonotrode oscillations through a range of amplitudes, pressures, speeds, foil materials, anvil temperatures and sonotrode textures. This full data may reveal any issues related to amplitude loss and would further the understanding of the UC process.

A more representative method of calculating the LWD could be to use a plan view of the weld area which would allow for the unprocessed foil material to be identified and a bonded to non-bonded ratio could be more accurately assessed. Due to the required sample destruction when peeling the bonded foils from each other, a non-destructive method of analysing the unbonded foil area would be highly beneficial in terms of accuracy. Further research would be required to find a suitable non-destructive method however a candidate could be X-ray Microtomography (μCT) analysis. The μCT may be able to internally characterise the UC sample in terms of foil/foil bond density and fibre/foil bond density. Future work could try to indentify how the possible void filling from foil plastic flow contributes, or not, to the strength of the UC samples and to the integrity of fibre/matrix interfaces. The use of μCT would be a step towards a quality control procedure for UC which would aid in the industrial application of the process.

The microhardness testing in the present work was inconclusive due to the relatively small area of the interlaminar peak structures. Future research could use a smaller indenter to accurately measure the hardness of the peak and trough material within the UC interlaminar region. Nano-indentation equipment would most likely be suitable for this future work. Future work could be conducted to verify if the material was undergoing work hardening or not which would further enlighten the understanding of the interlaminar UC landscape.

Full layer penetration by the larger SMA fibres was apparent through the course of the research. To prevent the penetration of the foil layer by larger diameter fibres the use of

thicker foils could be researched in the future as well as possibly using materials with higher yield strength to determine the possible restrictions on fibre embedding, during UC, imposed by a material with superior mechanical properties to Al 3003 (T0). Future work into the embedding of SMA fibres into harder matrices via the use of UC may help elucidate the enabling mechanisms. Materials such as strain hardened Al 3003 (e.g. H18) will offer more resistance to fibre embedding and the ability of SMA fibres to full layer penetrate would be tested. The combination of SMAs with aerospace grade material such as Al 7000 series or Ti-6-4 would improve the industry interest in the use of UC for creating smart structures. This loss may be less if a matrix material with higher yield strength was used; this may be covered in future work.

Due to the significant influence of the sonotrode topology on bond quality it was theorised that an optimised sonotrode topology could increase the effectiveness of UC bonding and possibly allow for an alteration to the UC processed sample properties. It would be of benefit to investigate various sonotrode topologies to attempt to optimise UC bonding. A specific sonotrode topology could be used to maximise the sonotrode intimate contact area during UC processing to help improve the energy transfer efficiency and the refinement of the interlaminar structure. This could potentially allow for denser and stronger components to be produced as well as allowing for a possible increase in processing speed which would help make UC even more attractive as a manufacturing process. As a result of this research an EPSRC project (IMCRC275) has been instigated at Loughborough University, in partnership with Solidica, Inc. which is investigating the alteration and analysis of various UC sonotrode topologies. The ultimate goal of this work is the optimisation of the sonotrode topology to maximise UC components for their intended end use.

The apparent bonding between NiTi SMA fibres and an Al 3003 (T0) matrix during UC processing was relatively weak and likely to be mechanical entrapment of the fibre within the metal matrix. Coating of the fibres, prior to UC, with a material known to bond well with the matrix during UC may also improve the mechanical performance of UC MMC’s. A method by which this may be achieved may be through vapour deposition onto the fibre material prior to embedding in UC; this would help avoid the loss of the SME of the SMA through aggressive thermal cycling. A protective jacket that facilitates

mechanical interlocking and insulates the fibre from the matrix material could also possibly be utilised to increase the efficacy of the SMA/Al MMC. The embedding of fibres in the un-strained state may also help the maximal performance of the SMA fibres.

The present research identified a sonotrode like effect by the SMA fibre on the metal matrix material. Future work could utilise this effect to create a work hardened internal structure. The strategic use of this work hardening effect could be used to create MMC's that are very hard, compared to the raw processing foil, and/or the creation of functionally graded MMC's (i.e. hard in desired areas). A set of experiments using various fibre diameters, fibre materials, matrix materials and processing parameters could be used in combination with microscopic inspection to characterise the potential design of the sonotrode like effect for material alteration.

Increase in matrix material temperature is known to improve bonding and plastic flow during the UC process. The use of raised temperature while embedding SMA fibres should be investigated to ascertain whether this can improve the fibre volume level, fibre diameter level available and allow the use of higher yield strength matrices. In addition to this the use of implanted seed crystals (a different material easily identifiable and immune to process alteration) within the aluminium matrix prior to UC may allow the accurate mapping of plastic flow during UC by having these potentially easily identifiable seeds that will flow with the grain structure and then be identifiable via microscopy.

Future work could investigate the use of large diameter SMA fibres as latent built in structural weaknesses. The present work identified that the expansion of the larger diameter SMA fibres can have a delaminating effect. Future study could use this delaminating ability to create quick release structures or sacrificial components.

A combination of actuators and sensors combined into a single UC sample should be investigated and a potential real world industrial application for a smart integrated device should be sourced to allow the progression of the UC research to further move from academia to market.

To enable UC to progress as a MMC technology the author suggests the following points should be prioritised:

- The optimum sonotrode texture and material should be researched and decided upon. This will then prevent a level of variation between UC machines caused by varying sonotrode surface roughness profiles.
- Standardisation of the UC apparatus should be decided so that standard operating procedures, best practices, and relevant standards can be put into place.
- Sample testing techniques should be decided and adhered to so as to allow for the production of material test data from UC equipment. This data is essential if industry is to put faith in the UC process.
- A method by which to automate the placement and tensioning of fibres during the UC process is desirable to allow accuracy and repeatability of fibre embedding via UC.
- The Computer Aided Manufacturing (CAM) software used with UC (RPCAM) should be adapted so that fibre pathways can be plotted into the software to prevent manual fibre layup being necessary during the process.
- Information about UC and its capabilities should be disseminated more vigorously to the advanced manufacturing community so that further potential applications can be identified and served.

11 References

Agarwala M. [et al.] Direct selective laser sintering of metals. Rapid Prototyping Journal. Emerald Group Publishing Limited, 1995. Vol. 1. pp. 26-36. ISSN: 1355-2546. DOI: 10.1108/13552549510078113.

Agnes G.S and Mall S. Structural Integrity Issues during Piezoelectric Vibration Suppression of Composite Structures. Composites Part B: Engineering, 1999. Vol. 30. No. 7. pp.727-738. ISSN 1359-8368. DOI: 10.1016/S1359-8368(99)00029-3.

Allan W.B. Fibre Optics: Theory and Practice [Book]. Basic Books, 1973. ISBN: 0306307359.

Allen J.J. Micro electro mechanical system design [Book]. London: Taylor & Francis, 2005. ISBN: 0824758242.

Ansari F. (Ed.), Maji, A. (Ed.), Leung, C. (Ed.) Intelligent Civil Engineering Materials and Structures: A Collection of State-of-the-art Papers in the Application of Emerging Technologies to Civil Structures and Materials [Book]. American Society of Civil Engineers, 1997. ISBN 0-7844-0248-5.

Armstrong W.D. [et al.] An experimental and modelling investigation of the external strain, internal stress and fibre phase transformation behaviour of a NiTi actuated aluminium metal matrix composite. Acta Materialia. Elsevier Science Ltd., 1998. Vol. 46. No. 10. pp. 3455-3466. ISSN: 1359-6454. DOI: 10.1016/S1359-6454(98)00020-2

Atkinson H.V. and Rickinson B.A. Hot isostatic processing [Book]. Bristol: Adam Hilger, 1991. ISBN: 0750300736.

Bannantine J.A., Comer J.J. and Handrock J.L. Fundamentals of Metal Fatigue Analysis [Book]. Prentice Hall, 1990. Vol. 1: p. 273. ISBN: 013340191X.

Barbarino S., Pecora, R., Lecce, L., Concilio, A., Ameduri, S., Calvi, E. A Novel SMA-based Concept for Airfoil Structural Morphing. Journal of Materials Engineering

and Performance. ASM International, August 2009. Vol. 18. pp.696-705. ISSN: 1059-9495. DOI: 10.1007/s11665-009-9356-3.

Bein B.K., Wojczak M. and Pelzl J. Analysis of plasma surface modifications by thermal depth profiling and correlation with plasma-surface interactions. Materials Science and Engineering: A. Elsevier B.V., 1989. Vol. 122. No. 1. pp.93-99. ISSN: 0921-5093. DOI: 10.1016/0921-5093(89)90778-8

Bennion I. [et al.] UV-Written In-Fibre Bragg Gratings. Optical and Quantum Electronics. Springer Netherlands, 1996. Vol. 28. No. 2. pp.93-135. ISSN: 1572-817X.

Bhatia V. [et al.] Optical Fibre Based Absolute Extrinsic Fabry - Pérot Interferometric Sensing System. Measurement Science and Technology. IOP Publishing, 1996. Vol. 7. No. 1. pp.58-61. ISSN: 1361-6501. DOI: 10.1088/0957-0233/7/1/008.

Bock W.J., Wolinski T.R. and Eftimov T.A. Polarimetric Fibre-Optic Strain Gauge using Two-Mode Highly Birefringent Fibres. Pure and Applied Optics: Journal of the European Optical Society Part A. IOP Publishing, 1996. Vol. 5. No. 2. ISSN: 1361-6617. DOI: 10.1088/0963-9659/5/2/001

Bonello P., Brennan, M.J., Elliott, S.J., Vincent, J.F.V., Jeronimidis, G. Designs for an Adaptive Tuned Vibration Absorber with Variable Shape Stiffness Element. Proceedings of the Royal Society A. Royal Society Publishing, 2005. Vol. 461. No. 2064. pp.3955-3976. ISSN: 1471-2946. DOI: 10.1098/rspa.2005.1547.

Bräutigam V. [et al.] Smart Structural Components by Integration of Sensor/Actuator Modules in Die Castings. Proceedings of SPIE - Automotive Applications. SPIE, 2007. Vol. 6527. No. 65270S. ISSN: 0277-786X. DOI: 10.1117/12.705831.

Calkins F.T., Mabe J.H. and Butler G.W. Boeing's variable geometry chevron: morphing aerospace structures for jet noise reduction. Proceedings of SPIE: Smart Structures and Materials, and Noise Reduction. San Diego, CA, USA : SPIE, 2006. Vol. 6171. No. 61710O. DOI: 10.1117/12.659664.

Chau H-L. and Wise K.D. An ultraminiature solid-state pressure sensor for a cardiovascular catheter. IEEE Transactions on Electron Devices. IEEE, 1988. Vol. 35. No. 12. pp.2355 - 2362. ISSN: 0018-9383. DOI: 10.1109/16.8814.

Chiodo J.D., Jones, N., Billett, E.H., Harrison, D.J. Shape memory alloy actuators for active disassembly using 'smart' materials of consumer electronic products. Materials & Design. Elsevier Ltd., 2002. Vol. 23. No. 5. pp.471-478. ISSN: 0261-3069. DOI: 10.1016/S0261-3069(02)00018-3.

Clyne T.W. and Withers P.J. An introduction to metal matrix composites [Book]. Cambridge University Press, 1993. ISBN: 0521418089.

Committee on Aeronautical Technologies National Research Council Aeronautical Technologies for the Twenty-First Century [Book]. Washington: National Academy Press, 1992. ISBN: 0-309-04732-3.

Coughlin J.P., Williams, J.J., Chawla, N. Mechanical Behavior of NiTi Shape Memory Alloy Fiber Reinforced Sn Matrix "Smart" Composites. Journal of Materials Science. Springer Netherlands, 2009. Vol. 44. No. 3. pp.700-707. ISSN: 0022-2461. DOI: 10.1007/s10853-008-3188-7.

Daghia F. [et al.] Shape Memory Alloy Hybrid Composite Plates for Shape and Stiffness Control. Journal of Intelligent Material Systems and Structures. Sage Publications, 2008. Vol. 19. No. 5. pp.609-619. ISSN: 1530-8138. DOI: 10.1177/1045389X07077901

Daniels H.P.C. Ultrasonic welding. Ultrasonics. Elsevier B.V., 1965. Vol. 3. No. 4. pp.190-196. ISSN: 0041-624X. DOI: 10.1016/0041-624X(65)90169-1.

Dawson G.R., Winsper C.E. and Sansome D.H. Application of high and low frequency oscillations to the plastic deformation of metals. Metal Forming. 1970. Vol. 37.No. 2. pp. 254-261.

de Vries E. Mechanics and Mechanisms of Ultrasonic Metal Welding. PhD Thesis. Ohio State University, 2004.

Dong B. and Li Z. Cement-Based Piezoelectric Ceramic Smart Composites. Composites Science and Technology. 2005. Vol. 65. No. 9. pp.1363-1371. ISSN: 0266-3538. DOI: 10.1016/j.compscitech.2004.12.006.

Dosch J.J. A Self-Sensing Piezoelectric Actuator for Collocated Control. Journal of Intelligent Material Systems and Structures: SAGE Publications, 1992. Vol. 3. No. 1. pp.166-185. ISSN: 1530-8138. DOI: 10.1177/1045389X9200300109.

Dyke S.J. [et al.] Modeling and control of magnetorheological dampers for seismic response reduction. Smart Material Structures: IOP Science, 1996. Vol. 5. No. 5. pp.565-575. ISSN: 1361-665X. DOI: 10.1088/0964-1726/5/5/006.

Evans A., Marchi C.S. and Mortensen A. Metal matrix composites in industry: an introduction and a survey [Book]. Dordrecht: Kluwer Academic Publishers, 2003. ISBN: 1-4020-7521-9.

Ferrasse S. [et al.] Microstructure and properties of copper and aluminum alloy 3003 heavily worked by equal channel angular extrusion. Metallurgical and Materials Transactions A.: Springer Boston, 1997. Vol. 28. No. 4. pp.1047-1057. ISSN:1073-5623. DOI: 10.1007/s11661-997-0234-z.

Friel R.J. [et al.] The effect of interface topography for ultrasonic consolidation of aluminium. Materials Science and Engineering: A. Elsevier Inc., 2010. Vol. 527. No. 16-17. pp.4474-4483. ISSN: 0921-5093. DOI: 10.1016/j.msea.2010.03.094.

Friel R.J. and Harris R.A. A nanometre-scale fibre-to-matrix interface characterization of an ultrasonically consolidated metal matrix composite. Proceedings of the Institution of Mechanical Engineers, Part L: Journal of Materials: Design and Applications.: Sage Publications, 2010. Vol. 224. No. 1. pp.31-40. ISSN: 2041-3076. DOI: 10.1243/14644207JMDA268.

Furukawaa M. [et al.] Microstructural characteristics of an ultrafine grain metal processed with equal-channel angular pressing. Materials Characterization: Elsevier Inc., November 1996. Vol. 37.No. 5. pp.277-283. ISSN: 1044-5803. DOI: 10.1016/S1044-5803(96)00131-3.

Furuya Y., Sasaki A. and Taya M. Enhanced mechanical properties of TiNi shape memory fiber/Al matrix composite. Materials Transactions: Japan Institute of Metals, 1993. Vol. 34. No. 3. pp.224-227. ISSN: 0916-1821.

Gad-el-Hak M. MEMS: introduction and fundamentals [Book]. Boca Raton: Taylor & Francis, 2006. 2nd Edition. ISBN: 0849391377.

Gärtner F. [et al.] The Cold Spray Process and Its Potential for Industrial Applications. Journal of Thermal Spray Technology.: Springer Boston, 2006. Vol. 15. No. 2. pp.223-232. ISSN: 1544-1016. DOI: 10.1361/105996306X108110.

Gautschi G. Piezoelectric sensorics: force, strain, pressure, acceleration and acoustic emission sensors, materials and amplifiers [Book]. Berlin: Springer-Verlag, 2002. ISBN: 3-540-42259-5.

German R.M. Sintering theory and practice [Book]. New York: Wiley, 1996. ISBN: 047105786X.

Gibson I., Rosen D.W. and Stucker B. Additive Manufacturing Technologies: Rapid Prototyping to Direct Digital Manufacturing [Book]. New York: Springer, 2009. ISBN: 9781441911193.

Goff D.R. Fiber Optic Reference Guide: A Practical Guide to Communications Technology [Book]. Focal Press, 2002. 3rd Edition. ISBN: 0-240-80486-4.

Griffith M.L. [et al.] Understanding thermal behavior in the LENS process. Materials & Design. : Elsevier Ltd., 1999. Vol. 20. No. 2-3. pp.107-113. ISSN: 0261-3069. DOI: 10.1016/S0261-3069(99)00016-3.

Guemes J.A. and Menéndez J.M. Response of Bragg Grating Fiber-Optic Sensors when Embedded in Composite Laminates. Composites Science and Technology.: Elsevier Ltd., 2002. Vol. 62. No. 7-8. pp.959-966. ISSN: 0266-3538. DOI: 10.1016/S0266-3538(02)00010-6.

Gunduz I.E. [et al.] Enhanced diffusion and phase transformations during ultrasonicwelding of zinc and aluminum. Scripta Materialia. : Elsevier, 2005. Vol. 52. No. 9. pp.939–943. ISSN: 1359-6462. DOI: 10.1016/j.scriptamat.2004.12.015.

Hahnlen R. and Dapino M.J. Active Metal-Matrix Composites with Embedded Smart Materials by Ultrasonic Additive Manufacturing. Industrial and Commercial Applications of Smart Structures Technologies. San Diego, CA : 2010. Vol. 7645. p.76450O.

Hahnlen R., Dapino, M.J., Short, M., Graff, K. Aluminum-Matrix Composites with Embedded Ni-Ti Wires by Ultrasonic Consolidation. Industrial and Commercial Applications of Smart Structures Technologies. San Diego, CA: 2009. Vol. 7290. p. 729009.

Hamada K. [et al.] Thermomechanical behavior of TiNi shape memory alloy fiber reinforced 6061 aluminum matrix composite. Metallurgical and Materials Transactions A. Springer, 1998. Vol. 29A. pp.1127-1135. ISSN: 1073-5623. DOI: 10.1007/s11661-998-1022-0.

Hansson I. and Thölen A. Plasticity due to superimposed macrosonic and static strains. Ultrasonics. 1978. Vol. 16. No. 2. pp.57-64. ISSN: 0041-624X. DOI: 10.1016/0041-624X(78)90090-2.

Hartl D.J. and Lagoudas D.C. Aerospace applications of shape memory alloys. Proceedings of the Institution of Mechanical Engineers, Part G: Journal of Aerospace Engineering. : Institution of Mechanical Engineers, 2007. Vol. 221. No. 4. pp.535-552. ISSN: 2041-3025. DOI: 10.1243/09544100JAERO211.

Hashim J., Looney L. and Hashmi M.S.J. Metal matrix composites: production by the stir casting method. Journal of Materials Processing Technology. : Elsevier B.V., 1999. Vol. 92. No. 93. pp.1-7. ISSN: 0924-0136. DOI: 10 .1016/S0924-0136(99)00118-1

He X.Q. [et al.] Active control of FGM plates with integrated piezoelectric sensors and actuators. International Journal of Solids and Structures. : Elsevier Ltd., 2001. Vol. 38. No. 9. pp.1641-1655. ISSN: 0020-7683. DOI: 10.1016/S0020-7683(00)00050-0.

Hill K.O. [et al.] Bragg Gratings Fabricated in Monomode Photosensitive Optical Fiber by UV Exposure through a Phase Mask. Applied Physics Letters.: American Institute of Physics, 1993. Vol. 62. No. 10. pp.1035-1037. ISSN: 1077-3118. DOI: 1 0.1063/1.108786.

Hill K.O. and Meltz G. Fiber Bragg Grating Technology Fundamentals and Overview. Journal of Lightwave Technology. : IEEE, 1997. Vol. 15. No. 8. pp.1263-1276. ISSN: 0733-8724. DOI: 10.1109/50.618320.

Hofmeister W. and Griffith M. Solidification in direct metal deposition by LENS processing. JOM Journal of the Minerals, Metals and Materials Society. Springer Boston, 2001. Vol. 53. No. 9. pp.30-34. ISSN: 1047-4838. DOI: 10.1007/s11837-001-0066-z.

Holzer H. and Dunand D.C. Phase transformation and thermal expansion of Cu/ZrW2O8. Journal of Materials Research. : Materials Research Society, 1999. Vol. 14. No. 3 pp.780-789. ISSN: 0884-2914. DOI: 10.1557/JMR.1999.0104.

Hopkinson N., Hague R. and Dickens P. Rapid Manufacturing : An Industrial Revolution for the Digital Age [Book]. John Wiley & Sons, Ltd., 2006. ISBN: 9780470016138.

Jaffe H. Piezoelectric Ceramics. Journal of the American Ceramic Society.: American Cermaic Society, 1958. Vol. 41. No. 11 pp.494-498. ISSN: 0002-7820. DOI: 10.1111/j.1151-2916.1958.tb12903.x

Janaki Ram G.D. [et al.] Improving Linear Weld Density in Ultrasonically Consolidated Parts. Solid Freeform Fabrication Proceedings, Austin, TX, USA. 2006. pp.692-708.

Janaki Ram G.D. [et al.] Interface Microstructures and Bond Formation in Ultrasonic Consolidation. Solid Freeform Fabrication Proceedings. Austin, TX, USA. 2007. pp.266-283.

Janaki Ram G.D., Yang Y. and Stucker B.E. Effect of Process Parameters on Bond Formation During Ultrasonic Consolidation of Aluminum Alloy 3003. Journal of Manufacturing Systems. 2006. Vol. 25. No. 3. pp. 221-238. ISSN: 0278-6125. DOI: 10.1016/S0278-6125(07)80011-2.

Jiang Q.C., Li X.L. and Wang H.Y. Fabrication of TiC particulate reinforced magnesium matrix composites. Scripta Materialia.: Elsevier, 2003. Vol. 48. No. 6. pp.713-717. ISSN: 1359-6462. DOI: 10.1016/S1359-6462(02)00551-1.

Johnson K Interlaminar subgrain refinement in ultrasonic consolidation. PhD Thesis, Loughborough University, 2008.

Johnson K. Ultrasonic Consolidation – A Viable Method of Smart Structure Manufacture. 4th International Conference on Rapid Manufacturing. Loughborough, UK: 8th - 9th July, 2009.

Jones J.B. and Powers Jr. J.J. Ultrasonic Welding. The Welding Journal. : American Welding Society, 1956. Vol. 35. pp.761-766. ISSN: 0043-2296.

Joshi K.C. The formation of ultrasonic bonds between metals. The Welding Journal. American Welding Society, 1971. Vol. 50. No. 12. pp.840-848. ISSN: 0043-2296.

Judy J.W. Microelectromechanical systems (MEMS): fabrication, design and applications. Smart Materials and Structures.: Institute of Physics Publishing, 2001. Vol. 10. No. 6. pp.1115–1134. ISSN: 0964-1726. DOI: 10.1088/0964-1726/10/6/301.

Jung B.S. [et al.] Fabrication of smart structure using shape memory alloy wire embedded hybrid composite. Materialwissenschaft und Werkstofftechnik. Verlag: John Wiley & Sons, Ltd, 2010. Vol. 41. No. 5. pp.320-324. ISSN: 1521-4052. DOI: 10.1002/mawe.201000604.

Kaczmar J.W., Pietrzak K. and Wlosinski W. The production and application of metal matrix composite materials. Journal of Materials Processing Technology. : Elsevier, B.V., 2000. Vol. 106. No. 1. pp.58-67. ISSN: 0924-0136. DOI: 10.1016/S0924-0136(00)00639-7

Kalpakjian S., Schmid S.R. and Kok C-W. Manufacturing Processes for Engineering Materials [Book]. London: Pearson Prentice-Hall, 2008. 5th Edition. ISBN: 981067953X.

Kanda Y. Piezoresistance effect of silicon. Sensors and Actuators A: Physical.: Elsevier B.V., 1991. Vol. 28. No. 2. pp.83-91. ISSN: 0924-4247. DOI: 10.1016/0924-4247(91)85017-I.

Kang I., Heung, Y.Y., Kim, J.H., et al. Introduction to Carbon Nanotube and Nanofiber Smart Materials. Composites Part B: Engineering.: Elsevier Ltd., 2006. Vol. 37. No. 6. pp.382-394. ISSN: 1359-8368. DOI: 10.1016/j.compositesb.2006.02.011.

Kersey A.D. A Review of Recent Developments in Fiber Optic Sensor Technology. Optical Fiber Technology.: Elsevier Inc., 1996. Vol. 2. No. 3. pp.291-317. ISSN: 1068-5200. DOI: 10.1006/ofte.1996.0036.

Kong C.Y. and Soar R.C. Fabrication of metal-matrix composites and adaptive composites using ultrasonic consolidation process. Materials Science and Engineering: A.: Elsevier, 2005. Vol. 412. No. 1-2. pp.12-18. ISSN: 0921-5093. DOI: 10.1016/j.msea.2005.08.041.

Kong C.Y. and Soar R.C. Method for embedding optical fibers in an aluminum matrix by ultrasonic consolidation. Applied Optics. 2005. Vol. 44. No. 30. pp.6325-6333. ISSN: 1559-128X. DOI: 10.1364/AO.44.006325.

Kong C.Y. Investigation of ultrasonic consolidation for embedding active/passive fibres in aluminium matrices. PhD Thesis. Loughborough University, UK. 2005.

Kong C.Y., Soar R.C and Dickens P.M. Characterisation of aluminium alloy 6061 for the ultrasonic consolidation process. Materials Science and Engineering: A.: Elsevier, 2003. Vol. 363. No. 1. pp.99-106. ISSN: 0921-5093. DOI: 10.1016/S0921-5093(03)00590-2.

Kong C.Y., Soar R.C. and Dickens P.M. A model for weld strength in ultrasonically consolidated components. Proceedings of the Institution of Mechanical Engineers, Part C: Journal of Mechanical Engineering Science. Professional Engineering Publishing, 2005. Vol. 219. No. 1. pp. 83-91. ISSN: 0 954-4062 . DOI: 10.1243/095440605X8315.

Kong C.Y., Soar R.C. and Dickens P.M. Optimum process parameters for ultrasonic consolidation of 3003 aluminium. Journal of Materials Processing Technology.: Elsevier, 2004. Vol. 146. No. 2. pp.181-187. ISSN: 0924-0136. DOI: 10.1016/j.jmatprotec.2003.10.016.

Kong C.Y., Soar R.C. and Dickens P.M. Ultrasonic consolidation for embedding SMA fibres within aluminium matrices. Composite Structures.: Elsevier, 2004. Vol. 66. No. 1-4. pp.421-427. ISSN: 0263-8223. DOI: 10.1016/j.compstruct.2004.04.064.

Kruth J-P. [et al.] Binding mechanisms in selective laser sintering and selective laser melting. Rapid Prototyping Journal.: Emerald Group Publishing Limited, 2005. Vol. 11. No. 1. pp.26-36. ISSN: 1355-2546. DOI: 10.1108/13552540510573365.

Kudva J.N. Overview of the DARPA Smart Wing Project. Journal of Intelligent Material Systems and Structures.: SAGE Publications, 2004. Vol. 15. No. 4. pp.261-267. ISSN: 1530-8138. DOI: 10.1177/1045389X04042796.

Langenecker B. Effects of ultrasound on deformation characteristics of metals. IEEE Transactions on Sonics and Ultrasonics.: IEEE, 1966. Vol. 13. ISSN: 0018-9537. DOI: 10.1109/T-SU.1966.29367.

Lendlein A. Shape-Memory Polymers [Book]. Berlin: Springer-Verlag, 2010. ISSN: 0065-3195.

Leo D.J. Engineering analysis of smart material systems [Book]. Hoboken: John Wiley and Sons, 2007. ISBN: 0471684775.

Lewis G.K. and Schlienger E. Practical considerations and capabilities for laser assisted direct metal deposition. Materials & Design.: Elsevier Ltd., 2000. Vol. 21. No. 4. pp.417-423. ISSN: 0261-3069. DOI: 10.1016/S0261-3069(99)00078-3.

Li D. and Soar R. Influence of sonotrode texture on the performance of an ultrasonic consolidation machine and the interfacial bond strength. Journal of Materials Processing Technology.: Elsevier Inc., 2009. Vol. 209. No. 4. pp.1627-1634. ISSN: 0924-0136. DOI: 10.1016/j.jmatprotec.2008.04.018.

Li D. and Soar R.C. Plastic flow and work hardening of Al alloy matrices during ultrasonic consolidation fibre embedding process. Materials Science and Engineering: A.: Elsevier Inc., 2008. Vol. 498. No. 1-2. pp.421-429. ISSN: 0921-5093. DOI: 10.1016/j.msea.2008.08.037.

Li D., Soar, R.C. Characterization of Process for Embedding SiC Fibers in Al 6061 O Matrix Through Ultrasonic Consolidation. Journal of Engineering Materials and Technology. 2009. Vol. 131. No. 2. p.021016. ISSN: 0094-4289. DOI: 10.1115/1.3030946.

Li L., Li Q. and Zhang F. Behavior of Smart Concrete Beams with Embedded Shape Memory Alloy Bundles. Journal of Intelligent Material Systems and Structures.: SAGE Publications, 2007. Vol. 18. No. 10. pp.1003-1014. ISSN 1530-8138. DOI: 10.1177/1045389X06071974.

Li X.C. and Prinz F. Metal Embedded Fiber Bragg Grating Sensors in Layered Manufacturing. Journal of Manufacturing Science and Engineering. 2003. Vol. 125. No. 3. pp.577-585. ISSN: 1087-1357.

Lira-Olivares J. [et al.] Microstructure Development and Mechanical Properties of Ni Matrix/Carbide Composites. Advanced Performance Materials.: Springer Netherlands, 1997. Vol. 4. No. 1. pp.95-103. ISSN: 1572-8765. DOI: 10.1023/A:1008628501114.

Liu C. and Qin H. and Mather, P.T. Review of progress in shape-memory polymers. Journal of Materials Chemistry.: Royal Society of Chemistry, 2007. Vol. 17. No. 1. pp. 1543-1558. ISSN: 1364-5501. DOI: 10.1039/B615954K.

Liu T. [et al.] A Multi-Mode Extrinsic Fabry - Pérot Interferometric Strain Sensor. Smart Materials and Structures. : IOP Publishing, 1997. Vol. 6. No. 4. pp.464-469. ISSN: 1361-665X . DOI: 10.1088/0964-1726/6/4/011.

Loewy R.G. Recent developments in smart structures with aeronautical applications. Smart Materials and Structures.: IOP Publishing Ltd., 1997. Vol. 6. No. 5. ISSN: 1361-665X. DOI: 10.1088/0964-1726/6/5/001.

Manz H., Breitbach, E.J. Application of Smart Materials in Automotive Structures. Proceedings of Society of Photo-Optical Instrumentation Engineers. 2001. Vol. 4332. pp.197-204. ISBN: 0-8194-4018-3.

Mariani E. and Ghassemieh E. Microstructure evolution of 6061 O Al alloy during ultrasonic consolidation: An insight from electron backscatter diffraction. Acta Materialia.: Pergammon Elsevier Science Ltd., 2010. Vol. 58. No. 7. pp.2492-2503. ISSN: 1359-6454. DOI: 10.1016/j.actamat.2009.12.035.

Michie C. Optical Fiber Sensors for Advanced Composite Materials. Comprehensive Composite Materials.: Elsevier Ltd., 2000. Vol. 5. pp.475-491. ISBN: 978-0-08-042993-9.

Mortensen A. and Cornie J.A. On the infiltration of metal matrix composites. Metallurgical and Materials Transactions A.: Springer Boston, 1991. Vol. 22. No. 1. pp.1160-1163. ISSN: 1543-1940. DOI: 10.1007/BF02668570.

Mou C. [et al.] Smart structure sensors based on embedded fibre Bragg grating arrays in aluminium alloy matrix by ultrasonic consolidation. Measurement Science and Technology. 2009. Vol. 20. No. 3. p.034013. ISSN: 0957-0233. DOI: 10.1088/0957-0233/20/3/034013.

Mussman S. Hot Isostatic Pressing [Article]. Materials World. 1999. November. Vol. 7. - No. 11. pp.677-678. ISSN: 0967-8638.

O'Brien R.L. Welding Handbook Eighth Edition, Volume 2 – Welding Processes [Book]. American Welding Society, 1991. pp.783-812. ISBN: 0871713543.

Obielodan J.O., Ceylan, A, Murr, L.E., Stucker, B.E. Multi-Material Bonding in Ultrasonic Consolidation. Rapid Prototyping Journal. 2010. Vol. 16. No. 3. pp.180-188. ISSN: 1355-2546. DOI: 10.1108/13552541011034843.

Okada M. [et al.] Joint mechanism o f ultrasonic welding. Transactions of the Japanese Institute of Metals.: The Japan Institute of Metals, 1963. Vol. 4. No. 1. pp.250-255. ISSN: 1347-5320.

Okazaki Y. A micro-positioning tool post using a piezoelectric actuator for diamond turning machines. Precision Engineering.: Elsevier Inc., 1990. Vol. 12. No. 3. pp.151-156. ISSN: 0141-6359. DOI: 10.1016/0141-6359(90)90087-F.

Orowan E. Internal Stresses and Fatigue in Metals [Book]. New York: Elsevier, 1959. pp.59-80. ISBN: 0444404678.

Ortin J. and Delaey L. Hysteresis in shape-memory alloys. International Journal of Non-Linear Mechanics.: Elsevier Ltd., 2002. Vol. 37. No. 8. pp.1275-1281. ISSN: 0020-7462. DOI: 10.1016/S0020-7462(02)00027-6.

Otsuka K. and Wayman C.M. Shape memory materials [Book]. Cambridge: Cambridge University Press, 1998. ISBN: 052144487 X.

Pang J.W.C., Bond, I.P. A Hollow Fibre Reinforced Polymer Composite Encompassing Self-Healing and Enhanced Damage Visibility. Composites Science and Technology. 2005. Vol. 65. No. 11-12. pp.1791-1799. ISSN: 0266-3538. DOI: 10.1016/j.compscitech.2005.03.008.

Papyrin A. [et al.] Cold spray technology [Book]. Amsterdam: Elsevier Ltd., 2007. ISBN: 0080451551.

Park S-E. and Shrout T.R. Ultrahigh strain and piezoelectric behavior in relaxor based ferroelectric single crystals. Journal of Applied Physics.: American Institute of Physics, 1997. Vol. 82. No. 4. pp.1804-1811. ISSN: 0021-8979. DOI: 10.1063/1.365983.

Peelamedu S.M., Naganathan G. and Buckley S.J. Impact analysis of automotive structures with distributed smart material systems. Proceedings of SPIE. 1999. Vol. 3667. pp.813-824. ISBN: 9780819431417. DOI: 10.1117/12.350138

Phulé P.P. Magnetorheological (MR) Fluids: Principles and Applications. Smart Materials Bulletin.:Elsevier Ltd., 2001. Vol. 2001. No. 2. pp. 7-10. ISSN: 1471-3918. DOI: 10.1016/S1471-3918(01)80040-X

Pinkerton J.L. [et al.] Controlled Aeroelastic Response and Airfoil Shaping using Adaptive Materials and Integrated Systems. Proceedings of the Society of Photo-optical Instrumentation Engineers. 1996. Vol. 2717. pp. 166-177. ISSN 0361-0748. DOI: 10.1117/12.239019

Potapov P.L. and Da Silva E.P. Time Response of Shape Memory Alloy Actuators. Journal of Intelligent Material Systems and Structures.: Sage Publications, 2000. Vol. 11. No. 2. pp.125-134. ISSN: 1530-8138. DOI: 10.1106/XH1H-FH3Q-1YEX-4H3F.

Rao Y-J In-Fibre Bragg Grating Sensors. Measurement Science and Technology.: IOP Publishing, 1997. Vol. 8. No. 4. pp.355-375. ISSN: 1361-6501. DOI: 10.1088/0957-0233/8/4/002.

Rawal S. Metal-Matrix Composites for Space Applications. Journal of Metals.: Springer Sciences & Business Media, 2001. Vol. 53. No. 4. ISSN: 1047-4838. DOI: 10.1007/s11837-001-0139-z.

Recarte V. [et al.] High Temperature β Phase Decomposition Process in a Cu–Al–Ni Shape Memory Alloy. Materials Science and Engineering A.: Elsevier B.V., 2004. Vol. 378. No. 1-2. pp.238-242. ISSN: 0921-5093. DOI: 10.1016/j.msea.2003.09.111.

Salamone S., Bartoli, I., Di Leo, P., Di Scala, F.L., Ajovalasit, A., D'Acquisto, L., Rhymer, J., Kim, H. High-velocity Impact Location on Aircraft Panels Using Macro-fiber Composite Piezoelectric Rosettes. Journal of Intelligent Material Systems and Structures.: SAGE Publications, 2010. Vol. 21. No. 9. pp. 887-896. ISSN: 1530-8138. DOI: 10.1177/1045389X10368450.

Schaller R. Metal matrix composites, a smart choice for high damping materials. Journal of Alloys and Compounds.: Elsevier Science B.V, 2003. Vol. 355. No. 1-2. pp.131-135. ISSN: 0925-8388. DOI: 10.1016/S0925-8388(03)00239-1.

Schwope L-A. [et al.] Field Repair and Replacement Part Fabrication of Military Components using Ultrasonic Consolidation Cold Metal Deposition. NATO RTO-MP-AVT-163 Additive Technology for the Repair of Military Hardware. Bonn: NATO, 2009, October 19-22. Paper 22.

Shi L., Yu C. and Zhou J. Thermal characterization and sensor applications of one-dimensional nanostructures employing microelectromechanical systems. The journal of physical chemistry. B.: American Chemical Society, 2005. Vol. 109. No. 74. pp. 22102-11. ISSN: 1520-5207. DOI: 10.1021/jp053904l.

Spearing S.M. Micro Devices and Micro Systems, Materials for [Book Section] Encyclopedia of Materials: Science and Technology / book auth. Buschow K.H.J. [et al.]. Oxford: Elsevier, 2001. ISBN: 978-0-08-043152-9.

Spillman Jr. W.B., Sirkis J.S. and Gardiner P.T. Smart materials and structures: what are they? Smart Materials and Structures.1996. Vol. 5. No. 3. pp. 247-254. ISSN: 1361-665X DOI: 10.1088/0964-1726/5/3/002.

Srivatsan T.S. and Lavernia E.J. Use of spray techniques to synthesize particulate-reinforced metal-matrix composites. Journal of Materials Science.: Springer Netherlands, 1992. Vol. 27. No. 22. pp.5965-5981. ISSN: 1573-4803. DOI: 10.1007/BF01133739.

Staszewski W.(Ed.), Boller, C.(Ed.), Tomlinson, G.(Ed.) Health Monitoring of Aerospace Structures: Smart Sensor Technologies and Signal Processing [Book]. Chichester: John Wiley & Sons Ltd, 2004. ISBN 0-470-84340-3.

Steinem C. and Janshoff A. Piezoelectric sensors [Book]. Berlin: Springer-Verlag, 2007. 1st Ed. Vol. 5. ISSN: 1612-7617.

Stoltenhoff T., H. Kreye and Richter H.J. An analysis of the cold spray process and its coatings. Journal of Thermal Spray Technology.: Springer Boston, 2002. Vol. 11. No. 4. pp.542-550. ISSN: 1544-1016. DOI: 10.1361/105996302770348682.

Straub F.K. [et al.] Smart Material-Actuated Rotor Technology – SMART. Journal of Intelligent Material Systems and Structures.: SAGE Publications, 2004. Vol. 15. No. 4. pp.249-260. ISSN: 1530-8138. DOI: 10.1177/1045389X04042795.

Tai W-P. and Kim S-H. Relationship between cyclic loading and degradation of piezoelectric properties in Pb(Zr,Ti)O3 ceramics. Materials Science and Engineering B.: Elsevier B.V., 1996. Vol. 38. No. 1-2. pp.182-185. ISSN: 0921-5107. DOI: 10.1016/0921-5107(95)01513-2

Takahashi K. Sensor Materials for the Future: Intelligent Materials. Sensors and Actuators. 1988. Vol. 13. No. 1. pp.3-10. ISSN 0250-6874. DOI: 10.1016/0250-6874(88)85024-8.

Takeda N. [et al.] Development of Smart Composite Structures with Small-Diameter Fiber Bragg Grating Sensors for Damage Detection: Quantitative Evaluation of Delamination Length in CFRP Laminates using Lamb Wave Sensing. Composites Science and Technology. Elsevier Ltd., 2005. Vol. 65. No. 15-16. pp.2575-2587. ISSN: 0266-3538. DOI: 10.1016/j.compscitech.2005.07.014.

Taminger K.M. and Hafley R.A. Electron Beam Freeform Fabrication for Cost Effective Near-Net Shape Manufacturing. RTO MP AVT 136 - Cost effective manufacture via net shape processing. Amsterdam: North Atlantic Treaty Organization, 2006. Paper 16.

Taminger K.M., Hafley R.A. and Domack M.S. Evolution and control of 2219 aluminum microstructural features through electron beam freeform fabrication. Materials Science Forum.: Trans Tech Publications, 2006. Vols. 519-521. pp.1297-1302. ISSN: 0255-5476.

Tang W.C. MEMS applications in space exploration. Micromachined Devices and Components III, Proceedings of SPIE. Austin, TX, USA, 1997. Vol.3224. pp.202-211. ISBN: 9780819426567.

Taya M. [et al.] Strengthening mechanisms of TiNi shape memory fiber/Al matrix composite. Proceedings of SPIE.: The International Society for Optical Engineering, 1993. Vol. 1916. No. 1. pp. 373-383.

Tennyson R.C., Mufti, A.A., Rizkalla, S., Tadros, G., Benmokrane, B. Structural Health Monitoring of Innovative Bridges in Canada with Fiber Optic Sensors. Smart Materials and Structures.: Institute of Physics Publishing, 2001. Vol. 10. No. 3. pp. 560-573. ISSN: 0964-1726. DOI: 10.1088/0964-1726/10/3/320.

Thompson B.S., Gandhi M.V. and Kasiviswanathan S. An introduction to smart materials and structures. Materials & Design.: Elsevier Ltd., 1992. Vol. 13. No. 1. pp.3-9. ISSN: 0261-3069. DOI: 10.1016/0261-3069(92)90045-J.

Thümmler F. and Oberacker R. An introduction to powder metallurgy [Book]. London: Institute of Materials, 1993. ISBN: 090171626X.

Torres B. [et al.] Oxy-Acetylene Flame Thermal Spray of Al/SiCp Composites with High Fraction of Reinforcements. Journal of Thermal Spray Technology.: Springer Boston, 2009. Vol. 18. No. 4. pp.642-651. ISSN: 1544-1016. DOI: 10.1007/s11666-009-9393-3.

Udd E. (ed) Fiber Optic Smart Structures [Book]. New York: John Wiley & Sons, Inc, 1995. ISBN: 0-471-55448-0.

Vogelesang L.B. and Vlot A. Development of Fibre Metal Laminates for Advanced Aerospace Structures. Journal of Materials Processing Technology.: Elsevier B.V., 2000. Vol. 103. No.1. pp.1-5. ISSN: 0924-0136. DOI: 10.1016/S0924-0136(00)00411-8.

White D. Ultrasonic Consolidation of Aluminium Tooling. Advanced Materials and Processes. 2003. Vol. 161. No. 1. pp. 64-65. ISSN: 0882-7958.

White D. Ultrasonic Object Consolidation [Patent] : 6519500. - United States of America, 23 March 2000.

White S.R. [et al.] Autonomic Healing of Polymer Composites. Nature. 2001. Vol. 409. pp.794-797. ISSN: 0028-0836. DOI: 10.1038/35057232.

Wood R.A., Han C.J. and Kruse P.W. Integrated uncooled infrared detector imaging arrays. Solid-State Sensor and Actuator Workshop, 5th Technical Digest. Hilton Head Island, SC , USA: IEEE, 1992. pp.132 - 135. ISBN: 0-7803-0456-X.

Wu X.D., Fan Y.Z. and and Wu J.S. A study on the variations of the electrical resistance for NiTi shape memory alloy wires during the thermo-mechanical loading. Materials & Design.: Elsevier Ltd., 2000. Vol. 21. No. 6. pp.511-515. ISSN: 0261-3069. DOI: 10.1016/S0261-3069(00)00022-4.

Yang Y., Janaki Ram G. D. and and Stucker B. E. Bond formation and fiber embedment during ultrasonic consolidation. Journal of Material Processing Technology.: Elsevier B.V., 2009. Vol. 209. No. 10. pp.4915–4924. ISSN: 0924-0136. DOI: 10.1016/j.jmatprotec.2009.01.014.

Yang Y., Janaki Ram, G.D., Stucker, B.E. An Experimental Determination of Optimum Processing Parameters for Al/SiC Metal Matrix Composites Made using Ultrasonic Consolidation. Journal of Engineering Materials and Technology. 2007. Vol. 129. No. 4. pp.538-549. ISSN: 0094-4289. DOI: 10.1115/1.2744431.

Yousefi-Koma A. and Zimcik D.G. Applications of Smart Structures to Aircraft for Performance Enhancement. Canadian Aeronautics and Space Journal.: Canadian Aeronautics and Space Institute, 2003. Vol. 49. No. 4. pp.163-172. ISSN: 1712-7998. DOI: 10.5589/q03-014.

Zagrai A., Doyle, D., Gigineishvili, V., Brown, J., Gardenier, H., Arritt, B. Piezoelectric Wafer Active Sensor Structural Health Monitoring of Space Structures. Journal of Intelligent Material Systems and Structures.: SAGE Publications, 2010. Vol. 21. No. 9. pp.921-940. ISSN 1530-8138. DOI: 10.1177/1045389X10369850.

Zhang X-P. [et al.] Investigation on diffusion bonding characteristics of SiC particulate reinforced aluminium metal matrix composites (Al/SiCp-MMC). Composites Part A: Applied Science and Manufacturing.: Elsevier B.V., 1999. Vol. 30. No. 12. pp.1415-1421. ISSN: 1359-835X. DOI: 10.1016/S1359-835X(99)00040-8.

Zhou G. and Sim L.M. Damage Detection and Assessment in Fibre-Reinforced Composite Structures with Embedded Fibre Optic Sensors - Review. Smart Materials and Structures.: IOP Publishing, 2002. Vol. 11. No. 6. pp.925-939. ISSN: 1361-665X. DOI: 10.1088/0964-1726/11/6/314.